Combining supramolecular cylinders with a platinum anticancer agent

UNIVERSITY OF BIRMINGHAM

Viktoriia Sadovnikova

A thesis submitted in partial fulfilment of the requirements for the degree of Doctor of Philosophy in Chemistry

University of Birmingham, School of Chemistry

August 2011

This thesis is dedicated to my parents for their unconditional love and endless support.

Acknowledgements

First of all, I would like to express my sincere gratitude to my supervisor, Prof. M. J. Hannon, who gave me an opportunity to carry out research in his group and provided support and guidance throughout my PhD studies.

I am very grateful to all the staff members of the analytical facilities for the technical support. In particular I would like to thank Dr. Neil Spencer for providing me assistance and advice with NMR experiments, Peter Ashton for help with Mass spectrometry data analysis, Louise Male for solving X-ray structures and helping me with interpretation of the X-ray data, Graham Burns for his great help with HPLC. I am very thankful to Ian Bodfish for doing a great job with chemical orders. I would also like to express my appreciation to Prof. Kevin Chipman, Dr. Chris Bunce and Dr. Nicholas Hodges for allowing me to use their facilities in the School of Biosciences at the University of Birmingham.

I would like to thank all the members of the Hannon group, past and present, for sharing their knowledge and experience, providing help and support, particularly I would like to thank Carlos for teaching me cell culture techniques and Jenna for proofreading of my thesis. Very special thanks to my dear friends and colleagues Anna and Siriporn for their friendship, care, immense support throughout the studies, great time shared and unforgettable trips.

Many people whom I met in Birmingham were important to me but some of them impacted my life in a very special way. I am very thankful to Fred, who became part of my life, for his great love and support and incredible moments we shared as well as for his help in proofreading of the thesis. To Giorgio, Bick, and Bene for great and fun

times in our home at the Wentworth road, Iryna and Maxim for amazing moments during my first year in Birmingham. Special thanks to my dear Cypriot friend and housemate Eleni, for being very helpful and supportive throughout the studies, for our long philosophical conversations and sharing good and bad moments together.

Many thanks to all my Russian friends especially Alice, Anastasia, Maria and Julia for their true friendship and support.

I would like to express my deepest gratitude to my parents. My father who offered me a great support, provided advice, and guidance throughout my life and gave me this opportunity to study abroad. My mother, for her deep love and care, long phone calls, sharing happiness and sadness with me. Without love and support of my family I would not be who I am at this point in life.

Finally, I would like to thank the EU DNAREC Marie Curie Training Site for funding.

Declaration

The work, observations and recommendations reported in this thesis are those of the author unless specifically stated and have not previously been submitted as part of a degree at the University of Birmingham or any other institution.

Viktoriia Sadovnikova

August 2011

List of papers published from this thesis

1. L. Cardo, V. Sadovnikova, S. Phongtongpasuk and M. J. Hannon, Arginine conjugates of metallo-supramolecular cylinders prescribe helicity and enhance DNA junction binding and cellular activity, *Chem Commun.*, 2011, **47**, 6575.

2. S. Vitorino, V. Sadovnikova, L. Male and M. J. Hannon, Synthesis, cytotoxic activity and DNA binding studies of rhodium(III) complexes. *Manuscript to be submitted to Chemistry - A European Journal.*

3. L. Cardo, S. Phongtongpasuk, V. Sadovnikova and M. J. Hannon, Iron(II) supramolecular helicate conjugated to amino acids. *Manuscript to be submitted to the Chemical Communications Journal.*

4. V. Sadovnikova, L. Male and M. J. Hannon, Introducing new properties on cylinders. *Manuscript in preparation.*

Contents

Abbreviations

3WJ	Three-way junction
1D	One dimensional
2D	Two dimensional
A	Adenine
Å	Angstoms
ATP	Adenosine triphosphate
AAS	Atomic Absorption Spectroscopy
Arg	Arginine
br	Broad
bpz	bipyrazine
Bn	Benzyl
^{t}Bu	*tert*-Butyl
Bpy	2,2'-bipyridine
CD	Circular Dichroism
^{o}C	degree Celsius
C	Cytosine
CD_3CN	deuterated acetonitrile
CD_3OD	deuterated methanol
$CDCl_3$	deuterated chloroform
ct-DNA	calf thymus DNA
DNA	Deoxyribonucleic acid
DAPI	4,6'-diamidio-2-phenylindole
DCM	Dichloromethane

DIPEA	*N*,*N*-diisopropylethylamine
DACH	1,2-diaminocyclohexane
DMDT	*N*,*N*-dimethyldithiocarbamate
DMF	*N*,*N*-dimethylformamide
DMSO	Dimethyl sulfoxide
dmtp	5,7-dimethyl-1,2,4-triazolo[1,5-*a*]pyrimidine
dpp	2,3'-bis(2-pyridyl)pyrazine
dpq	dipyrido[3,2-d:2',3'-f]quinoxaline
dppz	dipyrido[3,2-a:2',3'-c]phenazine
dppn	3,6-bis(2'-pyridyl)pyridazine
d	doublet
dd	doublet of doublets
DMEM	Dulbecco`s modified Eagle`s medium
ESI	Electrospray Ionisation (Mass Spectrometry)
EGF	Epidermal Growth Factor
EGFR	Epidermal Growth Factor Receptor
ESDT	Ethylsarcosinedithiocarbamate
ε	Extinction coefficient
EtOAc	Ethyl Acetate
en	Ethylenediamine
EDTA	Ethylenediaminetetraacetic acid
FBS	Foetal bovine serum
5-FU	5-fluorouracil
Fig	Figure

FAB	Fast-atom Bombardment (Mass Spectrometry)
G	Guanine
5’-GMP	guanosine 5’-monophosphate
g	gram
Gly	Glycine
Hz	Hertz
HMG	High-Mobility Group proteins
HPLC	High-performance liquid chromatography
HEPES	4-(2-hydroxyethyl)-1-piperazineethanesulfonic acid
IR	Infrared spectroscopy
ICP-MS	Inductively Coupled Plasma Mass Spectrometry
IC_{50}	half maximal inhibitory concentration
J	NMR coupling constant
LD	Linear Dichroism
MLCT	Metal to Ligand Charge Transfer
Me	Methyl
MALDI	Matrix-Assisted Laser Desorption Ionization
m	medium
M	molar
mL	millilitre
μM	micromolar
mmol	millimole
m/z	mass to charge ratio
mM	millimolar

min	minute
MTT	3-(4,5-dimethylthiazol-2-yl)-2,5-diphenyltetrazolium bromide
NMR	Nuclear Magnetic Resonance
nm	nanometre
PBS	Phosphate Buffered Saline
PAGE	Polyacrylamide gel electrophoresis
ppm	parts per million
phi	9,10-phenanthrenequinone diimine
p	page
phen	1,10-phenanthroline
pyr	pyridine
qpy	2,2’:6’2’’:6’’,2’’’:6’’’,2’’’’-quinquepyridine
RNA	Ribonucleic acid
RPMI-1640	Roswell Park Memorial Institute medium
SD	Standard deviation
s	strong (IR), singlet (NMR)
SWNT	Single Wall Carbon Nanotube
td	triplet of doublets
T	Thymine
trien	triethylenetetramine
TAE	Tris-Acetate EDTA
TEMED	tetramethylenediamine
tpy	2,2’:6’,2’’-terpyridine
UV/Vis	Ultraviolet/Visible spectroscopy

Abstract

Chapter 1 reviews DNA structure and DNA molecular recognition by synthetic agents, including supramolecular helicates and cisplatin. An overview of various types of helicates and cisplatin anticancer drugs and their mechanisms of action is discussed. Examples of non-platinum anticancer drugs are also presented.

In Chapter 2, the synthesis of novel metal-based supramolecular helicates and attempts to combine them with the cisplatin anticancer agent are described. In some cases X-ray crystallography data are presented and discussed in detail. In addition, the synthesis of the fluorescent europium helicate is described.

In Chapter 3, stability and DNA binding properties of the synthesised metallo-helicates are investigated using UV/Vis spectroscopy, CD and LD techniques. The ability of the complexes to unwind plasmid DNA and stabilise DNA three-way junction formation is explored by gel electrophoresis experiments. The results demonstrate that the geometry and size of the helicates are crucial for DNA three-way junction recognition.

In Chapter 4, biological evaluation of antineoplastic activity of the metallo-helicates synthesised in this work, as well as of the compounds supplied by other members of the group, is studied using an MTT colorimetric assay. The results of the study reveal that some of the complexes exhibit a potent cytotoxic activity.

Chapter 1

Introduction

1.1 Overview

The structures and effects of many biologically active molecules within biological systems are mediated by non-covalent interactions. It is essential to study these interactions, in order to understand function and mechanisms of action and to design synthetic analogues that will possess similar or even better biological activity. DNA, for instance, is a key molecule of the cell and its structure is held together by non-covalent interactions. Some proteins are able to bind to specific sites of the DNA and take part in gene regulation. Understanding the mechanism and principle of these interactions gives an opportunity to design new synthetic agents similar to their biological counterparts that could control gene expression. Supramolecular chemistry is a powerful tool in the creation of such synthetic analogues that could be used as therapeutic agents.

1.2 Supramolecular chemistry

The term supramolecular chemistry was first introduced by French chemist Jean-Marie Lehn.[1] Supramolecular chemistry is a field of chemistry based on non-covalent interactions between molecules including electrostatic interactions, van der Waals forces, hydrophobic effects, aromatic π-π stacking, metal coordination, dipole-dipole bonds, and hydrogen bonding.[2] Covalent bonds introduce some rigidity within molecules whereas non-covalent intermolecular interactions introduce some flexibility to the molecular assemblies. Control of the geometry and rigidity of the molecular components gives opportunities to build molecules which can spontaneously generate well defined supramolecular assemblies. Thus, supramolecular chemistry allows the development of highly complex, functional chemical systems from individual components which are held together by intermolecular forces.[3]

1.3 DNA

1.3.1 Background

DNA or deoxyribonucleic acid is a highly ordered molecule with a helical structure. DNA was first isolated by the Swiss scientist Friedrich Miescher in 1869 from cell nuclei.[4] The structure of DNA remained unknown for many years and only in 1953 the double helical structure of DNA was identified by James Watson and Francis Crick.[5] DNA encodes the genetic information of most living organisms and thus is responsible for their development and functioning. Moreover, DNA is used as a template for the synthesis of RNA which in turn encodes amino-acid sequence as proteins. Understanding the structure of DNA and the mechanisms of DNA recognition provides opportunities to control genetic information.

1.3.2 DNA structure

The DNA molecule consists of individual units called nucleotides which are linked together by 3'-5' phosphodiester bond (Fig. 1.0).[6]

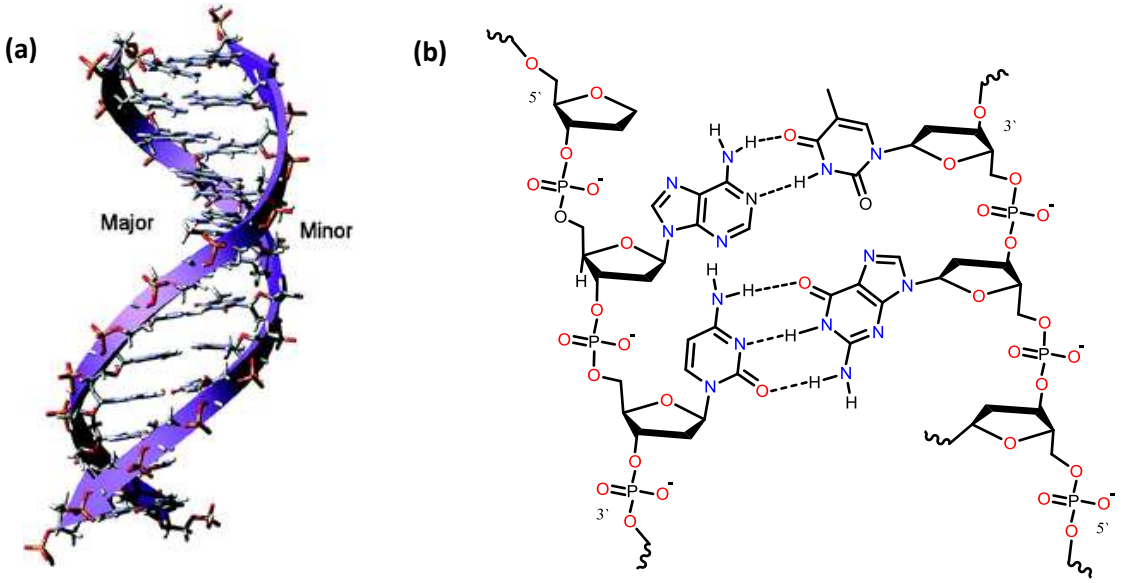

Figure 1.0 Schematic representation of B-DNA.[7]

The B-form of the DNA, as established by Watson and Crick[8], consists of two polynucleotide strands which form a ~ 20 Å diameter double helix by winding about a common axis. The helix is right-handed and the two strands run in opposite directions. Four different nitrogenous bases are present in the DNA: purines (adenine (A) and guanine (G)) and pyrimidines (cytosine (C) and thymine (T)). Bases from one strand of the DNA are paired with bases on the other strand of the DNA by hydrogen bonds thus forming base pairs (Fig. 1.1). Adenine is always paired with thymine and cytosine is paired with guanine. These interactions are called complementary base pairing.[8]

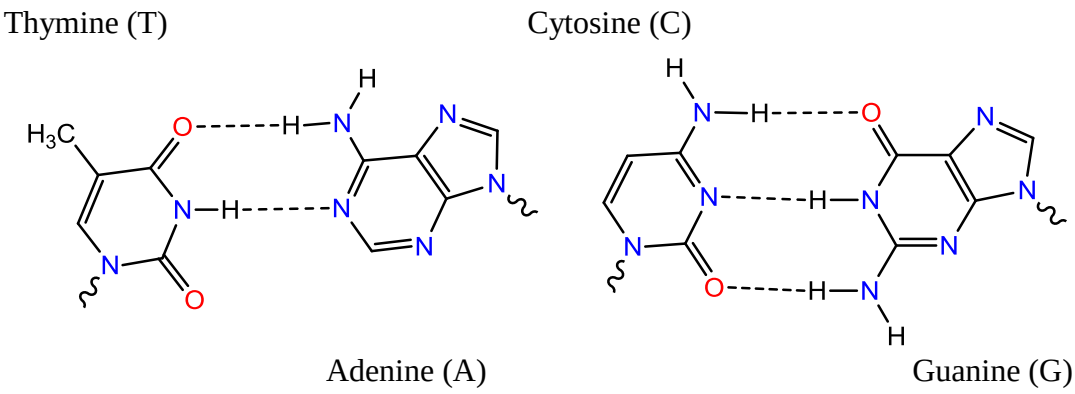

Figure 1.1 Watson-Crick base pairs.

The paired bases are perpendicular to the helix axis and are π-stacked on each other forming a hydrophobic core of the DNA. Thus, the center of the helix is a chemically inert place to store genetic information. The DNA itself is negatively charged due to the presence of phosphate groups. One of the most important characteristics of B-DNA is the occurrence of two distinct grooves known as the major groove and the minor groove. These grooves play a significant role in the recognition of DNA, providing distinct surfaces with which proteins, certain chemicals and drugs can interact.[6, 8]

The DNA molecule can exist in several various conformations. A, B and Z forms of the DNA have been found in living organisms (Fig. 1.2). The B-DNA is the prevailing form present in the cell. A-DNA is a right-handed double helix with inclined base pairs wrapping around a cylindrical hole. It is wider and flatter than B-DNA with a shallow minor groove and deep major groove. The A-form of DNA occurs in dehydrated samples of DNA and it can be found in hybrid DNA and RNA strands or in protein-DNA complexes.[9] Z-DNA is a left-handed double helix with a zigzag pattern which has only one deep and narrow minor groove and no distinct major groove. The Z-conformation of the DNA is not a stable feature; the Z-structure is induced by biological activity and then it disappears.[10]

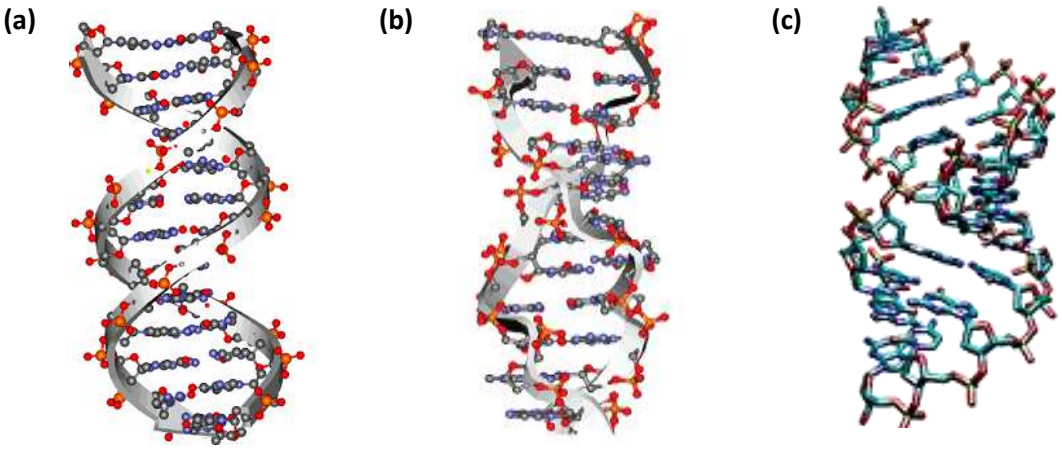

Figure 1.2 DNA conformations **(a)** B-DNA **(b)** Z-DNA[10] **(c)** A -DNA.[11]

Other unique DNA structures that are believed to play important roles in gene expression include DNA junctions and DNA tetraplex.[12] DNA junctions are intermediate structures that are formed during DNA replication (three-way junction) and homologous recombination (four-way junction) (Fig. 1.3).[13]

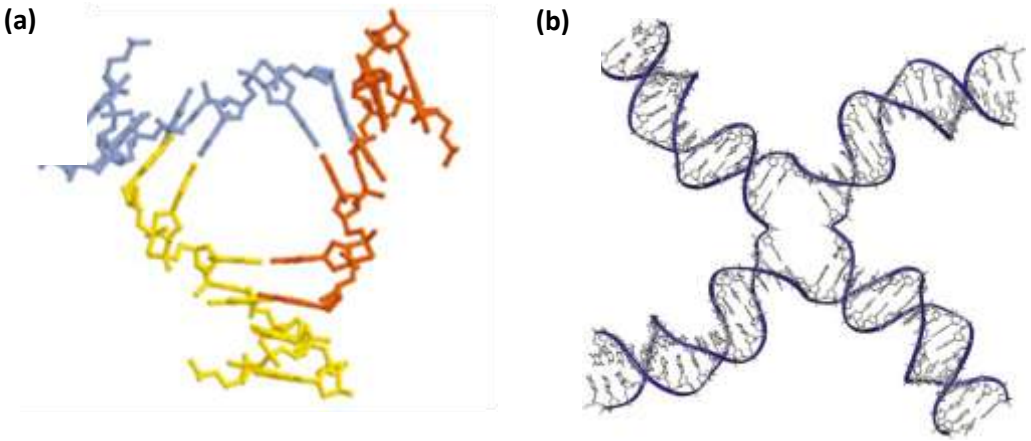

Figure 1.3 DNA junction structures **(a)** DNA three-way junction[14] **(b)** DNA four-way junction.[15]

Tetraplex DNA or G-quadruplex has a four-stranded helical structure which consists of stacked quartets known as G-quartets (Fig. 1.4). Each of the quartets involves the planar association of four guanine bases with a cyclic hydrogen bonding arrangement between them.[16]

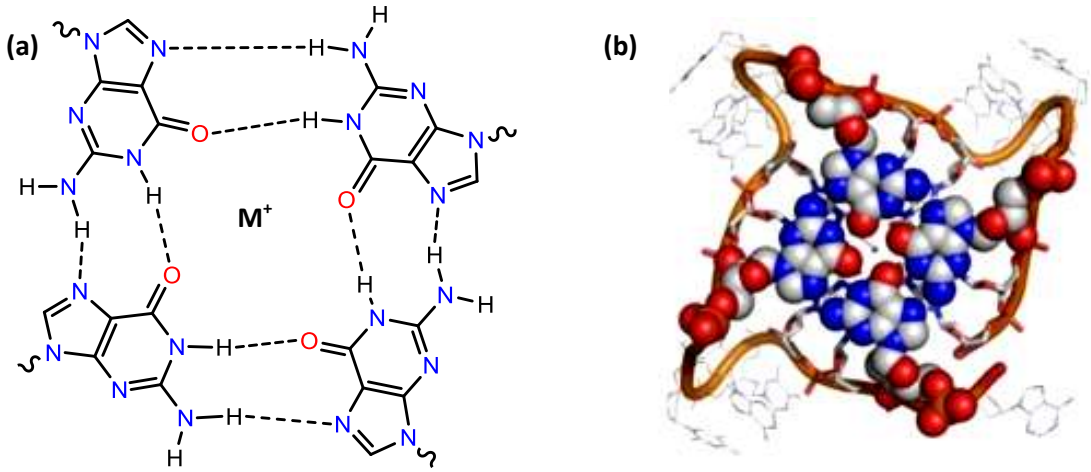

Figure 1.4 DNA tetraplex **(a)** Schematic structure of the guanine quartet **(b)** Top view of the X-ray crystal structure of a human telomeric quadruplex DNA generated with PyMol.[17, 18]

Telomeres, the ends of the chromosomes, are guanine rich sequences. They protect chromosomes from damage and recombination. Telomeric sequences of DNA are capable of tetraplex formation therefore there is a significant interest in these kind of structures as potential targets for anticancer therapy.[19]

1.3.3 DNA recognition

DNA recognition plays a crucial role in the functioning of living systems. In biological systems the control of genetic information occurs through the non-covalent recognition of DNA by regulatory proteins. Understanding the mechanism of DNA recognition is important to design and develop synthetic agents that are able to recognize and bind to the DNA with selectivity and control gene expression. Molecular recognition of B-DNA can take place in different ways such as sugar-phosphate backbone binding, intercalation between base pairs, coordinative binding, groove binding, DNA junction and G-quadruplex recognition.[20]

1.3.3.1 DNA sugar-phosphate backbone binding

The sugar phosphate backbone of DNA is an oxygen-rich polyanionic surface. Hydrogen bonding and electrostatic interactions are predominant in this type of DNA recognition. Farrell`s compound TriplatinNC is an example of a DNA backbone binder (Fig. 1.5). TriplatinNC has a strong selectivity for phosphate oxygens forming bidentate complexes through hydrogen bonding.[21]

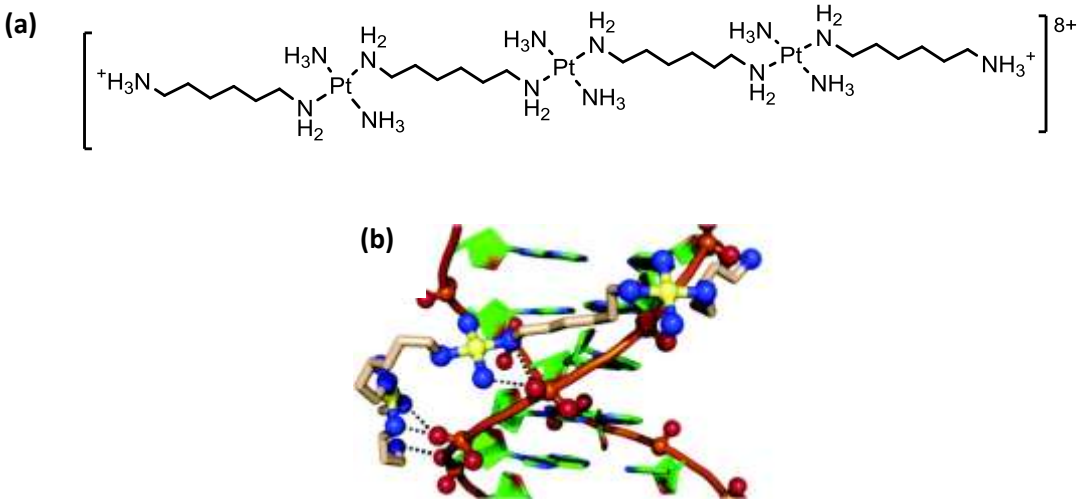

Figure 1.5 Farrell`s trinuclear platinum backbone binder **(a)** Structure of TriplatinNC **(b)** TriplatinNC bound to the DNA backbone.[21]

1.3.3.2 DNA intercalation

DNA intercalation is based on insertion of a planar aromatic molecule or a fragment between two adjacent base-pairs of the DNA, forming sandwich-like structures. Intercalation leads to an opening between base pairs and unwinding of the DNA. DNA intercalators are mostly polycyclic, aromatic, and planar molecules.[22] An anticancer drug doxorubicin is an example of a DNA intercalator (Fig. 1.6 (a, b)).[23]

Metallo-intercalators are metal complexes containing one or several intercalating ligands. An example of a metallo-intercalator is $[Rh(phi)(Me_2trien)]^{3+}$ complex of Barton (Fig. 1.6 (c, d)).[24] When the metal complex binds to the DNA its planar phi ligand is inserted between base pairs forming face-face π-π interactions while the metal and other co-ligands reside in one of the DNA grooves.[25]

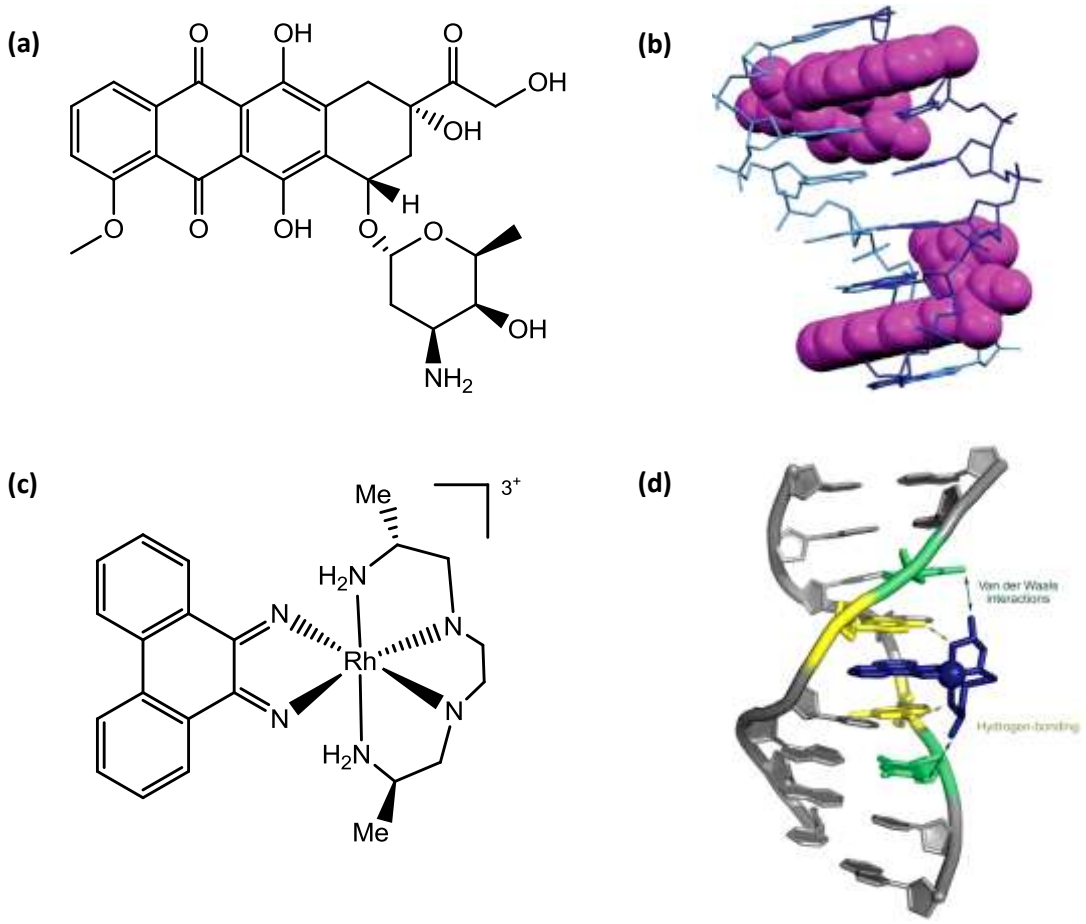

Figure 1.6 DNA intercalators **(a)** Structure of doxorubicin **(b)** Intercalation of doxorubicin between DNA base pairs[23] **(c)** Structure of $[Rh(phi)(Me_2trien)]^{3+}$ **(d)** Binding of $[Rh(phi)(Me_2trien)]^{3+}$ to DNA by intercalation.[24, 25]

1.3.3.3 Coordinative binding

The coordinative binding of synthetic agents to the DNA is irreversible and can lead to cell death by interfering in the processes of DNA functioning. Nitrogen mustards such as the drug chlorambucil and mustine (Fig. 1.7) are examples of coordinative binders.[26] They alkylate DNA primarily at the N7 position of guanine by displacement of the chlorine and thus, are involved in the arrest of processes of replication and transcription.

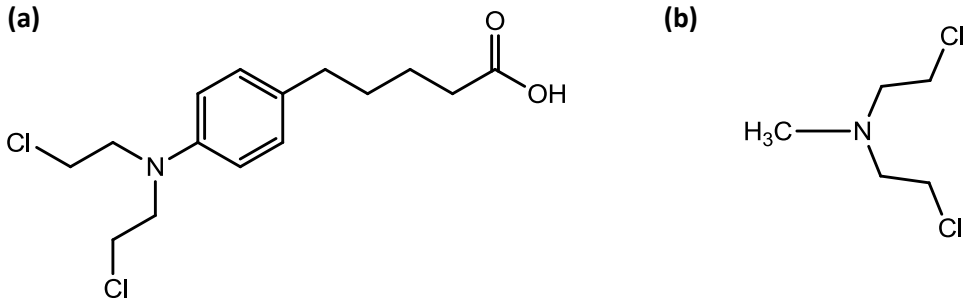

Figure 1.7 Nitrogen mustards **(a)** Chlorambucil **(b)** Mustine.

The most successful in clinics anticancer drug cisplatin is a DNA alkylating agent. It binds to DNA by forming coordinative bonds mostly to the N7 position of adjacent guanine residues on one strand of the DNA (Fig. 1.8).[27] The mechanism of action of cisplatin is discussed in more detail in section 1.5 of chapter 1.

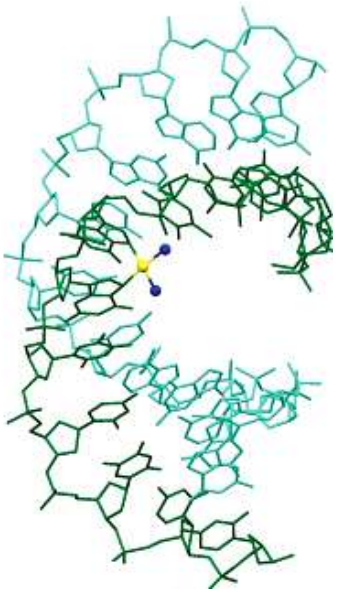

Figure 1.8 Cisplatin bound to DNA.[28]

Another example of coordinative binder is antitumour antibiotic anthramycin (Fig. 1.9) which belongs to the pyrollo(1,4)benzodiazepine antibiotic group.[30] Antibiotics of

this group are able to inhibit nucleic acid synthesis by forming coordinative adducts with DNA.

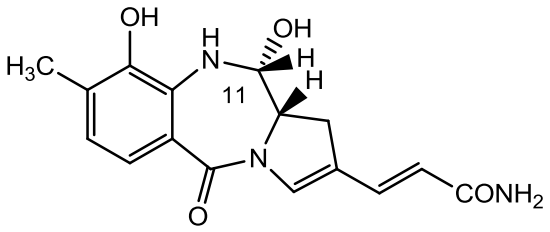

Figure 1.9 Structure of anthramycin.

The binding of anthramycin to DNA occurs by forming a covalent bond between C11 and N2 of guanine. The structure is further stabilized by hydrogen bonding. Anthramycin has a preference for purine-G-purine sequences and binds to the middle guanine.[29, 30]

1.3.3.4 Minor groove binding

The minor groove of DNA is an interaction site of some enzymes and regulatory proteins and thus is an attractive target for small synthetic molecules. Minor groove binders have specificity for AT regions of DNA and bind to DNA non-covalently. An example of such a binder is DAPI (Fig. 1.10). DAPI (4,6-diamidino-2-phenylindole) is an anti-parasitic agent that binds to AT-rich regions of the DNA minor groove with phenyl and indole rings parallel to the groove walls covering the three-base pair sequence ATT.[31]

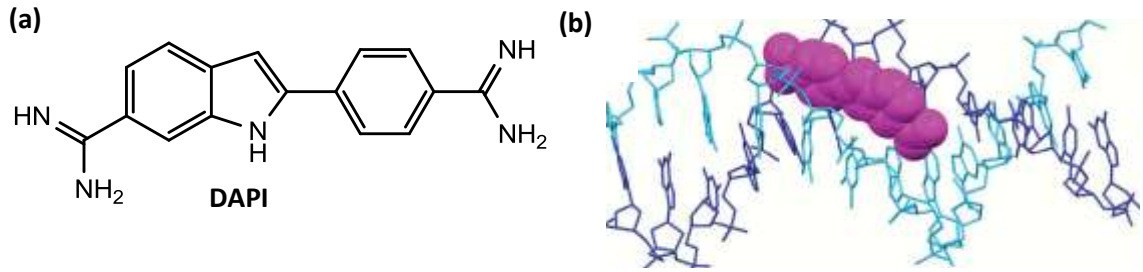

Figure 1.10 Minor groove binder **(a)** The structure of DAPI **(b)** DAPI (pink) bound in the minor groove of the DNA.[32]

One of the most well-known anti-microbial DNA minor groove binders is pentamidine (Fig. 1.11).[33] It is an aromatic diamidine which is active against *Pneumocystis pneumonia* caused by yeast-like fungus. It also favors AT rich regions upon binding to DNA.

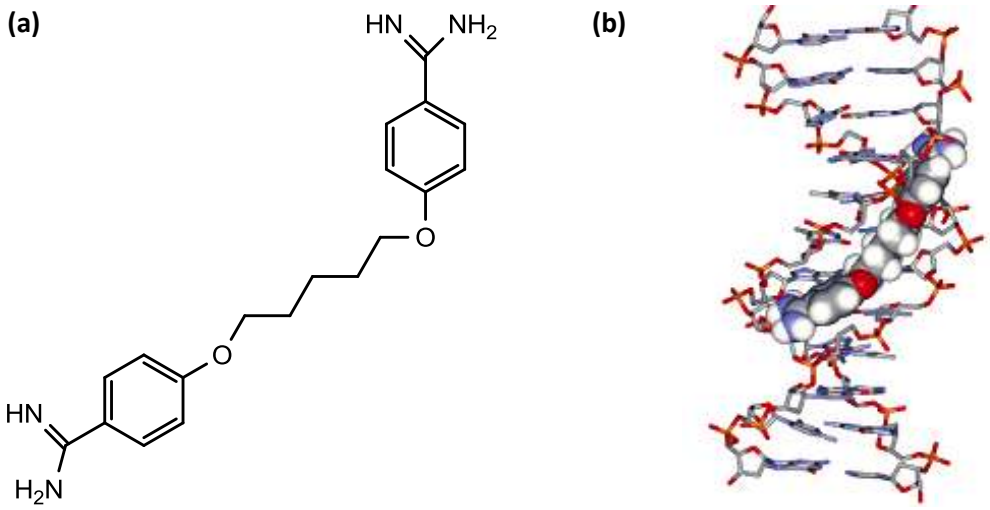

Figure 1.11 (a) Chemical structure of pentamidine **(b)** Pentamidine bound in the minor groove of the DNA.[31, 33]

Dervan *et al.* reported polyamides as sequence specific DNA binders.[34] A set of codes was established in Dervan`s laboratories by which synthetic molecules based on

dystamycin-type structures can recognize the DNA sequence via minor groove. In the first step of the experimental procedure a methylpyrrole of dystamycine was substituted with a methylimidazole group (Fig. 1.12 (a, b)). The nitrogen in the ring system is able to form hydrogen bonds to NH_2 group of guanine base in the minor groove. Interestingly, at high drug loading two pyrrole/imidazole peptide strands could bind side-by-side in the minor groove (Fig. 1.12 (c)). This demonstrates that DNA is not a rigid molecule and in order to accommodate two peptide strands the minor groove of DNA must increase in size. The two polyamide strands lie head-to-tail in the groove with guanadinium ends located away from each other. Each polyamide strand interacts with bases of one strand of the DNA. The pyrrole/imidazole rings of one strand form π-stacking interactions with amide carbonyls of the other.[35]

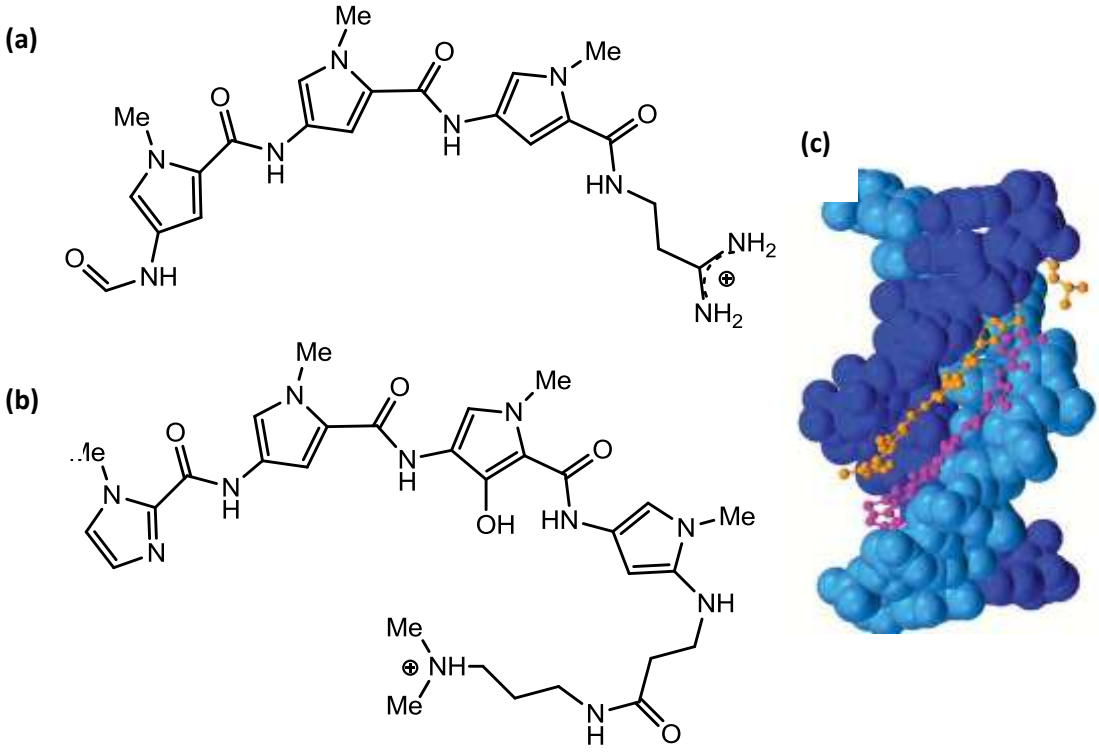

Figure 1.12 (a) Chemical structure of dystamycine **(b)** Chemical structure of the polyamide strand **(c)** Two polyamide strands bound in the DNA minor groove.[35]

1.3.3.5 Major groove binding

The DNA major groove is an attractive site for protein binding rather than for small synthetic molecules as it is wider and has a greater number of hydrogen donor and acceptor units than the minor groove.[35] Binding of proteins to DNA occurs through DNA binding domains such as zinc finger, α-helix-turn-α-helix, leucine zipper, and etc.

Likewise proteins, oligonucleotides can bind to the DNA major groove and form Hoogsteen or reverse-Hoogsteen base pairing leading to a triple-stranded DNA formation (Fig. 1.13). The triplex is formed in areas of the DNA rich in purines (adenine and guanine) which can interact with pyrimidines on the third additional strand of the DNA by forming additional hydrogen bonds. Triple-stranded DNA structures are suggested to play a role in DNA transcription, recombination and condensation.[36, 37]

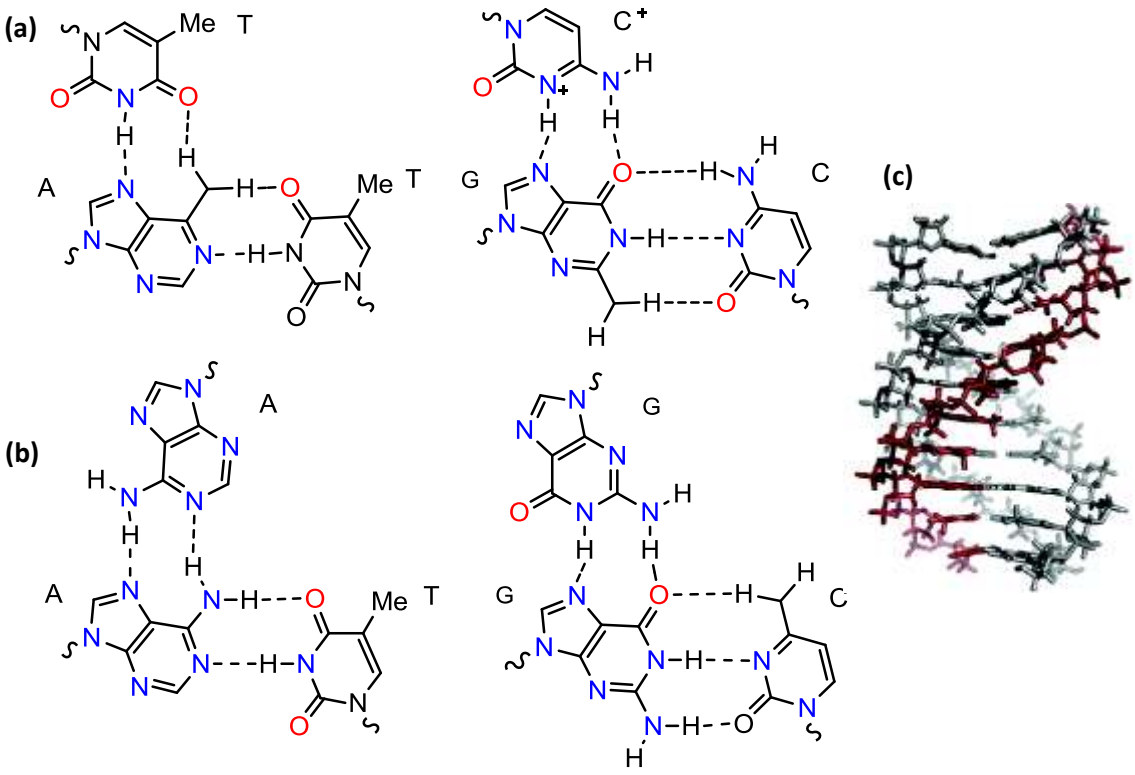

Figure 1.13 Hydrogen bonding involved in DNA triplex formation **(a)** Hoogsteen base paring **(b)** Reverse-Hoogsteen base paring **(c)** Structure of DNA triple helix.[37]

A synthetic metal-based supramolecular cylinder (Fig. 1.14) synthesized in Hannon`s laboratory can bind to the DNA major groove and induce intramolecular DNA coiling. The iron triple-stranded helicate is ~ 2 nm length and ~ 1nm in diameter and these dimensions are similar to those of the α-helical DNA recognition unit of zinc fingers.[38]

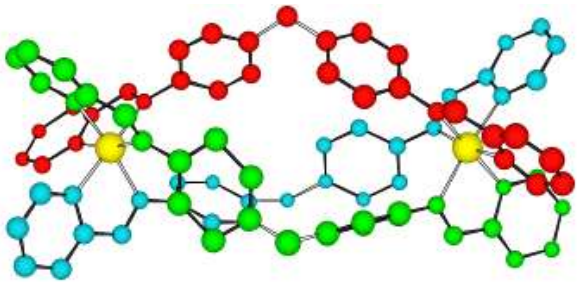

Figure 1.14 Crystal structure of iron(II) triple-stranded helicate synthesized in Hannon`s laboratory.[38]

1.3.3.6 DNA three-way junction recognition

Hannon`s tetracationic iron(II) supramolecular helicate is able to recognize DNA three-way junction structures. It was crystallized with DNA palindromic hexanucleotide. The recognition of the junction was observed with a helicate located in the central cavity of the junction (Fig. 1.15). The structure is stabilized by π-stacking interactions between the helicate surface and the adenine and thymine bases of the junction, and electrostatic interactions between the positively charged cylinder and polyanionic surface of DNA.[39] The ability of cylinder to recognize DNA three-way junction is a key discovery that underpins work in this thesis and is discussed in more detail in chapter 3 section 3.10.

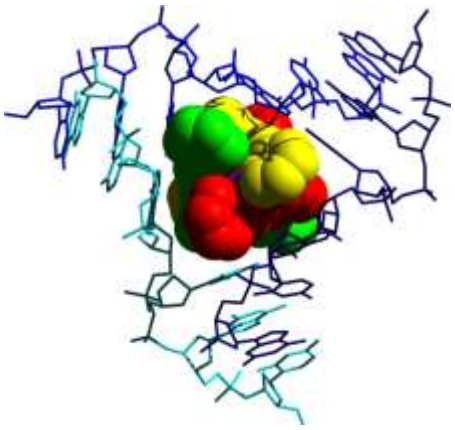

Figure 1.15 Crystal structure of the iron(II) triple helicate bound to the center of the DNA three-way junction.[39]

1.3.3.7 Recognition of DNA G-quadruplex

Guanine rich regions of the DNA such as telomeres are able to form tetra-stranded structures known as G-quadruplexes. These DNA structures are involved in the regulation of some key biological processes. Promoter regions of some oncogens consist of G-quadruplexes. Over the last years, there has been a great interest in these DNA sequences as potential targets for novel anticancer drugs.[18] An example of a molecule that binds to DNA G-quadruplex is a platinum molecular square developed by Sleiman and co-workers (Fig. 1.15).

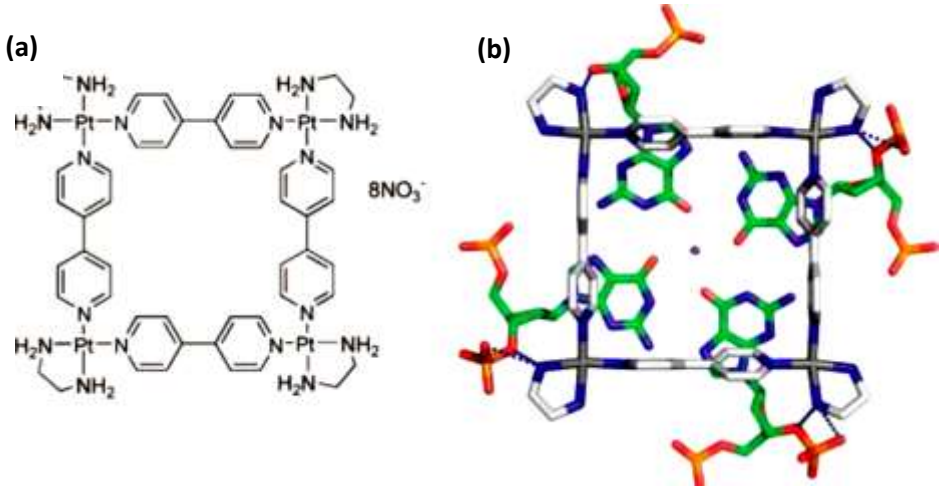

Figure 1.15 (a) Structure of the platinum molecular square **(b)** Structure of the complex with a DNA G-quadruplex. The complex is displayed in grey and blue; hydrogen bonding to phosphates is represented by a blue dotted line.[40]

It has been proposed that cylinders developed by Hannon and co-workers bind to G-quadruplex DNA[41, 42] although the results were not reproducible in our laboratory.[43]

In this section of chapter 1, DNA structure and DNA recognition by various agents was discussed. DNA molecule is considered to be one of the key targets for anticancer treatment therefore compounds that bind to DNA are of great interest. Supramolecular assemblies such as helicates have been shown to bind to the major groove of DNA and induce intramolecular DNA coiling. In the following section examples of supramolecular helicates will be presented.

1.4. Supramolecular helicates

The term helicate was first introduced by French chemist Jean-Marie Lehn in 1987 to describe a metal-based helix with one or more ligands coordinated to metal ions.[44] Metallo-helicates can be viewed as simple models of more complex natural

structures such as DNA and viruses. They play an important role in the understanding and development of self-processes in supramolecular chemistry.[45, 46]

1.4.1 Introduction to helicate formation

Supramolecular helicates are formed by a spontaneous self-assembly process of wrapping ligand strands around the metal ions. According to the concept of coordination chemistry, different metal ions prefer different coordination environments such as square planar, tetrahedral, or octahedral. This geometrical preference of the metal ion can be used to control the orientation of coordinating ligands in space.[47] Generally, helicates are Werner-type coordination compounds consisting of two or several units connected by a spacer. Depending on the number of coordinated ligands, helicates are divided into single, double and triple-stranded. If helicates are formed from symmetrical ligand strands they are homotopic, whereas helicates formed from asymmetrical ligand strands are heterotopic (Fig. 1.16).[46]

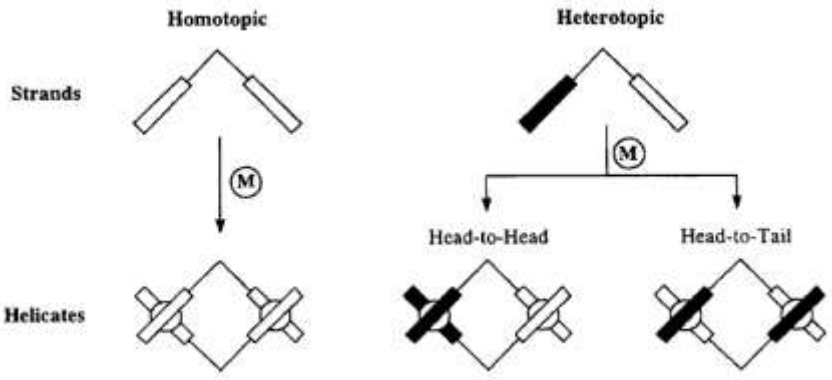

Figure 1.16 Homotopic and heterotopic helical configurations.[46]

One of the intrinsic characteristics of helicates is chirality. They can be right-handed (plus, P) or left-handed (minus, M), depending on whether the rotation is

clockwise or anticlockwise when a helicate is considered to wind from the eye of the viewer towards a distant point. The self-assembly of helicates from achiral ligands and metal ions results in racemates containing both right-handed and left-handed helicates.[48]

1.4.2 Single-stranded helicates

Mononuclear single-stranded helical compounds can be formed when a central metal ion is too small to fit in the cavity of a bound multidentate ligand. A small twist of the ligand decreases the steric constraints of the molecule.[46] Monohelices with chiral ligands are of particular interest due to their high asymmetry, well-defined reaction centers, and potential as asymmetric catalysts. Single-stranded monohelical molecules are synthetically complicated targets since flexible multidentate ligands often prefer to bridge metal centers and produce helicates.[49]

Constable and co-workers have shown that the 2,2’:6’,2’’:6’’,2’’’:6’’’,2’’’’-quinquepyridine ligand (qpy) (Fig. 1.17) and its substituted analogues are able to form mononuclear single-stranded complexes. When the qpy ligand is reacted with Ag(I), the ligand wraps around the small silver metal ion forming a helical structure.[50]

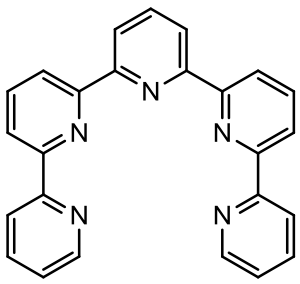

Figure 1.17 The structure of 2,2’:6’,2’’:6’’,2’’’:6’’’,2’’’’- quinquepyridine ligand.

Another example is a mononuclear Co(II) complex, with a 4',4'''-bis(p-chlorophenyl)- 2,2':6',2'':6'',2''':6''',2'''':6'''',2''''- quinquepyridine (bcpqpy = L) acting as a pentadentate ligand with a shallow helical twist about the metal centre (Fig. 1.18). The helical configuration is achieved through individual twisting about the interannular C-C bonds of the adjacent pyridine rings.[51]

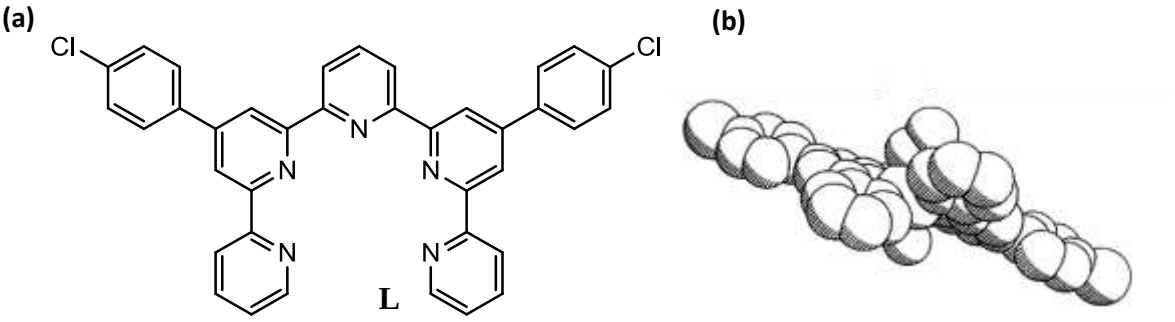

Figure 1.18 (a) Structure of ligand L **(b)** Space filling model of $[Co(L)(CH_3OH)(OH_2)]^{2+}$.[51]

Recently, Levy and co-workers synthesized a monohelical zinc complex of a salen ligand containing benz[α]-anthracene side arms (Fig. 1.19). The benz[α]anthryl sidearms are significantly overlapped, but the large angle between them and the relatively large space shows that little face-to-face π-π interaction can occur.[49]

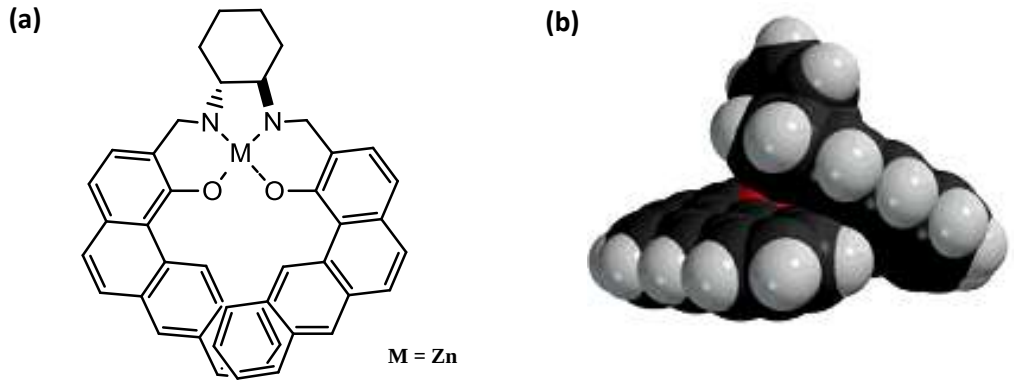

Figure 1.19 (a) Structure of Levy`s Zn complex **(b)** Space filling model of Levy`s Zn complex.[49]

More recently, Datta *et al.* reported a mononuclear single helicate of europium(III). The ligand employed in complexation with europium metal ion is a condensate of benzildihydrazone and 2-acetylpyridine (Fig. 1.18 (a)). The europium metal centre in the complex is coordinated to three molecules of nitrate and four nitrogen of the ligand in a bidentate fashion (Fig. 1.20 (b)).[52]

(a) **(b)**

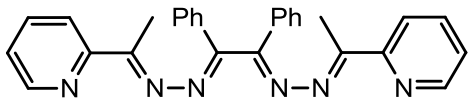

Figure 1.20 (a) Structure of the ligand reported by Datta **(b)** A space-filling model of europium(III) metal compex (Eu, white; N, black; C, dark gray; O, light gray).[52]

1.4.3 Double-stranded helicates

Since early studies by the groups of Lehn, Constable, and Potts, versatile complexation properties of the oligo-pyridine derivatives and a wide range of polydentate ligands has been developed for the formation of helicate complexes.[53] Double-stranded helicates are formed by the reaction of binucleating ligands with metal cations with tetrahedral coordination geometry such as Cu(I) and Ag(I).[54]

Lehn`s group developed a ligand containing 6,6'-dimethyl-2,2'-bipyridine moieties which form a double-stranded helicate with copper(I) ions (Fig. 1.21).[55]

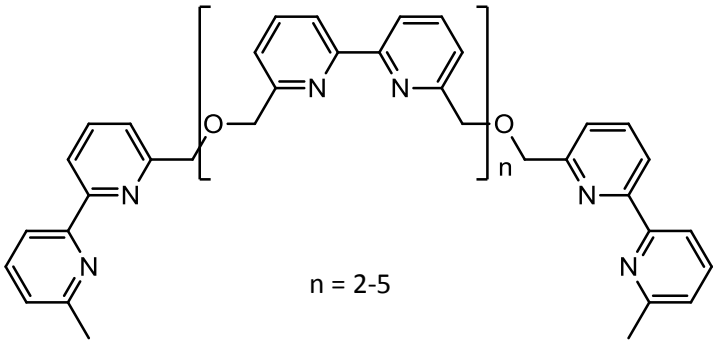

Figure 1.21 Structure of the ligand developed by Lehn`s group.

Jeffery *et al.* designed a double-stranded dinuclear copper(I) helicate based on the pyridyl-thiazole ligand L_1 (Fig. 1.22). Two ligands are being divided into two bis-bidentate pyridine-thiazole binding domains by rotation about the central pyridine-pyridine bond. The metal ions are coordinated to one pyridyl-thiazole binding domain from each ligand. The formed complex exhibits strong π-π interactions between pyridyl-thiazole rings on adjacent strands.[53]

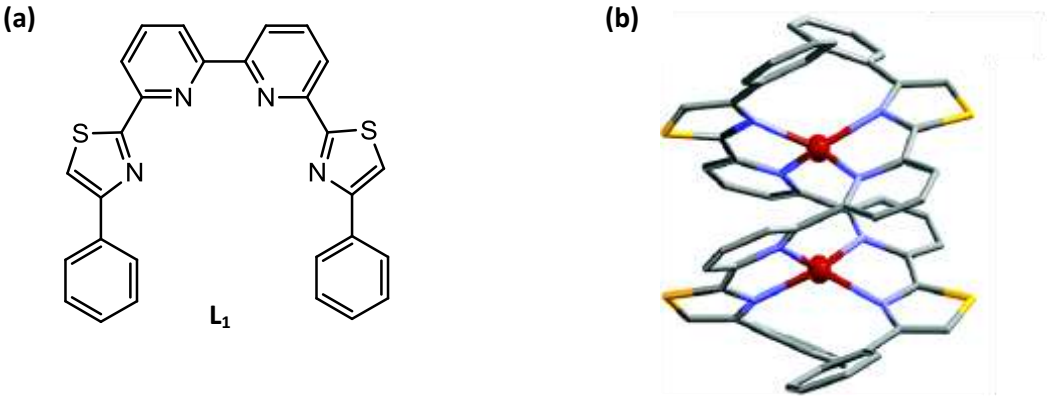

Figure 1.22 (a) Structure of the pyridyl-thiazole-based ligand L_1 **(b)** Solid state structure of the double stranded copper(I) complex of L_1.[53]

Metals subject to octahedral coordination, e.g. Ni(II), Co(II), Zn(II) will form double-strand helicates with ligands having terdentate subunits. In 1992, Crane and Sauvage reported the synthesis of a dinuclear double helix from a bis-terpyridine ligand system using both iron- and ruthenium(II) ions as templates (Fig. 1.23).[55]

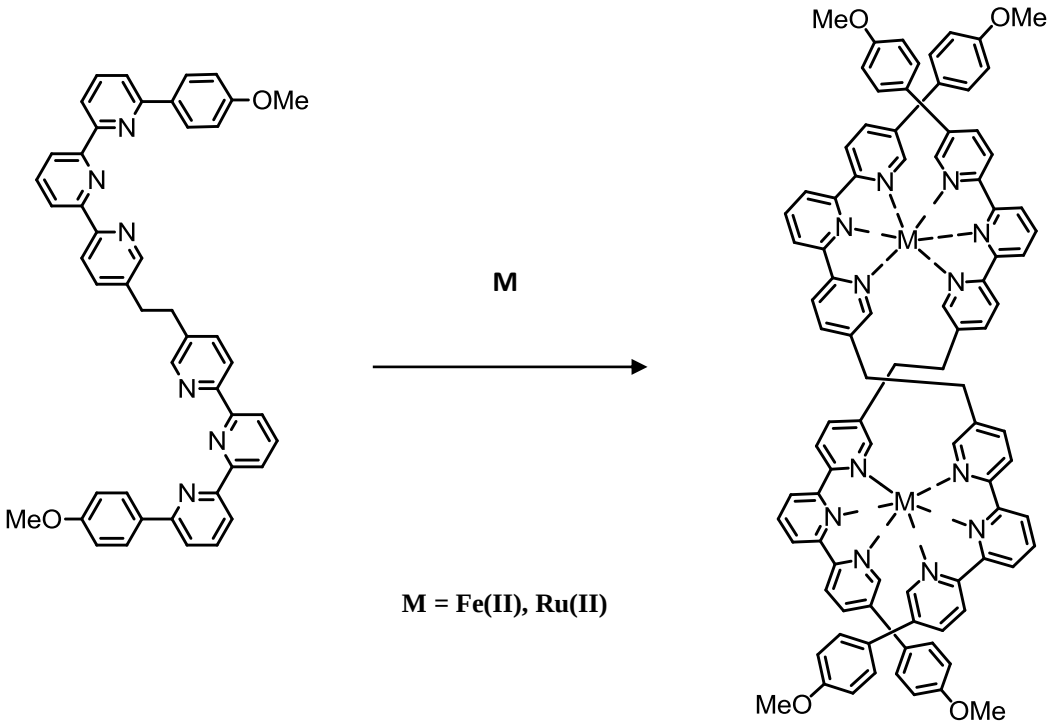

Figure 1.23 Self-assembly of double-stranded helicate reported by Sauvage and Crane.

More recently, Kwong and co-workers reported binuclear double-stranded manganese(II) helicates[56] which are formed by the reaction of manganese(II) perchlorate and chiral phenyl- and polyphenyl-bridged oligopyridines (Fig. 1.24).

(a)

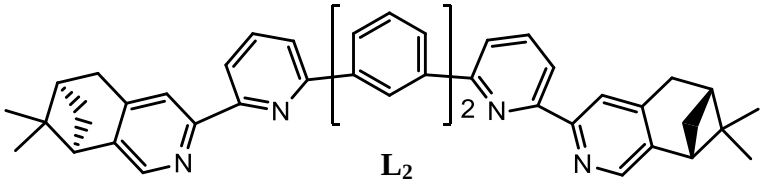

L_2

(b)

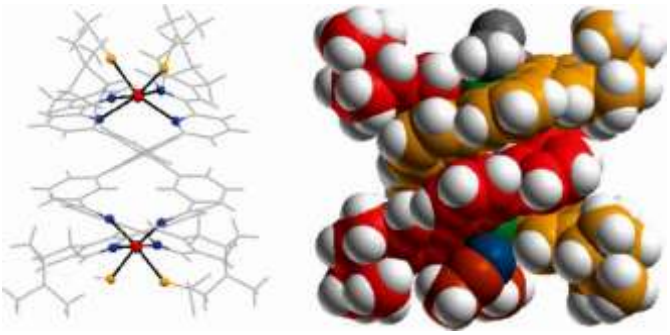

Figure 1.24 (a) Chemical structure of the ligand L_2 **(b)** Crystal structure and space-filling model of the $[Mn_2(L_2)_2(H_2O)(CH_3OH)(CH_3CN)(ClO_4)]^{3+}$ complex.[56]

The manganese(II) complex of L_2 contains one diastereomer which is a double-stranded helicate with P chirality. Both manganese metal centers have distorted octahedral geometry and are coordinated to two nitrogen binding sites from each L_2 ligand. Additional manganese binding sites are filled by solvent molecules and a perchlorate ion. The major helical twists take place between the 2,2'-bipyridine units and bridged phenyl rings.[56]

A number of cyclic molecules with double-helical structures have also been synthesized. A Schiff based helical microcycle containing pyridine-2,6-diiyldiimine moieties and divalent metals have been reported in literature (Fig. 1.25 (a)).[55]

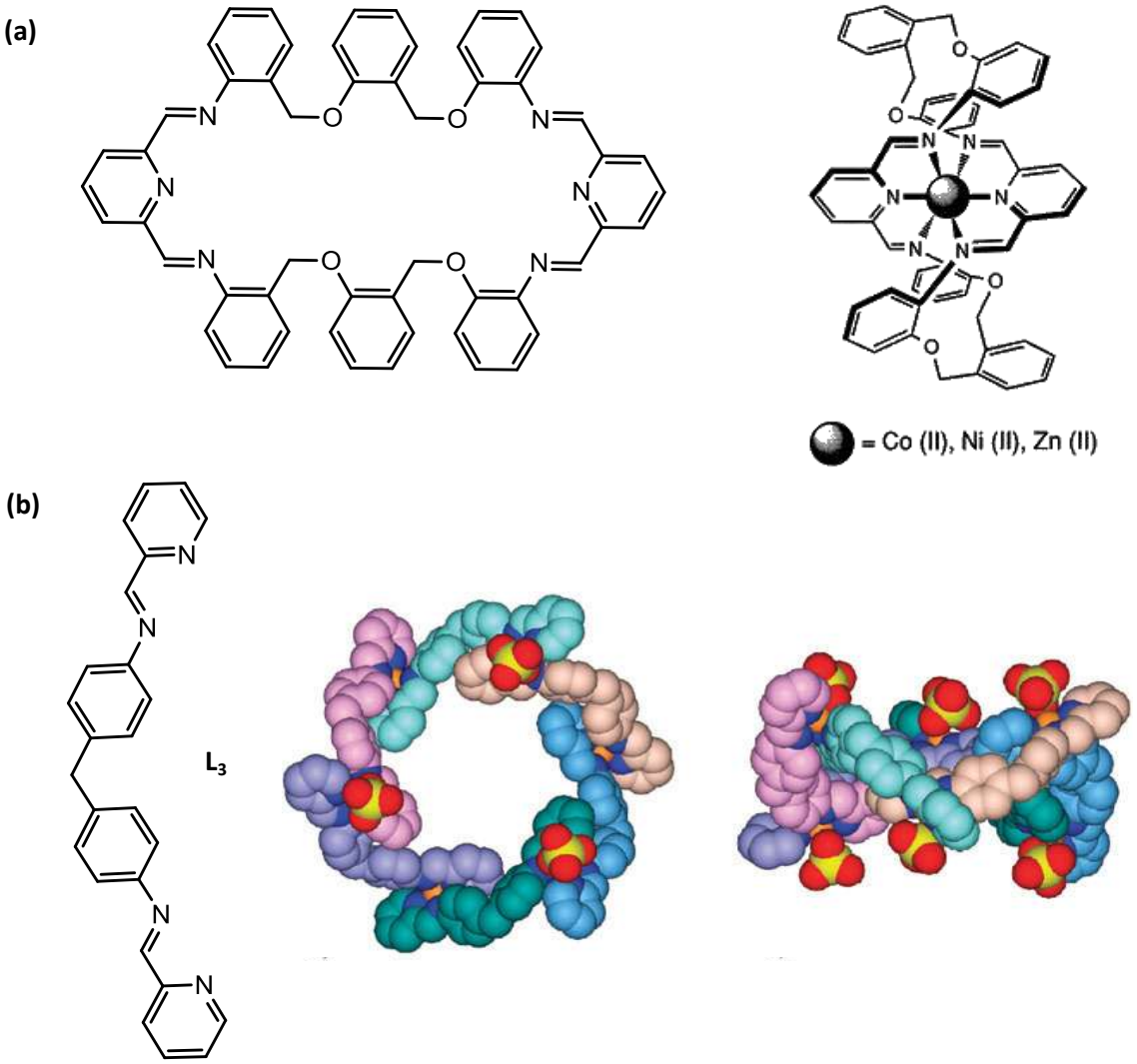

Figure 1.25 (a) Double-helical Schiff based macrocyclic complex with divalent metal ions.[55] **(b)** Space-filling representation of $[CuL_3(SO_4)]_6$: top view and side view. The six ligands L_3 are drawn in different colours, Cu in orange, N in blue, O in red, S in yellow; H atoms are omitted for clarity.[57]

According to the X-ray crystal structures of the complexes, the orientation of the two ligating groups induce helicity within the macrocycle in a six-coordinate nucleus.[55]

A hexanuclear circular copper(II) meso-helicate based on the bis-pyridylimine ligand has been reported by Gloe *et al.* (Fig. 1.25 (b)).[57] Topological control of the

assembly process is associated with the bidentate coordination of the sulfate anions to the metal center which direct the formation of a double-stranded stracture. The formed complex is a neutral circular helicate assembled around Cu(II) metal centres by hydrogen bonding and π–π stacking interactions.

1.4.4 Triple-stranded helicates

An early triple-stranded helicate was structurally characterized by Raymond and co-workers in 1985.[58] It is formed by self-assembly of three 1,5-bis[(1,2-di-hydro-1-hydroxy-2-oxopyridin-6-yl)carbonyl]-1,5-diazapentane (5,"3-HOPOCAM-1,2") ligands (Fig. 1.26) with three iron (III) metal ions. The ligand has similarity with rhodotorulic acid which is a naturally occurring siderophore.[59]

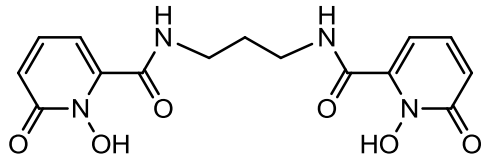

Figure 1.26 Structure of the 5,"3-HOPOCAM-1,2" ligand developed by Raymond and co-workers.

Triple-stranded helicates are formed by the coordination of bidentate ligands to metals with octahedral coordination and wrapping around them. The europium(III) complex developed by Albrecht-Gary and co-workers is an example of such a helicate (Fig. 1.27). Albrecht-Gary`s helicate is based on a ligand L_4, containing tridentate bis(benzimidazolyl)pyridine subunits. Two europium metal ions are coordinated by six nitrogen atoms of the benzimidazole moieties and three nitrogen atoms of the pyridine groups.[60]

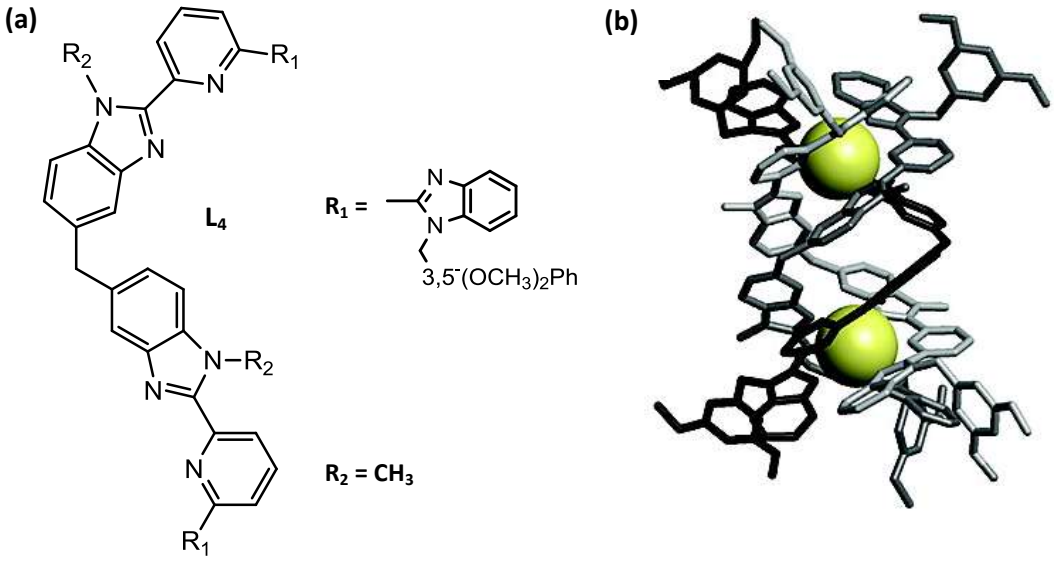

Figure 1.27 (a) Structure of the ligand L_4 **(b)** Molecular structure of the $[Eu_2(L_4)_3]^{6+}$ complex.[60]

Hahn`s group prepared triple-stranded helicates with titanium(IV) metal ions using bis(benzene-o-dithiol) based ligands and a reactive metal compound $[Ti(OC_2H_5)_4]$ (Fig. 1.28).[61] Titanium metal ions are coordinated to six thiolato donors in a slightly distorted octahedral fashion and the rigid ligand L_5 leads to a helical twist of the molecule.

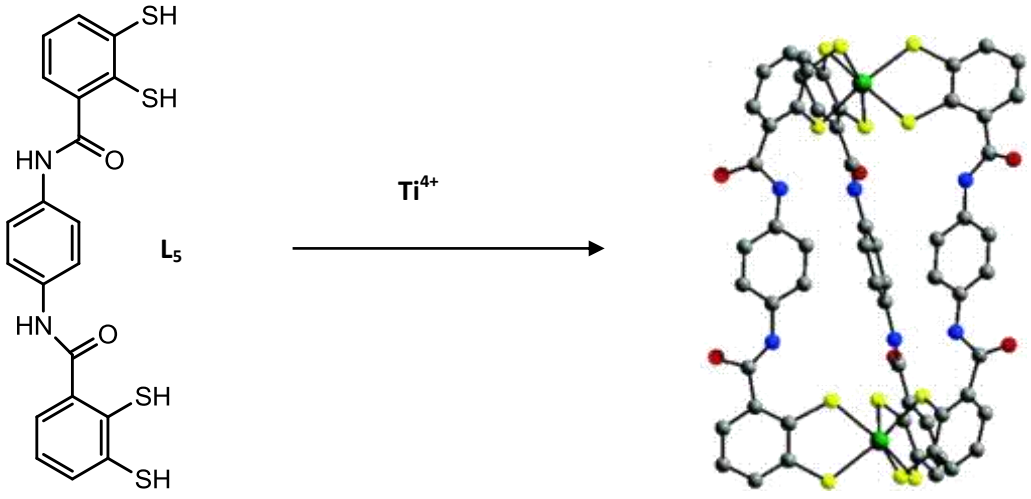

Figure 1.28 Schematic procedure for the synthesis of $[Ti_2(L_5)_3]^{4-}$ complex.[61]

Hannon and co-workers developed a dinuclear iron(II) triple-stranded helicate in a simple reaction by mixing imine-based ligand with an iron(II) chloride salt (Fig. 1.29).[62]

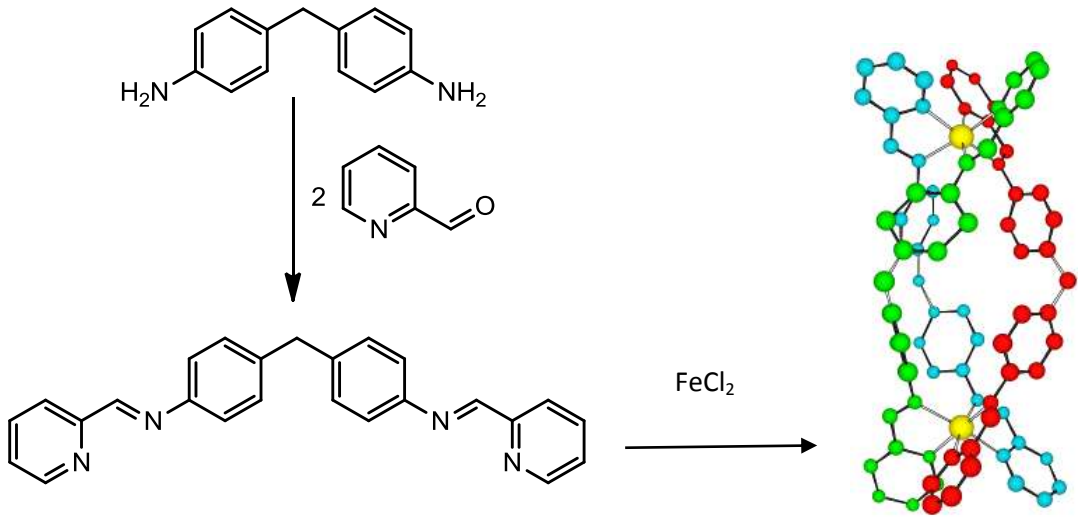

Figure 1.29 Schematic representation of iron(II) triple helicate formation.[62]

Three strands of the ligand are coordinated to two octahedral iron(II) metal ions. Coordination to the metal centre induces twisting between the phenylene ring and the pyridylimine unit and as a result, the formation of a triple-helical assembly. The helicate is chiral and has two enantiomeric forms (M and P).[62]

Recently, Dolphin *et al.* described diamagnetic cobalt and gallium triple-stranded helicates based on β,β`-linked bis(dipyrromethene) ligand L_6 (Fig. 1.30).[63]

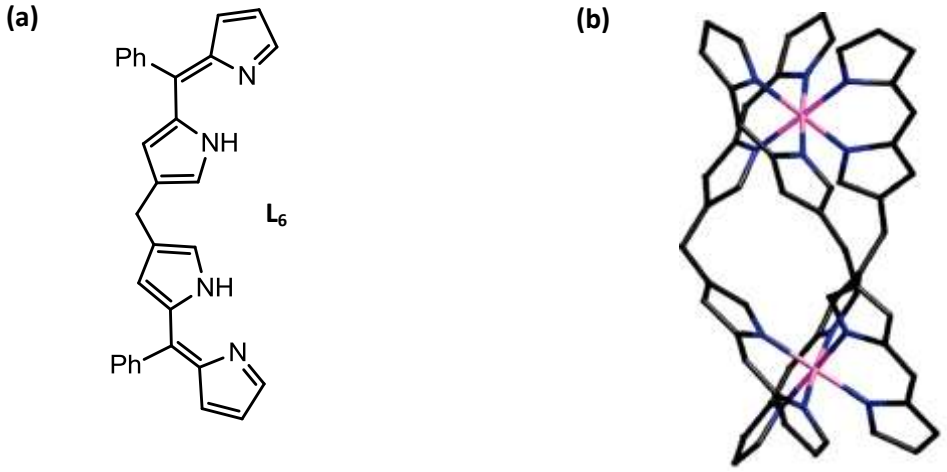

Figure 1.30 (a) Chemical structure of the ligand L_6 **(b)** Crystal structure of the $[Co_2(L_6)_3]$ helicate. Phenyl groups and hydrogen atoms have been omitted for clarity.[63]

The formed triple helicates are uncharged due to the nature of the ligand. Deprotonated dipyrromethenes (known as dipyrrins) act as monoanionic ligands that can produce uncharged complexes upon coordination to di- or tri-valent metals.[63]

1.4.5 Quadruple-stranded helicates.

The first example of a quadruple-stranded helicate was reported by McMorran and Steel in 1998 (Fig. 1.31). The helicate was prepared using four 1,4-bis(3-pyridyloxy)benzene ligands L_7 and two square planar Pd(II) centers. The complex formed represents a helical cage in which a hexafluorophosphate anion is incapsulated.[64]

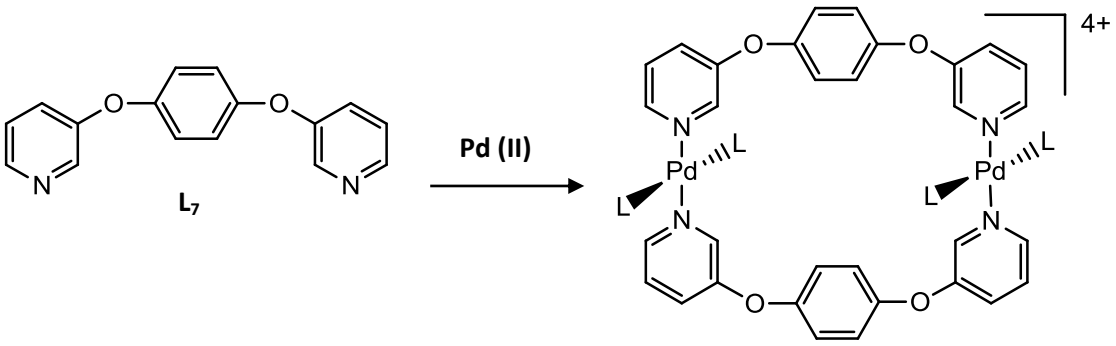

Figure 1.31 Self-assembly of McMorran and Steel quadruple-stranded helicate.

More recently, Raymond reported a quadruple-stranded helical complex containing bis-diketonate 4-acyl-2-pyrazolin-5-one ligands L_8 and thorium(IV) as a metal (Fig. 1.32). Each actinide metal center in the helicate is nine coordinated by four bisbidentate 4-acylpyrazolone chelating units and *N,N'*-dimethylformamide solvent molecules. This complex is the first example of a structurally characterized bisbidentate quadruple-stranded helicate.[65]

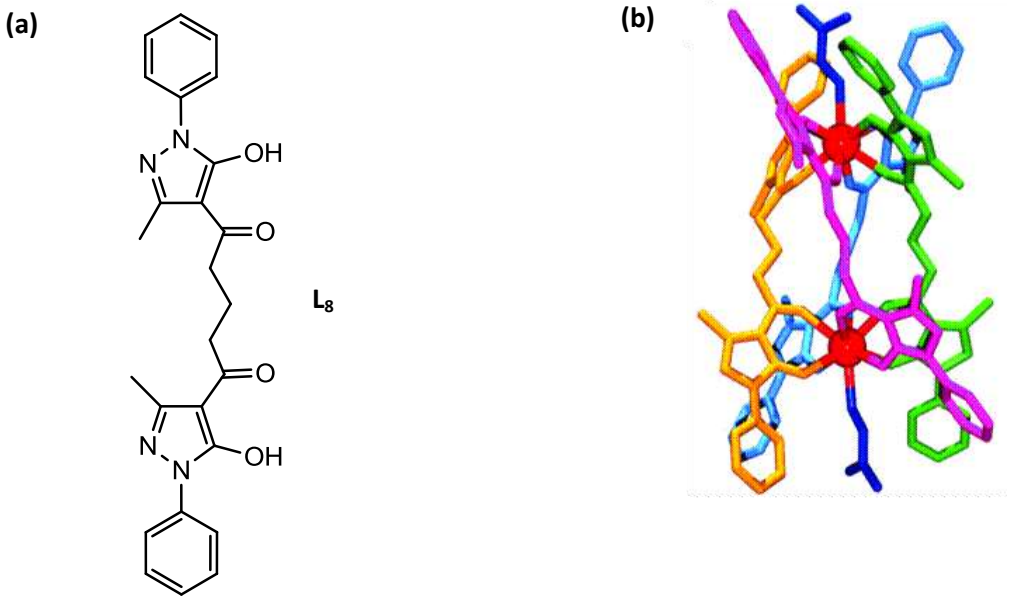

Figure 1.32 (a) Structure of the ligand L_8 **(b)** Structure of the $[Th_2(L^8)_4(DMF)_2]$ quadruple-stranded helicate.[65]

Chand and co-workers described palladium quadruple-stranded metallohelicate with *N*,*N'*-bis(3-pyridylformyl)piperazine ligand (Fig. 1.33).[66]

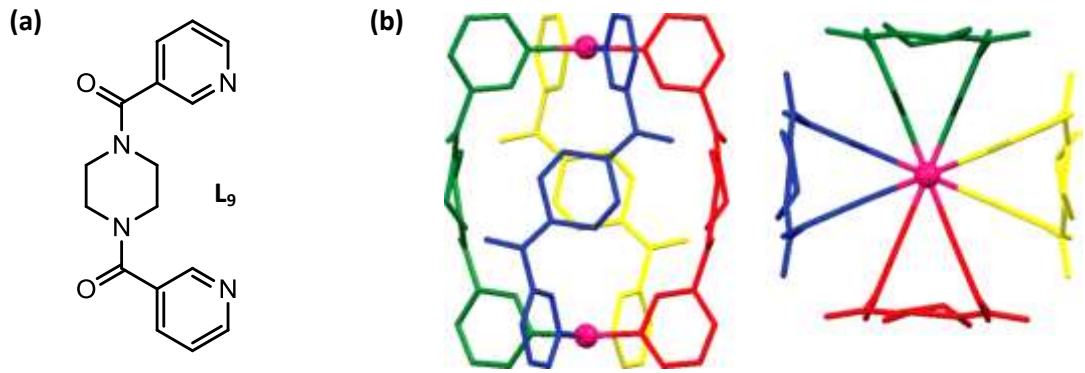

Figure 1.33 (**a)** Structure of the ligand L_9 (**b)** Crystal structure of $[Pd_2(L_9)_4]^{2+}$ viewed perpendicular to the four fold axis and along the Pd–Pd axis.[66]

The synthesised molecule represents a helical cage where each metal centre has a planar square geometry and each plane consists of four pyridyl nitrogen atoms from different ligands. The crystal structure of $[Pd_2(L_9)_4]^{2+}$ revealed that the metallohelicate encapsulates nitrate anion between two metal centres.[66]

Various supramolecular metallo-helicates formed in a self-assembly process have been discussed in section 1.4. Our interest in metal-based helicates originates from the discovery of their anticancer activity and this stimulated us to explore the effect of the synthesised cylinders in combination with cisplatin anticancer agent. The focus of the next two sections (1.5 and 1.6) of this chapter is platinum-based anticancer drugs and cisplatin anticancer therapy.

1.5 Platinum based anticancer drugs

Metal-based compounds have an enormous impact on medicine as they offer possibilities to design new therapeutic agents to treat different types of disease.[67] The variety of coordination numbers and geometries, intrinsic properties of the cationic metal ion and ligand give a wide range of reactivities that can be exploited. Platinum coordination compounds have found application as active antitumour agents after the discovery of the biological activity of cisplatin. Nowadays, this drug remains one of the most effective therapeutic agents in a clinical use.[68, 69]

1.5.1 Cisplatin

Cisplatin (*cis*-$[PtCl_2(NH_3)_2]$) or *cis*-diamminedichloroplatinum(II) possesses high cytotoxic activity and is used to treat epithelial malignancies such as lung, head and neck, bladder and cervical cancer but it was found to be particularly effective in the treatment of testicular and ovarian cancers.[70] The drug molecule contains a square-planar platinum(II) center coordinated to two ammonia and two chloride ligands. This platinum complex exists in two different isomeric forms, *trans*- and *cis*- (Fig. 1.34). *Trans*-structures are inactive however at high concentration they start to restrain cell growth.[27]

Figure 1.34 Chemical structures of **(a)** Cisplatin **(b)** Transplatin.

Cisplatin was first identified in 1847 and was known as peyrone`s chloride.[71] The antitumour activity of cisplatin was discovered by chance in 1970 by Barnett Rosenberg while investigating the effect of the electric field on the growth of the bacteria *Escherichia coli*. It was found that a platinum compound generated by the reaction of platinum electrodes with ammonium chloride in a buffer solution stopped cell division and caused filamentous growth of the bacteria cells. Further testing of the compound revealed its anticancer activity. [27]

The synthesis of cisplatin is based on the Dhara method reported in 1970 (Scheme 1.0).[72] The success of this procedure depends on the *trans* effect introduced by Chernyaev in 1926. According to this concept, the rate of substitution of a ligand in a square planar or octahedral metal complex depends on the group opposite (*trans*) to it.[73] The stronger *trans*-directing influence of the iodo ligand relative to the ammonia ligand in the intermediate means that the ligand *trans* to the iodide is more liable and is the first one to be displaced, resulting in a desired *cis*-configuration.[71]

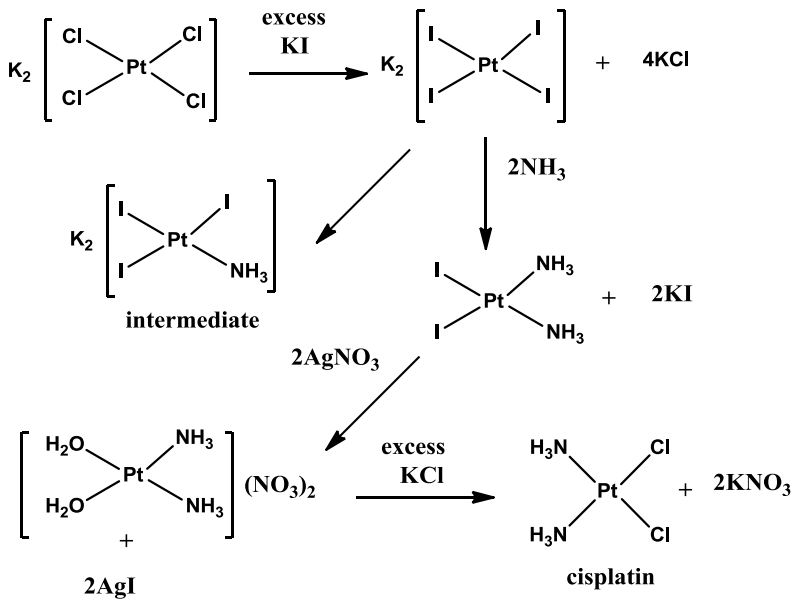

Scheme 1.0 Dhara synthesis of cisplatin.

1.5.2 Mechanism of action

DNA is considered to be the primary target of cisplatin. The drug is injected into the bloodstream and is believed to stay in a neutral state due to the high concentration of chloride ions that prevent hydrolysis. Cisplatin enters the cell by passive diffusion through the cell membrane or it can be partly transferred by an active transport mechanism. The concentration of chloride ions inside the cell is quite low and this results in the formation of aquated forms of cisplatin (*cis*-$[Pt(NH_3)_2Cl(H_2O)]^+$ or *cis*-$[Pt(NH_3)_2(H_2O)_2]^{2+}$) which are more reactive molecules. Inside the cell the activated platinum complexes of cisplatin react with different components of the cell (proteins, membrane phospholipids, RNA, thiol-containing molecules), including DNA however, it is not fully understood how platinum complexes reach their biological targets.[74] Because of the high nucleotide concentration in the cell nucleus, cisplatin will react primarily with DNA. The mechanism of action is based on substitution of aqua or chloride ions of these cationic aqua complexes and interaction with DNA bases mostly at N7 position of purine bases (with guanine favored over adenine).[75] Cisplatin binds to a guanine N7 on DNA and if the complex contains another exchangeable ligand it provides different crosslinks: intra- or interstrand with available binding sites. *Cis*-diamminedichloroplatinum(II) predominantly forms intrastrand adducts with the adjacent bases. 1,2 Intrastrand GG adducts account for more than 70 % of all adducts formed; 1,2 intrastrand AG adducts are the next most common at around 20 %: 1,3 adducts and monoadducts are much less common.[27, 76] The formation of a cisplatin-DNA adduct alters the structure of DNA. The 1,2 intrastrand adducts unwind the DNA at the site of platination, bending it towards the major groove and creating a shallow

minor groove. The interstrand DNA-cisplatin adducts bend the helix towards the minor groove, where the platinum moiety is located (Fig. 1.35).[69]

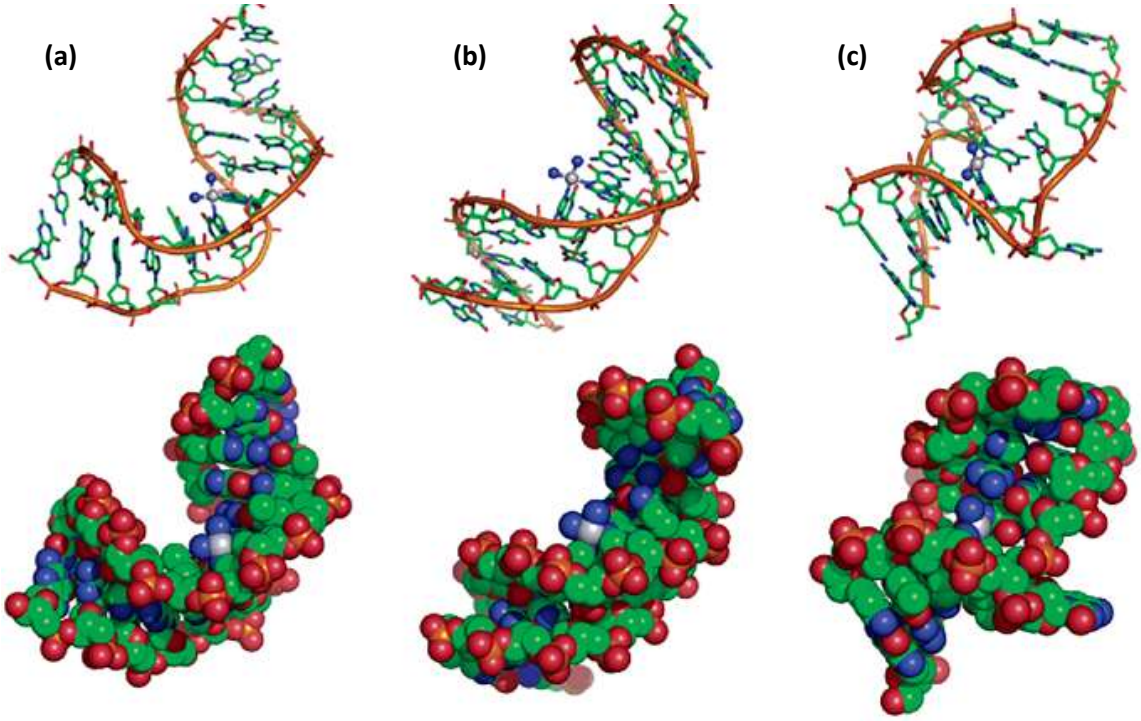

Figure 1.35 Platinum-DNA adduct structures. Duplex DNA containing **(a)** Cisplatin 1,2-d(GpG), **(b)** 1,3-d(GpTpG) Intrastrand, and **(c)** Interstrand cross-links, generated by PyMol. The DNA sequences are d(CCTCTG*G*TCTCC)·d(GGAGACCAGAGG), d(CTCTAG*-TG*CTCAC)·d(GTGAGCACTAGAG), and d(CCTCG*CTCTC)·d(GAGAG*CGAGG) for the cisplatin 1,2-d(GpG), 1,3-d(GpTpG) intrastrand, and interstrand cross-links, respectively. Guanine residues cross-linked by cisplatin at the N7 position are indicated by asterisks.[69]

The alteration in DNA structure caused by cisplatin is recognized by proteins of the High Mobility Group class. High Mobility Group (HMG) is a group of chromosomal proteins that help with transcription, replication, recombination, and DNA repair.[77] When the protein is bound to DNA it inserts a phenyl group of the phenylalanine from the minor groove into a wedge-like interaction site created by the bent (Fig. 1.36). This causes destacking of nucleotide bases resulting in the DNA helix

being kinked. With HMG protein bound to DNA, the modified strand is not repaired properly and the cell dies.[78, 79]

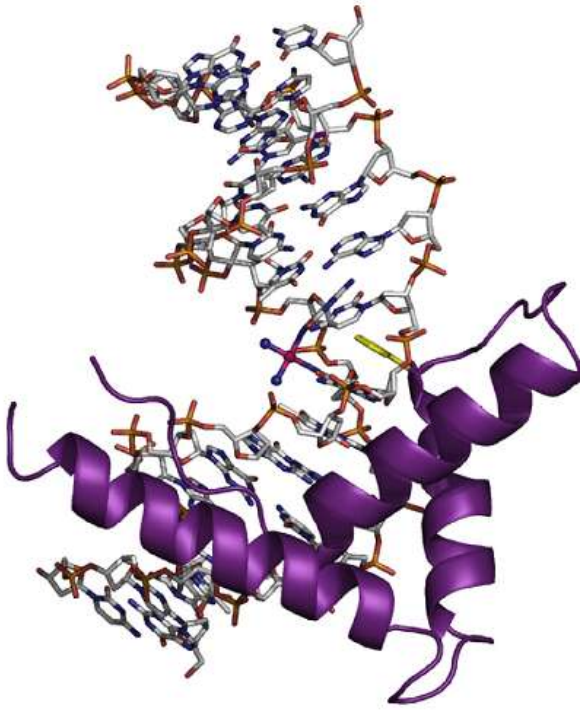

Figure 1.36 A model of HMG protein (violet) binding to the platinated DNA with phenylalanine (yellow) as the intercalating residue.[80]

1.5.3 Cisplatin Pharmacology

Cisplatin (*cis*-DDP) is an effective antineoplastic agent, however its clinical application is limited due to its severe side effects. Cisplatin is administered as an intravenous infusion, with extensive hydration of the patient before and after administration in order to reduce kidney damage.[81] The typical frequency of administration of *cis*-DDP is every three weeks or for high dosages every four weeks. Cisplatin acts nonselectively and affects the growth of rapidly dividing cancer cells as well as other healthy rapidly dividing cells in the body such as cells from

gastrointestinal tract, hair follicles and bone marrow. This causes hair loss, nausea and toxicity of blood forming elements.

The main side effects of cisplatin are:

- Nephrotoxicity (kidney damage)
- Gastrointestinal toxicity (nausea, vomiting)
- Neurotoxicity (abnormalities of the nervous system, including muscle cramps, seizures and a loss of taste)
- Ototoxicity (hear loss resulting from damage to the sound-detecting hair cells in the inner ear)[82]
- Hematologic toxicity (low levels of platelets, white blood cells, red blood cells)
- Hyperuricemia (an increase in uric acid)

To minimize adverse toxic side effects, cisplatin can be used in combination with two or more chemotherapeutic agents. The use of cisplatin is also limited by the tumour resistance to the drug. Resistance takes place when the cancer cell is treated with a drug and destroyed and then does not respond to that drug treatment again. Some tumours are intrinsically resistant to cisplatin (e.g. colon cancer) whereas others gain their resistance after exposure to the drug over a period of time (e.g. ovarian cancer).[27] The resistance is believed to be caused by low drug uptake by the cell or accumulation in the cell, increased levels of intracellular thiols that can bind to cisplatin and deactivate it, and increased level of repair of the DNA damage caused by cisplatin due to the presence of certain DNA repair proteins.[83, 84, 85] Inside the cell cisplatin can interact with thiol containing species (e.g. metallotheonein, glutathione) by coordination of sulfur donor to the platinum(II).[86] It is suggested that altered expression of oncogens limits the formation of DNA-cisplatin adducts and activates antiapoptotic mechanisms.[87]

1.5.4 Third and second generations of platinum drugs

The success of cisplatin as an anticancer agent stimulated the design and development of more effective and less toxic platinum-based anticancer agents. Thus the second generation platinum drugs carboplatin and nedaplatin has been synthesized (Fig. 1.37).[88]

Figure 1.37 Structures of the second generation platinum drugs: **(a)** Carboplatin (approved worldwide) **(b**) Nedaplatin (approved for clinical use in Japan).

Carboplatin was synthesized by the substitution of the chloride ligands of cisplatin with a bidentate 1,1-cyclobutanedicarboxilic acid ligand. Carboplatin is less reactive, more stable, with lower binding to the plasma proteins. It is administered by infusion into vein and is used to treat ovarian, head and neck, lung, breast, and cervical cancers. The side effects of the carboplatin therapy are less severe than in the case of cisplatin. Reduced nephrotoxicity and neurotoxicity are observed for carboplatin, while hematological side effects are prevalent.[89] Carboplatin has a lower cytotoxicity compared to cisplatin therefore it has to be administered at much higher doses in order to achieve a similar antineoplastic effect to cisplatin. However, the equivalent anticancer activity is observed for ovarian cancer. The mechanism of action of carboplatin, through generation of aqua species, is believed to be similar to cisplatin and therefore the formation of DNA adducts is identical.[90]

Nedaplatin (*cis*-diammine-glycolate-O,O'-platinum(II)) is a square planar platinum(II) complex that is comprised of a glycolic acid bidentate ligand with one carboxylic acid and one hydroxyl donor. This agent has shown high antitumour activity, less renal, gastrointestinal and neurotoxicity. Nedaplatin is efficient against lung, head and neck, testicular, and gynecological cancers.[91]

The third generation of platinum-based drugs includes oxaliplatin, lobaplatin, satraplatin, picoplatin, heptaplatin (Fig. 1.38). They show less toxicity, wider antitumour activity, little or no resistance compared to *cis*- or carboplatin.

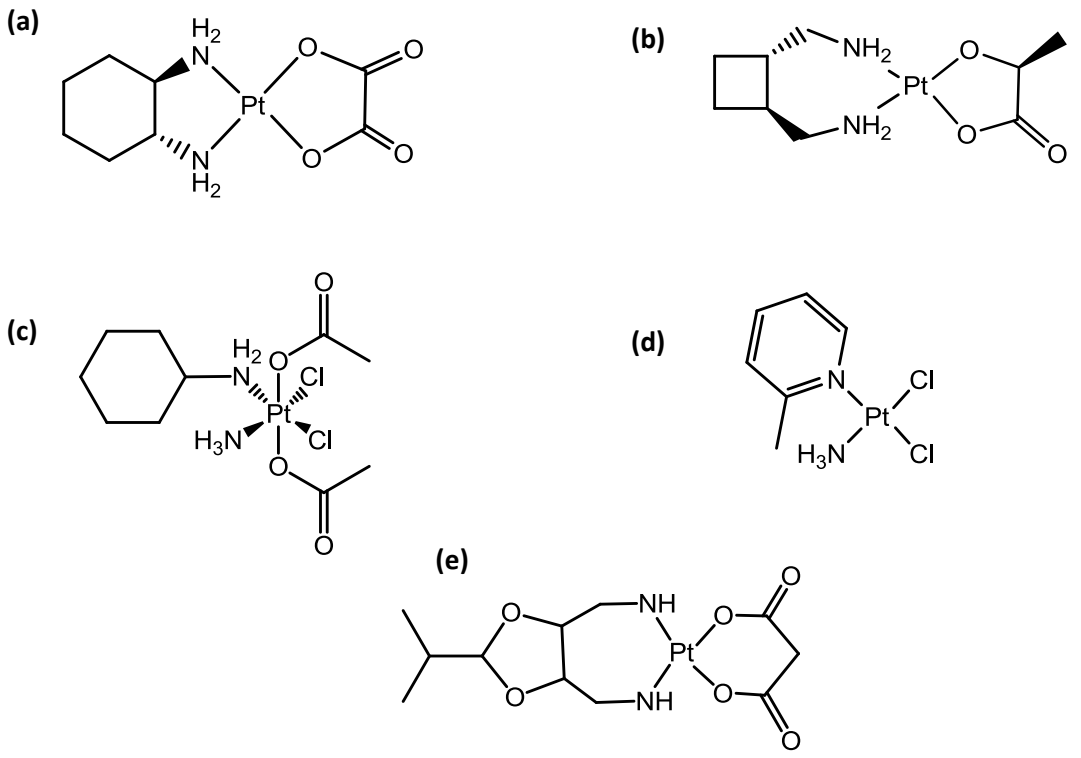

Figure 1.38 The third generation platinum drugs: **(a)** Oxaliplatin (approved worldwide) **(b)** Lobaplatin (approved for clinical use in China) **(c)** Satraplatin (in clinical trials) **(d)** Picoplatin (in clinical trials) **(e)** Heptaplatin (approved in South Korea).

Oxaliplatin is a square planar platinum(II) complex incorporating a 1,2-diaminocyclohexane (DACH) ligand and an oxalic acid leaving group. Compounds

containing DACH have lower solubility than cisplatin. In combination with other anticancer agents oxaliplatin is used to treat colorectal cancer. Oxaliplatin has shown minimal toxicity in clinical studies, except for reversible damage to peripheral sensory nerves.[92] However, the efficacy and toxicity of the drug varies from patient to patient, mostly because of the intrinsic or acquired resistance.[93]

Lobaplatin, a square planar platinum(II) complex, is a mixture of diastereomers (50:50) with a 1,2-diaminomethylcyclobutane ligand and a lactic acid as a leaving group. It is a water soluble and stable compound that exhibits antitumor effects on human esophageal, ovarian, breast and small cell lung cancers. Lobaplatin has a higher antineoplastic activity than cisplatin or carboplatin and is less toxic. The main drawback of lobaplatin is associated with myelosuppression.[94, 95]

Satraplatin is a platinum(IV) complex with octahedral geometry around the metal center. It has ammine and cyclohexylammine ligands as well as two chloride ions in a *cis*-conformation and two axial acetate ligands. It is believed to be reduced to platinum(II) complex, the active form, by losing acetate ligands. The inertness of the platinum(IV) drug and the presence of carboxylate ligands increase lipophilicity and thus, the oral bioavailability of the drug. Satraplatin has a smiliar activity to cisplatin and carboplatin but it is also active against some cisplatin-resistant cell lines. It is in phase III clinical trials to treat prostate, ovarian and lung cancers.[96, 97]

Picoplatin is a platinum drug with *cis*-conformation of ammine, and methyl pyridine and chloride ligands at the metal center. It was designed in an attempt to overcome cisplatin resistance. Picoplatin contains a bulky methylpyridine ligand and therefore has a lower rate of interaction with sulphur containing molecules. Picoplatin has a poor solubility and is administered intravenously. Low solubility in water causes

problems to create effective oral dosage forms. Picoplatin is active against lung, ovarian, prostate and colorectal cancers. There is no nephrotoxicity observed for picoplatin, however, myelosupression is the main drawback of the drug.[97, 98]

Heptaplatin exhibits equivalent antitumor activity and less toxicity compared to cisplatin. Moreover, it is effective against cisplatin-resistant L1210 leukemia cells, probably owing to its unique amine carrier. Heptaplatin is used in the South of Korea for the treatment of advanced gastric cancer and lung cancer. Nonetheless, treatment with heptaplatin causes significant side-effects including nephrotoxicity, myelosuppression, heptatoxicity, and nephrotoxicity.[99]

1.5.5 Platinum(IV) complexes

There is a great interest in platinum(IV) compounds as potential antineoplastic agents, with higher anticancer activity than cisplatin. These compounds may act as pro-drugs which can be reduced in hypoxic environment of cancer cells to their active form and are believed to be able to overcome cisplatin-resistance and severe side-effects. Platinum(IV) complexes have some advantages over platinum(II) compounds. They are relatively inert and thus undergo less side-reactions upon reaching their target. Platinum(IV) species can offer greater structural variety of the complexes due to the higher coordination number and good aqueous solubility.[100] As it was previously discussed, the platinum(IV) complex satraplatin is an orally administrable drug.

Some platinum(IV) compounds, such as iproplatin and tetraplatin, (Fig. 1.39) entered into clinical trials.

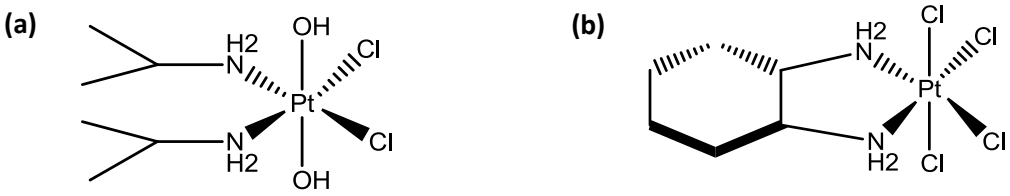

Figure 1.39 Structures of platinum(IV) complexes **(a)** Iproplatin **(b)** Tetraplatin.

Iproplatin (JM9, *cis,trans,cis*-[$PtCl_2(OH)_2$ $(isopropylamine)_2$]) has a high solubility but turned out to be less active than cisplatin and therefore has not been approved. Tetraplatin (ormaplatin, [$PtCl_4$(D,L-cyclohexane-1,2-diamine)]) showed great results in preclinical studies in cisplatin-resistant cell lines but caused severe neurotoxicity in treated patients and was abandoned.[101]

Introducing specific functionality to platinum compounds can help to improve drug uptake or overcome drug resistance. Lippard and co-workers proposed the trans-Pt(IV) carboxylate moiety for incorporation of functional groups into platinum-based compounds. They introduced an estrogen fragment to the platinum(IV) carboxylate structure by using a succinate linker (Fig. 1.40 (a)) and that resulted in increased sensitivity of the estrogen receptor of mammalian tumour cells to treatment.[102]

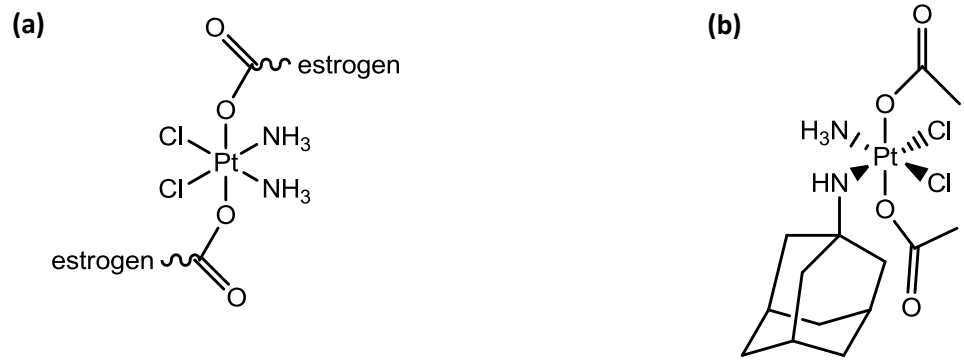

Figure 1.40 Structures of platinum(IV) complexes **(a)** Lippard`s estrgogen-platinum(IV) complex **(b)** LA-12 complex.

Kozubik and collaborators have reported the synthesis of a highly lipophilic platinum(IV) complex LA-12 ((OC-6-43)-bis(acetato)adamantylamine(ammine) dichloroplatinum(IV)) (Fig. 1.40 (b)) which showed similar activity to satraplatin and no cross-resistance with cisplatin. It exhibits higher activity than cisplatin in A2780 and A2780 *cis*-resistant cell lines. The mechanism of action of LA-12, as other platinum(IV) complexes, is considered to be through reduction to the active platinum(II) species. The drug has entered phase I clinical trials.[103]

Sadler and Bednarski have developed *trans*-dihydroxo platinum(IV) complexes that have azide ligands instead of chloro leaving groups as in cisplatin (Fig. 1.41). These complexes are stable in the dark and, upon irradiation with light of different wavelengths, they undergo reduction and bind to DNA nucleotides. The synthesized compounds are active against 5637 human bladder cancer cell lines including *cis*-resistant cell lines.[100, 104]

Figure 1.41 Structures of Sadler and Bednarski`s photoactive platinum(IV) complexes.

Kim and co-workers reported a *cis*,*trans*-[$PtCl_2(OAc)_2$(1,4-butanediamine)] complex which showed improved activity against colorectal and breast cancers (Fig. 1.42). The drug had lower toxicity in experiments with mice and was chosen for further studies.[96]

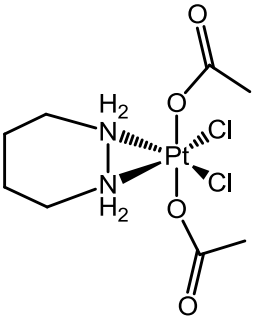

Figure 1.42 Chemical structure of Kim`s platinum(IV) complex.

Numerous platinum(IV) complexes with anticancer activity have been synthesized but only a few have entered into clinical trials.

1.6 Cisplatin combination therapy

1.6.1 Cisplatin in combination with other therapeutics

Cisplatin is a potent anticancer drug that can be used in cancer therapy as a single agent or in combination with other drugs. The multicomponent strategy is becoming of great importance as combination therapy can offer a significant advantage over monotherapy. Treatment with a single agent often fails due to developed drug resistance in cancer cells. Combining drugs that have different modes of action can exhibit synergism in activity and can even help to overcome the problem of drug resistance.[105] The drug synergy effect takes place when one drug interacts with the other in such a way that leads to a significantly greater activity than each single component itself. Synergism in multicomponent therapy depends on various factors such as the mechanism of action of individual drugs, phenotypes of targeting cells, dosing period and combination ratio of each drug.[106]

Combination chemotherapy consisting of gemcitabine hydrochloride with cisplatin is used to treat non-small cell lung cancer and advanced stage bladder, cervical, pancreatic and epithelial ovarian cancers. Gemcitabine or 2',2'-difluoro-2'-deoxycytidine is a nucleoside type molecule where the two hydrogen atoms in the second position of deoxycytidine are substituted by fluorine atoms (Fig. 1.43).

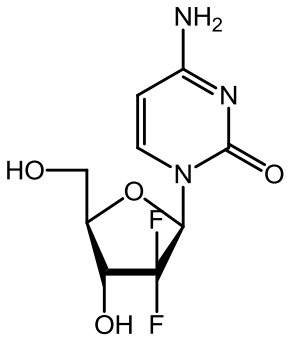

Figure 1.43 Chemical structure of gemcitabine.

Gemcitabine acts as a prodrug which is converted in the body to the corresponding 5'-diphosphate and triphosphate metabolites by deoxycitidine kinase. These two molecules are responsible for the cytotoxic effects of gemcitabine. The diphosphate molecule is capable of inhibiting ribonucleotide reductase which is involved in the catalysis of the reaction to produce deoxyribonucleotides, essential components for DNA synthesis and repair. Therefore, the number of DNA monomers in the cell is reduced. The triphosphate metabolite acts by competing with the natural deoxycytidine 5-triphosphate by incorporation into replicating DNA. Once the triphosphate molecule has incorporated into the DNA, another deoxyribonucleotide is included and thus DNA synthesis is prevented.[107, 108] It is believed that when administered together with cisplatin, gemcitabine helps to prevent cell resistance to cisplatin treatment.

Combining cisplatin with doxorubicin has improved its anticancer efficacy in endometrial carcinoma in phase III clinical trials. Doxorubicin, or Adriamycin, (Fig. 1.6 (a), page 9) is anthracycline antibiotic intensively used in anticancer therapy to treat hematological cancers, several carcinomas and soft tissue sarcomas. Doxorubicin itself is cardiotoxic but together with cisplatin in combination therapy it induces a higher level of hematological and gastrointestinal toxicity.[109] Doxorubicin acts by intercalation between the bases of the DNA, binding to the DNA polymerase and inhibiting DNA synthesis.[110]

Cisplatin in combination with 5-fluorouracil (5-FU) is widely used to treat advanced nasopharyngeal carcinoma and advanced gastric carcinoma.[111, 112] 5-Fluorouracil is an analogue of uracil with a hydrogen atom at C5 position being substituted by a fluorine atom (Fig. 1.44 (a)).

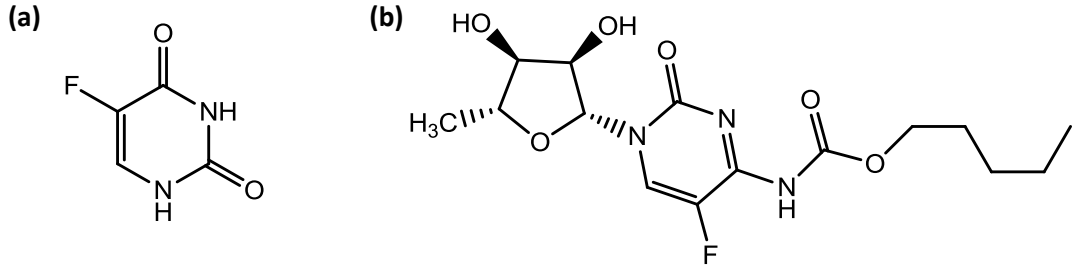

Figure 1.44 (a) Structure of 5-fluorouracil **(b)** Structure of capecitabine.

5-Fluorouracil as a single agent is used to treat colorectal and pancreatic cancers. Within the cell, the drug is converted into toxic metabolites fluorodeoxyuridine monophosphate, fluorodeoxyuridine and fluorouridine triphosphates, which are then incorporated into RNA and DNA molecules inhibiting the DNA synthesis.[112] Previous clinical studies revealed that platinum-based multicomponent therapy for treatment of

metastatic and recurrent nasopharyngeal carcinoma results in higher response rates than any other drug combinations, approximately 50 - 90 % with a complete response rate of 5 - 30 %. However, continuous infusion of 5-FU requires chronic venous excess which is inconvenient, expensive and very often leads to a venous thrombosis and sepsis. Therefore to overcome these complications an alternative to 5-FU was created; the oral drug fluoropyrimidine capecitabine.[113]

Capecitabine (Fig. 1.44 (b)) is an oral prodrug that is converted into 5-fluorouracil by a series of enzymatic reactions in tumour tissue. It inhibits DNA synthesis and precludes cell growth. Capecitabine shows a single-agent activity against advanced pancreas and metastatic breast cancers.[114, 115] It was reported that in combination with cisplatin it is effective and well-tolerated by patients with advanced gastric cancer, biliary cancer and squamous cell carcinoma of the head and neck.[111] Capecitabine combined with oxaliplatin shows a good activity profile and thus this combination of drugs can be used as a first-line therapy in advanced gastric cancer. Oxaliplatin is less toxic than cisplatin and no renal or ototoxicity is observed. The combination of capecitabine and oxaliplatin does not require hydration, like cisplatin, and therefore is more convenient to use.[113]

The cisplatin combination therapy was proven to be more effective in treatment of some types of cancers than drug monotherapy however high toxicity of cisplatin remains the main drawback of its dose-limiting application. Oxaliplatin was found to be a good alternative for cisplatin with lower toxicity and good antitumour profile.

1.6.2 Cisplatin conjugates.

In the search for novel anticancer agents with higher cytotoxic activity and less toxicity, numerous compounds have been synthesised by modifying the cisplatin moiety and incorporating it into various molecules.

Brunner and co-workers incorporated the cisplatin moiety to a porphyrin system by attaching it to the carboxylate groups of the propionic acid side chains of porphyrin in order to accumulate cisplatin specifically in a tumour tissue (Fig. 1.45).[116] Porphyrins are used to treat tumours in photodynamic therapy. When irradiated with light of 630 nm, they produce singlet oxygen which kills tumour cells. The cytotoxic activity of the synthesised compounds was investigated in breast cancer cell line MDA-MB-231. It was found that porphyrin ligand itself is not active without irradiation; however upon irradiation it reduces cell proliferation to ~ 81 %. The porphyrin complex with cisplatin showed activity without irradiation decreasing cell proliferation to ~ 63 % and upon irradiation to ~ 38 %. Cisplatin alone was found to reduce cell proliferation by ~ 50 % upon irradiation. This demonstrates the additive effect of porhpyrins and cisplatin.[116]

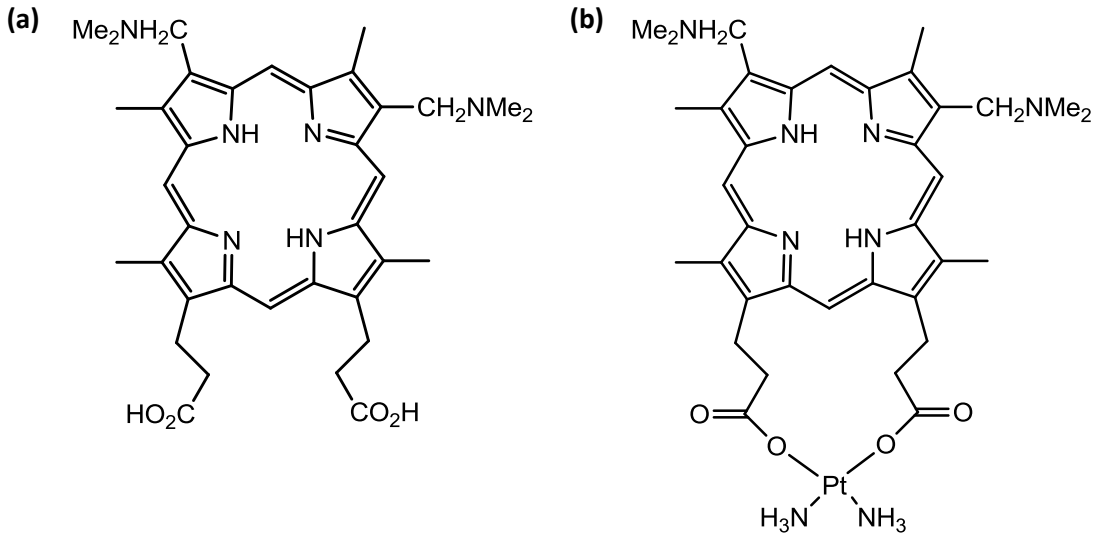

Figure 1.45 Structure of porphyrin **(a)** with propionic acid side chains **(b)** with cisplatin moiety.

Brabec and co-workers combined the cisplatin moiety with the DNA minor groove binder distamycin (Fig. 1.46). Distamycin is a known antibacterial, antiviral and antineoplastic agent whose activity is thought to be associated with its ability to bind to DNA. This molecule has a preference for AT rich regions of DNA. Cisplatin-distamycin complex binds to DNA and induces a higher number of interstrand cross-links than cisplatin itself. This in turn causes a bend of the helix of ~ 35º towards the DNA minor groove and unwinding of the DNA by approximately 95º. However, there is no systematic data and evidence of the activity of the cisplatin-dystamycin complex.[117]

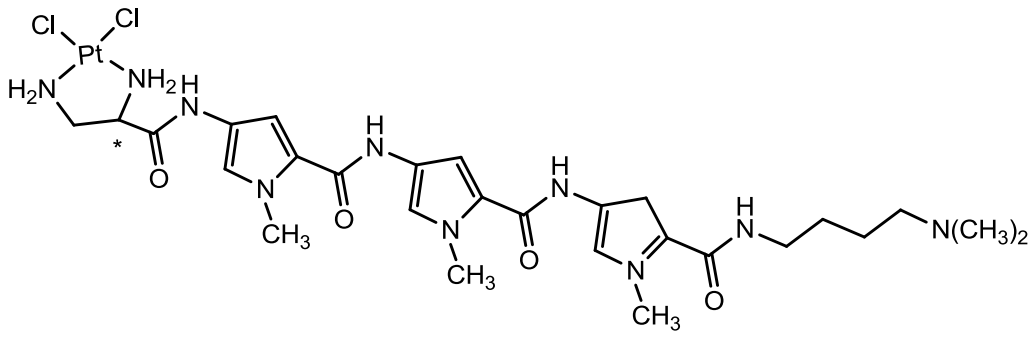

Figure 1.46 Cisplatin moiety attached to distamycin.

Reedijk *et al.* have reported mononuclear and dinuclear platinum(II) compounds containing a 5,7-dimethyl-1,2,4-triazolo[1,5-*a*]pyrimidine (dmtp) moiety as a ligand (Fig. 1.47). Triazolopyrimidine derivatives are similar in structure to purines and differ from them by the presence of an additional pyrimidine nitrogen.[118]

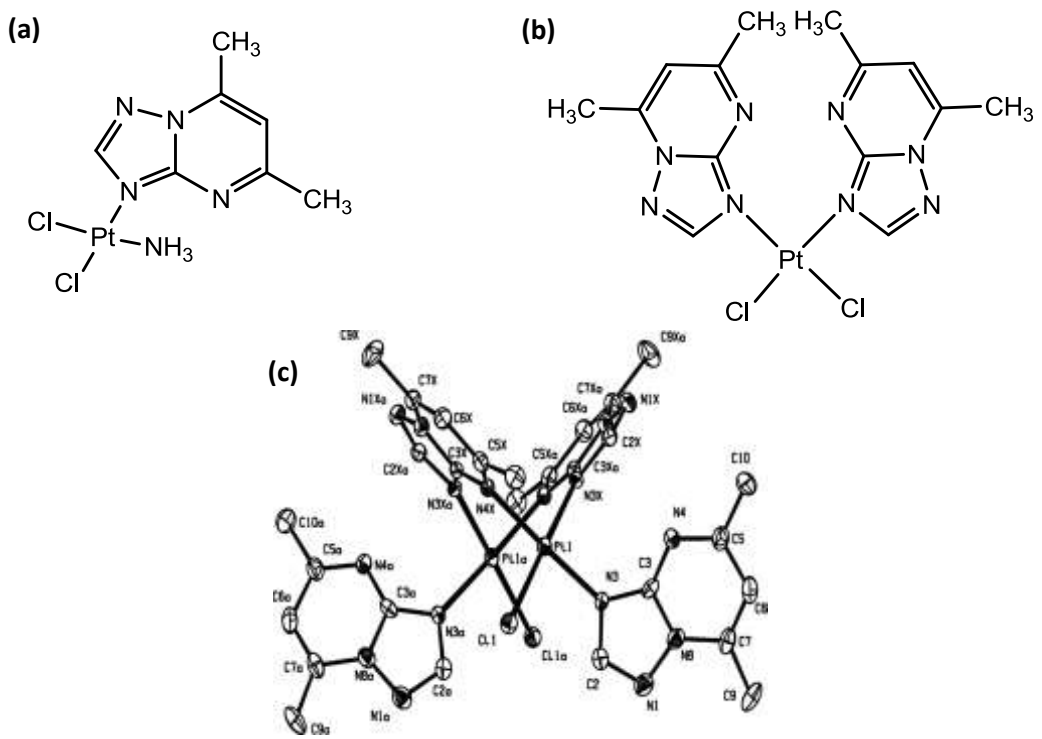

Figure 1.47 (a) Structure of *cis*-$[PtCl_2(NH_3)(dmtp)]$ **(b)** Structure of *cis*-$[PtCl_2(dmtp)_2]$ **(c)** Crystal structure of $[Pt_2(\mu\text{-}dmtp)_2Cl_2(dmtp)_2]^{2+}$.[118]

The reaction of the synthesised compounds with 5'-GMP revealed the site of platination at the N7 position of 5'-GMP. The complexes have been tested for their antitumor activity in T47D breast and HCV29T bladder cancer cell lines. *Cis*-$[PtCl_2(NH_3)(dmtp)]$ and *cis*-$[PtCl_2(dmtp)_2]$ did not show any activity, whereas the dinuclear complex $\{H^+[Pt_2(\mu\text{-}dmtp)_2Cl_2(dmtp)_2]^{2+}(NO_3)_3(H_2O)_6\}$ was active against T47D breast cancer cell line with an IC_{50} of 2.3 μM compared to that of cisplatin (10.7 μM).[118]

Herman and co-workers reported a heteronuclear ruthenium(III)-platinum(II) complex that resembles cisplatin and NAMI-A anticancer compounds (Fig. 1.48).[119]

This trinuclear complex contains two ruthenium(III) metal centres that can undergo reduction to Ru(II) under biological conditions and one platinum(II) metal centre.

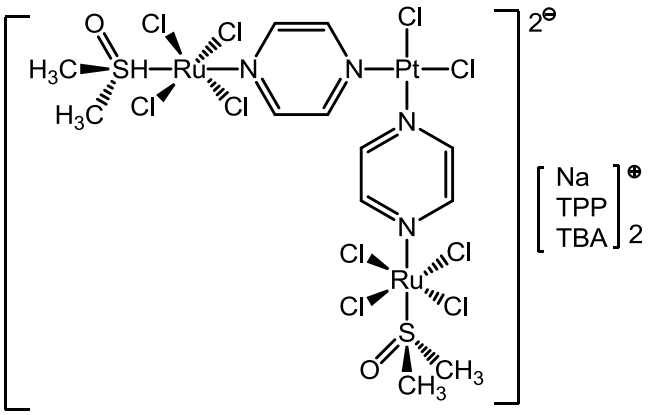

Figure 1.48 Structure of mixed ruthenium(III)-platinum(II) complex.

DNA binding studies by gel electrophoresis showed that the compound binds strongly to the DNA and has a higher effect on the DNA electrophoretic mobility than cisplatin. The complex has been tested for its cytotoxic activity, together with cisplatin as a control, in CCRF-CEM leukemia cells (IC_{50} = 4.3 and 4.8 μM, respectively), HOP-62 NSC lung cells (IC_{50} = 5.0 and 4.5 μM, respectively), and BT-549 breast cells (IC_{50} = 14.4 and 14.8 μM, respectively). The IC_{50} values revealed that the heteronuclear mixed-metal complex has a moderate activity. The activity of the complex was mostly associated with the presence of cisplatin moiety group.[119]

More recently Brewer *et al.* described mixed-metal ruthenium(II)-platinum(II) complexes with substituted terpyridine ligands (Fig. 1.49).[120]

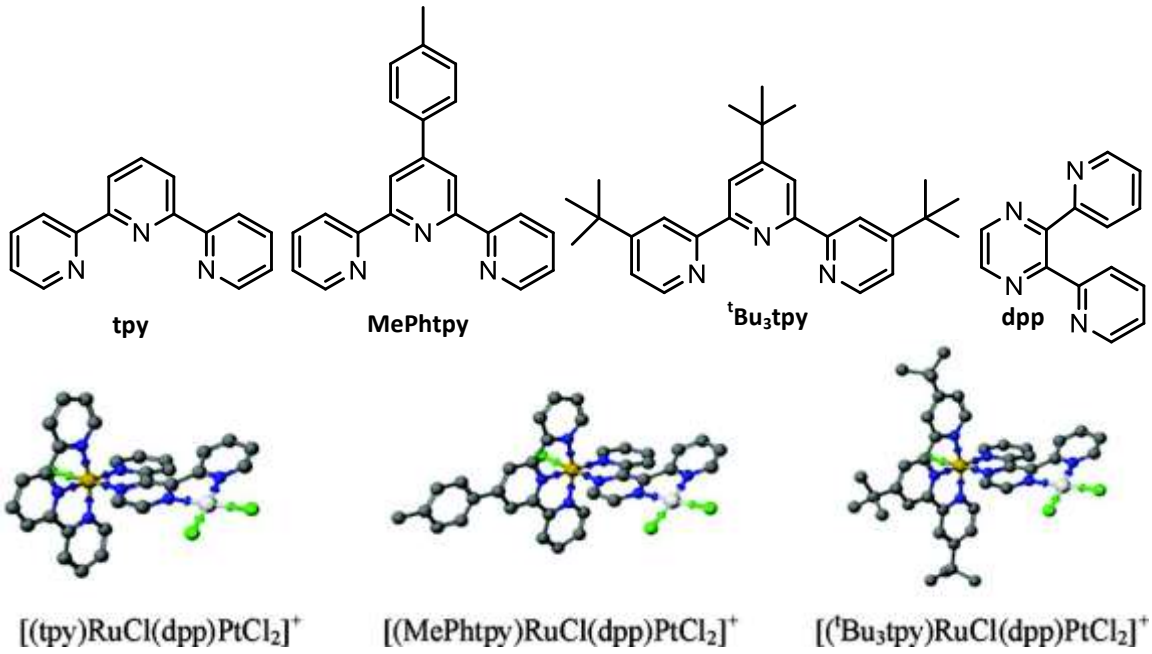

Figure 1.49 Structures of the ligands and the mixed-metal ruthenium(II)-platinum(II) complexes; grey-carbon, blue-nitrogen, green-chlorine, gold-ruthenium, and white-platinum.

Mixed-metal complexes consisting of ruthenium light absorbers and bioactive molecules such as cisplatin attracted a lot of attention for their potential anticancer properties. Mixed-metal complexes show enhanced covalent binding to DNA compared to cisplatin itself, and the positive charge introduced by Ru(II) improves water solubility. The coordinative binding of the synthesised complexes was demonstrated by agarose gel electrophoresis using linear DNA. The retardation of migration through the gel was greater for these compounds than for cisplatin. Introduction of bulky $^{t}Bu_3$ groups caused slower migration through the gel due to steric factors. All the complexes have been shown to bind to the guanine residues of DNA. The photocleavage studies using gel electrophoresis with plasmid DNA were carried out. The compounds were shown to photocleave DNA upon irradiation with visible light. The $[(MePhtpy)RuCl(dpp)PtCl_2](PF_6)$ complex is significantly more efficient in

photocleaving DNA, whereas for the [(^{t}Bu$_3$tpy)RuCl(dpp)PtCl$_2$](PF$_6$) metal complex minimal to no photocleavage was observed.[120]

Guo *et al.* from China linked the cisplatin moiety to bisphosphonate tetraethyl esters (Fig. 1.50).[121] Biphosphonates are well known for their bone targeting properties and they are widely used as therapeutics to treat bone–related diseases. According to the CD studies data obtained compounds **1** - **4** hardly interact with the DNA, suggesting that DNA is not the primary target of these compounds. Interestingly, compounds **2** and **4** exhibit cytotoxic activity in MG-63 osteosarcoma and COC1 ovarian cancer cell lines with IC_{50} values higher than cisplatin whereas compounds **1** and **3** do not show any activity, which can be explained by the length of the linker between the chelating moiety and the bisphosphonate esters.[121]

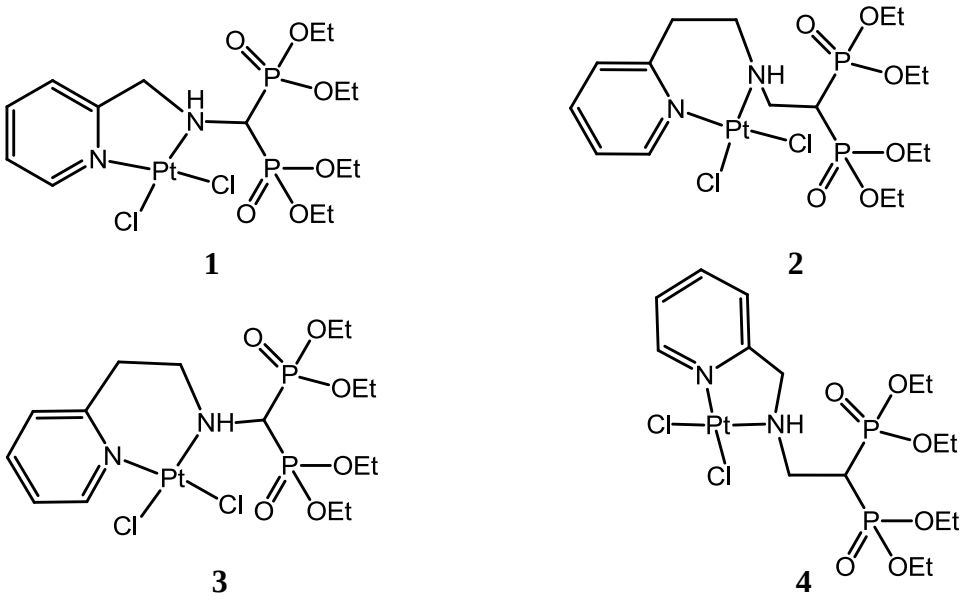

Figure 1.50 Structures of platinum(II) complexes synthesised by Guo *et al.*

Rusling and co-workers combined cisplatin and epidermal growth factor (EGF) with a single wall carbon nanotube (SWNT) in order to specifically target head and

neck squamous cancer cells (Fig. 1.51).[122] The synthesised nanotubes are able to enter the cells by endocytosis and other mechanisms. Functionalised SWNTs provide high surface area for drug loading and the ability to transport the drug across the cell membrane with low toxicity. Functionalised with cisplatin and epidermal growth factor, SWNTs have an affinity to the cell-surface receptor (EGFR) which is overexpressed in squamous cancer cells. By using these EGF-EGFR interactions, SWNTs can selectively target and kill cancer cells. The synthesised SWNT-cisplatin-EGF conjugate has been tested for its antitumor activity in head and neck squamous carcinoma cell lines, and a significant decrease in a tumour volume has been observed.

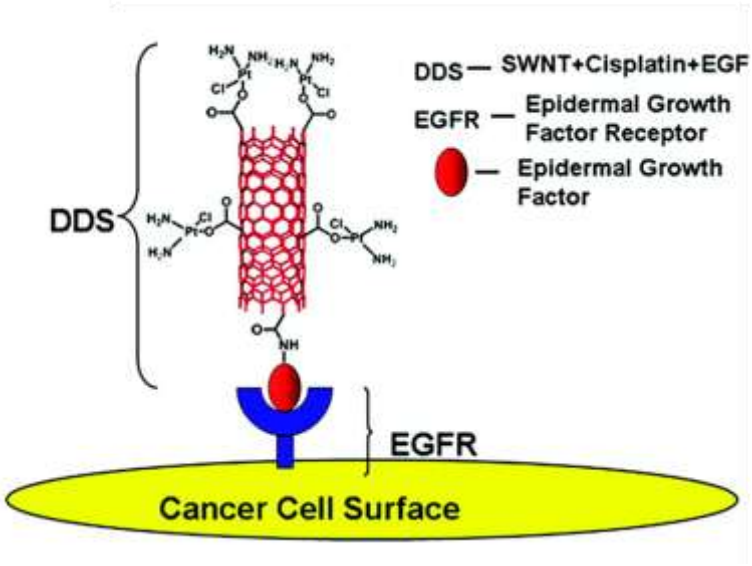

Figure 1.51 Schematic representation of SWNTs targeting the EGFR receptor on the cell surface.[122]

In the previous sections 1.5 and 1.6, platinum anticancer drugs and cisplatin combination therapy were discussed. Cisplatin is one of the most common drugs used in clinics to treat patients with different types of cancers. However, severe side effects,

absence of specificity of this drug and efficiency against platinum-resistant and metastasis tumours stimulated research in the area of non-platinum-based anticancer drugs.[123] The success of advances in this area is discussed in the following section.

1.7 Non-platinum metal compounds as anticancer drugs

1.7.1 Ruthenium metal complexes

Ruthenium compounds show great promise as potential therapeutics, although there are no analogues in the clinic as yet. Nevertheless two ruthenium compounds entered human clinical trials, NAMI-A and KP-1019 (Fig. 1.52).[124]

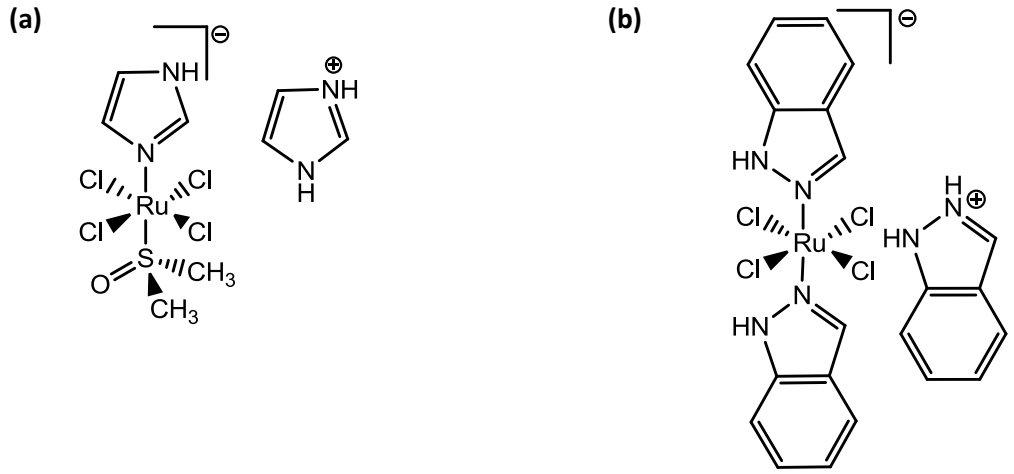

Figure 1.52 Structures of **(a)** NAMI-A **(b)** KP1019.

NAMI-A shows anti-metastatic properties and it is active against lung metastasis. KP1019 is active against colorectal cancer and primary explants of tumours that are resistant to standard chemotherapeutic agents. It is believed that ruthenium compounds convert to their active form after entering the cell. Ruthenium complexes tend to accumulate in tumour cells rather than healthy tissues by utilising the transferrin molecule to enter the cell.[124]

Several ruthenium arene-based compounds with cytotoxic properties have been designed. Sadler *et al.* developed ruthenium anticancer compounds consisting of an aryl ruthenium with a "piano-stool" type of conformation, with a bidentate ethylenediamine and a chloride occupying the remaining coordination sites (Fig. 1.53).[125] The compounds showed a wide spectrum of activity including cisplatin resistant tumours. Interestingly, the activity of Sadler`s ruthenium compounds is dependent on the size of the aryl unit, the more extended aryls exhibit higher activity. The complexes can bind to DNA with a preference for guanine residues and large aryl groups can partially insert between DNA bases creating a bifunctional lesion.[126]

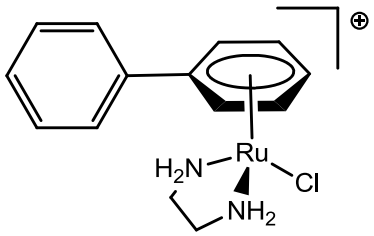

Figure 1.53 Sadler`s piano-stool ruthenium complex.

Dyson and co-workers synthesised RAPTA-C and RAPTA-T ($RuCl_2(\eta^6$-arene)(PTA)) ruthenium(II) arene complexes based on the 1,3,5-triaza-7-phosphaadamantane (PTA) ligand (Fig. 1.54). RAPTA-C is based on p-cymene whereas RAPTA-T is toluene based.[127]

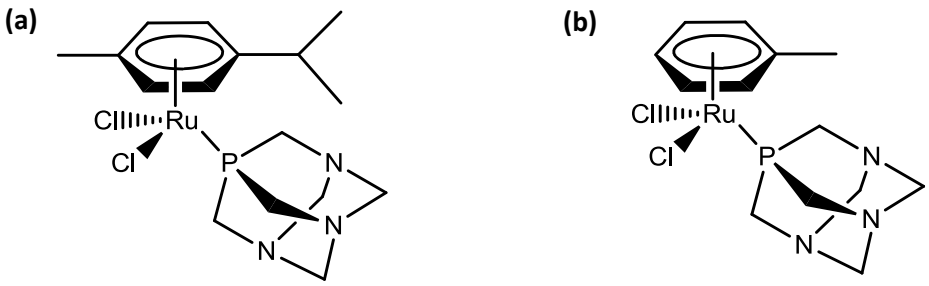

Figure 1.54 Structures of ruthenium arene-based compounds **(a)** RAPTA-C **(b)** RAPTA-T.

RAPTA compounds showed moderate cytotoxic activity in various cancer cell lines and significant activity in metastatic cancers, by reducing number and weight of solid metastases without affecting the primary tumour. The anticancer activity of RAPTA-T is associated with interaction of the compound with extracellular components such as collagenIV and fibronectin. Treatment of Ehrlich ascites carcinoma cells with RAPTA-C induces high accumulation of tumour suppressor gene p53 responsible for cell apoptosis in response to DNA damage and cell stress, and thus the arrest of the cell cycle occurs. RAPTA-C also provokes high levels of the p21 gene associated with cell cycle inhibition, differentiation, and cellular senescence. Low levels of cyclin E, a central regulator in transition of G1-S/G2-M was observed, which demonstrates the ability of RAPTA-C to slow down cell division.[124, 128]

More recently, Navarro and co-workers reported a half-sandwiched ruthenium(II) complex that binds non-covalently to DNA.[129] Cationic cyclic polynuclear half-sandwiched ruthenium(II) complexes of general formula $[(cymene)_4Ru_4(\mu\text{-Hoxonato})_2(\mu\text{-N,N}'\text{-L})_2]\text{-}(CF_3SO_3)_4$ (L = 4,4'-bpy; L = 4,7-phen) contain Hoxonato bridges (H_3oxonic = 4,6-dihydroxy-2-carboxy-1,3,5-triazine acid) and N,N'-linkers (4,4'-bipyridine (4,4'-bpy), 4,7-phenanthroline (4,7-phen) (Fig. 1.55). Both compounds

were shown to bind to the DNA and induce significant alterations in its conformation. They were found to change shape of the DNA strands, mainly by stiffening and strand aggregation. The compounds exhibited a good cytotoxic profile in A2780 and A2780 cisplatin-resistant cancer cell lines with significant activity in the A2780cisR cell line (IC_{50} = 2.4 μM for compound **5**, 4.6 μM for compound **6** and 3.7 μM for cisplatin) which is quite striking due to their non-covalent nature of binding.

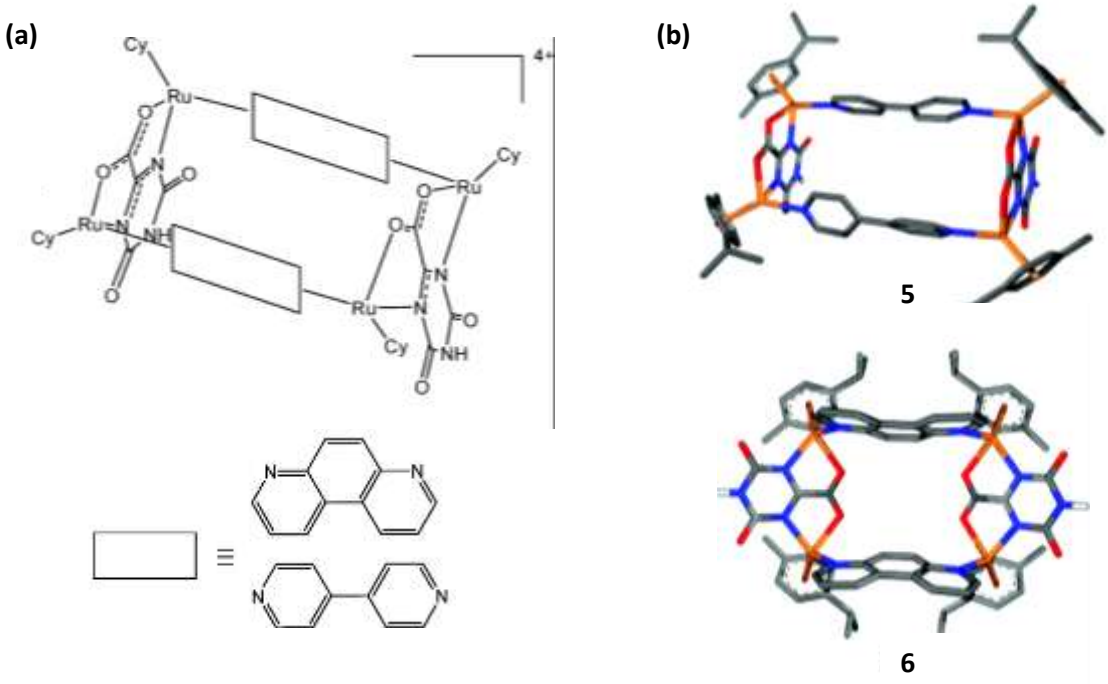

Figure 1.55 Structures of half-sandwiched ruthenium(II) complexes **(a)** Schematic representation of $[(cymene)_4Ru_4(\mu\text{-Hoxonato})_2(\mu\text{-N,N'-L})_2]\text{-}(CF_3SO_3)_4$ **(b)** Molecular force field models of $[(cymene)_4Ru_4(Hoxonato)_2(4,4'\text{-bpy})_2]^{4+}$ **5** and $[(cymene)_4Ru_4(Hoxonato)_2(4,7\text{-phen})_2]^{4+}$ **6**.[129]

1.7.2 Rhodium metal complexes

There has been a significant interest in rhodium compounds and their antitumor properties since the discovery of dirhodium(II) carboxylates. The dirhodium tetracarboxylate complexes of formula [$(RCOO)_4L_2Rh_2$(II)] (where R = Me, Et, Ph or CF_3; L = H_2O or other solvents) (Fig. 1.56) exhibit cytotoxic activity in leukemia L1210 tumors, Ehrlich ascites, sarcoma 180, and P388 murine leukemia tumour cell lines.[130] The rhodium(II) carboxylate compounds are known to bind to the DNA and inhibit DNA, RNA and protein synthesis, however, the mechanism of their action is not fully understood.[131] It was found that with increasing lipophilicity of the alkyl group, the compounds showed higher activity, with pentanoate being the most active in Ehrlich ascites tumor cell lines.[130]

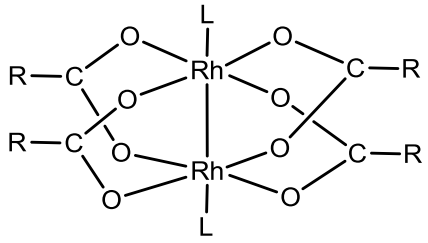

Figure 1.56 General structure of dirhodium(II) tetracarboxylate.

Sheldrick *et al.* recently reported several complexes of general formula [$RhCl_3$(DMSO-*κS*)(pp)] with a series of aromatic polypyridyl ligands (Fig. 1.57). Interestingly, these compounds do not show binding to the DNA neither by intercalation nor by covalent binding. The characteristic DNA CD spectrum is unchanged upon titration of the rhodium(III) polypyridyl compounds with ct-DNA.[132]

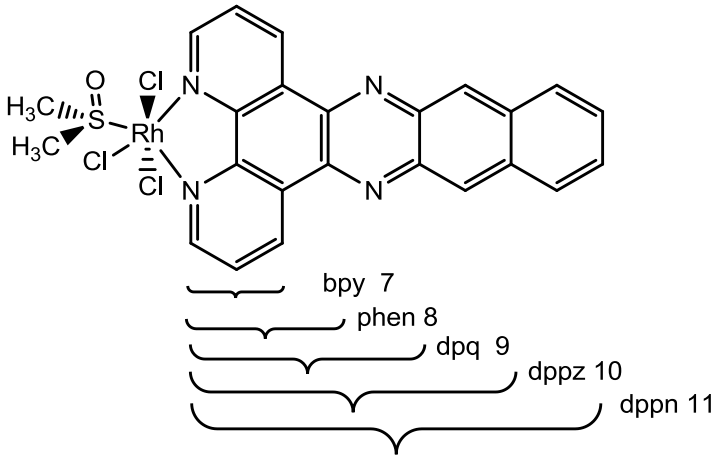

Figure 1.57 Structures of the trichloridorhodium (III) polypyridyl complexes *mer*-[$RhCl_3$(DMSO-κS)(pp)] **7 - 11** (pp = bpy, phen, dpq, dppz, dppn).

Despite the absence of DNA binding, the trichloridorhodium(III) polypyridyl complexes exhibit potent cytotoxic activity in MCF-7 breast cancer and HT-29 colon cancer human cell lines. The IC_{50} values for the complexes **7 - 9** are strongly dependant on the size of the polypyridyl ligand (bpy > phen > dpq). There is no further significant increase for complexes **10** and **11**. Compounds **9 - 11** showed significantly high antitumor activity with IC_{50} values in the range of 0.069 - 0.079 μM, which is two times lower than for cisplatin (IC_{50} range 2 - 7 μM). Moreover, a high level of cellular uptake of these complexes was observed, with compound **9** causing a significant decrease in cellular oxygen consumption and rate of cellular acidification.[132, 133]

Lorenz and co-workers described a new rhodium(III) complex with 1-nitroso-2-naphthol chelating as a 1,2-naphthoquinone-1-oximato ligand (Fig. 1.58).[134] This compound binds to the DNA in a suggested non-covalent manner and has no effect on the stability of the DNA.

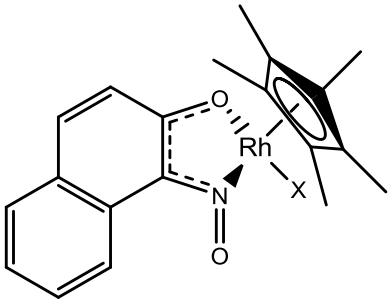

Figure 1.58 Chemical structure of rhodium(III) chelate complex.

The cytotoxic activity of the rhodium(III) chelate complex was tested on HeLa cervical carcinoma and HL60 leukemia cancer cell lines. The compound showed a good activity profile in both cancer cell lines, however the highest activity was observed in the HeLa cancer cell line with IC_{50} values higher (IC_{50} = 6.5±5.9 μM) than those of cisplatin (IC_{50} = 25±4.2 μM).[134]

The drive to synthesise metal-based anticancer compounds with a high antitumour activity is not limited to ruthenium and rhodium chemistry. Various iron and gold compounds with anticancer activity have also been reported.

1.7.3 Iron metal complexes

The salts of ferrocenium picrate and ferrocenium trichloroacetate were the first iron compounds to be discovered to have cytotoxic activity.[135] Substituted ferrocene compounds are active, though ferrocene itself does not exhibit any activity. The antitumour activity of ferrocene derivatives is linked to the oxidative DNA damage caused by oxygen species produced by the compounds. Iron(II) ferrocene is interconverted into iron(III) ferrocenium ions within cancer cells which are then involved in the production of reactive oxygen species. Ferrocifens are ferrocene

derivatives of anti-estrogen tamoxifen with one phenyl ring of tamoxifen replaced with ferrocene (Fig. 1.59).

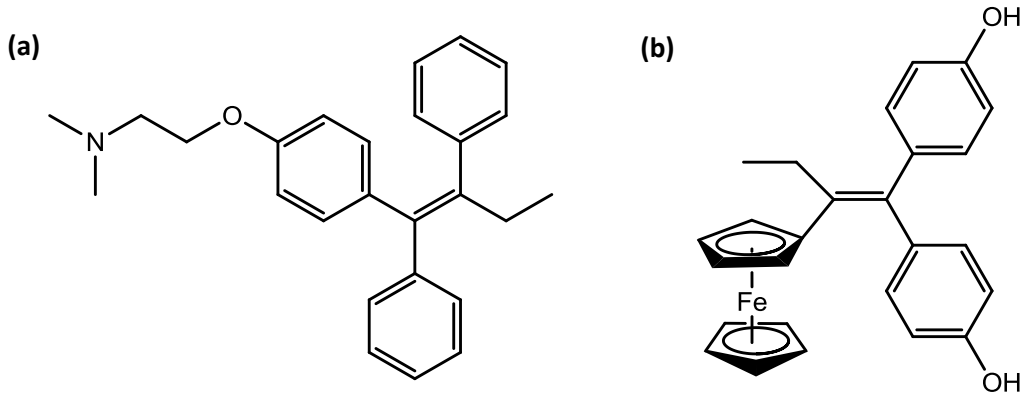

Figure 1.59 Structure of **(a)** Tamoxifen **(b)** Ferrocifen.

Ferrocifens are highly active towards breast cancer cell lines that are ERα –ve (ERβ +ve) as well as breast cancers that are ERα +ve, whereas tamoxifen itself is active only in cancers that are rich in ERα (ERα +ve).[126, 135]

Iron(II)-bleomycin compounds have shown antineoplastic activity against various malignancies including testicular cancer and certain types of lymphomas.[136] Bleomycins are a group of glycopeptides isolated from bacterium *Streptomyces verticillus*. Bleomycin (BLM) has four functional domains: the metal binding domain responsible for DNA recognition and oxygen activation, the bithiazole and C-terminal substituents involved in DNA binding, the linker region for DNA cleavage and carbohydrate moiety for cell surface recognition and efficient DNA cleavage (Fig. 1.60).

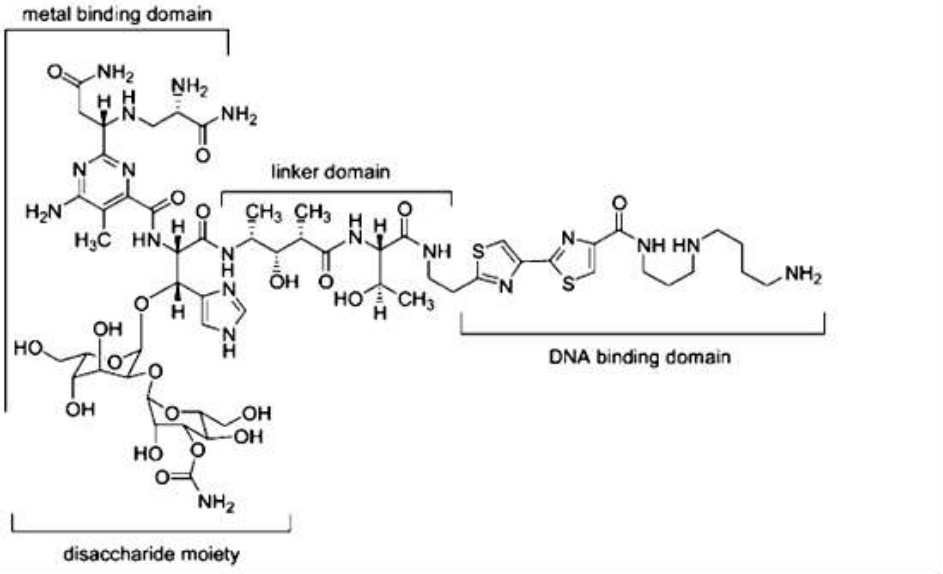

Figure 1.60 Structure of BLM A_5.[136]

When complexed to Fe(II) metal ions bleomycins have been shown to degrade DNA by forming single-stranded lesions and double-stranded breaks in the DNA backbone. Single-stranded lesions are caused by both direct breaks in the DNA backbone and release of bases from deoxyribose moiety. Regions in which the bases are removed then undergo to alkaline lysis. Double-stranded breaks in the DNA are thought to be due to two independent breaks on opposite strands of the DNA. The ability of iron(II)-bleomycin complex to degrade DNA is believed to be responsible for its antineoplastic activity.[137]

An iron(III)-salophen compound recently reported in the literature is an organometallic complex with antitumour properties.[138] Salophens are organic compounds composed of two Schiff`s bases linking three aromatic moieties (Fig. 1.61). It was shown that iron(III)-salophen complex is a potential candidate for the treatment of ovarian cancer. Treatment of SKOV-3 cancer cell line with iron (III)-salophen complex for 24 hours caused reduction of cell proliferation with an IC_{50} value of 300

nM. At a concentration of 2 μM in the SKOV-3 cell line the complex caused nuclear fragmentation, chromatin condensation and DNA fragmentation leading to apoptosis. It is believed that iron (III)-salophen forms active hydroxyl radicals that cleave DNA.[138]

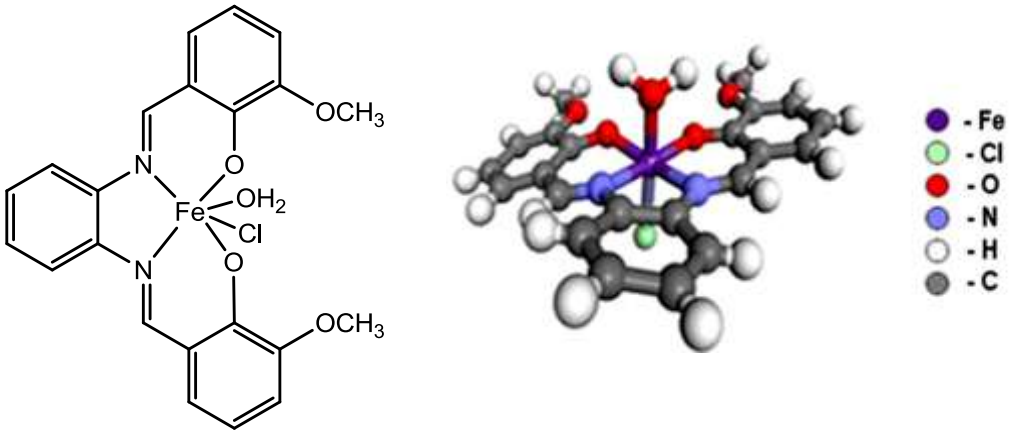

Figure 1.61 Chemical and X-ray structures of iron(III)-salophen complex.[138]

Recently, Chakravarty and co-workers described photoactive ternary iron(III) complexes containing tertiary butyl groups with a tetradentate phenolate-based ligand and phenanthroline (phen, **12**), dipyridoquinoxaline (dpq, **13**) and dipyridiphenazine (dppz, **14**) moieties (Fig. 1.62).[139] These compounds bind to the DNA in a groove-binding nature rather than intercalation due to the presence of the steric bulky tetradentate ligand. They induce photocleavage of the DNA in the presence of visible light through the formation of active hydroxyl radicals. Among the series of compounds, complex **14** was found to show high cytotoxicity in HeLa cervical (IC_{50} = 3.59 μM) and keratinocyte HaCaT (IC_{50} = 6.07 μM) cancer cell lines in visible light and low toxicity in the dark. Rapid cancer cell death observed after 2 hours of photoirradiation of this compound makes it a potential candidate for photodynamic anticancer therapy.[139]

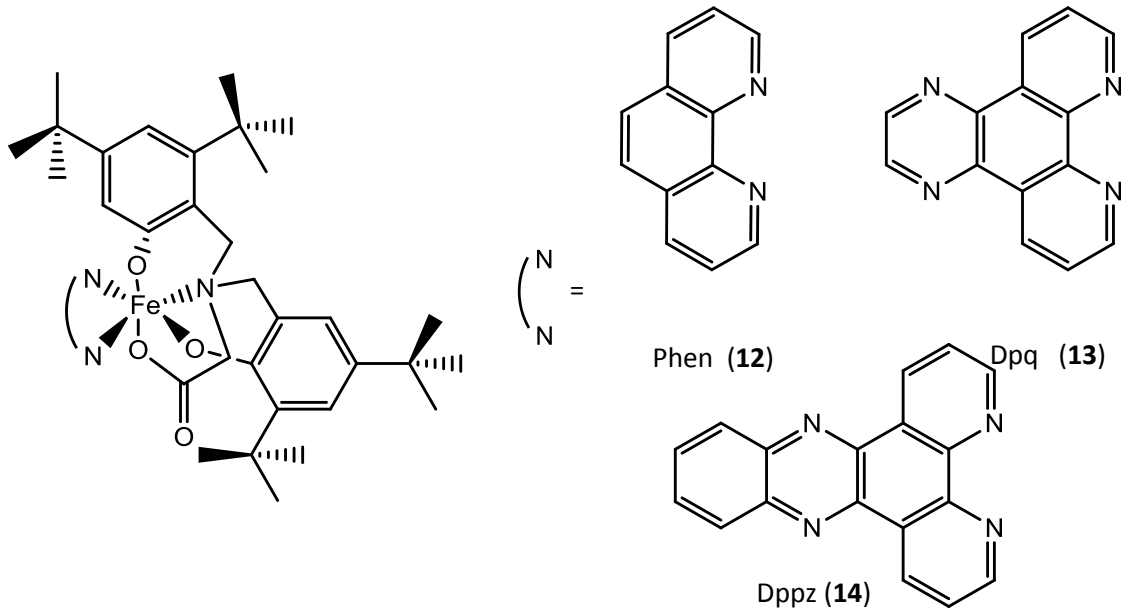

Figure 1.62 Structures of iron(III) complexes reported by Chakravarty.

1.7.4. Gold complexes

Gold compounds have attracted the interest of many research groups for their great potential in anticancer treatment, however, the mechanism of their action is not yet fully understood. It is suggested that gold compounds induce apoptosis through various cellular processes such as direct DNA damage, modification of the cell cycle, mitochondrial damage, proteasome inhibition, modulation of specific kinases and others.[140]

Gold(I) compounds have been extensively studied for their antiarthritic properties and moreover, several gold compounds such as Auranofin and related thiolate gold phosphane derivatives have shown a good cytotoxic activity (Fig. 1.63). Gold(I) complexes act by inhibiting mitochondrial functions and induce conditions for the release of cytochrome c which leads to apoptosis.[140, 141]

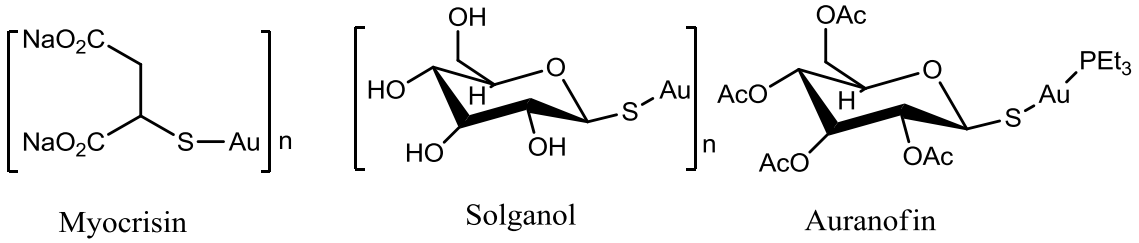

Figure 1.63 Structures of gold (I) complexes with antiarthritic and antitumour properties.

Dyson *et al.* have developed alkynyl phosphane gold(I) complexes with the PTA and DAPTA co-ligands (Fig. 1.64).[141] The antitumour properties of these compounds were analysed using A2780 and A2780cisR ovarian cancer cell lines. All the complexes **15 - 18** showed from good to moderate anticancer activity with IC_{50} values falling in the 0.8 - 14 μM range. The compound **15b** is the most cytotoxic and it exhibits 20-fold higher activity than cisplatin in the A2780cisR cancer cell line. The synthesised complexes do not damage DNA, they act via interactions with proteins and enzymes.

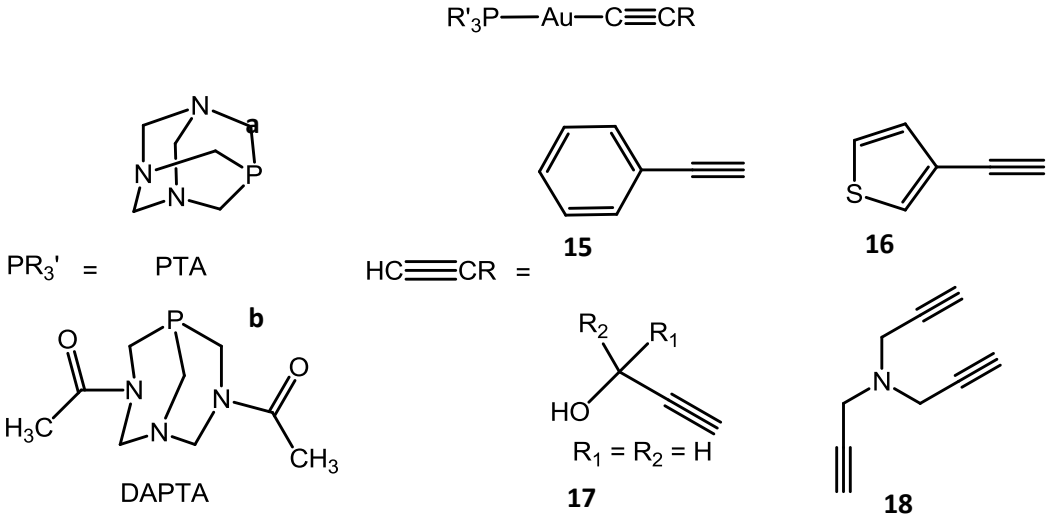

Figure 1.64 Structures of alkynyl gold(I) derivatives.

Messori and co-workers reported dinuclear gold(III) compounds where two square-planar gold(III) moieties are linked together by nitrogen atoms from the bidentate 2,2'-bipyridine ligand and two adjacent oxygen atoms (Fig. 1.65).[142] The cytotoxic activity of the synthesised compounds was explored on A2780 and A2780cisR ovarian cancer cell lines. All the compounds **19** - **24** exhibit antitumour activity, however compound **24** possess the highest activity with IC_{50} values comparable to cisplatin (IC_{50} in A2780cisR = 1.79 μM **24**, 2.1 μM cisplatin; A2780 IC_{50} = 4.81 μM **24**, 24.4 μM cisplatin).

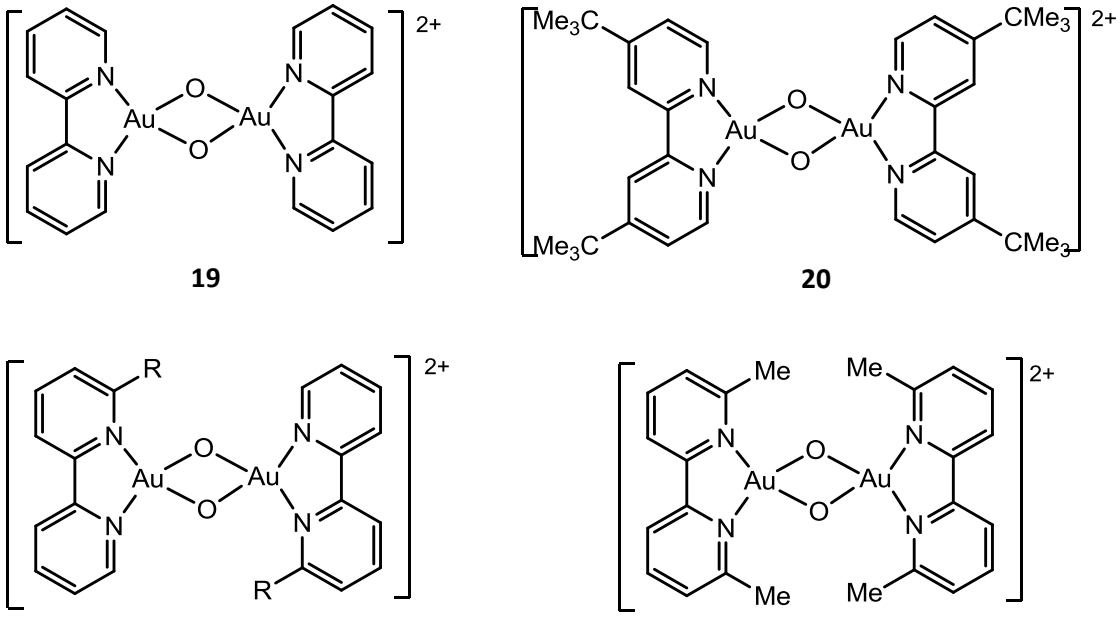

Figure 1.65 Chemical structures of dinuclear gold (III) complexes.

The CD experiment data obtained suggest that compounds **19** and **24** bind to the ct-DNA, with compound **24** showing more effective binding which is most likely due to its specific redox processes.[142]

Gold(III) dithiocarbonato complexes have recently attracted lot of attention for their high *in vitro* and *in vivo* anticancer activity and low renal toxicity.[143] Dithiocarbamates are bidentate chelating ligands and coordination of the metal ions to these ligands results in a chelating complex (Fig. 1.66).

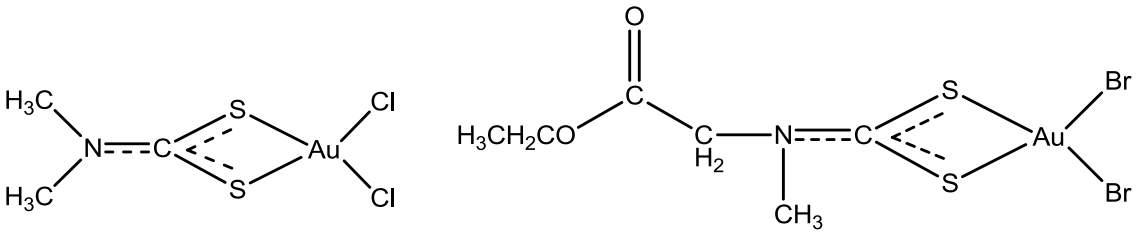

[$AuCl_2$(DMDT)] **25**

[$AuBr_2$(ESDT)] **26**

Figure 1.66 Chemical structures of gold(III) dithiocarbonato complexes (DMDT = *N*,*N*-dimethyldithiocarbamate, ESDT = ethylsarcosinedithiocarbamate).

Gold(III) dithiocarbonato complexes showed in vitro activity higher than cisplatin and more interestingly even in cisplatin-resistant cancer cell lines. Treatment of PC3, DU145 and R-PC3 (cisplatin-resistant) human prostate cancer cell lines with compounds **25** and **26** inhibited cell proliferation, with compound **25** being the most effective. *In vivo* testing in prostate cancer-bearing mice showed that compound **25** actively inhibited the tumour growth. The mechanism of action of these compounds is believed to be different from cisplatin. It was found that compound **25** changes mitochondrial functions, induces formation of reactive oxygen species and inhibits selenoenzyme overexpressed in prostate cancer. The reported results demonstrate that the gold(III) dithiocarbamato complexes have a great potential to be used for prostate cancer treatment.[14]

1.8 References:

1. L. Lestel, I. Tkatchenko, *Eur. J. Org. Chem.*, 2007, **19**, 3064-3067.

2. J. M. Lehn, *Chem. Soc. Rev.*, 2007, **36**, 151-160.

3. J. Vicens, Q. Vicens, *J. Incl. Phenom. Macrocycl. Chem.*, 2009, **65**, 221-235.

4. R. Dahm, *Hum. Genet.*, 2008, **122**, 565-581.

5. J. D. Watson, F. H. C. Crick, *Nature*, 1953, **171**, 737-738.

6. S. Neidle, *DNA structure and recognition*, Oxford University Press, Oxford, 1994.

7. F. R. Keene, *Dalton. Trans.*, 2011, **40**, 2405-2418.

8. D. Voet, J. G. Voet, *Biochemistry*, 2d edn., John Wiley&Sons, USA, 1995.

9. A. K. Mazur, *J. Am. Chem. Soc.*, 2003, **125**, 7849-7859.

10. M. A. Fuertes, V. Cepeda, C. Alonso, J. M. Pérez, *Chem. Rev.*, 2006, **106**, 2045-2064.

11. M. Trieb, C. Rauch, B. Wellenzohn, F. Wibowo, T. Loerting, K. R. Liedl, *J. Phys. Chem. B*, 2004, **108**, 2470-2476.

12. Y. Xu, R. Ikeda, H. Sugiyama, *J. Am. Chem. Soc.*, 2003, **125**, 13519-13524.

13. R. Assenberg, A. Weston, D. L. N. Cardy1, K. R. Fox, *Nucleic Acids Res.*, 2002, **30**, 5142-5150.

14. K. C. Woods, S. S. Martin, V. C. Chu and E. P. Baldwin, *J. Mol. Biol.*, 2001, **313**, 49-69.

15. D. M. J. Lilley, *Q. Rev. Biophys.*, 2000, **33**, 109-159.

16. H. Mita, T. Ohyama, Y. Tanaka, Y. Yamamoto, *Biochemistry*, 2006, **45**, 6765-6772.

17. K. Suntharalingam, A. J. P. White, R. Vilar, *Inorg. Chem.*, 2010, **49**, 8371-8380.

18. S. N. Georgiades, N. H. Abd Karim, K. Suntharalingam, R. Vilar, *Angew. Chem. Int. Ed.*, 2010, **49**, 4020-4034.

19. L. Petraccone, E. Erra, V. Esposito, A. Randazzo, L. Mayol, L. Nasti, G. Barone, C. Giancola, *Biochemistry*, 2004, **43**, 4877-4884.

20. M. J. Hannon, *Chem. Soc. Rev.*, 2007, **36**, 280-295.

21. S. Komeda, T. Moulaei, K. K. Woods, M. Chikuma, N. P. Farrell, L. D. Williams, *J. Am. Chem. Soc.*, 2006, **128**, 16092-16103.

22. S. Li, V. R. Cooper, T. Thonhauser, B. I. Lundqvist, D. C. Langreth, *J. Phys. Chem. B*, 2009, **113**, 11166-11172.

23. C. A. Frederick, L. D. Williams, G. Ughetto, G. A. van der Marel, J. H. van Boom, A. Rich, A. H. Wang, *Biochemistry*, 1990, **29**, 2538-2549.

24. K. E. Erkkila, D. T. Odom, J. K. Barton, *Chem. Rev.*, 1999, **99**, 2777-2295.

25. B. M. Zeglis, V. C. Pierre, J. K. Barton, *Chem. Commun*., 2007, **44**, 4565-4579.

26. M. R. Osborne, D. E. V. Wilman, P. D. Lawleyt, *Chem. Res. Toxicol.*, 1995, **8**, 316-320.

27. B. Lippert, *Cisplatin, Chemistry and Biochemistry of a Leading Anticancer Drug*, Wiley-VCH, Weinheim, 1999.

28. P. M. Takahara, A. C. Rosenzweig, C. A. Frederick, S. J. Lippard, *Nature*, 1995, **377**, 649-652.

29. L. H. Hurley, R. Petrusek, *Nature*, 1979, **282**, 529-531.

30. M. Rettig, M. Weingarth, W. Langel, A. Kamal, P. P. Kumar, K. Weisz, *Biochemistry*, 2009, **48**, 12223-12232.

31. X. Cai, P. J. Gray, D. D. Von Hoff, *Cancer Treat. Rev.*, 2009, **35**, 437–450.

32. T. A. Larsen, D. S. Goodsell, D. Cascio, K. Grzeskowiak and R. E. Dickerson, *J. Biomol. Struct. Dyn.*, 1989, **7**, 477-491.

33. T. Grawe, G. Schafer, T. Schrader, *Org. Lett.*, 2003, **5**, 1641-1644.

34. P. B. Dervan, *Bioorg. Med. Chem.*, 2001, **9**, 2215-2235.

35. M. J. Hannon, *Chem. Soc. Rev.*, 2007, **36**, 280-295.

36. R. Goobes, O. Cohen, A. Minsky, *Nucleic Acids Res.*, 2002, **30**, 2154-2161.

37. T. Ihara, T. Ishii, N. Araki, A. W. Wilson, A. Jyo, *J. Am. Chem. Soc.*, 2009, **131**, 3826- 3827.

38. M. J. Hannon, V. Moreno, M. J. Prieto, E. Moldrheim, E. Sletten, I. Meistermann, C. J. Issak, K. J. Sanders, A. Rodger, *Angew. Chem., Int. Ed.*, 2001, **40**, 879-884.

39. A. Oleksi, A. G. Blanco, R. Boer, I. Usón, J. Aymamí, A. Rodger, M. J. Hannon, M. Coll, *Angew. Chem., Int. Ed.*, 2006, **45**, 1227-1231.

40. R. Kieltyka, P. Englebienne, J. Fakhoury, C. Autexier, N. Moitessier, H. F. Sleiman, *J. Am. Chem. Soc.*, 2008, **130**, 10040-10041.

41. H. Yu, X. Wang, M. Fu, J. Ren, X. Qu, *Nucleic Acids Res.*, 2008, **36**, 5695-5703.

42. C. Zhao, J. Geng, L. Feng, J. Ren, X. Qu, *Chem. Eur. J.*, 2011, **17**, 8209-8215.

43. S. Phongtongpasuk personal communication.

44. J.-M. Lehn, A. Rigault, J. Siegel, J. Harrowfield, B. Chevrier, D. Moras, *Proc. Natl. Acad. Sci. U.S.A.*, 1987, **84**, 2565-2569.

45. M. Meyer, B. Kersting, R. E. Powers, K. N. Raymond, *Inorg. Chem.*, 1997, **36**, 5179-5191.

46. C. Piguet, G. Bernardinelli, G. Hopfgartner, *Chem. Rev.*, 1997, **97**, 2005-2062.

47. M. Albrecht, R. Fröhlich, *Bull. Chem. Soc. Jpn.*, 2007, **80**, 797-808.

48. C. He, Y. Zhao, D. Guo, Z. Lin, C. Duan, *Eur. J. Inorg. Chem.*, 2007, **22**, 3451-3463.

49. A. V. Wiznycia, J. Desper, C. J. Levy, *Inorg. Chem.*, 2006, **45**, 10034-10036.

50. E. C. Constable, M. G. B, Drew, G. Forsyth, M. D. Ward, *J. Chem. Soc., Chem. Commun.*, 1988, **22**, 1450-1451.

51. E. C. Constable, M. A. M. Daniels, M. G. B. Drew, D. A. Tocher, J. V. Walkera, P. D. Wooda, *J. Chem. Soc. Dalton Trans.*, 1993, **13**, 1947-1958.

52. S. De, M. G. B. Drew, D. Datta, *Inorg. Chim. Acta*, 2010, **363**, 4123-4126.

53. J. C. Jeffery, T. Riis-Johannessen, C. J. Anderson, C. J. Adams, A. Robinson, S. P. Argent, M. D. Ward, C. R. Rice, *Inorg. Chem.*, 2007, **46**, 2417-2426.

54. V. Amendola, M. Boiocchi, V. Brega, L. Fabbrizzi, L. Mosca, *Inorg. Chem.*, 2010, **49**, 997-1007.

55. D. Amabilino, J. F. Stoddart, *Chem. Rev.*, 1995, **95**, 2725-2828.

56. K.-C. Sham, H.-L. Yeung, S.-M. Yiu, T.-C. Lau, H.-L. Kwong, *Dalton Trans.*, 2010, **39**, 9469-9471.

57. H. B. T. Jeazet, K. Gloe, T. Doert, O. N. Kataeva, A. Jäger, G. Geipel, G Bernhard, B. Büchnerd, K. Gloe, *Chem. Commun.*, 2010, **46**, 2373-2375.

58. M. Albrecht, *Chem. Eur. J.*, 2000, **6**, 3485-3489.

59. R. C. Scarrow, D. L. White, K. N. Raymond, *J. Am. Chem. Soc.*, 1985, **107**, 6540-6546.

60. J. Hamacek, S. Blanc, M. Elhabiri, E. Leize, A. Van Dorsselaer, C. Piguet, A. M. Albrecht-Gary, J. Am. Chem. Soc., 2003, **125**, 1541-1550.

61. T. Kreickmann, C. Diedrich, T. Pape, H. Vinh Huynh, S. Grimme, F. E. Hahn, *J. Am. Chem. Soc.*, 2006, **128**, 11808-11819.

62. M. J. Hannon, C. L. Painting, A. Jackson, J. Hamblin, W. Errington, *Chem. Commun.*, 1997, 1807-1808.

63. Z. Zhang, D. Dolphin, *Inorg. Chem.*, 2010, **49**, 11550-11555.

64. D. A. McMorran, P. J. Steel, *Angew. Chem., Int. Ed.*, 1998, **37**, 3295-3297.

65. J. Xu, K. N. Raymond, *Angew. Chem., Int. Ed.*, 2006, **45**, 6480-6485.

66. H. S. Sahoo, D. K. Chand, *Dalton Trans.*, 2010, **39**, 7223-7225.

67. N. P. Farrell, *Comprehensive Coordination Chemistry II*, 2003, **9**, 809-840.

68. P. C. A. Bruijnincx, P. J. Sadler, *Curr. Opin. Chem. Biol.*, 2008, **12**, 197-206.

69. Y. Jung, S. J. Lippard, *Chem. Rev.*, 2007, **107**, 1387-1407.

70. J. Reedijk, *Chem. Commun.*, 1996, **7**, 801-806.

71. R. A. Alderden, M. D. Hall, T. W. Hambley, *J. Chem. Ed.*, 2006, **83**, 728-734.

72. S. C. Dhara, *Indian J. Chem.*, 1970, **8**, 193-134.

73. F. Basolo, *Coord. Chem. Rev.*, 1996, **154**, 151-161.

74. S. J. Lippard, E. R. Jamieson, *Chem. Rev.*, 1999, **99**, 2467-2498.

75. J. Reedijk, *Pure Appl. Chem.*, 1987, **59**, 181.

76. P. M. Takahara, A. C. Rosenzweig, C. A. Frederick, S. J. Lippard, *Nature*, 1995, **377**, 649-652.

77. M. R. Rajeswari, A. Jain, *Curr. Sci.*, 2002, **82**, 838-844.

78. U. M. Ohndorf, M. A. Rould, Q. He, C. O. Pabo, S. J. Lippard, *Nature*, 1999, **399**, 708-712.

79. M. J. Hannon, *Chem. Soc. Rev.*, 2007, **36**, 280-295.

80. A. M. Pizarro, P. J. Sadler, *Biochimie*, 2009, **91**, 1198-1211.

81. D. Wang, S. J. Lippard, *Nat. Rev. Drug. Discov.*, 2005, **4**, 307-320.

82. B. Rosenberg, *Nucleic Acid-Metal Ion Interactions*, John Wiley & Sons, New York, 1980.

83. G. Chu, *J. Biol. Chem.*, 1994, **269**, 787-790.

84. K. Kartalou, *Mutat. Res.*, 2001, **478**, 23-43.

85. E. R. Jamieson, S. J. Lippard, *Chem. Rev.*, 1999, **99**, 2467-2498.

86. Z. Guo, P. J. Sadler, *Adv. Inorg. Chem.*, 2000, **49**, 183-306.

87. K. Woźniak, J. Błasiak, *Acta Biochim. Pol.*, 2002, **49**, 583-596.

88. M. J. Hannon, *Pure and Appl. Chem.*, 2007, **79**, 2243-2261.

89. S. B. Duffull, B. A. Robinson, *Clin. Pharmacokinet.*, 1997, **33**,161-183.

90. R. S. Go, A. A. Adjei, *J. Clin. Oncol.*, 1999, **17**, 409-422.

91. N. E. Alberto, M. F. A. Lucas, M. Pavelka, N. Russo, *J. Phys. Chem. B.*, 2009, **113**, 14473-14479.

92. J. Graham, M. Muhsin, P. Kirkpatrick, *Nat. Rev. Drug Discovery*, 2004, **3**, 11-12.

93. S. S. Hah, R. A. Sumbad, R. W. de Vere White, K. W. Turteltaub, P. T. Henderson, *Chem. Res. Toxicol.*, 2007, **20**, 1745-1751.

94. M. J. McKeage, *Expert Opin. Investig. Drugs*, 2001, **10**, 119-128.

95. J. A. Gietema, G. J. Veldhuis, H. J. Guchelaar, *Br. J. Cancer*, 1995, **71**, 1302-1307.

96. M. D. Hall, H. R. Mellor, R. Callaghan, T. W. Hambley, *J. Med. Chem.*, 2007, **50**, 3403-3411.

97. K. J. Haxton, H. M. Burt, *J. Pharm. Sci.*, 2009, **98**, 2299-2316.

98. L. Kelland, *Expert Opin. Invest. Drugs*, 2007, **16**, 1009-1021.

99. W. Liu, X. Chen, Q. Ye, Y. Xu, C. Xie, M. Xie, Q. Chang, L. Lou, *Inorg. Chem.*, 2011, **50**, 5324-5326.

100. A. M. Pizarro, P. J. Sadler, *Biochimie*, 2009, **91**, 1198-1211.

101. M. D. Hall, T. W. Hambley, *Coord. Chem. Rev.*, 2002, **232**, 49-67.

102. W. H. Ang, S. Pilet, R. Scopelliti, F. Bussy, L. Juillerat-Jeanneret, P. J. Dyson, *J. Med. Chem.*, 2005, **48**, 8060- 8069.

103. M. D. Hall, H. R. Mellor, R. Callaghan, T. W. Hambley, *J. Med. Chem.*, 2007, **50**, 3403-3411.

104. U. Schatzschneider, *Eur. J. Inorg. Chem.*, 2010, **10**, 1451-1467.

105. F. Huq, A. Alshehri, P. Beale, J. Q. Yu, Biomedical and Pharmaceutical Engineering, ICBPE, 2009, *Synergism from combination of platinum in ovarian cancer*, 1-3.

106. S. Lee, T. V. O'Halloran, S. T. Nguyen, *J. Am. Chem. Soc.*, 2010, **132**, 17130-17138.

107. N. M. F. S. A. Cerqueira, P. A. Fernandes, M. J. Ramos, *Chem. Eur. J.*, 2007, **13**, 8507-8515.

108. A. M. Bergman, P. P. Eijk, V. W. Ruiz van Haperen, K. Smid, G. Veerman, I. Hubeek, P. van den Ijssel, B. Ylstra, G. J. Peters, *Cancer Res.*, 2005, **65**, 9510-9516.

109. J. T. Thigpen, M. F. Brady, H. D. Homesley, J. Malfetano, B. DuBeshter, R. A. Burger, S. Liao, *J. Clin. Oncol.*, 2004, **22**, 3902-3908.

110. A. D. K. Sauter, E. A. Magun, M. S. Iordanov and B. E. Magun, *Cancer Biol. Ther.*, 2010, **10**, 258-266.

111. Y. H. Li, F. H. Wang, W. Q. Jiang, X. J. Xiang, Y. M. Deng, G. Q. Hu, D. M. Xu, Y. Chen, Q. Lin, Y. J. He, *Cancer Chemother. Pharmacol.*, 2008, **62**, 539-544.

112. D. B. Longley, D. P. Harkin, P. G. Johnston, *Nat. Rev. Cancer*, 2003, **3**, 330-338.

113. Y. H. Park, J. L. Lee, B. Y. Ryoo, M. H. Ryu, S. H. Yang, B. S. Kim, D. B. Shin, H. M. Chang, T. W. Kim, Y. J. Yuh, Y. K. Kang, *Cancer Chemother. Pharmacol.*, 2008, **61**, 623-629.

114. D. B. Smith, J. P. Neoptolemos, *Expert Opin. Pharmaco.*, 2006, **7**, 1633-1639.

115. C. Andreetta, C. Puppin, A. Minisini, F. Valent, E. Pegolo, G. Damante, C. Di Loreto, S. Pizzolitto, M. Pandolfi, G. Fasola, *Ann. Oncol.*, 2009, **20**, 265-71.

116. H. Brunner, H. Obermeier, *Angew. Chem., Int. Ad. Engl.*, 1994, **33**, 2214-2215.

117. H. Kostrhunova, V. Brabec, *Biochemistry*, 2000, **39**, 12639-12649.

118. I. Łakomska, H. Kooijman, A. L. Spek, W. Z. Shen, J. Reedijk, *Dalton Trans.*, 2009, **48**, 10736-10741.

119. A. Herman, J. M. Tanski, M. F. Tibbetts, C. M. Anderson, *Inorg. Chem.*, 2008, **47**, 274-280.

120. A. Jain, J. Wang, E. R. Mashack, B. S. J. Winkel, K. J. Brewer, *Inorg. Chem.*, 2009, **48**, 9077-9084.

121. Z. Xue, M. Lin, J. Zhu, J. Zhang, Y. Lia and Z. Guo, *Chem. Commun.*, 2010, **46**, 1212-1214.

122. A. A. Bhirde, V. Patel, J. Gavard, G. Zhang, A. A. Sousa, A. Masedunskas, R. D. Leapman, R. Weigert, J. S. Gutkind, J. F. Rusling, *ACS Nano*, 2009, **3**, 307-316.

123. V. Moreno, J. Lorenzo, F. X. Aviles, M. H. Garcia, J. P. Ribeiro, T. S.Morais, P. Florindo, M. P. Robalo, *Bioinorg. Chem. Appl.*, 2010, 1-11.

124. E. S. Antonarakis, A. Emadi, *Cancer Chemother. Pharmacol.*, 2010, **66**, 1-9.

125. Y. K. Yan, M. Melchart, A. Habtemariam, P. J. Sadler. *Chem. Commun*, 2005, 4764-4776.

126. M. J. Hannon, *Pure Appl. Chem.*, 2007, **79**, 2243-2261.

127. C. Scolaro, A. Bergamo, L. Brescacin, R. Delfino, M. Cocchietto, G. Laurenczy, T. J. Geldbach, G. Sava and P. J. Dyson, *J. Med. Chem.*, 2005, **48**, 4161-4171.

128. S. Chatterjee, S. Kundu, A. Bhattacharyya, C. G. Hartinger, P. J. Dyson, *J. Biol. Inorg. Chem.*, 2008, **13**, 1149-1155.

129. F. Linares, M. A. Galindo, S. Galli, M. A. Romero, J. A. R. Navarro and E. Barea, *Inorg. Chem.*, 2009, **48**, 7413-7420.

130. N. Katsaros, A. Anagnostopoulou, *Crit. Re*v. *Oncol. Hemat.*, 2002, **42**, 297–308.

131. H. T. Chifotides and K. R. Dunbar, *Acc. Chem. Res.*, 2005, **38**, 146-156.

132. M. Harlos, I. Ott, R. Gust, H. Alborzinia, S. Wölfl, A. Kromm, and W. S. Sheldrick, *J. Med. Chem.*, 2008, **51**, 3924-3933.

133. M. Dobroschke, Y. Geldmacher, I. Ott, M. Harlos, L. Kater, L. Wagner, R. Gust, W. S. Sheldrick, A. Prokop, *Chem. Med. Chem.*, 2009, **4**, 177-187.

134. S. Wirth, C. J. Rohbogner, M. Cieslak, J. Kazmierczak-Baranska, S. Donevski, B. Nawrot, I. P. Lorenz, *J. Biol. Inorg. Chem.*, 2010, **15**, 429-440.

135. I. Ott and R. Gust, *Arch. Pharm. Chem. Life Sci.*, 2007, **340**, 117-126.

136. R. A. Giroux, S. M. Hecht, *J. Am. Chem. Soc.*, 2010, **132**, 16987-16996.

137. L. R. Solomon, R. D. Bereelli, P. L. Moselei, *Biochemistry*, 1989, **28**, 9932-9937.

138. T. S. Lange1, K. K. Kim, R. K. Singh, R. M. Strongin, C. K. McCourt1, L. Brard, *Plos one*, 2008, **3**, 1-10.

139. S. Saha, R. Majumdar, M. Roy, R. R. Dighe, A. R. Chakravarty, *Inorg. Chem.*, 2009, **48**, 2652-2663.

140. S. Nobili, E. Mini,1 I. Landini, C. Gabbiani, A. Casini, L. Messori, *Med. Res. Rev.*,

141. E. Vergara, E. Cerrada, A. Casini, O. Zava, M. Laguna, P. J. Dyson, *Organometallics*, 2010, **29**, 2596-2603.

142. A. Casini, M. A. Cinellu, G. Minghetti, C. Gabbiani, M. Coronnello, E. Mini, L. Messori, *J. Med. Chem.*, 2006, **49**, 5524-5531.

143. L. Cattaruzza, D. Fregona, M. Mongiat1, L. Ronconi, A. Fassina, A. Colombatti, D. Aldinucci, *Int. J. Cancer*, 2011, **128**, 206-215.

Chapter 2

Introducing new properties on cylinders

2.1 Introduction

Cisplatin is the most effective antineoplastic agent used in clinics to treat various types of cancers, particularly head and neck, testicular, ovarian, bladder and small cell lung cancers. However, undesirable side-effects such as nephrotoxicity, ototoxicity, neurotoxicity, bone marrow suppression and acquired resistance associated with cisplatin treatment are the main drawbacks which limit the use of this drug.[1] In the search for more effective and less toxic antitumor agents, various metal-based compounds have been synthesised. Among them is an iron(II) triple stranded helicate developed in Hannon`s laboratory.[2]

The synthesised supramolecular helicate (see Fig. 1.29, page 28) is a dinuclear tetracationic metal-based complex which is similar in size (approximately 2 nm in length and 1 nm in diameter) and shape to the DNA zinc finger motif present in some regulatory proteins. The iron(II) helicate is based on bis-pyridylimine ligands wrapped around two iron(II) metal centres in a helical fashion. The compound binds non-covalently to the DNA major groove and induces intramolecular DNA coiling.[3] Moreover, the iron(II) triple helicate can also bind to the DNA three way junction with a helicate located in the centre of the junction.[4] Biological testing of the synthesized complex revealed a good cytotoxic profile. The iron(II) tetracationic cylinder affects mitochondrial function by reducing its activity, inhibits the cell cycle and induces apoptosis, programmed cell death.[5]

Cisplatin and the iron(II) triple-stranded helicate are examples of compounds with anticancer properties that act by different molecular mechanisms. Cisplatin is a coordinative DNA binder whereas Hannon`s iron(II) helicate binds non-covalently to the DNA major groove or in the cavity of a DNA three way junction. It would be an

interesting approach to design a synthetic agent that would combine these two different modes of action as that might result in higher cytotoxic activity.

2.2 Research aims and molecular design

The aim of this project is to synthesise novel supramolecular cylinders by using simple metal–ligand interactions and combine them with cisplatin in order to create a synthetic agent that will act in biological systems by two different molecular mechanisms and have enhanced antitumor properties against a wide spectrum of cancers. Additional metal binding units will be introduced onto the outside of the supramolecular architecture to attach a cisplatin moiety (Fig. 2.0). The mixed-metal iron(II)–platinum(II) helicate will possess a high cationic charge which will contribute to the interaction with negatively charged DNA.

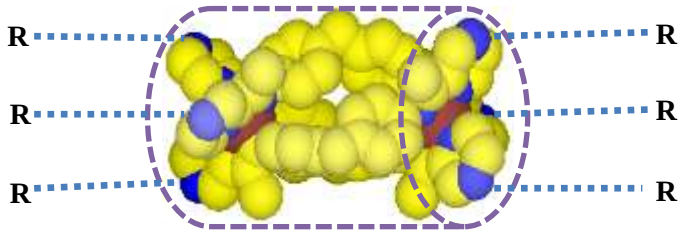

Figure 2.0 Schematic illustration of iron(II) pyrazine supramolecular cylinder[6] (iron, brown; nitrogen, blue; hydrocarbon framework, yellow) with attached cisplatin (R).

Using various techniques from chemistry and biology, the properties and biological activity of the synthesised polynuclear metal compounds will be characterised and explored.

2.3 Multinuclear platinum metal complexes

A few multinuclear platinum metal complexes, where several platinum metal centres are linked together by ligand have been reported in the literature, including Farrell's trinuclear platinum compound that binds to the DNA sugar phosphate backbone[7] (see chapter 1, 1.3.3.1) and a tetranuclear platinum molecular cage reported by Sleiman and co-workers[8] that binds to the DNA G-quadruplex (see chapter 1, 1.3.3.7). Examples of other multinuclear platinum agents are relatively rare and only a few of them are presented in this thesis.

Lippert and co-workers have reported a mixed-metal molecular triangle formed from [(en)Pd(2,2'-bpz-N^1,$N^{1'}$)]$^{2+}$ and *trans*-$(NH_3)_2$Pt(II) (Fig. 2.1).[9]

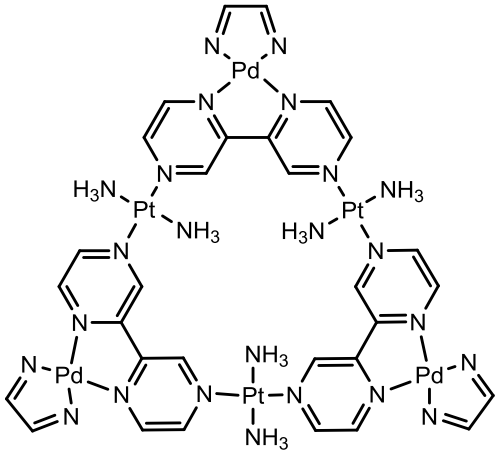

Figure 2.1 Lippert's mixed-metal molecular triangle.

The palladium(II) ions form three vertices of molecular triangle whereas platinum(II) ions are located in the sides. The NH_3 ligands of platinum(II) metal ions are roughly perpendicular to the triangle plane. The triangle encapsulates a single ClO_4^- anion which is held by hydrogen bonding.9 The activity of the synthesised triangle has

not been reported however, the anticancer properties of related compounds will be discussed in chapter 4 (see 4.3.2).

Lowe *et al.* have synthesised polynuclear 2,2':6',2''-terpyridineplatinum(II) complexes that exhibit cytotoxic activity against a number of ovarian cancer cell lines including cell lines resistant to cisplatin and doxorubicin (Fig. 2.2).[10]

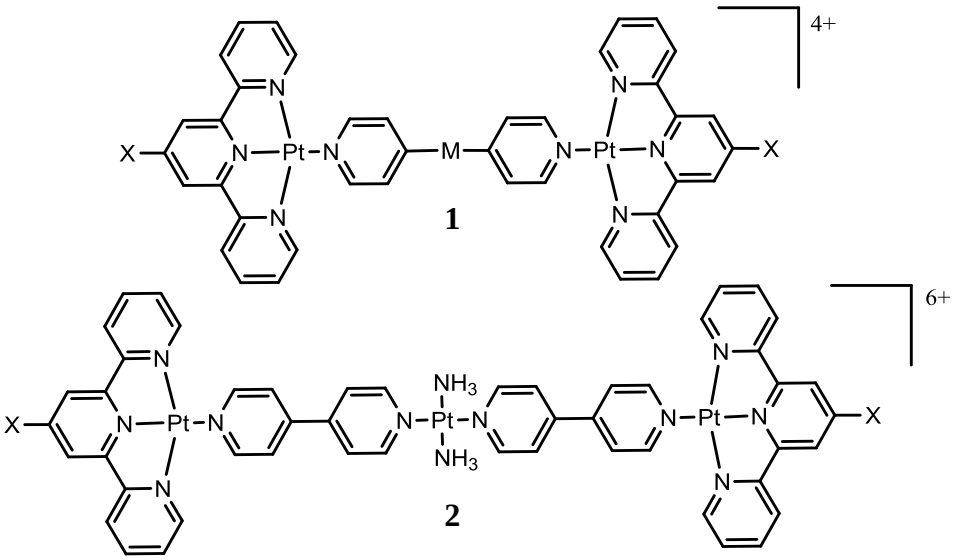

Figure 2.2 Structures of Lowe`s platinum(II) complexes.

2,2':6',2''-Terpyridineplatinum(II) complexes are known to intercalate into DNA. The antitumour activity of these compounds is strongly dependent on the nature of the linker. The complexes with a short and rigid linker are among the most effective however, complex **2** (X = H and Cl) with a long linker exhibited high activity in most ovarian cancer cell lines which suggests that activity may correlate with charge density and electrostatic stress within these molecules caused by the double positive charge on each Pt(II). The bis-intercalator **1** (X = H, M = *trans*-CH=CH-) showed the lowest IC_{50} values in CH1, A2780 and SKOV-3 and was found effective against cisplatin-resistant cell lines.[10]

Sun and Shao have described a trinuclear cyclometalated Pt(II) 4,6-diphenyl-2,2'-bipyridyl complex with a bis-(diphenylphosphinomethyl)phenylphosphine bridging ligand (Fig. 2.3).[11]

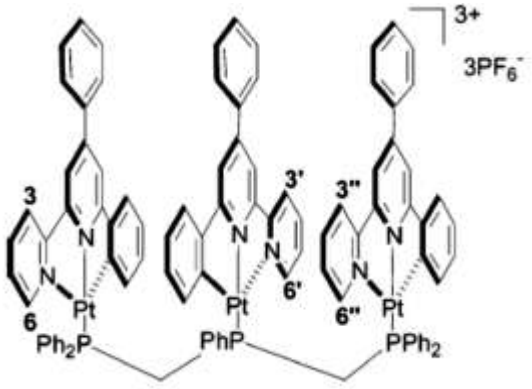

Figure 2.3 Structure of trinuclear platinum complex reported by Sun and Shao.[11]

According to the X-ray crystal structure, each platinum(II) metal center has a distorted square-planar geometry. Three cyclometalated platinum(II) 4,6-diphenyl-2,2'-bipyridyl moieties are arranged in a linear face-to-face configuration by the bridging ligand and are almost parallel to each other. This complex has relatively strong Pt-Pt interactions.[11] The activity and DNA binding studies of these polynuclear species has not been reported.

Lusby *et al.* reported a tetranuclear platinum square containing 4,4'-bipyridine units and 2,6-diphenyl pyridine as a ligand (Fig. 2.4).[12] Remarkably, the complex assembles in the presence of acid and dissembles in the presence of base. The X-ray structure confirmed the formation of tetrameric molecular-square structure. The 4,4'-bipyridine units that are located *trans*- to the nitrogen donor of the ligand have a planar conformation and lie perpendicular to the plane of the four platinum metal ions. The other 4,4'-bipyridine units have nonplanar conformation with two hydrogen atom from

each pyridine component slightly pointing to the centre of the square. Such a conformation of the complex is due to π-π interactions between these constituent pyridine components and phenyl groups of the ligand. To avoid steric effects the phenyl moieties are located above or below the plane of the four platinum metal ions.[12]

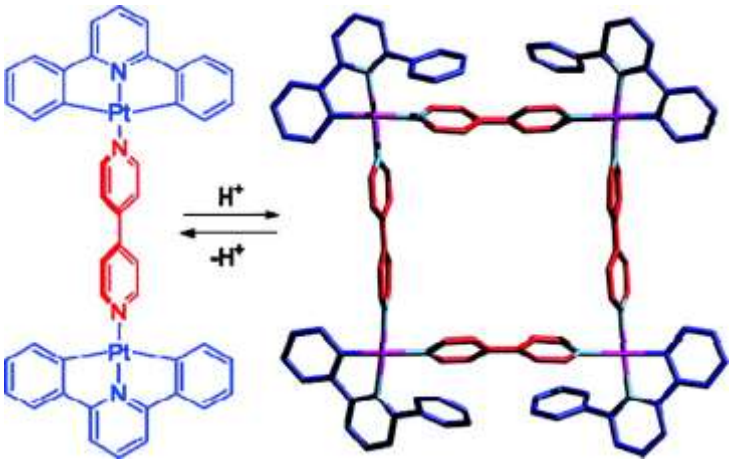

Figure 2.4 X-ray structure of molecular square reported by Lusby. The carbon atoms of 4,4'-bipyridine are shown in red, carbon atoms of ligand in dark blue, platinum atoms in pink, and nitrogen atoms in pale blue. Four PF_6 counteranions and five nitromethane solvent molecules have been omitted for clarity.[12]

Despite the similarity to the Fujita`s square studied by Moreno and Sleiman,8 DNA binding studies and cytotoxic activity of this cationic square have not been investigated.

More recently, Brabec and co-workers described dinuclear platinum(II) complexes containing aromatic linkers (Fig. 2.5).[13] Both of the compounds exhibited antineoplastic activity in A2780 cancer cell lines comparable to cisplatin with compound **4** being less cytotoxic. Importantly, **3** and **4** were more active than cisplatin in cisplatin-resistant A2780cisR cancer cell line and again **4** was less active than **3**. The compounds were shown to bind to ct-DNA and form a higher percentage of interstrand

cross-links (**3** ~ 48 %; **4** ~ 20 %) than cisplatin. A considerably lower level of repair synthesis was observed for DNA adducts formed by **3** and **4** than for cisplatin suggesting enhanced resistivity against repair processes which contribute to the ability of these compounds to overcome resistance of cancer cells to cisplatin.

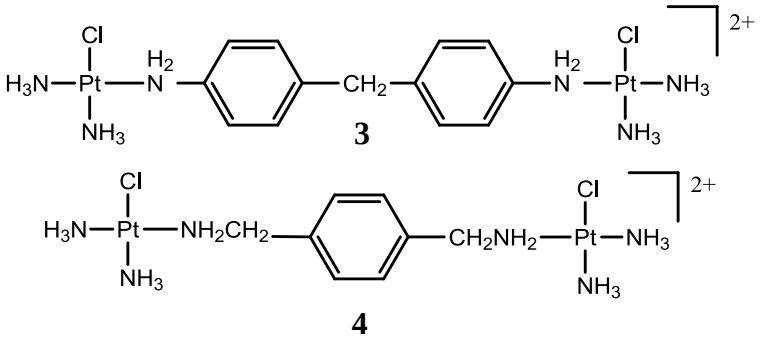

Figure 2.5 Structures of the platinum complexes reported by Brabec.

2.4 Synthesis of metal-based supramolecular helicates and combining them with cisplatin.

2.4.1 Ligand L_1

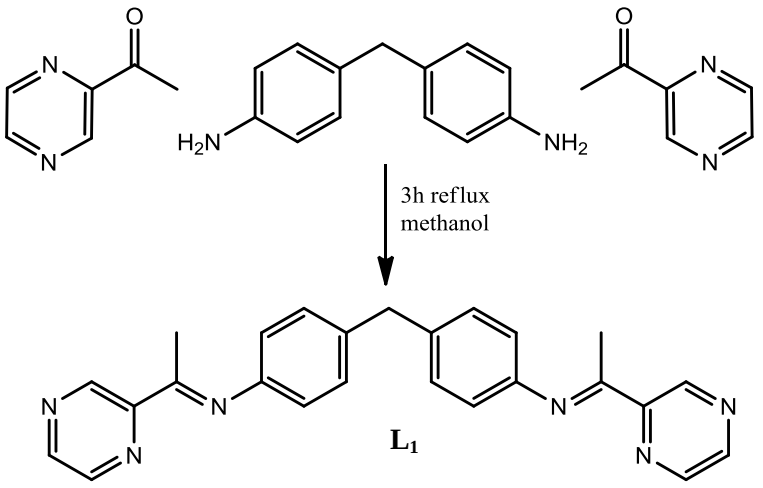

Scheme 2.0 Schematic procedure for the synthesis of ligand L_1

Ligand L_1 was synthesised according to a similar procedure reported in the literature.[14] Two equivalents of 2-acetylpyrazine were mixed with one equivalent of

4,4'-methylenedianiline using a few drops of acetic acid as a catalyst. The reaction mixture was heated to reflux for 3 hours under an atmosphere of nitrogen to yield the crude product as a yellow sticky oil. The ESI mass spectrum data shows a dominant single peak at *m/z* = 429 which corresponds to $[L_1 + Na]^+$ and a small peak at *m/z* = 325 which corresponds to $C_{19}H_{18}N_4$ (incomplete ligand). ^{1}H NMR confirms the formation of the ligand L_1 as the major product, however unreacted starting materials and incomplete ligand were also present in the mixture (Fig. 2.6).

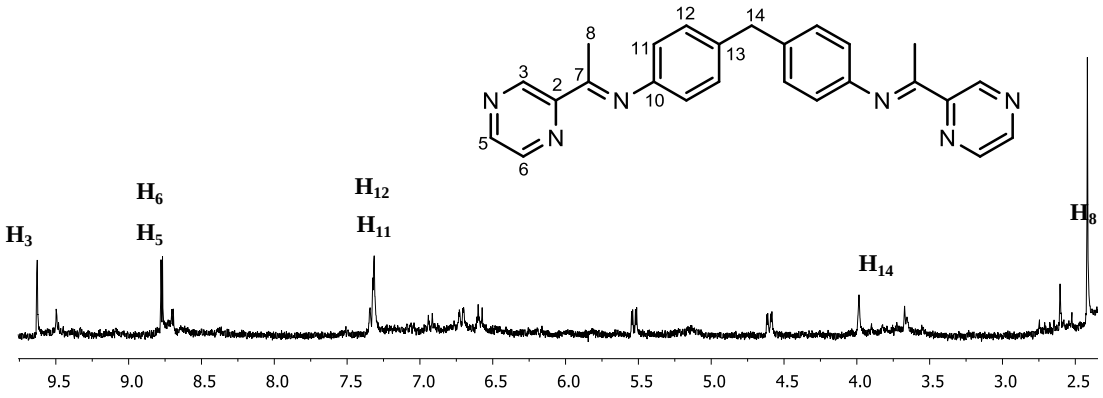

Figure 2.6 300 MHz ^{1}H NMR spectrum (CD_3CN, 298 K) of the ligand L_1.

Attempts to separate the ligand L_1 from the impurities using column chromatography failed. Therefore the following step was carried out without purification of the ligand.

2.4.1.1 Synthesis of iron(II) complex of L_1

To a solution of ligand L_1 in methanol, iron(II) chloride tetrahydrate was added and the reaction mixture was heated to reflux for 1 hour.[14] The formed purple solution was cooled down and the metal complex was precipitated with diethyl ether. The ^{1}H NMR spectrum revealed a broad set of signals for the iron(II) complex of L_1 with impurities present in the mixture. In order to purify the compound, it was crystallised in

an H-tube. One arm of the H-tube was filled with a methanolic solution of the chloride salt of the crude mixture of the complex and the other with a saturated methanolic solution of ammonium hexafluorophosphate. Both arms of the H-tube were filled to the top with methanol and covered with parafilm. After 4 - 5 days crystals of the $[Fe_2(C_{25}H_{22}N_6)_3](PF_6)_4$ complex were formed and those were collected from the H-tube by filtration.

The ESI spectrum shows a peak at *m/z* = 332 which corresponds to a $[Fe_2(C_{25}H_{22}N_6)_3]^{4+}$ species. The UV/Vis absorption spectrum reveals a broad band located at 570 nm (ε = 16500 $mol^{-1}dm^3cm^{-1}$) corresponding to a metal-ligand charge transfer which confirms coordination of the iron(II) to L_1 ligands. Partial elemental analysis supports the formation of the complex with an empirical formula of $[Fe_2(C_{25}H_{22}N_6)_3](PF_6)_4 \bullet H_2O$. The ^1H NMR spectrum of the iron(II) complex was recorded in CD_3CN (Fig. 2.7).

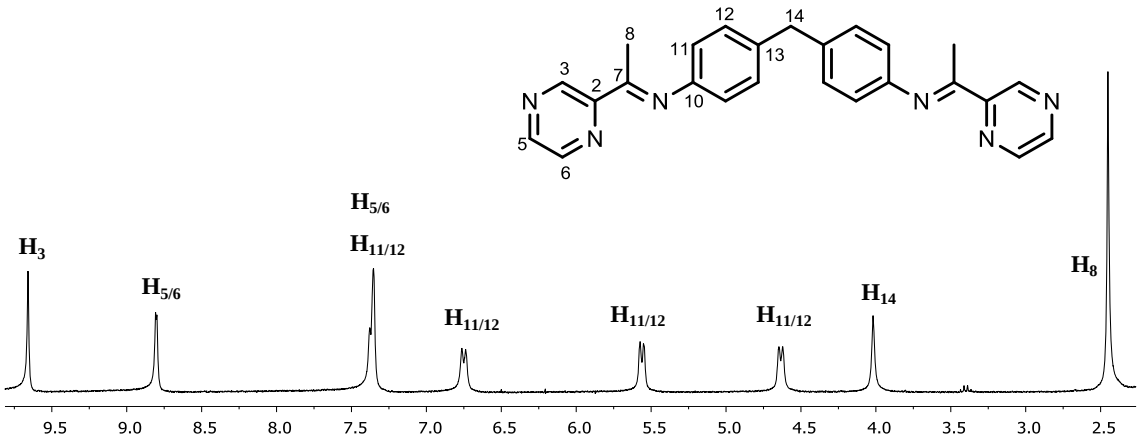

Figure 2.7 300 MHz ^1H NMR spectrum (CD_3CN, 298 K) of $[Fe_2(L_1)_3](PF_6)_4$.

The ^1H NMR spectrum shows a single set of peaks corresponding to a single symmetrical species of the complex formed in solution. The resonance corresponding to

the methyl protons H_8 appears as a singlet in the aliphatic region of the spectrum. Pyrazine protons H_3, H_5, H_6 experience reduced electronic density due to the presence of electronegative nitrogen atoms and their chemical shifts appear downfield in the spectrum. The ^{1}H NMR signal of one of the pyrazine protons $H_{5/6}$ overlaps with one of the signals arising from phenyl rings. Phenyl resonances H_9, H_{10} appear as four separate resonances as the phenyl rings are spinning slowly. It was previously reported by the Hannon group that with an increase in temperature the spinning of the phenyl rings increases and these resonances appear as two sharp singlets.[15]

2.4.1.2 Combining $[Fe_2(L_1)_3](PF_6)_4$ with cisplatin

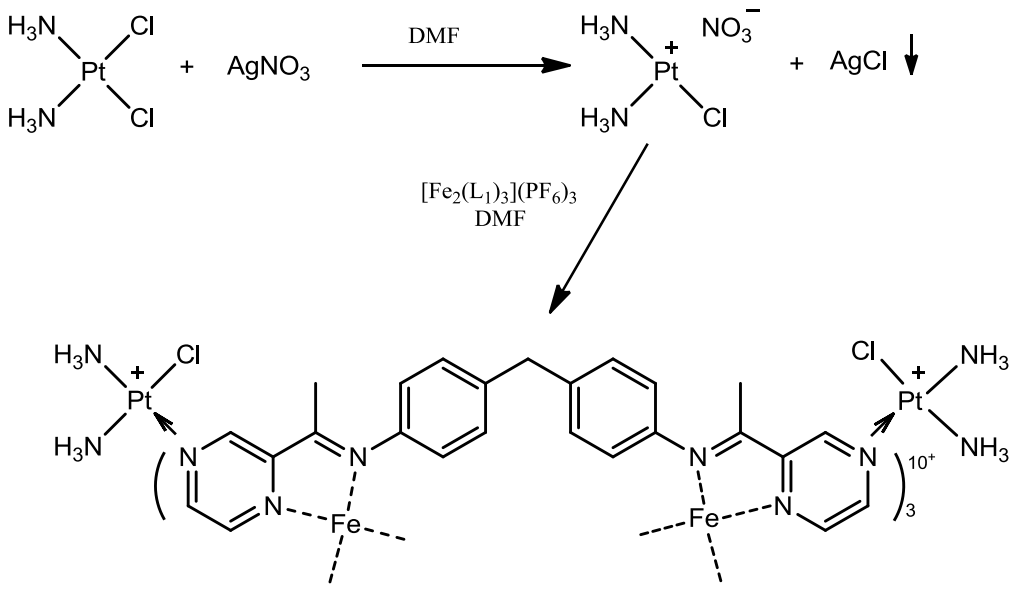

Scheme 2.1 Schematic procedure for combining cisplatin with $[Fe_2(L_1)_3](PF_6)_4$

Silver nitrate was stirred with cisplatin overnight in DMF with light exclusion. The $[Fe_2(L_1)_3](PF_6)_4$ complex in DMF was then added to the resulting solution and the reaction mixture was stirred for 3 hours at -18 ºC and 1 hour at room temperature. The

resulting blue solution was passed though celite to remove silver chloride that had precipitated. Direct precipitation of the complex from DMF with diethyl ether resulted in $[Fe_2(L_1)_3](PF_6)_4$ without cisplatin attached which was confirmed by NMR. Therefore the solvent was removed *in vacuo* without heating to avoid decomposition of the complex. The synthesised compound is poorly soluble in water but very soluble in DMF and thus it is unsuitable for DNA-binding studies where solubility is a crucial criterion. The complex itself is not stable at room temperature when dissolved in water or DMF and therefore the solution was kept at low temperatures. Attempts to grow crystals of the synthesised complex for X-ray analysis were unsuccessful.

Various mass spectrometry techniques such as MALDI, FAB and ESI were used in order to characterise the synthesised compound, however no peaks corresponding to the desired complex were observed. The ESI spectrum of counteranions of the iron(II)–platinum(II) complex was recorded. The spectrum shows two peaks corresponding to NO_3^- and PF_6^- species present in the complex. The infrared spectrum shows signals that can be assigned as υN-H stretching at 3210 cm^{-1} and υN-H symmetrical bending at 1323 cm^{-1}. Partial microanalysis is consistent with the empirical formula of $[Fe_2(C_{25}H_{22}N_6(Pt_2Cl_2(NH_3)_4))_3](PF_6)_4(NO_3)_6$. A ^1H NMR spectrum of the complex was recorded in d_6-DMF solution and compared to the one of the $[Fe_2(L_1)_3](PF_6)_4$ complex in d_6-DMF (Fig. 2.8).

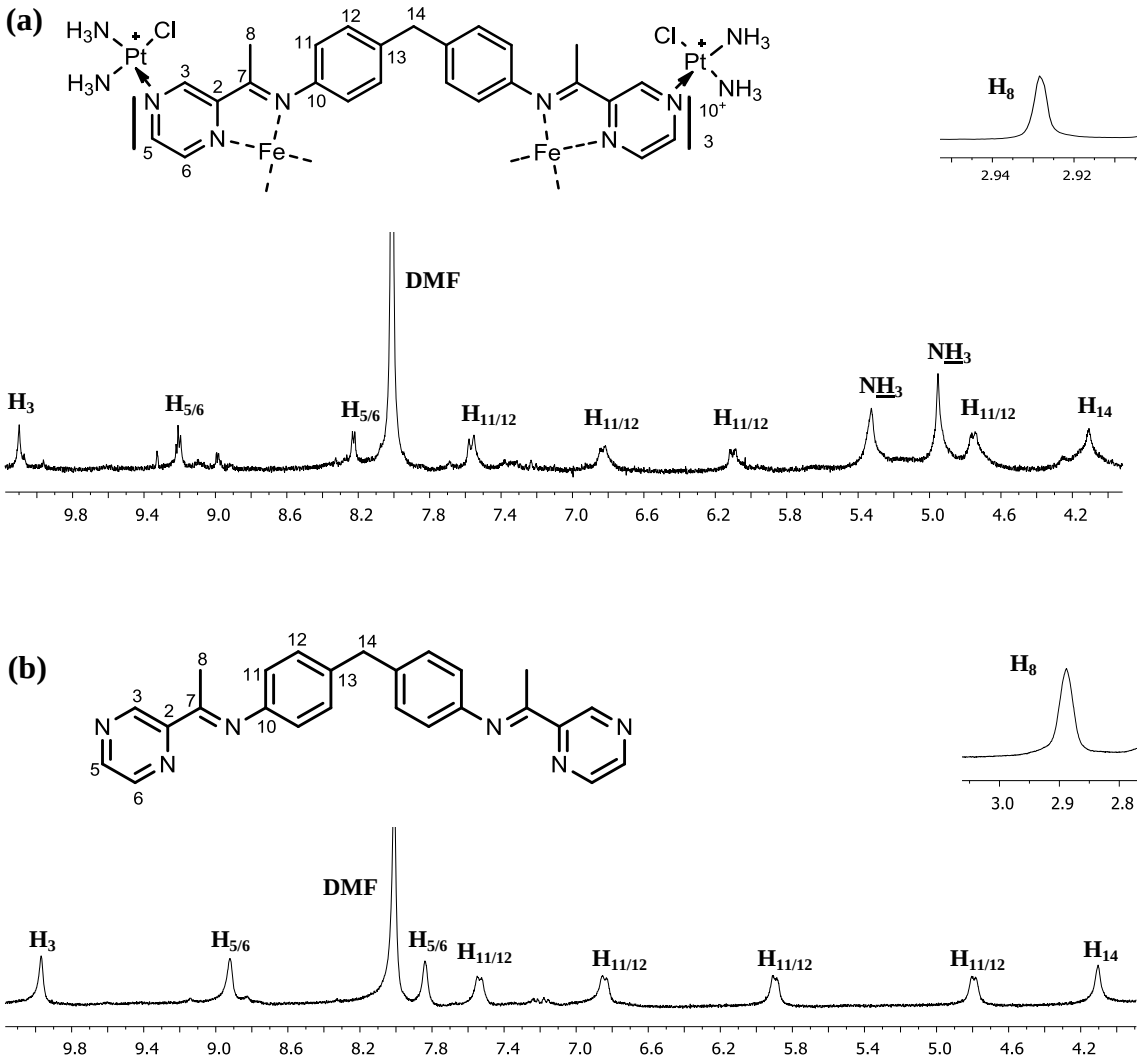

Figure 2.8 300 MHz ^{1}H NMR spectra (d_6-DMF, 298 K) **(a)** $[Fe_2(L_1)_3](PF_6)_4$ with attached cisplatin **(b)** $[Fe_2(L_1)_3](PF_6)_4$

The ^{1}H NMR spectrum of the $[Fe_2(L_1)_3](PF_6)_4$ complex with attached cisplatin shows a significant shift some of the proton resonances downfield (Table 2.0) compared to non-platinated complex and thus, indicate coordination of cisplatin to $[Fe_2(L_1)_3](PF_6)_4$. Two single peaks, both with integration three which appear at 5.35 ppm and 4.35 ppm, correspond to two ammine groups of cisplatin and confirm a *cis*-configuration.

H^1 NMR	Chemical shift δ (ppm)	
Protons	$[Fe_2(L_1)_3](PF_6)_4$	$[Fe_2(L_1)_3](PF_6)_4$ with attached cisplatin
H_3	9. 97	10.10
$H_{5/6}$	8.92 7.84	9.21 8.23
$H_{11/12}$	7.54 6.84 5.90 4.79	7.56 6.83 6.10 4.75
H_{14}	4.10	4.11
H_8	2.89	2.95

Table 2.0 H^1 NMR chemical shifts of $[Fe_2(L_1)_3](PF_6)_4$ and $[Fe_2(L_1)_3](PF_6)_4$ with attached cisplatin in d_6-DMF.

The UV/Vis spectrum of $[Fe_2(L_1)_3](PF_6)_4$ complex with attached cisplatin recorded in DMF reveals shift of the MLCT band from 570 nm to 599 nm (ε = 9400 mol^{-1} dm^3cm^{-1}) with a shoulder at 695 nm (ε = 6800 mol^{-1} dm^3cm^{-1}) which indicates that the coordination of cisplatin to $[Fe_2(L_1)_3](PF_6)_4$ was achieved and a new complex is formed.

2.4.1.3 Combining $[Fe_2(L_1)_3]Cl_4$ with cis-bis(dimethylsulphoxide)dichloro-platinum(II)

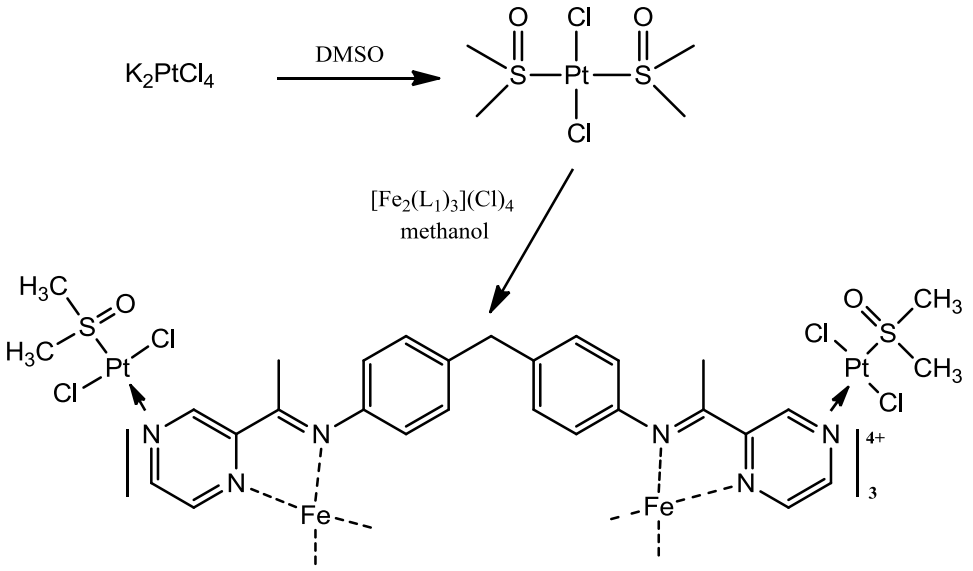

Scheme 2.2 Schematic procedure for $[Fe_2(C_{25}H_{22}N_6Pt_2Cl_4S_2O_2(CH_3)_4)]_3Cl_4$ synthesis.

Cis-bis(dimethylsulphoxide)dichloroplatinum(II) was synthesised from potassium tetrachloroplatinate and dimethylsulfoxide according to the published procedure.[16] One equivalent of the $[Fe_2(L_1)_3]Cl_4$ metal complex was stirred with six equivalents of $PtCl_2(SO(CH_3)_2)_2$ in methanol overnight at room temperature. The resulting violet complex precipitated from the methanol. All attempts to crystallise the synthesised complex were unsuccessful.

As in the case of the iron(II) complex with attached cisplatin, there were no peaks corresponding to the synthesised complex observed in the ESI and MALDI mass spectra. The IR spectrum shows a υS=O stretching band at 1127 cm^{-1}, CH_3 rocking mode at 1020 cm^{-1} and υC-S assymetrical stretching at 740 cm^{-1}. The complex is not

soluble in water and methanol but rather soluble in acetonitrile and DMF. A ^{1}H NMR spectrum of the obtained compound was recorded in CD_3CN (Fig. 2.9).

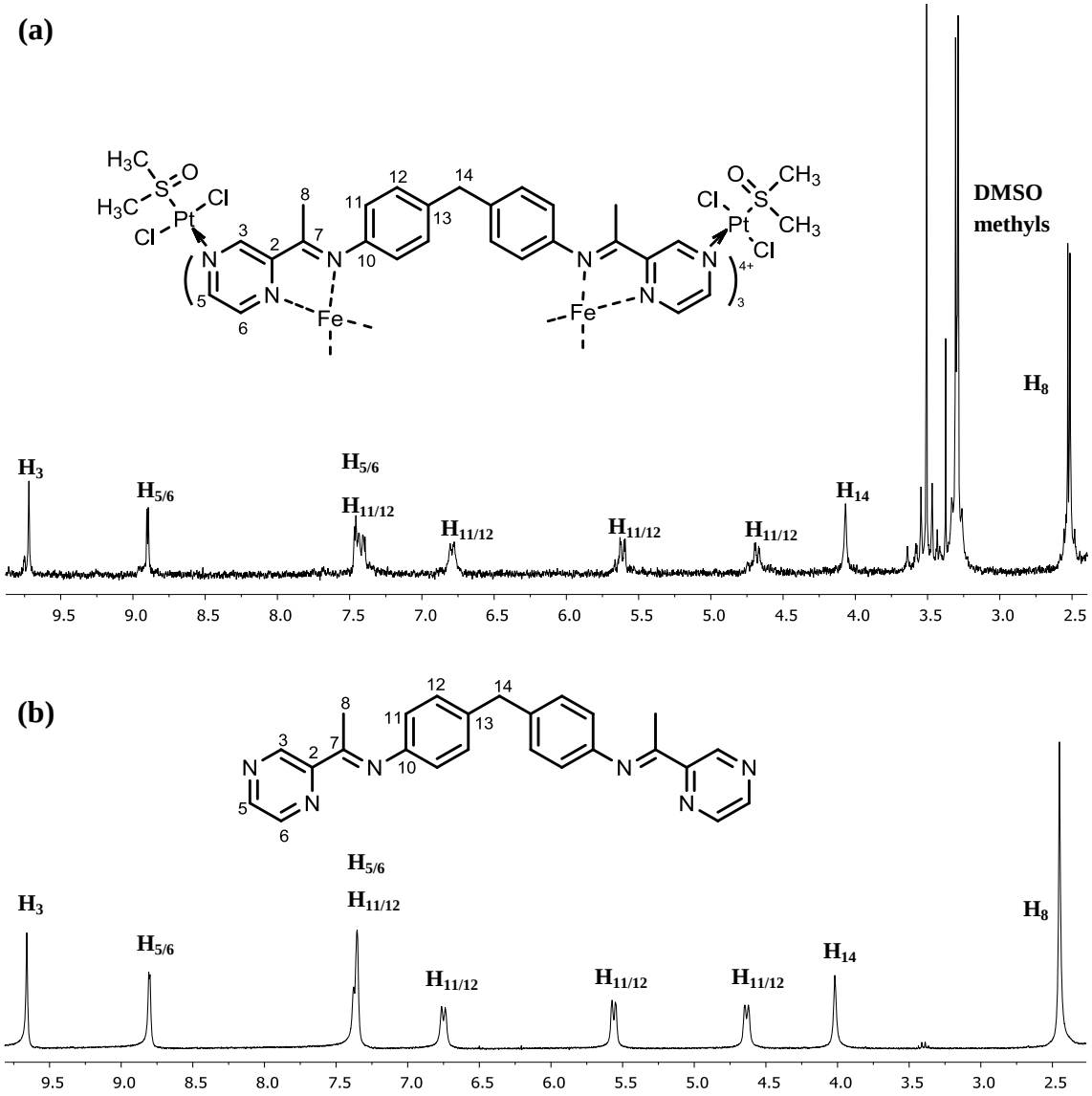

Figure 2.9 300 MHz ^{1}H NMR spectra (CD_3CN) of **(a)** $[Fe_2(C_{25}H_{22}N_6Pt_2Cl_4S_2O_2(CH_3)_4)_3]Cl_4$ **(b)** $[Fe_2(L_1)_3](PF_6)_4$.

The ^{1}H NMR spectrum shows a single set of peaks confirming the presence of a single symmetrical species in the solution. A slight shift of the proton resonances of platinated complex compared to non-platinated is observed. The signal resulting from

the methyl protons of ketimine bond is observed as a doublet or two adjacent singlets with integration of three. The proton resonance appearing as a doublet at 3.30 ppm with integration of six was assigned as a signal for DMSO methyls indicating the coordination of *cis*-bis(dimethylsulphoxide)dichloroplatinum(II) to the iron(II) complex of L_1. Additional single peak of unknown origin is observed at 3.51 ppm with integration of three. Interestingly, the methyl groups of platinum bound DMSO exhibit a single peak in ^{1}H NMR spectrum in chlorinated solvents (Fig 2.10 (a)). However in non-chlorinated solvents the band is split into a doublet (Fig. 2.10 (b)).

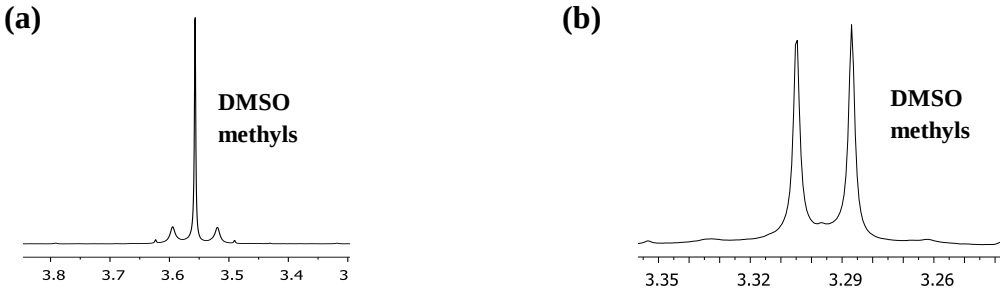

Figure 2.10 300 MHz ^{1}H NMR spectra of DMSO methyls recorded at 298 K in **(a)** Chloroform **(b)** Acetonitrile.

If the non-chlorinated solvent is evaporated and the sample is dissolved in a chlorinated solvent, the signal will be displayed as a singlet suggesting there must be an unknown solvent effect present. The similar solvent effect was previously reported by the Hannon group.[17]

In the case of the iron(II) complex with attached $Pt(DMSO)Cl_2$ there were two peaks observed in the region of 3.20 - 3.60 ppm one of which was assigned as a signal for DMSO methyls. The presence of additional single peak as well as the splitting of H_8 signal at 2.25 ppm is unclear.

2.4.2 Ligand L_2

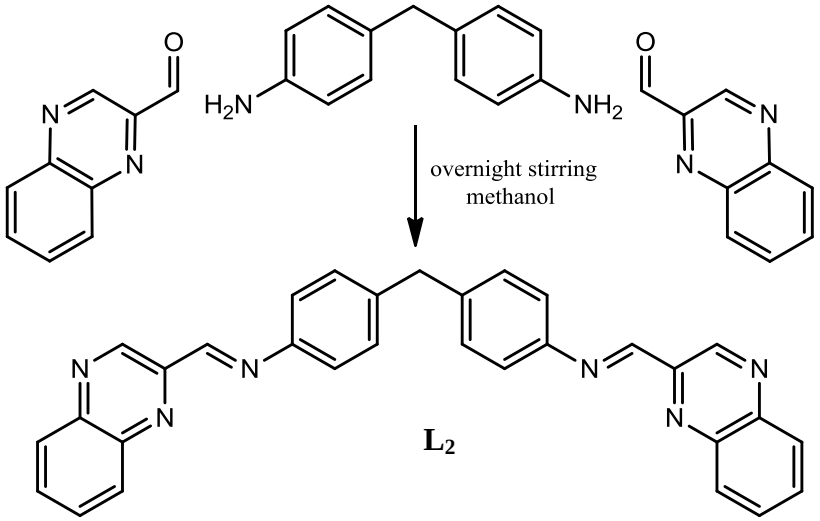

Scheme 2.3 Schematic procedure for the synthesis of ligand L_2

Ligand L_2 was synthesised by stirring two equivalents of quinoxaline-2-carboxaldehyde with one equivalent of spacer (4,4'-methylendianiline). The ligand was prepared in 55 % yield from these commercially available starting materials. The ESI spectrum shows a peak at *m/z* = 501 which corresponds to $[L_2 + Na]^+$. Partial elemental analysis supports the formation of the ligand with an empirical formula of $C_{31}H_{22}N_6$. A ^1H NMR spectrum of the ligand was recorded in $CDCl_3$ (Fig. 2.11).

The ^1H NMR spectrum displays 9 proton resonances consistent with a single solution species with a symmetrical configuration. The H_3 and H_{11} protons are shifted downfield as they experience reduced electronic density due to proximity to a negatively charged nitrogen atom. The resonances from phenyl protons appear as mutliplet at 7.40 – 7.30 ppm. The signals from quinoxaline protons H_6, H_9, H_7, and H_8 are displayed as multiplets.

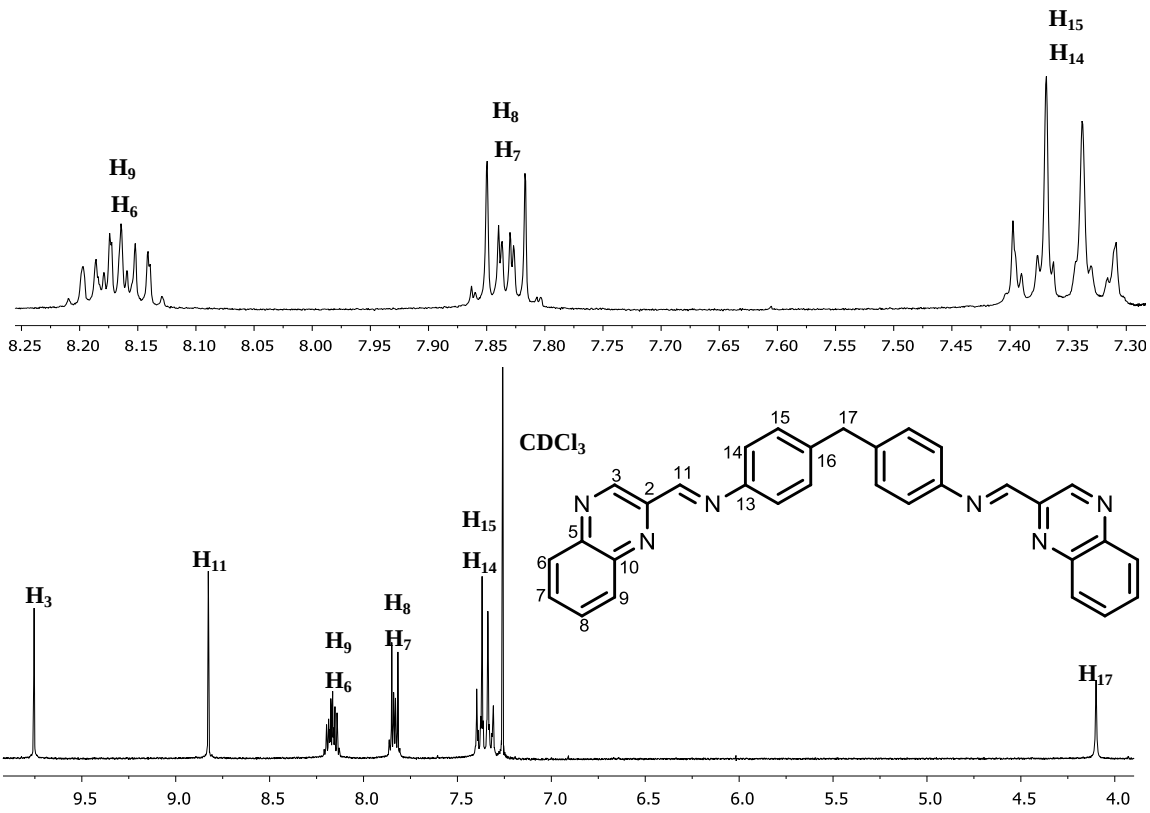

Figure 2.11 300 MHz ^{1}H NMR spectrum ($CDCl_3$, 298 K) of ligand L_2 with an expansion of the aromatic region.

Coordination of the ligand L_2 with metals of tetrahedral and octahedral configuration was investigated.

2.4.2.1 Silver(I) complex of L_2

The reaction of one equivalent of L_2 with one equivalent of silver acetate in methanol resulted in a yellow solution, from which a yellow solid precipitated upon addition of ammonium hexafluorophosphate. Partial microanalytical data is consistent with the empirical formula of $\{[Ag(C_{31}H_{22}N_6)](PF_6)\}_n$. The ESI mass spectrum displays peaks corresponding to $[[Ag_2(C_{31}H_{22}N_6)_2](PF_6)]^+$ (*m/z* = 1317) and $[Ag_2(C_{31}H_{22}N_6)_2]^{2+}$

(*m/z* = 586) which are consistent with a dinuclear complex formation. A ^{1}H NMR spectrum of the complex was recorded in d_6-DMF (Fig. 2.12).

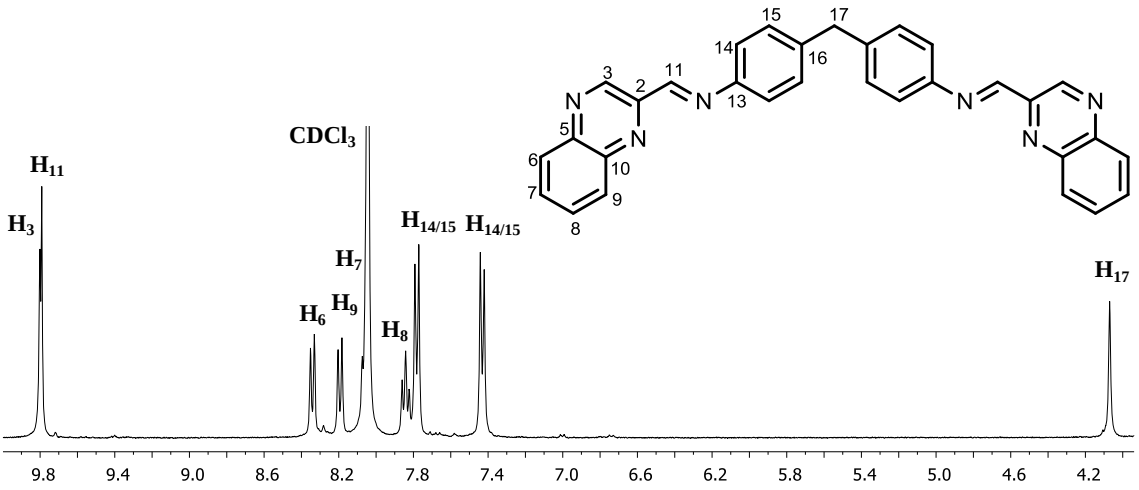

Figure 2.12 300 MHz ^{1}H NMR spectrum (d_6-DMF, 298 K) of $\{[Ag(C_{31}H_{22}N_6)](PF_6)\}_n$.

The ^{1}H NMR spectrum shows a single set of peaks that suggest that single symmetrical species are present in the solution. The resonances of the H_3 and H_{11} protons are readily identified in the downfield region of the spectrum. The quinoxaline protons H_6 and H_9 appear as doublets and H_8 as a triplet. The H_7 proton of quinoxaline is obscured by the solvent peak.

On reaction of the ligand L_2 with tetrahedral metal ions there are two possible conformations that can be obtained: helix or box (Fig. 2.13). Both structures differ from each other by the fashion in which ligands are surrounding the metal ion. In the helix conformation both of the ligand strands are located above one metal ion and below another metal ion. In the box conformation one ligand strand lies above the metal axis and another one below.[18] The CH_2 signal in the ^{1}H NMR spectrum is crucial in determination of the presence of box or helix species in solution. In the helix the CH_2 protons are equivalent which gives a single peak on the spectrum, whereas in the case of

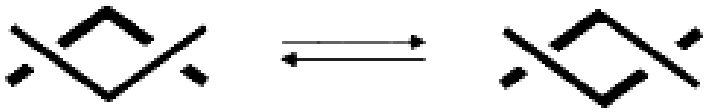

Box *meso* isomer Helix *rac* isomer

Figure 2.13 Schematic representation of box and helix conformations.[18]

the box conformation these protons are non-equivalent with one proton pointing out of the box and another proton pointing down towards the plane of the box assembly which gives a split CH_2 signal in the spectrum.[15]

In the case of $\{[Ag(C_{31}H_{22}N_6)](PF_6)\}_n$ in d_6-DMF solution at 298 K a single set of peaks have been observed. In solution the complex interconverts between helix and box conformations and in order to identify if there are any other species present, ^{1}H NMR experiments were performed at low temperatures (Fig. 2.14). In some cases there can be a rapid exchange between two species that cannot be recorded by NMR even at low temperatures.

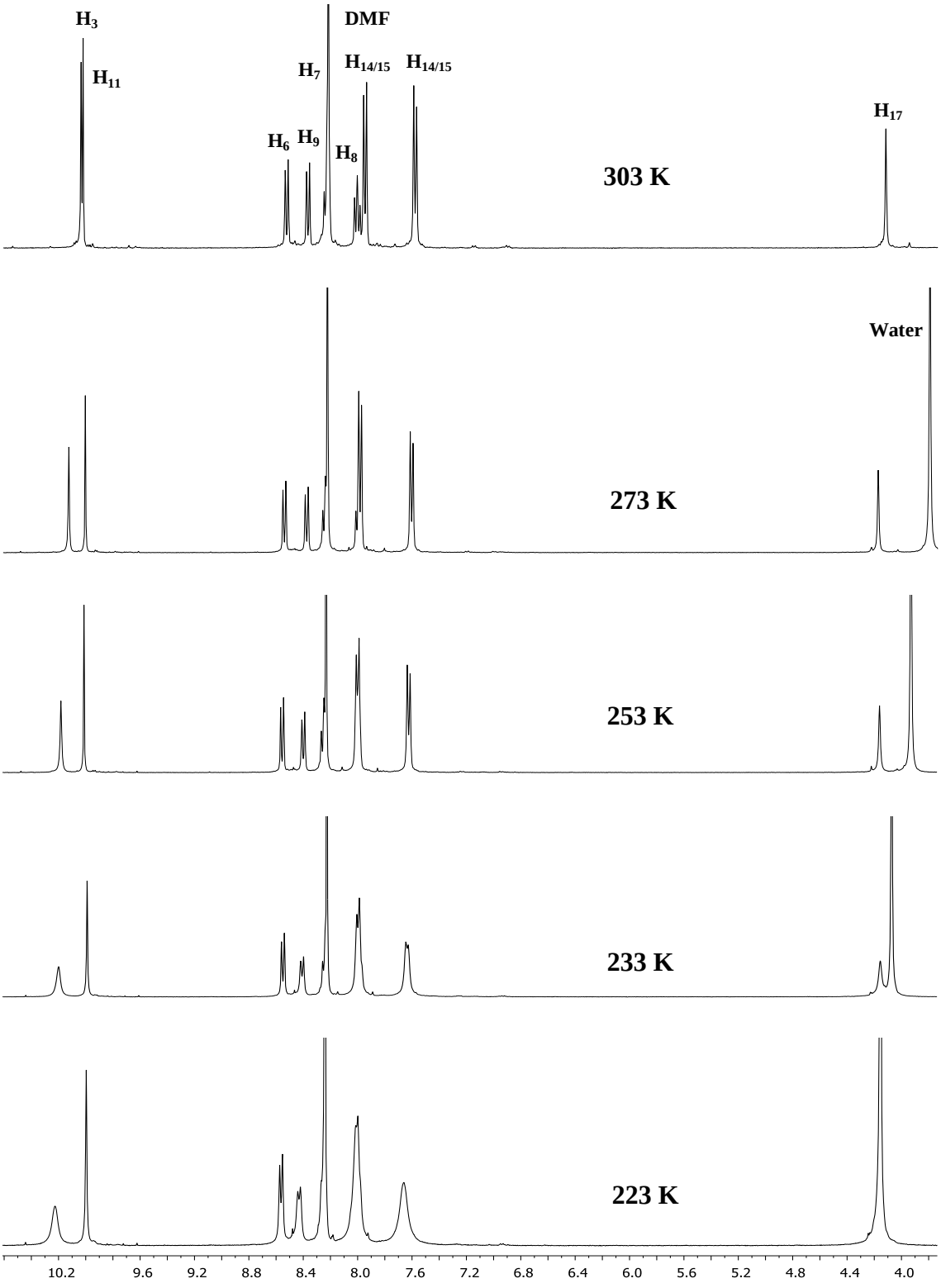

Figure 2.14 400 MHz ^{1}H NMR spectra (d_6-DMF, 303 K, 273 K, 253 K, 233 K, 223 K) of $\{[Ag(C_{31}H_{22}N_6)](PF_6)\}_n$.

^{1}H NMR experiments of $\{[Ag(C_{31}H_{22}N_6)](PF_6)\}_n$ in d_6-DMF performed at low temperatures did not reveal any distinct species present in the solution. If there are two species in the solution as was previously found in similar ligand systems, they exist in a rapid exchange on the NMR timescale.[19]

Crystals of the $\{[Ag(C_{31}H_{22}N_6)](PF_6)\}_n$ complex for X-ray analysis were obtained by slow diffusion of diethyl ether into a solution of the complex in DMF, however they were found to be of too poor quality to obtain the crystal structure.

2.4.2.2 Copper(I) complex of L_2

The formation of the copper(I) complex of ligand L_2 was achieved by refluxing L_2 with $[Cu(MeCN)_4](PF_6)$ (1:1) in methanol overnight. The dark brown solid precipitated upon addition of ammonium hexafluorophosphate. Partial microanalytical data are consistent with the empirical formula of $[Cu_2(C_{31}H_{22}N_6)_2](PF_6)_2$. The ESI mass spectrum displays a peak at *m/z* = 542 which corresponds to $[Cu_2(C_{31}H_{22}N_6)_2]^{2+}$. The brown color of the complex arises from the metal-to-ligand charge transfer (MLCT) transition. UV/Vis absorbtion spectrum shows a broad band at 577 nm (ε = 2200 mol^{-1} dm^3cm^{-1}) which is a characteristic of copper(I) in a bis-diimine environment.

The ^{1}H NMR spectrum of the $[Cu_2(C_{31}H_{22}N_6)_2](PF_6)_2$ complex was recorded in CD_3CN solution. At room temperature there is a single set of resonances observed as the ligand exchange is very rapid in acetonitrile at this temperature (Fig. 2.15). The resonance corresponding to the CH_2 appears as a singlet in the aliphatic region of the spectrum. Some of the quinoxaline peaks are broadened with the H_3 resonance overlapping with H_{11} signal. Phenyl protons appear as two sharp doublets at 7.49 ppm and 7.24 ppm respectively.

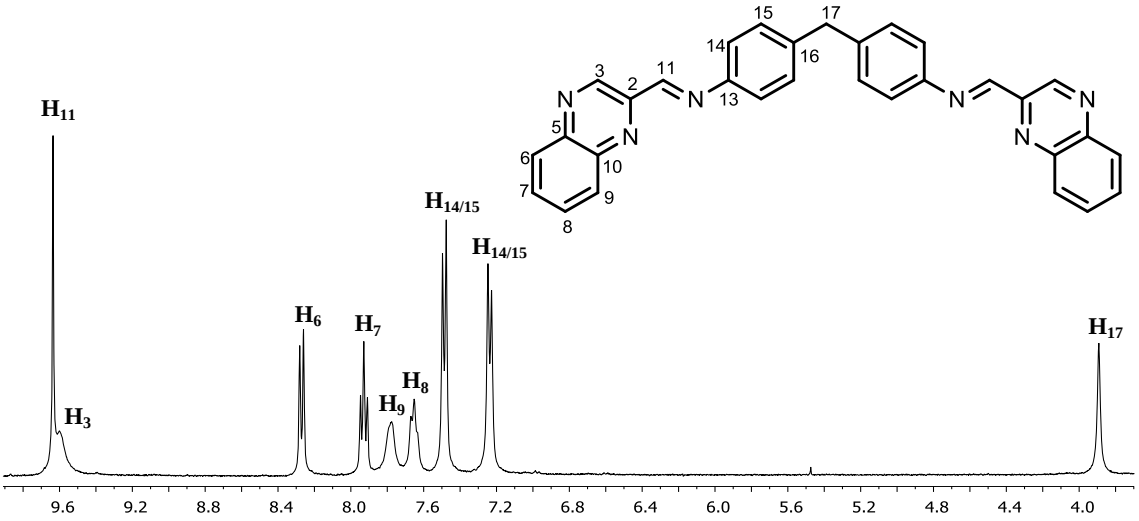

Figure 2.15 300 MHz ^{1}H NMR spectrum (CD_3CN, 298 K) of the $[Cu_2(L_2)_2](PF_6)_2$ complex.

In order to define the presence of other species in the solution, ^{1}H NMR experiments were performed at variable temperatures in $(CD_3)_2CO$. At 333 K additional peaks are observed, however they are not very distinctive. At lower temperatures another set of peaks becomes more obvious, revealing the presence of box conformation. The CH_2 protons are non-equivalent and split into two doublets (Fig. 2.16).

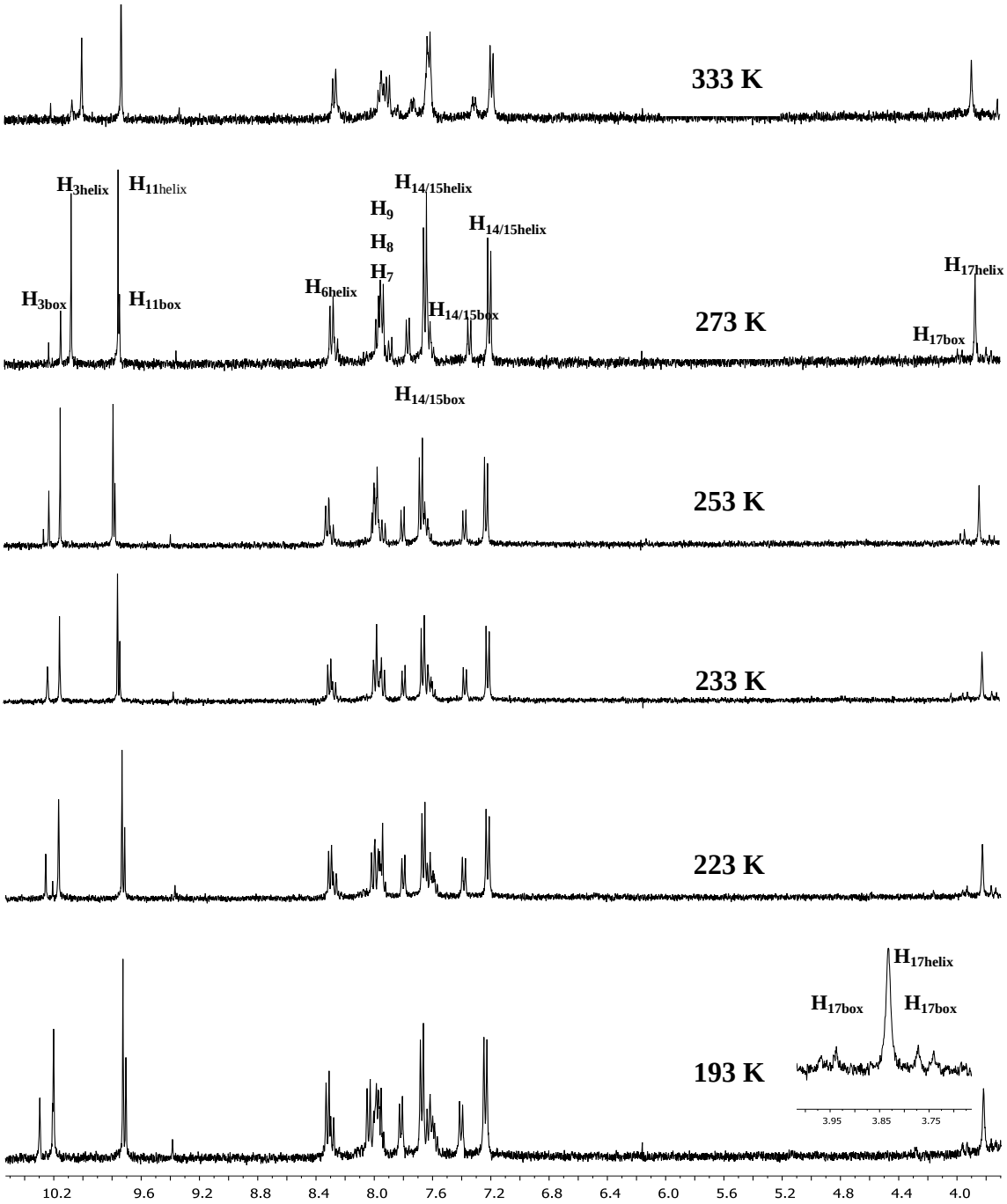

Figure 2.16 400 MHz ^{1}H NMR spectra ($(CD_3)_2CO$, 333 K, 273 K, 253 K, 233 K, 223 K, 193 K) of $[Cu_2(L_2)_2](PF_6)_2$ complex.

To identify the ratio helix:box in the solution, the integration of box and helix proton resonances was performed. At 273 K the ratio between helix and box is around

3:1. When the temperature is decreased up to 193 K the ratio is 2:1. The change in ratio helix:box with a temperature demonstrates that the helix conformation is favoured entropically whereas box conformation is enthalpically favoured.

Brown crystals of the $[Cu_2(L_2)_2](PF_6)_2$ complex suitable for X-ray analysis were obtained by slow diffusion of diethyl ether into a solution of the complex in acetonitrile. The X-ray structure confirms the formation of a double-stranded dinuclear copper(I) helicate (Fig. 2.17).

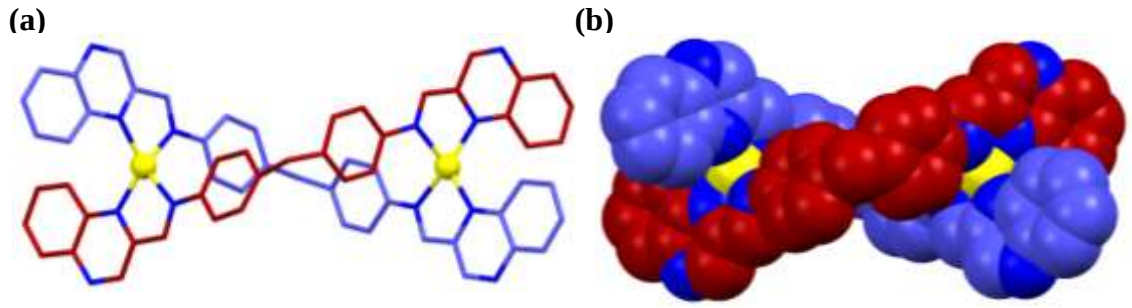

Figure 2.17 X-ray structure of $[Cu_2(L_2)_2](PF_6)_2$ complex **(a)** Perspective view **(b)** Space-filling representation of $[Cu_2(L_2)_2]^{2+}$ cation. Solvent molecules, hydrogen atoms and anions are omitted for clarity.

Each metal centre is four-coordinate and has a pseudo-tetrahedral geometry with $Cu\text{-}N_{imine}$ bond distances of 2.005(13)-2.108(13) and $Cu\text{-}N_{quinoxaline}$ distances of 1.999(10)-2.035(10) Å with N-Cu-N angles of 80.4(5)-82.7(5)º. Two ligand strands are coordinated to the copper(I) metal ions in such a way that leads to a Cu-Cu distance of 11.1 Å. The angles between the central phenyl rings are of 112.6º(14) and 113.7(13)º. The phenylene rings are slightly twisted with respect to the imine metal chelating unit with torsion angles of 9º and 170º. The quinoxaline rings from different ligand strands are located at angles of 121.3(5)º and 126.0(5)º with respect to each other. The copper(I) cylinder has two PF_6 counteranions and bears a double charge. The highly disordered

solvent molecules were present in the structure however the attempts to identify them failed. The crystal packing diagram of $[Cu_2(L_2)_2](PF_6)_2$ is shown in Figure 2.18.

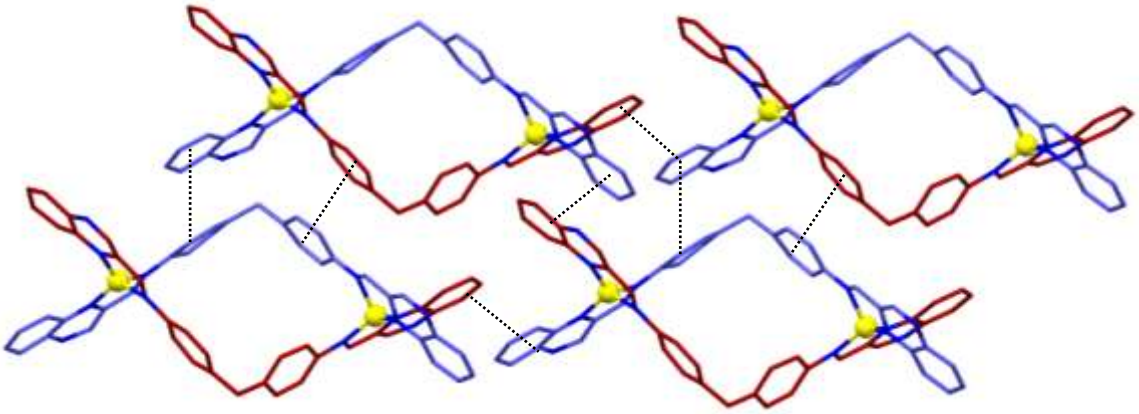

Figure 2.18 Packing diagram of $[Cu_2(L_2)_2]^{2+}$ showing π-π stacking interactions between phenyl and quinoxaline rings. Solvent molecules, hydrogen atoms and anions are omitted for clarity.

The crystal packing diagram shows that the helical architectures are arranged in a chain network with face to face π-π stacking interactions between the phenylene and quinoxaline rings of different helical assemblies. The centroid-centroid distances of the aromatic rings involved in π-π stacking are in the range of 3.5 - 3.9 Å.

Attempts to synthesise a helicate with metal ions of octahedral geometry were unsuccessful. No metal complex was formed upon stirring ligand L_2 with octahedral metal ions suggesting there are steric constraints due to the presence of bulky quinoxaline rings that prevent the formation of the complex.

2.4.3 Ligand L_3

A multiple step synthesis has been performed in order to obtain ligand L_3. L_3 is based on 4,4'-bypiridine units connected by an imine bond with a 4,4'-methylenedianiline. 4,4'-Bipyridine-2-carboxaldehyde is not commercially available therefore the first task was to synthesize the aldehyde through a three-step procedure.

2.4.3.1 Synthesis of 4,4'-bipyridine-2-carboxaldehyde

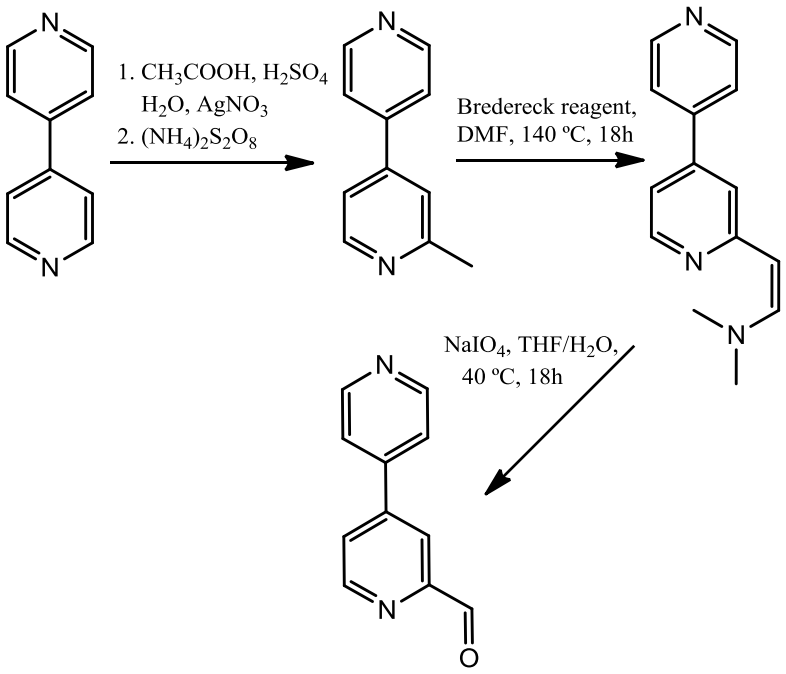

Scheme 2.4 Synthetic procedure for 4,4'-bipyridine-2-carboxaldehyde synthesis.

The first step was carried out according to the published literature procedure.[20] 2-Methyl-4,4'-bipyridine was prepared by radical alkylation of commercially available 4,4'-bipyridine using the procedure of Minisci et al.[21] 4,4'-bipyridine was dissolved in a solution of 98 % sulfuric acid and water. Subsequently acetic acid and a solution of silver nitrate in water were added to the mixture. The mixture was heated to 110 ºC and

maintained at that temperature for 30 min, after which ammonium persulfate was added portionwise. Ammonium persulfate is a very strong oxidizing agent and together with catalytic amounts of silver it is used for decarboxylation of acids and radical formation. When the release of carbon dioxide ceased the reaction was heated for another 30 minutes then cooled down and made alkaline with ammonia to pH ~ 8. The reaction products were extracted with ether, dried over $MgSO_4$ and evaporated *in vacuo* to yield a yellow solid. The crude mixture was purified by HPLC column chromatography using water-methanol in a ratio of 60:40. The separation gave 4 bands. The first band eluted was identified as unreacted 4,4'-bipyridine, the second band was 2-methyl-4,4'-bipyridine, the third band 2,2'-dimethyl-4,4'-bipyridine and the fourth band 2,2',6 – trimethyl-4,4'-bipyridine.

The second step involved enamination of 2-methyl-4,4'-bipyridine using Bredereck reagent, tert-butoxybis(dimethylamino)methane. The formation of enamine with Bredereck reagent is facilitated by the acidity of the methyl group.[22] 2-Methyl-4,4'-bipyridine with Bredereck reagent in DMF were heated at 140 ºC under an argon atmosphere for 18h. The pale orange solution was cooled down, hydrolyzed by addition of water and extracted with dichloromethane. The combined organic layers were dried and the solvent evaporated *in vacuo* to yield brown oil. The desired product was recrystallized from DCM-pentane to give orange crystals. The advantage of this procedure is the formation of enamine crystals upon cooling of the crude mixture. The synthesized 2-methyl-(*N*-dimethylaminovinyl)-[4,4']-bipyridine is unstable and slowly decomposes.[23]

The synthesised enamine was then converted to the aldehyde by oxidation with sodium periodate in aqueous THF at 40 ºC under an argon atmosphere. The reaction

was stirred for 18 hours, the solvent evaporated then the crude product dissolved in DCM and washed with water. The organic layers were dried and the solvent evaporated *in vacuo* to yield an off white solid. The aldehyde was obtained as a white solid after purification on a silica column using a combination of DCM/CH_3OH as an eluent. The mechanism of this transformation from enamine to aldehyde with sodium periodate is unknown.[23]

The ^{1}H NMR experiment confirms the formation of the 4,4'-bipyridine-2-carboxaldehyde (Fig. 2.19).

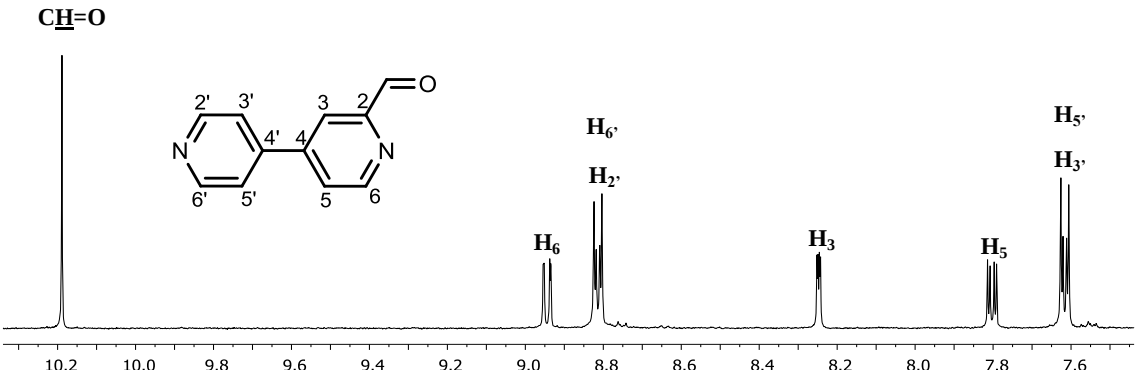

Figure 2.19 300 MHz ^{1}H NMR spectrum ($CDCl_3$, 298K) of 4,4'-bipyridine-2-carboxaldehyde.

The ^{1}HNMR spectrum reveals five signals in the aromatic region and one signal corresponding to the aldehyde proton at 10.17 ppm. The H_6, $H_{2'}$ and $H_{6'}$ resonances appear downfield in the spectrum as two doublet of doublets. The signal for H_3 arises as a doublet of doublets at 8.23 ppm. The remaining peaks at 7.78 and 7.60 ppm with integrations of one and two were assigned as H_5, $H_{3'}$ and $H_{5'}$ respectively.

The EI mass spectrum shows a peak at *m/z* = 184 which corresponds to $\{C_{11}H_8N_2O\}^+$. The IR spectrum reveals a υC=O stretching band at 1708 cm^{-1} and υC-H aldehyde stretching at 2858 cm^{-1} which supports the formation of the aldehyde. The

obtained 4,4'-bipyridine-2-carboxaldehyde was used in the next step for the ligand L_3 synthesis.

2.4.3.2 Synthesis of L_3

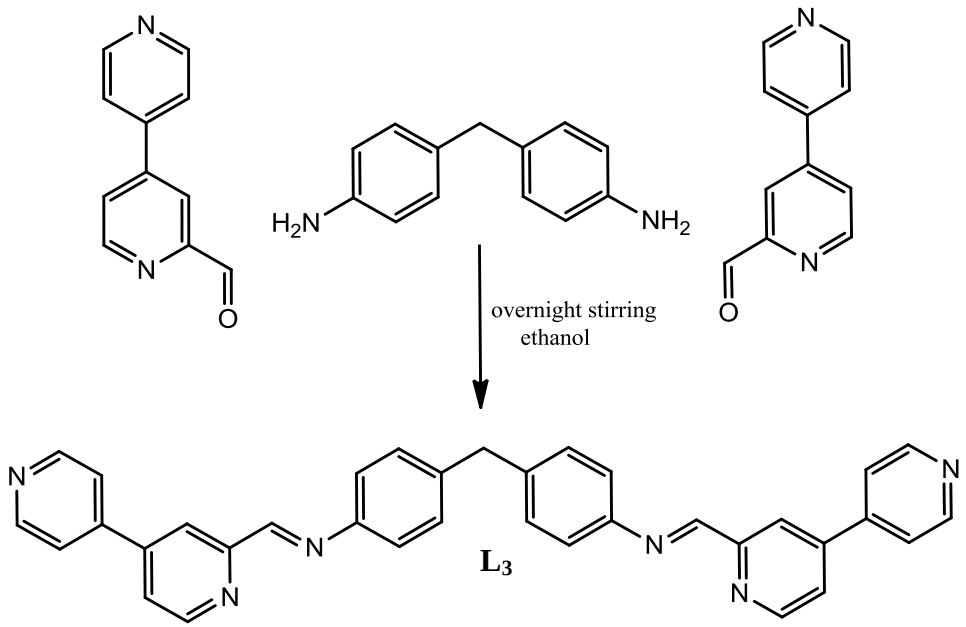

Scheme 2.5 Synthetic procedure for ligand L_3 preparation

The ligand L_3 was synthesised by stirring two equivalents of 4,4'-bipyridine-2-carboxaldehyde with one equivalent of 4,4'-methylendianiline in ethanol overnight. The resulting product precipitated from the mixture as a yellow solid. The ESI spectrum shows a peak at *m/z* = 553 which corresponds to $[L_3 + Na]^+$.

The ^1H NMR spectrum of the ligand L_3 recorded in $CDCl_3$ shows eight signals (Fig. 2.20). The resonances corresponding to H_2, $H_{2'}$, $H_{6'}$ and H_7 appear as two doublet of doublets and a singlet and are readily identified downfield in the spectrum. The H_3 signal appears as a doublet at 8.51 ppm, the remaining doublet of doublets at 7.67 ppm and at 7.64 ppm with integration of two and one were assigned as $H_{3'}$ and $H_{5'}$ and H_5

respectively. The signal from the phenylene protons appears as a doublet at 7.32 ppm and is overlapped with a solvent peak. The resonance corresponding to the CH_2 protons appears in the aliphatic region of the spectrum as a singlet at 4.09 ppm.

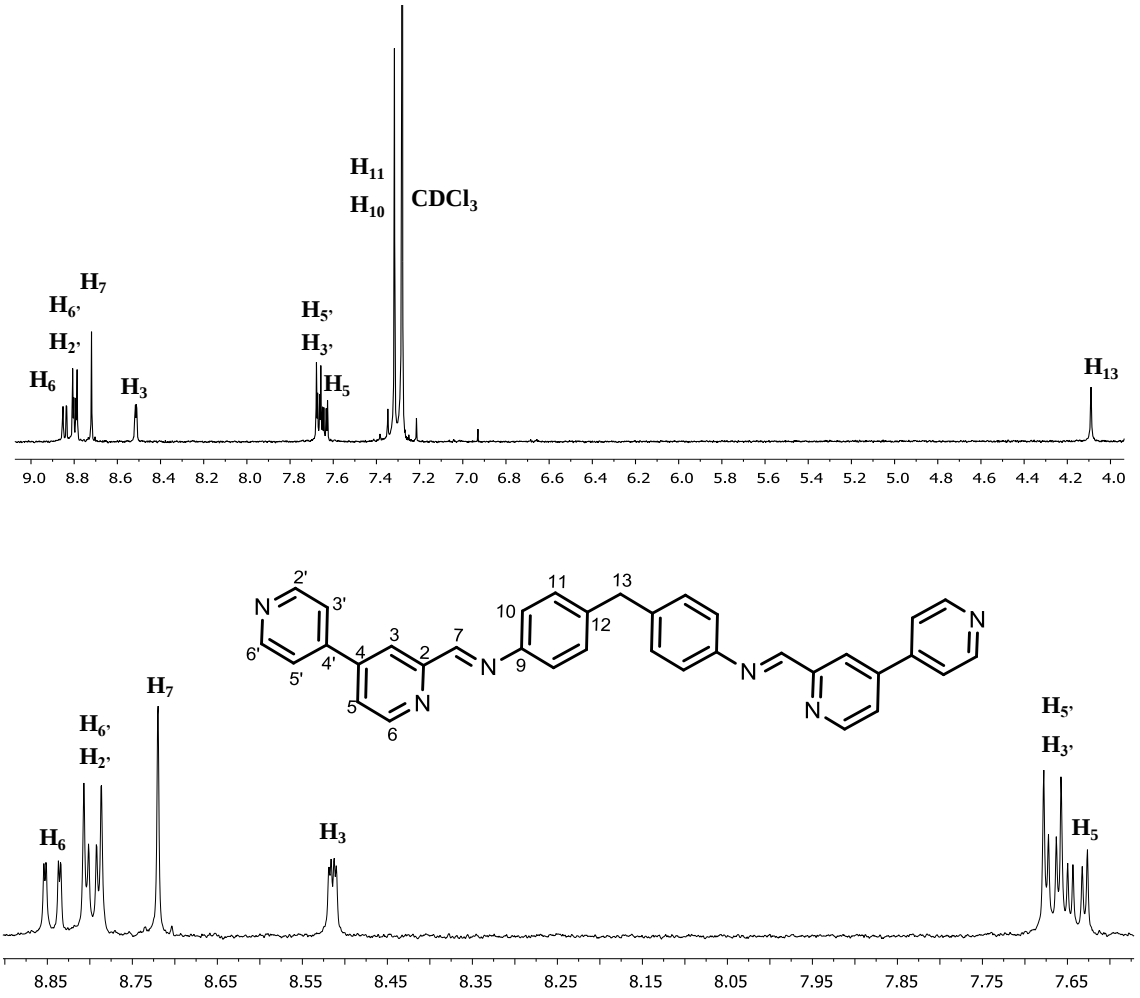

Figure 2.20 300 MHz ^{1}H NMR spectrum ($CDCl_3$, 298K) of the ligand L_3 with an expansion of the aromatic region.

2.4.3.3 Iron(II) complex of L_3

The coordination of iron(II) metal ions to the ligand L_3 was achieved by stirring L_3 with iron(II) chloride tetrahydrate in methanol for 3 hours at room temperature. A dark violet solid precipitated from the solution upon addition of ammonium

hexafluorophosphate. The ESI mass spectrum displays a peak *m/z* = 426 which corresponds to $[Fe_2(C_{35}H_{26}N_6)_3]^{4+}$. The elemental analysis data is consistent with the formation of the complex, with an empirical formula of $[Fe_2(L_3)_3](PF_6)_4 \bullet 2H_2O$. The violet colour of the complex arises from the MLCT absorption band located at 586 nm (ε = 15100 $mol^{-1}dm^3cm^{-1}$).

The ^1H NMR spectrum recorded in CD_3CN indicates the formation of the iron(II) complex of L_3 (Fig. 2.21).

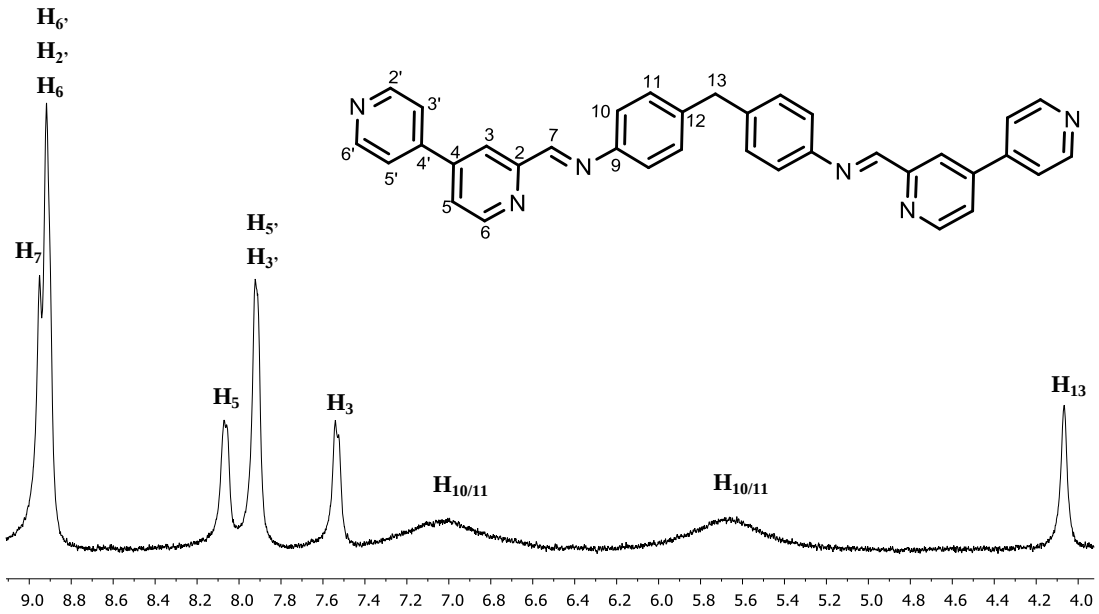

Figure 2.21 300 MHz ^1H NMR spectrum (CD_3CN, 298 K) of $[Fe_2(L_3)_3](PF_6)_4$.

The H_7, H_6, $H_{2'}$ and $H_{6'}$ resonances are overlapped in the spectrum. Signals for $H_{3'}/H_{5'}$, H_3 and H_5 are slightly broaden and appear as a singlet and two doublets, respectively. The $H_{10/11}$ protons are broadened due to a slow rotation of the phenyl rings at room temperature and there is no coupling observed. The H_{13} signal appears in the aliphatic region of the spectrum as a singlet at 4.07 ppm.

Crystals of the $[Fe_2(L_3)_3](PF_6)_4$ complex for X-ray analysis were obtained by slow diffusion of benzene into a solution of the compound in acetonitrile, however the crystals were of insufficient quality to obtain the crystal structure.

Attempts to attach cisplatin on to the outside of the formed iron(II) triple helicate were unsuccessful. The complex fell apart upon addition of cisplatin in DMF resulting in a colourless solution.

2.4.4 Ligand L_4

A two-step synthesis was employed to obtain ligand L_4. The starting material 1-pyridine-2-ylmethyl-1H-imidazole carboxaldehyde is not commercially available therefore the first step was to synthesise the aldehyde.

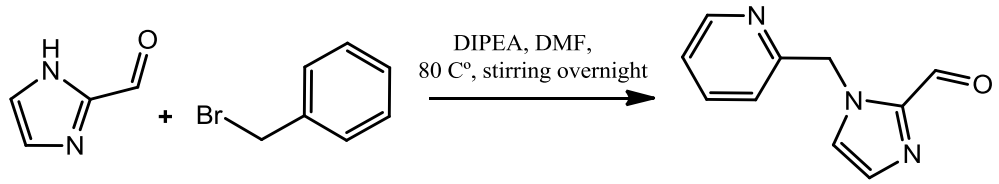

Scheme 2.6 Schematic procedure for the synthesis of 1-pyridine-2-ylmethyl-1H-imidazole carboxaldehyde

1-Pyridine-2-ylmethyl-1H-imidazole carboxaldehyde was synthesised according to a published procedure by reacting imidazole with 2-(bromomethyl)pyridine hydrobromide in DMF in the presence of Hunig`s base, *N*,*N*-diisopropylethylamine (DIPEA).[24, 25] Hunig`s base is a non-nucleophilic strong base that is able to accommodate a proton between the isopropyl groups. In this experimental procedure it was used to deprotonate the imidazole. The reaction mixture was stirred at 80 ºC under a nitrogen atmosphere overnight and then quenched by the addition of $NaHCO_3$. The

resulting solution was extracted with DCM; the organic layers were collected and washed with brine, dried over $MgSO_4$ and evaporated *in vacuo* to yield a brown oil. The final product was purified by HPLC on a solvent gradient starting from 100 % water to 33 % of acetonitrile. The separation gave three peaks; the second peak eluted was identified as 1-pyridine-2-ylmethyl-1H-imidazole carboxaldehyde. The prepared aldehyde was used for the synthesis of the ligand L_4.

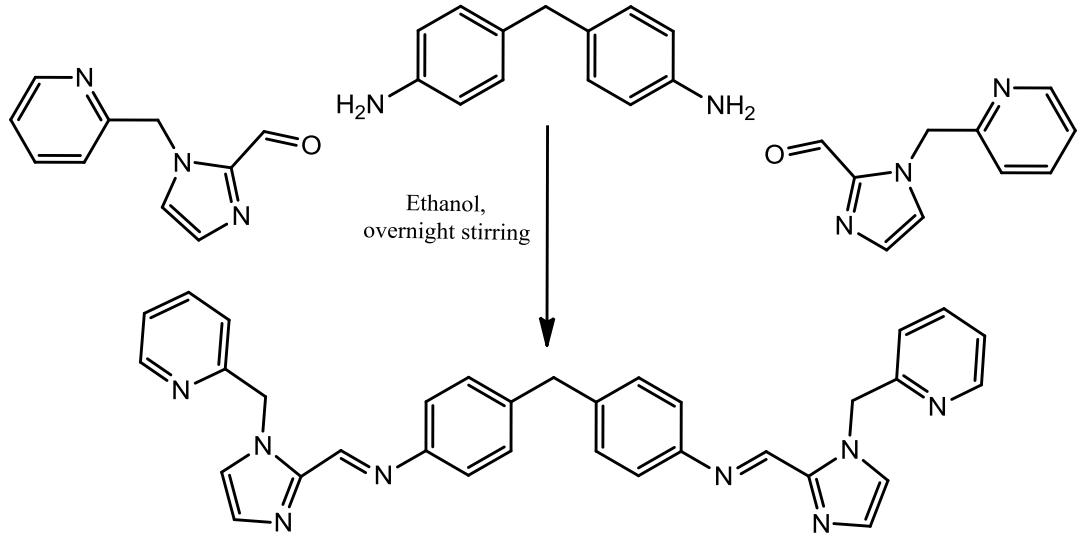

Scheme 2.7 Schematic procedure for the synthesis of L_4.

The ligand L_4 was synthesized by stirring two equivalents of 1-pyridine-2-ylmethyl-1H-imidazole carboxaldehyde with one equivalent of 4,4'-methylendianiline in ethanol overnight. The off-white solid precipitated from the solution upon stirring. The peak found at *m/z* = 559 in the ESI mass spectrum corresponds to $[L_4 + Na]^+$. Partial elemental analysis data are consistent with the formation of the ligand with the empirical formula of $C_{33}H_{28}N_8$.

The ^1H NMR spectrum recorded in $CDCl_3$ confirms the formation of the ligand L_4 (Fig. 2.22). All the protons were assigned using 1D and 2D NMR experiments.

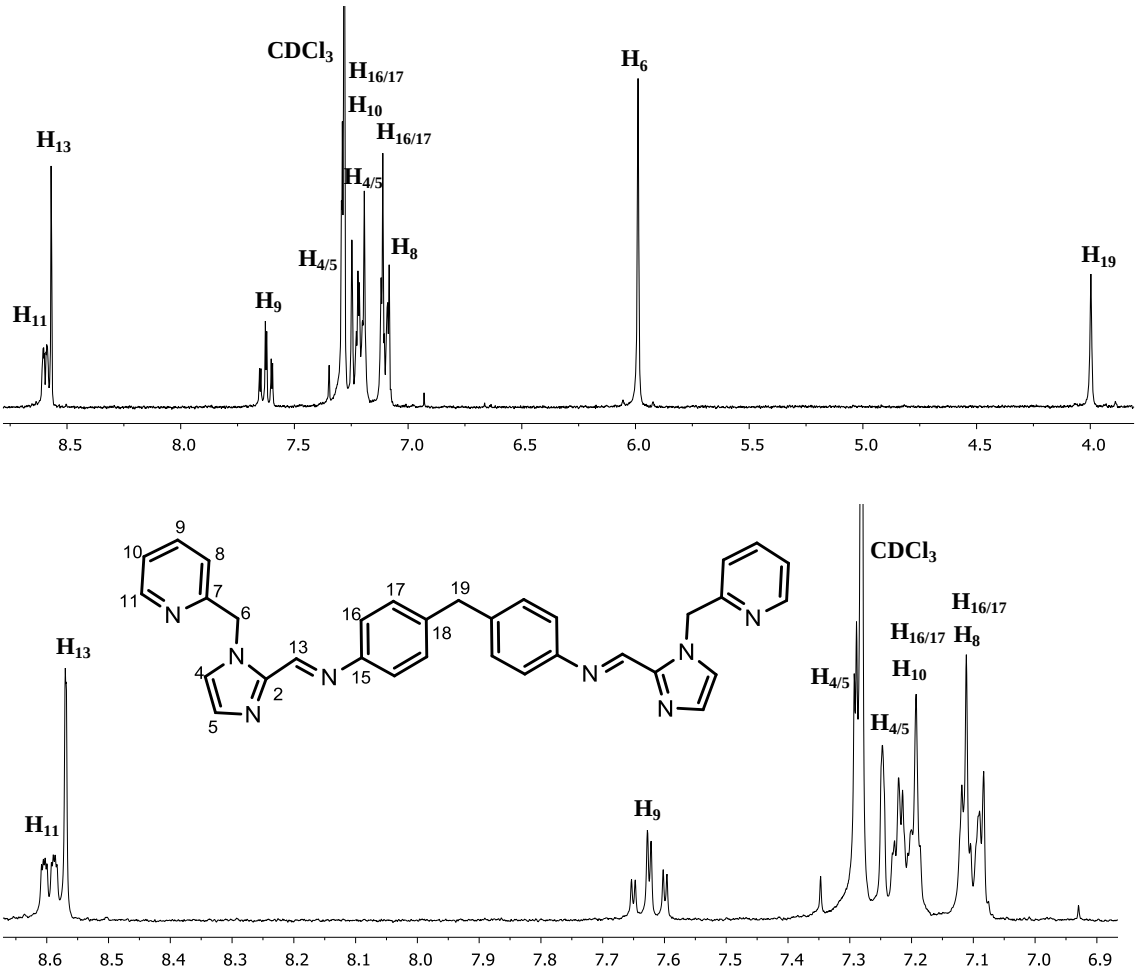

Figure 2.22 300 MHz ^{1}H NMR spectrum ($CDCl_3$, 298 K) of the ligand L_4 with an expansion of the aromatic region.

The ^{1}H NMR spectrum reveals 11 proton resonances. Two singlet peaks in the aliphatic region of the spectrum at 5.99 and 4.00 ppm are readily assigned as H_6 and H_{19} respectively. The signals for pyridine proton H_{11} (doublet of doublets) and imine proton H_{13} (singlet) appear downfield in the spectrum at 8.60 and 8.57 ppm. The H_8 and H_{10} pyridine resonances overlap with the signals from the phenylene protons, whereas H_9 appears as a triplet of doublets at 7.62 ppm. One of the imidazole proton resonances $H_{4/5}$ is partially hidden by the solvent peak.

2.4.4.1 Iron(II) complex of L_4

The formation of the iron(II) complex of L_4 was achieved by stirring L_4 with iron(II) chloride tetrahydrate at room temperature. A dark red solid precipitated from the solution upon addition of ammonium hexafluorophosphate. The ESI mass spectrum displays three peaks at *m/z* = 430 $[Fe_2(L_4)_3]^{4+}$, 622 $[[Fe_2(L_4)_3](PF_6)]^{3+}$, 1006 $[[Fe_2(L_4)_3](PF_6)_2]^{2+}$ which indicates the formation of the complex. The elemental analysis data is consistent with the empirical formula of $[Fe_2(C_{33}H_{28}N_8)_3](PF_6)_4 \bullet 3H_2O$. The red colour of the complex arises from the MLCT absorption band located at 553 nm (ε = 2400 $mol^{-1}dm^3\ cm^{-1}$). A ^1H NMR spectrum of the complex was recorded in CD_3CN solution (Fig. 2.23).

The ^1H NMR spectrum of $[Fe_2(L_4)_3](PF_6)_4$ displays 10 proton resonances. The signals corresponding to the H_{13} imine and imidazole protons H_4 and H_5 are significantly shifted downfield upon coordination to iron(II) metal ions compared to the free ligand. The H_6 protons are diastereotopic and appear as two doublets at 4.69 and 3.02 ppm. The pyridine signals for H_8 and H_{10} are overlapped and shown as a multiplet in the spectrum whereas the H_9 resonance and H_{11} appear as a triplet of doublets and doublet of doublets at 7.89 and 8.66 ppm respectively. The signal from imine proton H_{13} is overlapped with a signal from $H_{4/5}$ and appears as a broad singlet at 13.65 ppm. The phenylene resonances H_{16} and H_{17} coalesce and appear as two broad singlets at 7.23 and 5.96 ppm. These signals can be viewed only by increasing the magnitude of the spectrum.

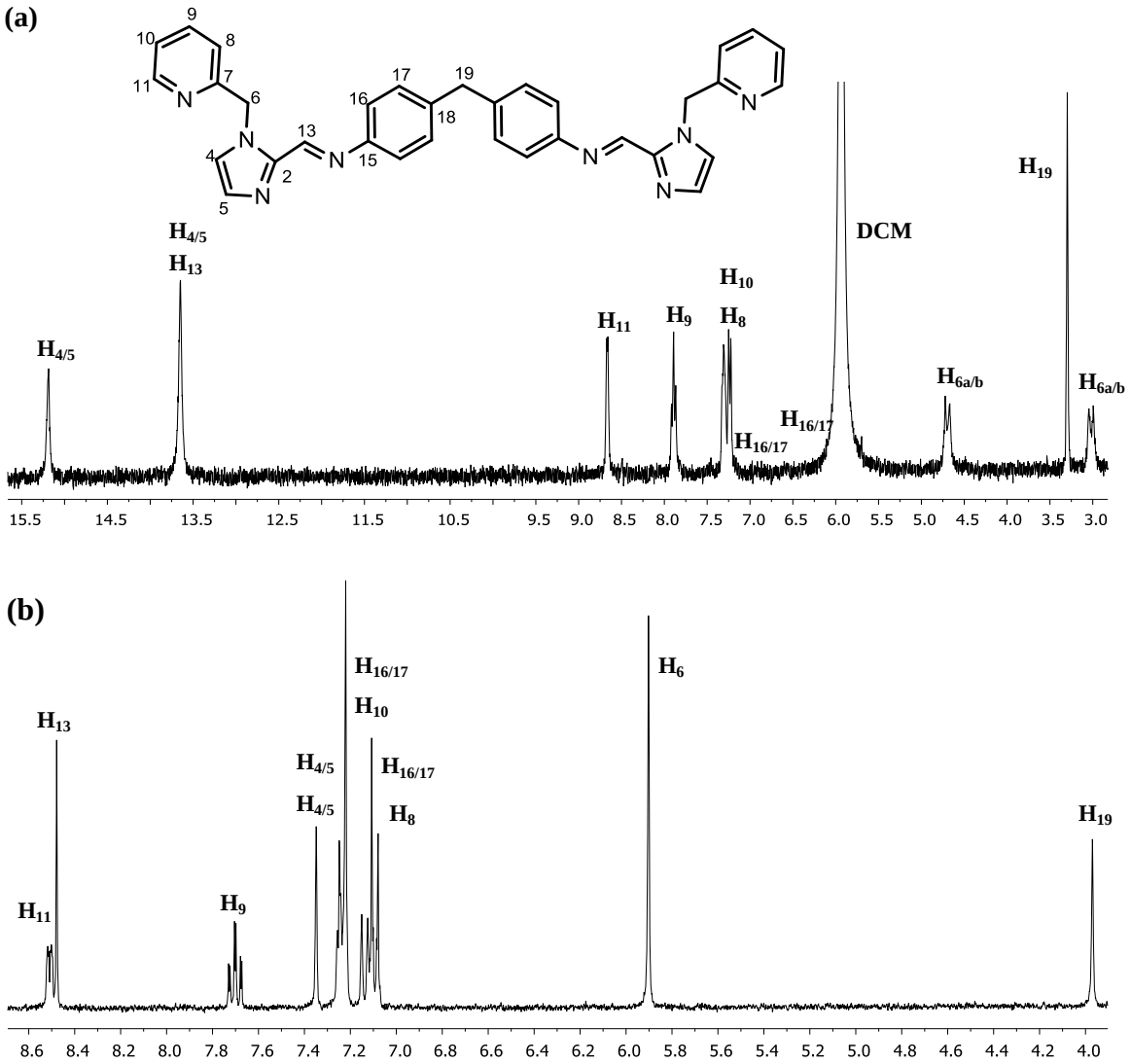

Figure 2.23 300 MHz ^{1}H NMR spectra (CD_3CN, 298K) of **(a)** $[Fe_2(L_4)_3](PF_6)_4$ **(b)** Ligand L_4.

Red crystals of $[Fe_2(L_4)_3](PF_6)_4$ complex suitable for X-ray analysis were obtained by slow diffusion of benzene into a solution of the complex in acetonitrile. The X-ray structure confirms the formation of the triple-stranded iron(II) helicate (Fig. 2.24).

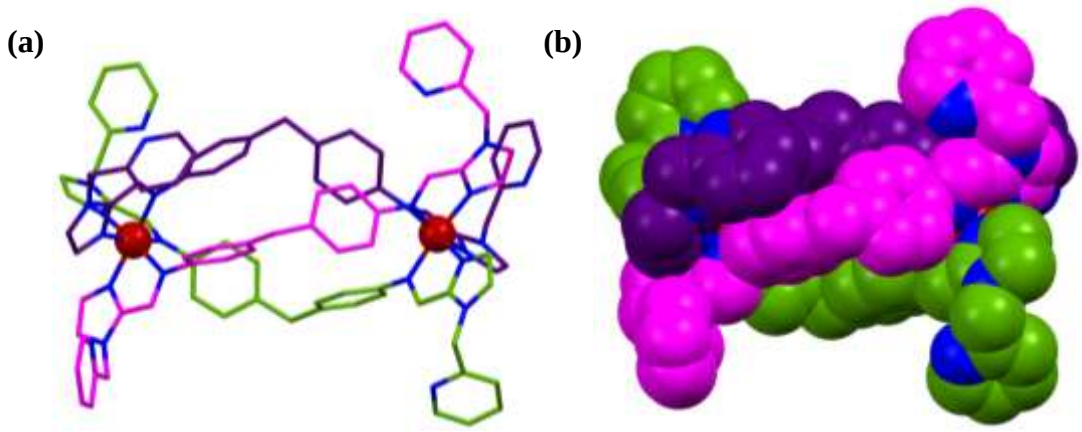

Figure 2.24 X-ray structure of $[Fe_2(L_4)_3](PF_6)_4$ complex **(a)** Perspective view **(b)** Space-filling representation of $[Fe_2(L_4)_3]^{4+}$ cation. Solvent molecules, hydrogen atoms and anions are omitted for clarity.

The metal centers are six-coordinate and have pseudo-octahedral geometry with Fe-N_{imine} bond distances of 1.970(5) - 2.026(5) and Fe-$N_{imidazole}$ distances of 1.956(5) - 1.972(5) Å with N_{imine}-Fe-$N_{imidazole}$ angles of 80.3(2) - 80.8(2)º. Each of the three ligand strands binds to two metal ions in such a way that they form a triple helical structure. The phenylene rings are located about the central CH_2 at angles to each other 113.4(5)º, 114.0(6)º and 113.7(5)º to allow intramolecular CH…π interactions in the centre of the helix. The phenylene rings are twisted at 73 - 89º with respect to the plane of imine chelating unit. The metal centres of the molecule are separated from each other by a distance of 11.4 Å. The pyridine rings are bent with respect to the imidazole units at different angles 109.2(10) - 113.4(6)º. There are four PF_6 counteranions along with benzene and acetonitrile solvent molecules found in the structure. The crystal packing diagram of the complex is shown in Figure 2.25.

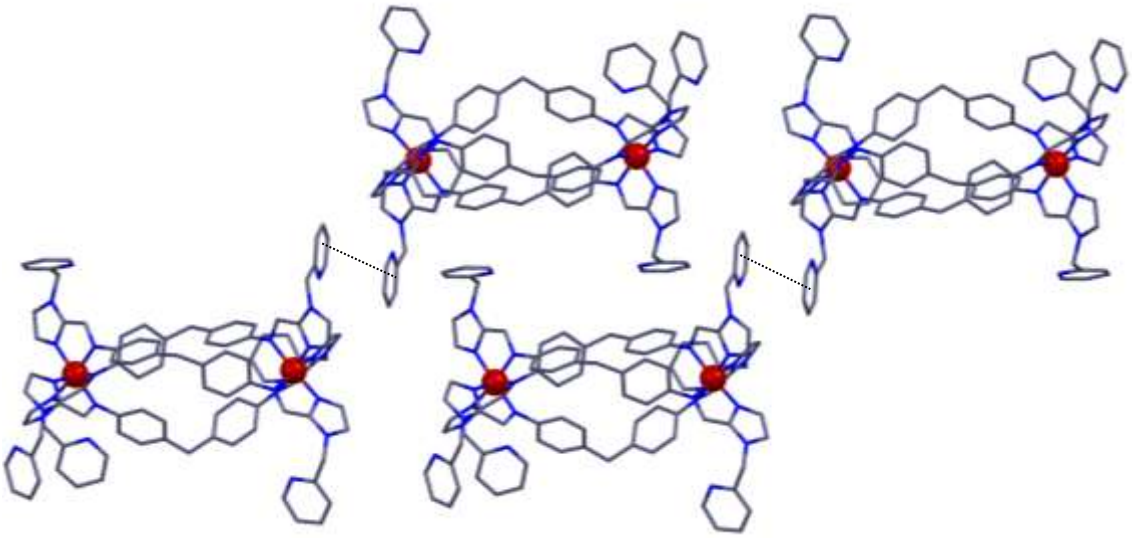

Figure 2.25 Packing diagram of $[Fe_2(L_4)_3](PF_6)_4$ showing π-π stacking interactions between the pyridine rings. Solvent molecules, hydrogen atoms and anions are omitted for clarity.

The crystal packing diagram reveals that the triple-helical architectures are arranged in a three-dimensional network with face to face π-π stacking interactions between the pyridine rings of different helical assemblies. The centroid-centroid distances of pyridine rings involved in π-π stacking are in the range of 4.1 - 4.5 Å.

The chloride salt of the synthesised iron(II) triple-stranded helicate is highly unstable when dissolved in water and falls apart within seconds. The complex is more stable in methanol although slow decomposition occurs as well.

The PF_6 salt of $[Fe_2(L_4)_3](PF_6)_4$ have been used in the experiment to attach cisplatin moieties onto the outside of the supramolecular assembly. However as in the case of the 4,4'-bipyridine based cylinder, upon addition of cisplatin in DMF the complex fell apart resulting in a colourless solution.

2.4.4.1 Nickel(II) complex of L_4

The nickel(II) complex was formed by stirring nickel(II) chloride hexahydrate with ligand L_4 under reflux in methanol overnight. The yellow solid precipitated from the mixture upon addition of diethyl ether. Partial microanalysis is consistent with the empirical formula of $[Ni_2(C_{33}H_{28}N_8)_3]Cl_4 \bullet 8H_2O$. The ESI mass spectrum shows three peaks at *m/z* = 432 $[Ni_2(C_{33}H_{28}N_8)_3]^{4+}$, 588 $[[Ni_2(C_{33}H_{28}N_8)_3]Cl]^{3+}$, 898 $[[Ni_2(C_{33}H_{28}N_8)_3]Cl_2]^{2+}$ and confirm the formation of the complex. The UV-Vis spectrum shows two broad bands at 260 nm (ε = 32600 $mol^{-1}dm^3cm^{-1}$) and 328 nm (ε = 55600 $mol^{-1}dm^3cm^{-1}$).

A paramagnetic NMR spectrum of the nickel(II) complex was recorded in CD_3OD (Fig. 2.26).

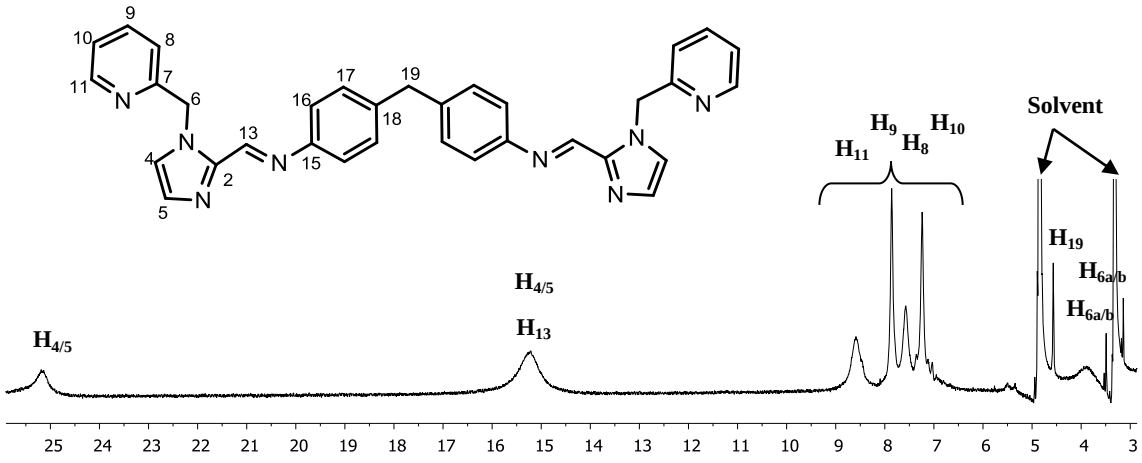

Figure 2.26 400 MHz paramagnetic ^1H NMR spectrum (CD_3OD, 298K) of the $[Ni_2(C_{33}H_{28}N_8)_3]Cl_4$ complex.

The proton resonances are considerably broadened and paramagnetically shifted. The single set of peaks suggests that the solutions species is symmetrical and consistent with a single species. There are 9 well-defined resonances, however it has not been

possible to fully assign the spectrum. The resonances from H_{16} and H_{17} have not been identified; apparently they are very weak and broadened.

Yellow crystals of the $[Ni_2(C_{33}H_{28}N_8)_3](PF_6)_4$ complex suitable for X-ray diffraction analysis were obtained by slow diffusion of benzene into a solution of the complex in acetonitrile. The X-ray structure confirms the formation of a triple-stranded Ni(II) helicate (Fig. 2.27).

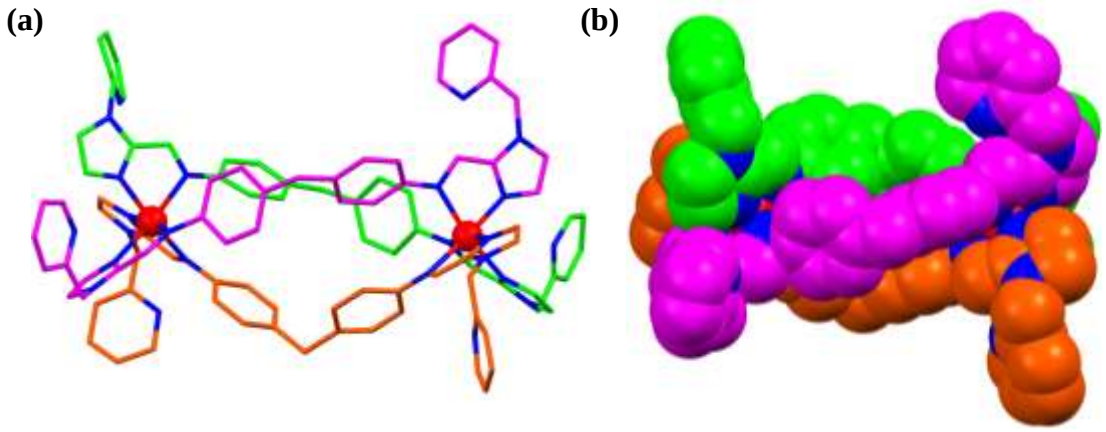

Figure 2.27 X-ray structure of $[Ni_2(L_4)_3](PF_6)_4$ complex **(a)** Perspective view **(b)** Space-filling representation of $[Fe_2(L_4)_3]^{4+}$ cation. Solvent molecules, hydrogen atoms and anions are omitted for clarity.

The Ni(II) metal centers are six-coordinate and have pseudo-octahedral geometry with Fe-N_{imine} bond distances of 2.106(13) - 2.207(11) and Fe-$N_{imidazole}$ distances of 2.051(11) - 2.095(16) Å with N_{imine}-Fe-$N_{imidazole}$ angles of 78.3(4) - 79.9(5)º. Three ligand strands of the complex are wrapped around two Ni(II) metal centres in a helical fashion. The phenylene rings are twisted at 80 - 89º with respect to the imine metal chelating unit. The Ni-Ni intermetallic distance in the complex is 11.6 Å. The pyridine rings are bent with respect to the imidazole units at different angles of 112.0(2) - 119.1(13). The nickel helicate is tetracationic and has four PF_6 counteranions. The

solvent molecules are present in the structure however they are highly disordered and it was not possible to successfully refine them.

The crystal packing diagram reveals that the triple-helical architectures are arranged in a three-dimensional chain network (Fig. 2.28). No π-π stacking interactions were found between the arrays of the helicates.

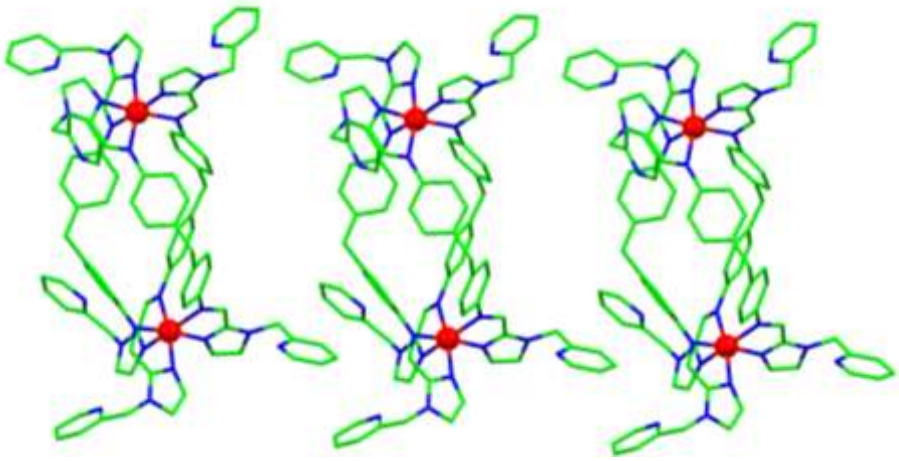

Figure 2.28 Packing diagram of $[Ni_2(L_4)_3]^{4+}$. Solvent molecules, hydrogen atoms and anions are omitted for clarity.

The chloride salt of Ni(II) triple-stranded helicate is very soluble in water and was used for DNA binding studies and biological evaluation.

2.5 Lanthanide helicates

2.5.1 Overview

Lanthanide helicates are of great interest to many research groups due to their ability to emit light in the visible or near-infrared region. These complexes can be used as bioprobes for cell and organ imaging and for tracking processes inside the cell. Wrapping ligand strands around lanthanide metal centres by self-assembly processes affords robust molecules with interesting chemical and photophysical properties. The characteristic luminescent properties of trivalent lanthanide metal ions such as sharp emission lines, large Stokes shifts upon ligand excitation, little or no photobleaching, and long lifetimes of the excited states, make them attractive bioprobes.[26, 27]

A few examples of lanthanide helicates have been reported in literature. Pikramenou and co-workers established the synthesis of highly luminescent, triple- and quadruple-stranded, dinuclear Eu, Nd, and Sm(III) lanthanide complexes based on bis-diketonate ligands (Fig 2.29).[28]

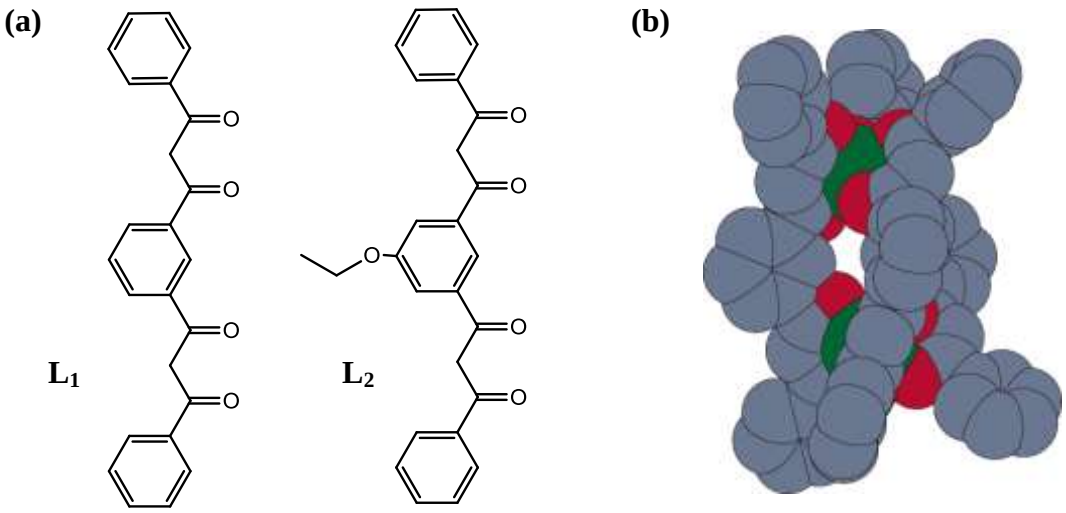

Figure 2.29 (a) Bis-diketonate ligands used in synthesis of lanthanide complexes **(b)** Molecular model of $[Eu_2(L_1)_3]$ complex.[28]

The ligands L_1 and L_2 have two conjugated diketonate binding sites which are connected together by a 1,3-phenylene spacer. The ligands bind to lanthanide metal ions to form neutral dinuclear triple-stranded complexes $[M_2(L_1)_3]$ (M = Eu, Nd, Sm, Y, Gd) and $[M_2(L_2)_3]$ (M = Eu, Nd) or anionic quadruple-stranded dinuclear lanthanide units $[Eu_2L^1{}_4]^{2-}$. The synthesised complexes show strong visible (red or pink) and near-infrared luminescence when irradiated at the ligand band, around 350 nm, and have 11 times more intense emission signals compared to their mononuclear analogues.[28]

Bünzli *et al.* reported europium(III) triple-stranded helicate based on ligand L_3 which was used in experiments to study the cellular distribution and cellular uptake of the complex (Fig. 2.30).[29]

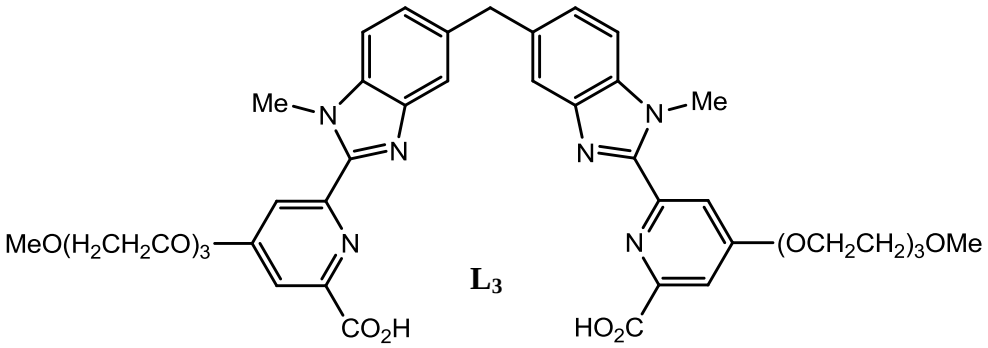

L3

Figure 2.30 Chemical structure of the ligand L_3.

The synthesised $[Eu_2(L_3)_3]$ helicate is water soluble, highly stable and non-cytotoxic. It displays strong luminescence and has a long luminescence lifetime. It was found out that europium(III) helicate is able to permeate into HeLa cells by endocytosis and stain their cytoplasm. The bimetallic complex was seen in endosomes and lysosomes which are predominantly located around the nucleus. Thus the $[Eu_2(L_3)_3]$ helicate behaves as an optical probe which can be used for the elucidation of cellular uptake and cellular localisation.[29]

More recently, Piguet and co-workers described a double-stranded bimetallic Lu(III) helicate using bis-tridentate ligand L_4 (Fig. 2.31). The flexibility of the spacer in the ligand is limited by the central rigid phenyl ring.[30]

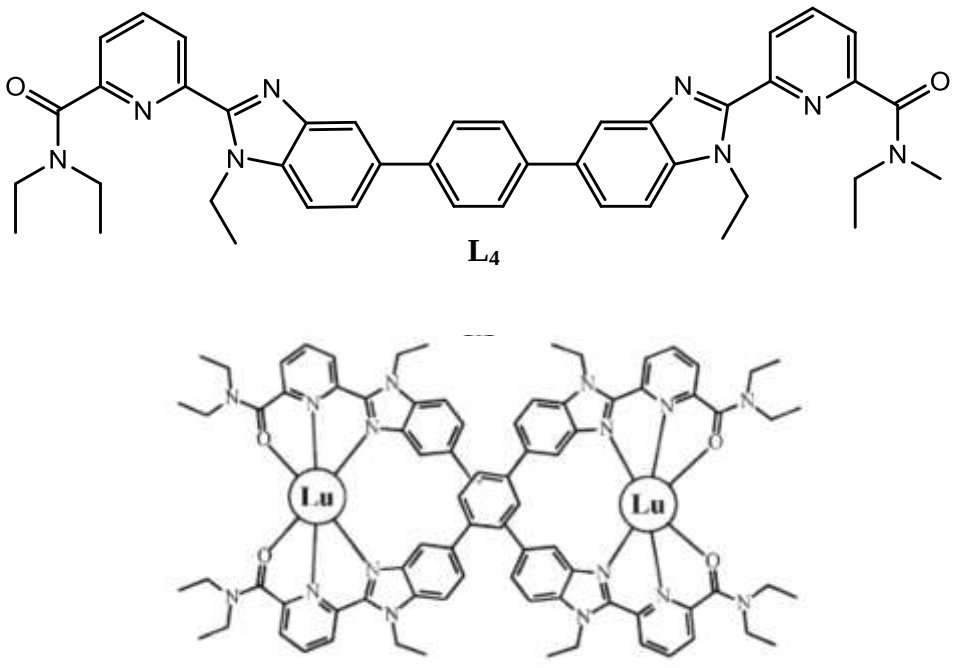

Figure 2.31 Schematic representation of ligand L_4 and $[Lu_2(L_4)_2]^{6+}$ complex.[30]

The X-ray structure reveals the double-helical nature of the complex. Each Lu(III) metal centre is octa-coordinate, with two tridentate binding units and two monodentate triflate anions. The main torsions in the ligands are caused by the rotation about the interannular C-C bond which links the aromatic benzimidazole and phenyl rings, forming slightly distorted dodecahedrons.[30]

Hamacek *et al.* reported the first pentanuclear lanthanide helicate formed from two different tripodal ligands and europium(III) metal ions (Fig. 2.32).[31] One ligand forms the base of the tetrahedron whereas three strands of the other form side faces and the linear part of the helical structure.

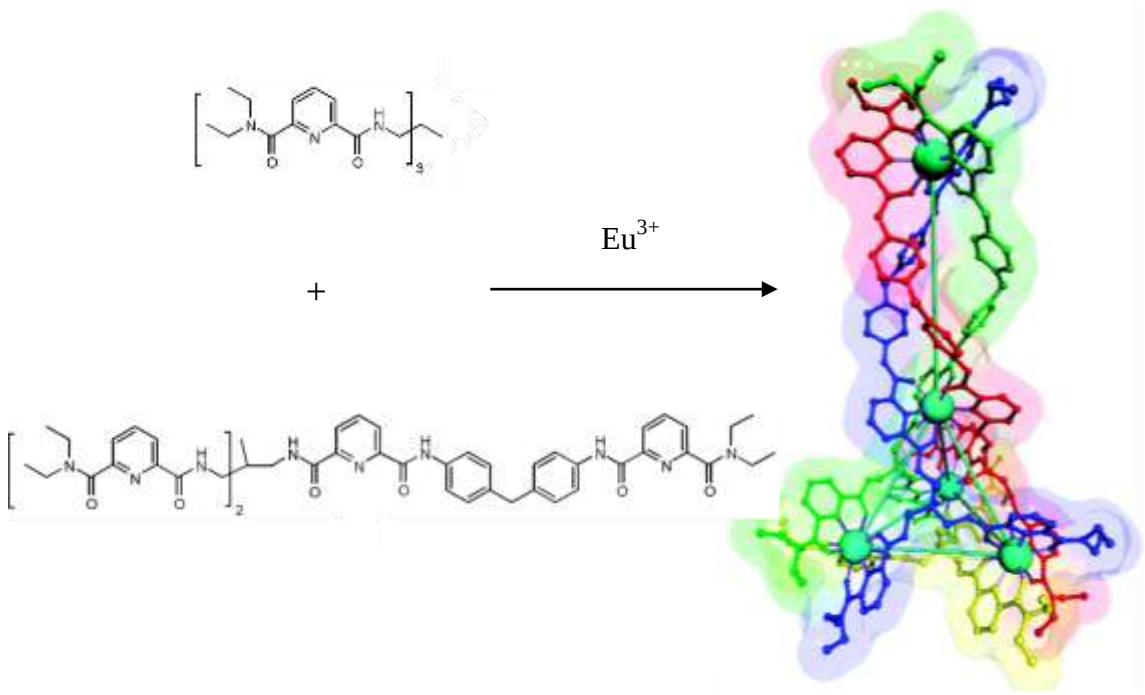

Figure 2.32 Self-assembly process of pentanuclear helicate. View of the calculated structure of $[Eu_5(L_5)(L_6)_3]^{15+}$ (SPARKLE/AM1 model). Hydrogen atoms are omitted for clarity.[31]

The self-assembly of the helicate was predicted on the structural basis obtained for linear and tetranuclear supramolecular compounds. The formation of the complex was experimentally evidenced by NMR and ESMS spectra.[31]

Herein we describe the synthesis of a europium(III) complex with a helical structure. The europium(III) complex was prepared according to a modified procedure reported in the literature.[32] This work was done in collaboration with Doctor Dave Lewis from Dr. Zoe Pikramenou`s group, who provided advice on the design of the europium(III) helicate.

2.5.2 Synthesis of europium(III) helicate

2.5.2.1 Synthesis of ligand L_5

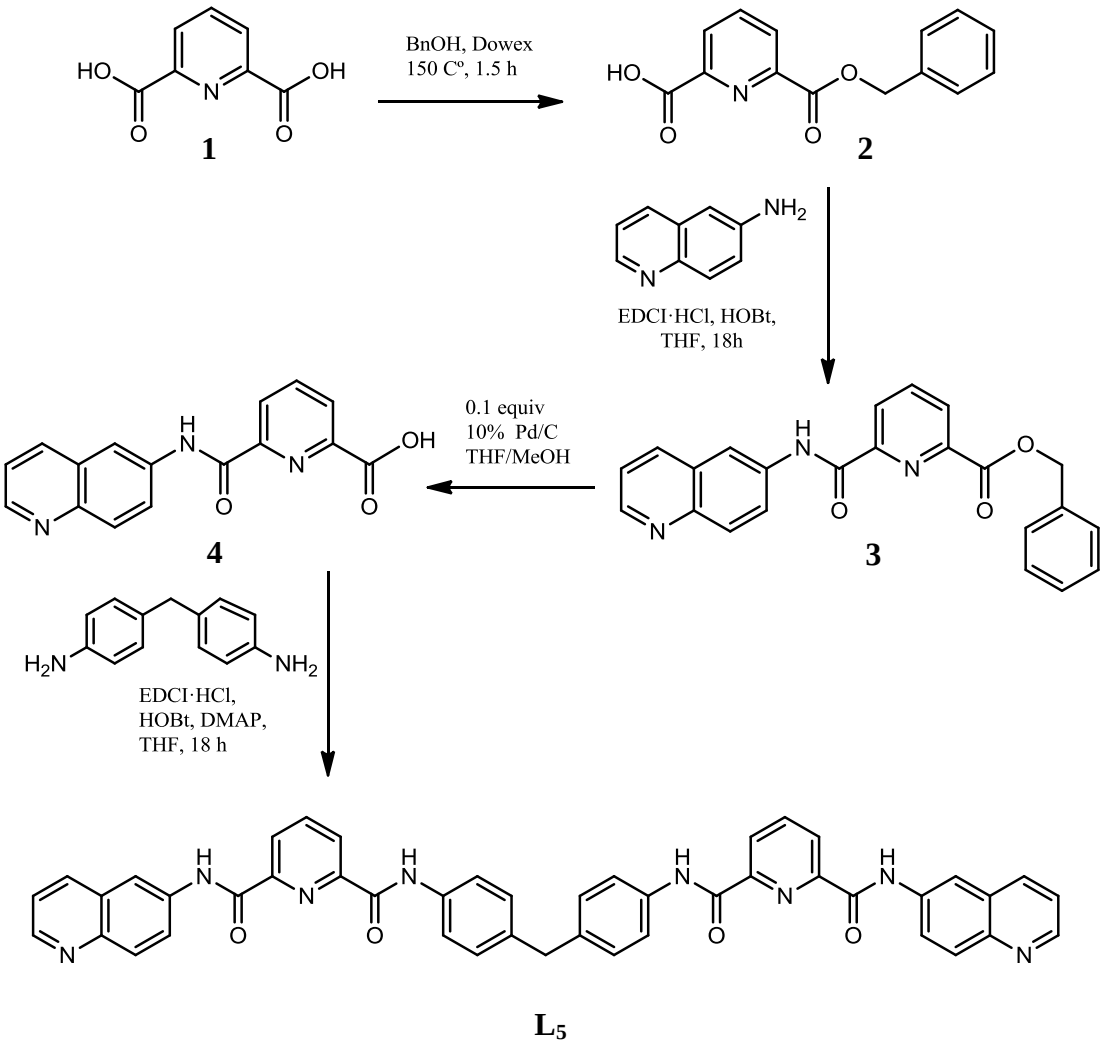

Scheme 2.7 Schematic procedure for the synthesis of $[Eu_2(L_5)_3]Cl_6$ complex

The ligand L_5 was developed to facilitate coordination of europium(III) to two pyridyl nitrogens and 2,6-dicarboxylic amides. The ligand was prepared by a multiple step synthesis from commercially available starting materials.

In the first step of the synthesis, 2,6-pyridinecarboxylic acid **1** was reacted with benzyl alcohol in the presence of ion exchange resin DOWEX 50-X8 H^+ to form 2,6-

pyridinecarboxylic acid mono benzyl ester **2** by a Fisher esterification mechanism.[32, 33] The reaction was refluxed for 1.5 hours and after work up the crude product was obtained as a colourless oil. Recrystallisation from ethyl acetate afforded the desired product as a white powder.

In the second step, the monoprotected 2,6-pyridine carboxylic acid **2** was reacted with 6-aminoquinoline using carbodiimide coupling methodology to yield 6-(quinoline-6-ylcarbamoyl) picolinate **3**. The reaction was carried out for 18 hours and the resulting crude product was purified by column chromatography using 2% DCM/CH_3OH solution as an eluent. The second band eluted was identified as the desired product **3**.

The third step of the synthesis involved deprotection of the benzyl ester using the hydrogenation technique. The intermediate compound **3** was stirred with 10 % Pd/C catalyst in a THF/CH_3OH (50:50) solution under a hydrogen atmosphere to yield 6-(quinoline-6-ylcarbamoyl) picolinic acid **4**. Completion of the reaction was followed by TLC. The isolated product, a yellow solid, was used in the next step without further purification.

The formation of the ligand L_5 was achieved by reacting intermediate **4** with 4,4'-methylenedianiline via a carbodiimide peptide coupling reaction. The crude product was purified on a silica column using 5 % DCM/CH_3OH solution as an eluent. The ligand was obtained as an off-white solid in approximately 37 % yield. The product was characterized by mass spectrometry and NMR techniques. The ESI mass spectrum of L_7 displays a peak at *m/z* = 771 which corresponds to $\{C_{45}H_{32}N_8O_4 + MeOH\}^+$. Partial elemental analysis is consistent with the formation of the ligand of the empirical formula of $C_{45}H_{32}N_8O_4$. The IR spectroscopy reveals several characteristic bands relating to the functional groups of ligand L_5. The υN-H strecthcing vibration of peptide

bond appears at 3303 and 3229 cm^{-1}. The strong band at 1525 cm^{-1} results from υN-H bending. Bands at 3027 and 1658 cm^{-1} are assigned as υC-H aromatic and υC=O stretching.

A ^{1}H NMR spectrum of the ligand was recorded in d_6-DMSO (Fig. 2.33). The spectrum displays 14 proton resonances and one solvent residue peak. All the protons were assigned using 1D and 2D NMR techniques.

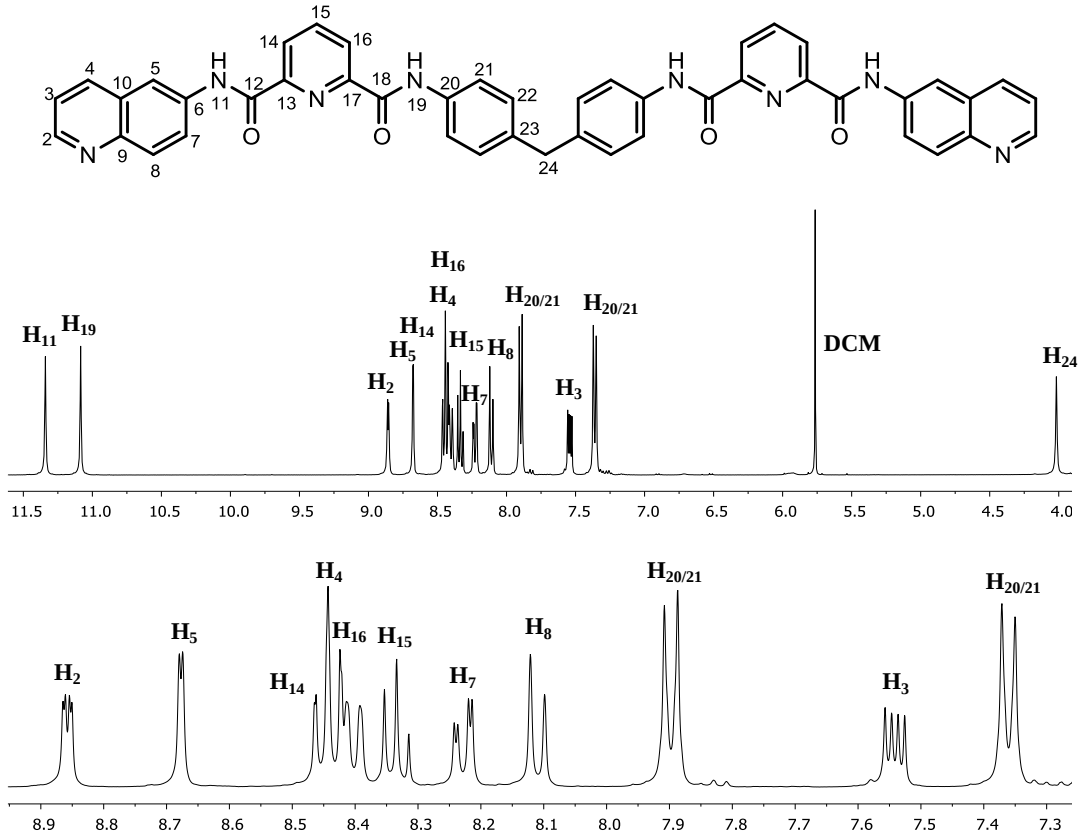

Figure 2.33 300 MHz ^{1}H NMR spectrum (d_6-DMSO, 298 K) of L_5 with an expansion of the aromatic region.

The single peak appearing at 4.02 ppm is readily assigned as H_{24}. Phenylene protons H_{20} and H_{21} are displayed in the spectrum as two sharp doublets at 7.80 and 7.36 ppm respectively. The resonances H_{11} and H_{19} of the peptide bond appear

downfield at 11.34 and 11.09 ppm as two singlets. The signal for H_2, displayed as a doublet of doublets at 8.86 ppm appears downfield due to its proximity to the nitrogen atom. The aminoquinoline proton resonances H_5 (doublet) at 8.68 ppm, H_7 (doublet of doublets) at 8.23 ppm, H_8 (doublet) at 8.11 ppm and H_3 (doublet of doublets) at 7.54 ppm can be assigned according to their characteristic splitting patterns. The signal from H_4 is overlapped with the signals from H_{14} and H_{16} of the pyridine. The resonance at 8.33 ppm appearing as a triplet results from H_{15}.

2.5.2.2 Synthesis of europium(III) complex of L_5

The europium(III) complex of L_5 was obtained by reacting two equivalents of the ligand with three equivalents of europium(III) chloride hexahydrate in a mixture of $CH_3OH/CHCl_3$ (1:1). The reaction was refluxed for 24 hours and the desired product was isolated by precipitation with diethyl ether. The elemental analysis is consistent with the formation of the europium(III) complex with the empirical formula of $[Eu_2(C_{45}H_{32}N_8O_4)_3]Cl_6 \bullet 3CHCl_3 \bullet H_2O$. Two different techniques, ESI and MALDI, were used in order to record a mass spectrum of the complex, however no peak was observed corresponding to the synthesised compound. The UV/Vis spectrum of the complex shows a broad band located at ~ 308 nm (ε = 84700 $mol^{-1}dm^3cm^{-1}$) nm.

A very weak ^1H NMR spectrum of the complex with broad proton resonances was obtained (not shown) and it has not been possible to fully assign it. Therefore to confirm the formation of the europium(III) complex, luminescence experiments were performed and the characteristic Eu(III) luminescent pattern upon excitation of the aminoquinoline units was recorded. The absorption spectrum of the europium(III) complex in DMSO showed the presence of a broad band for the aminoquinoline moieties (Fig. 2.34 (a)).

Excitation of this band resulted in an Eu(III) emission with λ_{max} = 613 nm (Fig. 2.34 (b)).

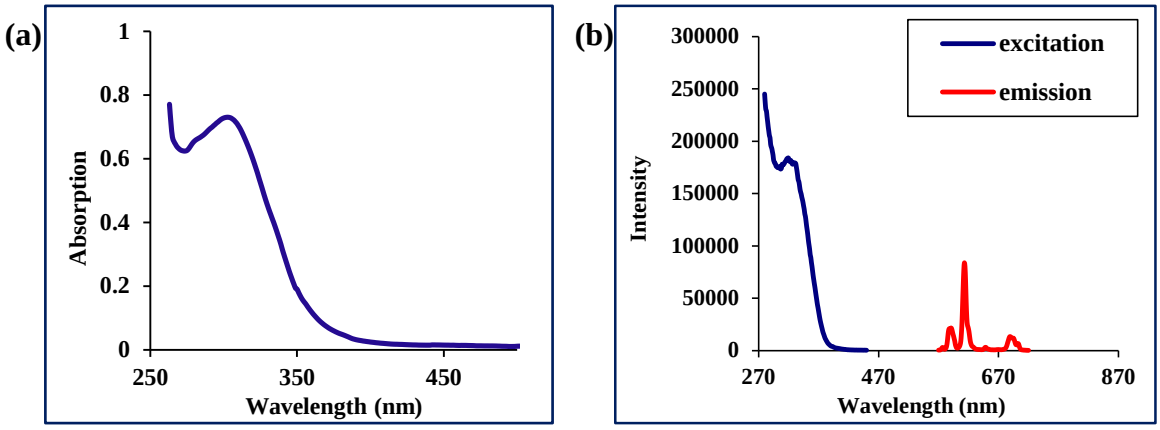

Figure 2.34 (a) Absorption spectrum of Eu(III) complex of L_5 **(b)** Excitation and luminescence spectra of europium(III) complex of L_5 recorded in DMF.

The characteristic fluorescence pattern of europium observed suggests that the europium(III) metal ions are bound to the ligand L_5. The quinoline units act as antennae to transfer energy to the lanthanide ions resulting in sensitized lanthanide emission. Narrow emission bands of the Eu(III) complex are observed at 572, 587, 613, 643, 687 nm respectively.

The obtained europium(III) complex is not soluble in water but is soluble in DMSO and DMF. The insolubility in water as well as poor yield of the europium(III) complex were the main drawbacks for performing DNA binding studies and other biological experiments and this was not pursued further.

2.6 Conclusions

In this chapter, the synthesis and characterisation of novel metallo-helicates has been discussed. The additional metal binding units were introduced on to the outside of ligands L_1, L_2, L_3, L_4 to afford binding of cisplatin. The attempts to attach cisplatin to $[Fe_2(L_3)_3](PF_6)_4$ and $[Fe_2(L_4)_3](PF_6)_4$ complexes failed as the compounds fell apart. Remarkably, combining $[Fe_2(L_3)_3](PF_6)_4$ complex with cisplatin was successful however the compound is poorly soluble in water and relatively stable only at low temperatures. The iron(II) triple-stranded helicate of ligand L_2 did not form due to steric constraints, nevertheless double-stranded helicates of L_2 with copper and silver tetrahedral metal ions were synthesized.

The ligand L_5 was designed to form luminescent europium(III) helicate. The formation of the complex was confirmed by elemental analysis and characteristic emission spectrum of europium(III) recorded in DMF.

2.7 References :

1. D. G. Sar, M. Montes-Bayon, E. B. Gonzalez, L. M. Sierra, A. Sanz-Medel, *Chem. Res. Toxicol.*, 2011, 1-33.
2. M. J. Hannon, C. L. Painting, A. Jackson, J. Hamblin, W. Errington, *Chem. Commun*., 1997, 1807-1808.
3. S. Khalid, M. J. Hannon, A. Rodger and P. M. Rodger, *Chem. Eur. J.*, 2006, **12**, 3493-3506.
4. A. Oleksi, A. G. Blanco, R. Boer, I. Usón, J. Aymamí, A. Rodger, M. J. Hannon, M. Coll, *Angew. Chem., Int. Ed.*, 2006, **45**, 1227-1231.
5. A. C. G. Hotze, N. J. Hodges, R. E. Hayden, C. Sanchez-Cano, C. Paines, N. Male, M.-K. Tse, C. M. Bunce, J. K. Chipman, M. J. Hannon, *Chem. Biol.*, 2008, **15**, 1258-1267.
6. M. Pascu, PhD thesis, University of Birmingham, 2007.
7. S. Komeda, T. Moulaei, K. K. Woods, M. Chikuma, N. P. Farrell, L. D. Williams, *J. Am. Chem. Soc.*, 2006, **128**, 16092-1610.
8. R. Kieltyka, P. Englebienne, J. Fakhoury, C. Autexier, N. Moitessier, H. F. Sleiman, *J. Am. Chem. Soc.*, 2008, **130**, 10040-10041.
9. R. D. Schnebeck, E. Freisinger, B. Lippert, *Chem. Commun.*, 1999, 675-676.
10. G. Lowe, A. S. Droz, T. Vilaivan, G. W. Weaver, J. J. Park, J. M. Pratt, L. Tweedale, L. R. Kelland, *J. Med. Chem.*, 1999, **42**, 3167-3174.
11. P. Shao, W. Sun, *Inorg. Chem.*, 2007, **46**, 8603-8612.

12. P. J. Lusby, P. Müller, S. J. Pike, and A. M. Z. Slawin, *J. Am. Chem. Soc.*, 2009, **141**, 16398-16400.

13. L. Zerzankova, H. Kostrhunova, M. Vojtiskova, O. Novakova, T. Suchankova, M. Lin, Z. Guo, J. Kasparkova,V. Brabec, *Biochem. Pharmacol.*, 2010, **80**, 344-351.

14. M. Pascu, F. Tuna, E. Kolodziejczyk, G. Pascu, G. Clarkson, M. J. Hannon, *Dalton Trans.*, 2004, 1546-1555.

15. C. Painting, PhD thesis, University of Warwick, 1999.

16. R. Cini, A. Donati, R. Giannettoni, *Inorg. Chem. Acta*, 2001, **315**, 73-80.

17. M. Huxley, PhD thesis, University of Warwick, 2006

18. L. J. Childs, M. Pascu, A. J. Clarke, N. W. Alcock, and M. J. Hannon, *Chem. Eur. J.*, 2004, **10**, 4291-4300.

19. M. Pascu, PhD thesis, University of Birmingham, 2008.

20. C.-L. Chen, J. M. Ellsworth, A. M. Goforth, M. D. Smith, C.-Y. Su, H.-C. zur Loye, *Dalton Trans*., 2006, 5278-5286.

21. F. Minisci, A. Citterio, *Acc. Chem. Res.*, 1983, **16**, 27-32.

22. J. Hodačová, M. Buděšínský, *Org. Lett.*, 2007, **9**, 5641-5643.

23. O. Maury, J.-P. Guégan, T. Renouard, A. Hilton, P. Dupau, N. Sandon, L. Toupet, H. le Bozec, *New J. Chem.*, 2001, **25**, 1553-1566.

24. G. J. Bridger, R. T. Skerlj, A. Kaller, C. Harwig, D. Bogucki, T. Wilson, J. Crawford, E. J. McEachern, B. Atsma, S. Nan et al, *PCT Int. Appl.*, 2003, WO 2003055876 A1 20030710.

25. J. L. Moore, S. M. Taylor, V. A. Soloshonok, *ARCHIVOC*, 2005, **6**, 287-292.

26. J.-C. G. Bünzli, A.-S. Chauvin, C. D.B. Vandevyver, S. Bo, S. Comby, *Ann. N.Y. Acad. Sci.*, 2008, **1130**, 97-105.

27. M. Albrecht, *Z. Anorg. Allg. Chem.*, 2010, 2198-2204.

28. A. P. Bassett, S. W. Magennis, P. B. Glover, D. J. Lewis, N. Spencer, S. Parsons, R. M. Williams, L. De Cola, Z. Pikramenou, *J. Am. Chem. Soc.*, 2004, **126**, 9413-9424.

29. B. Song, C. D. B. Vandevyver, A.-S. Chauvin, J.-C. G. Bünzli, *Org. Biomol. Chem.*, 2008, **6**, 4125-4133.

30. J.-F. Lemonnier, L. Guénée, G. Bernardinelli, J.-F. Vigier, B. Bocquet, C. Piguet, *Inorg. Chem.*, 2010, **49**, 1252-1265.

31. B. E. Aroussi, S. Zebret, C. Besnard, P. Perrottet, J. Hamacek, *J. Am. Chem. Soc.*, 2011, **133**, 10764-10767.

32. F. Stomeo, C. Lincheneau, J. P. Leonard, J. E. O'Brien, R. D. Peacock, C. P. McCoy, T. Gunnlaugsson, *J. Am. Chem. Soc.*, 2009, **131**, 9636-9637.

33. Y. Hamuro, S. J. Geib, and A. D. Hamilton, *J. Am. Chem. Soc.*, 1997, **119**, 10587-10593.

Chapter 3

DNA binding studies

3.1 Introduction

The medicinal applications of metal complexes are of increasing interest due to their unique physico-chemical properties together with their biological activity. Thus, for example, transition metal complexes are being investigated as potential chemotherapeutic agents.[1] It is believed that DNA is the main target for metallo-anticancer drugs currently in the clinic. Molecules that are able to bind to the DNA can access cellular information and hence take part in controlling gene expression.

The supramolecular iron(II) helicate designed in Hannon`s laboratory and formed by wrapping three ligand strands around transition metal ions was shown to bind to the major groove of the DNA, induce dramatic intermolecular coiling and exhibit biological activity in cancer cell lines. Circular and linear dichroism studies confirmed the binding of the complex to the DNA in an oriented fashion. Furthermore the iron(II) complex stabilises DNA three-way junctions with a helicate residing in the cavity of the junction. All these examples of the interaction of the iron(II) cylinder with DNA suggest that the biological activity of the complex can be associated with DNA as one of the main targets for the synthesised helicate.[2, 3]

By modulating the structure of the parent iron(II) cylinder, novel metallo-supramolecular helicates have been synthesised and characterised in chapter 2 . In this chapter DNA binding studies of the helicates are explored using circular and linear dichroism, UV/Vis spectroscopy and gel electrophoresis techniques.

3.2 UV/Vis spectroscopy

UV/Vis spectroscopy is used to provide information about the structure of the molecule and the electronic transitions occurring in the molecule upon excitation with light, as well as to perform quantitative analysis of the sample. Light is electromagnetic radiation. When radiation of wavelength between 200 to 700 nm (UV/Vis) interacts with a molecule it can stimulate the transition of p-, d- or π- electrons from bonding or lone pair orbitals to unfilled non-bonding or anti-bonding orbitals, increasing the energy of the sample.[4]

The amount of light absorbed by the sample is proportional to the number of absorbing molecules in the solution and length of the light pathway. The absorbance of the sample can be calculated using the following equation:

$$\mathbf{A = \log_{10} (I_0 / I)}$$

$\mathbf{I_0}$ is incident intensity of the light and **I** is transmitted intensity of the light.

To define the concentration of the sample with known absorbance the Beer-Lambert law can be used.

$$\mathbf{A = \varepsilon\, c\, l}$$

A – absorbance (arbitrary units), **ε** – molar absorption or extinction coefficient (mol^{-1} dm^3 cm^{-1}), **c** – concentration of the sample (mol dm^3), **l** is a length of the light pathway (cm).

UV/Vis spectroscopy is utilised in the work herein to obtain information about the stability of the synthesised complexes, to define their molar absorption coefficients and to calculate the concentration of ct-DNA for circular and linear dichroism experiments. The characteristic UV/Vis spectrum of ct-DNA gives a maximum peak at 260 nm (Fig.

3.0) which corresponds to π→π* transitions of the delocalised electrons of the DNA bases.

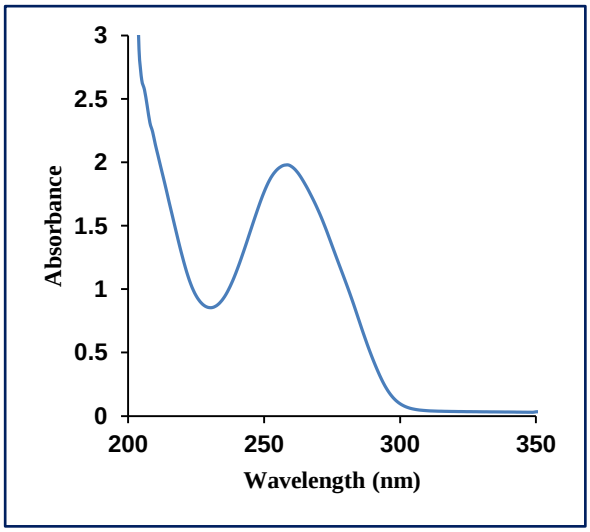

Figure 3.0 UV/Vis spectrum of 300 μM ct-DNA.

The concentration of DNA can be calculated by measuring the absorbance at 260 nm and using the Beer-Lambert law with a known molar absorption coefficient (e.g. ε = 6600 mol^{-1} dm^3 cm^{-1} for ct-DNA at 260 nm).[4]

3.3 Circular dichroism spectroscopy.

The circular dichroism (CD) technique is applied to study chiral molecules and their interactions. Circular Dichroism is the difference in absorption of left and right circularly polarised light and can be expressed by the following equation:

$$\mathbf{CD = A_L - A_R}$$

Achiral molecules and racemic mixtures do not give rise to a CD signal. Chiral molecules do not have a reflection plane and neither do their electrons, thus the electrons move in some kind of helix. In circularly polarized light electric field vectors

trace out helices. Therefore the interactions of the chiral molecule with left- and right-circularly polarised light will be different.

DNA is a chiral molecule due to the presence of chiral sugar units. Phosphates and the bases of the DNA are individually achiral but when bound all together with chiral sugars they become a part of the chiral molecule. When a CD spectrum of DNA is measured, a CD signal corresponding to transitions of the nucleobases (as a result of their coupling with backbone) is detected. The characteristic CD spectrum of the B-DNA has a positive band at ~ 275 nm, a negative band at ~ 240 nm with the zero being around 258 nm (Fig. 3.1 (a)).

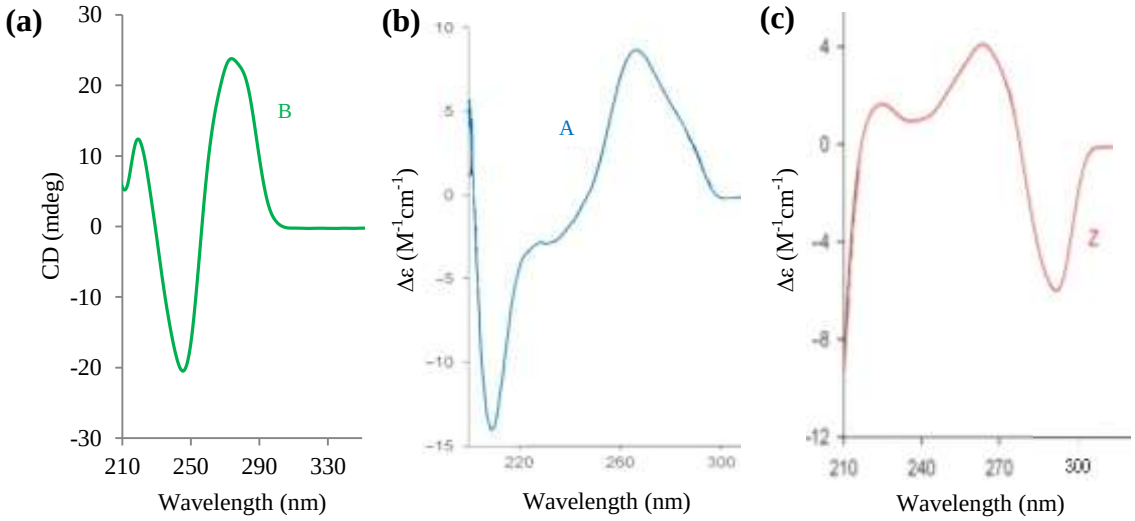

Figure 3.1 Circular dichroism spectra of (a) B-DNA (b) A-DNA (c) Z-DNA.[5]

A-DNA is characterized by a positive CD band at ~ 260 nm, a negative band at ~ 210 nm and a very intense positive band at 190 nm (Fig. 3.1 (b)).

Z-form DNA is formed for poly[d(G-C)]$_2$ in the presence of highly charged cations. The CD spectrum of Z-DNA is characterised by a negative CD band at ~ 290 nm and a positive band at ~ 260 nm (Fig. 3.1 (c)).

Many DNA binding molecules are achiral themselves and do not give rise to any CD signal. However, when they bind to DNA they experience a chiral environment and can exhibit a CD signal which indicates an interaction with the chiral DNA. In this work CD titrations of the synthesised metal complexes with DNA have been performed. Any changes in the shape of the characteristic DNA CD spectrum imply DNA-metal complex interactions.[6]

3.4 Linear dichroism spectroscopy

Linear Dichroism (LD) is the difference in the absorption of light linearly polarised parallel and perpendicular to an orientation axis of the molecule.

$$\mathbf{LD = A_{\parallel} - A_{\perp}}$$

In linearly polarised light all the photons have their electric component oscillating in one plane. In order to obtain an LD signal the molecule has to be oriented. Flow orientation is one of the methods used to orient the molecule. Orientation is achieved by viscous drag resulting from the flowing the solution between narrow walls. In this work a couette flow cell was used to orient the DNA molecule (Fig. 3.2).

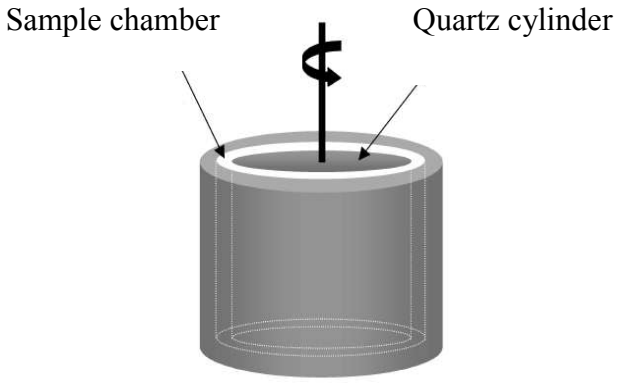

Figure 3.2 Schematic representation of couette flow cell.[6]

The molecule to be investigated is placed in a sample chamber between two quartz cylinders, one of which can rotate. When rotation is applied the sample is oriented by the direction of the flow. The speed of the rotation should be fast enough in order to orient molecules but not so fast as to cause turbulent flow.

The LD signal for B-DNA is depicted in Figure 3.3. The bases of the DNA are arranged approximately at right angle to the direction of the orientation which in turn leads to a negative band at ~ 260 nm as the electronic transitions occur parallel to the DNA bases.

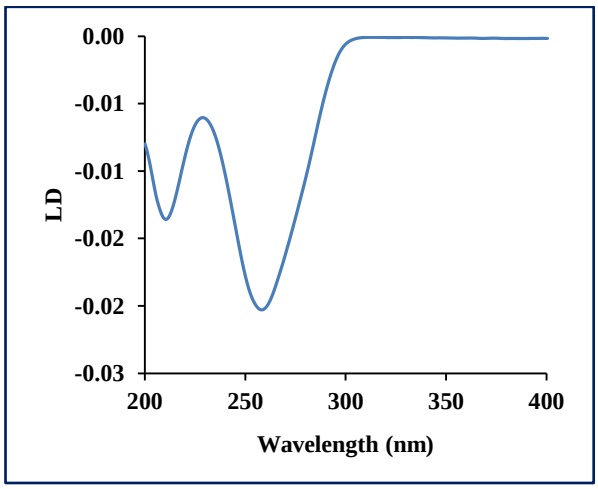

Figure 3.3 Linear dichroism spectrum of 300 μM ct-DNA.

LD measures an average signal from all the bases of oriented DNA. The DNA for LD experiments has to be at least 1000 base pairs in length to get a significant orientation. In this work linear dichroism is used to study interactions of different molecules with ct-DNA. Compounds that bind to the DNA in a specific way (major groove, covalent binding or intercalation between base pairs) will cause change in the DNA LD signal which is a characteristic of their interaction with DNA.[6]

3.5 CD and LD DNA binding studies

3.5.1 DNA binding studies of $[Fe_2(L_1)_3]Cl_4$

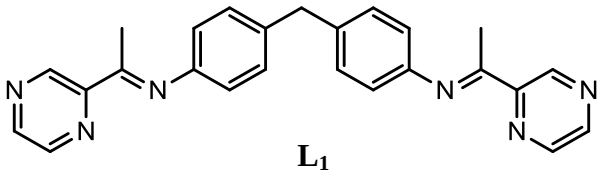

L_1

The synthesised $[Fe_2(L_1)_3]Cl_4$ is readily soluble in water which makes it a perfect candidate for DNA-binding studies. The stability of the complex was examined by UV/Vis spectroscopy in aqueous solution for 12 hours (Fig 3.4).

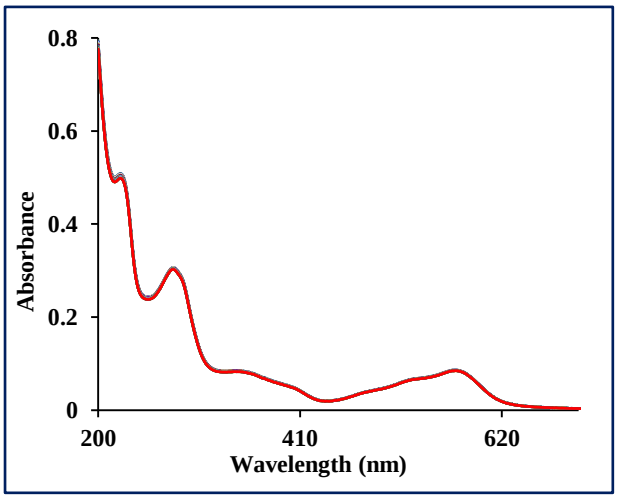

Figure 3.4 UV/Vis stability test spectrum of $[Fe_2(L_1)_3]Cl_4$ complex recorded in water for 12 hours (the spectra over 12 hours period overlay almost perfectly).

The UV/Vis spectrum reveals that the $[Fe_2(L_1)_3]Cl_4$ complex is stable in water for 12 hours. No significant changes are observed during this time period. Interestingly, the chloride salt of pyrazine analogue of the complex, with a hydrogen atom instead of the

methyl group in the imine position, is highly unstable and degrades within seconds of formation (data not shown).

The $[Fe_2(L_1)_3]Cl_4$ complex does not give a CD signal itself because it exists as a racemic mixture. A 300 μM ct-DNA CD spectrum, recorded in aqueous-buffer solution, gave a characteristic B-DNA pattern below 300 nm with a negative band at 247 nm and a positive band at 278 nm. The CD titrations of the complex in to ct-DNA were performed at constant DNA concentration (Fig. 3.5). The experiments were carried out in a 1 cm cuvette in order to visualise better a weak signal in the MLCT region and in 1 mm cuvette to avoid saturation of the signal between 200 and 300 nm that occurs at high concentrations of complex loading.

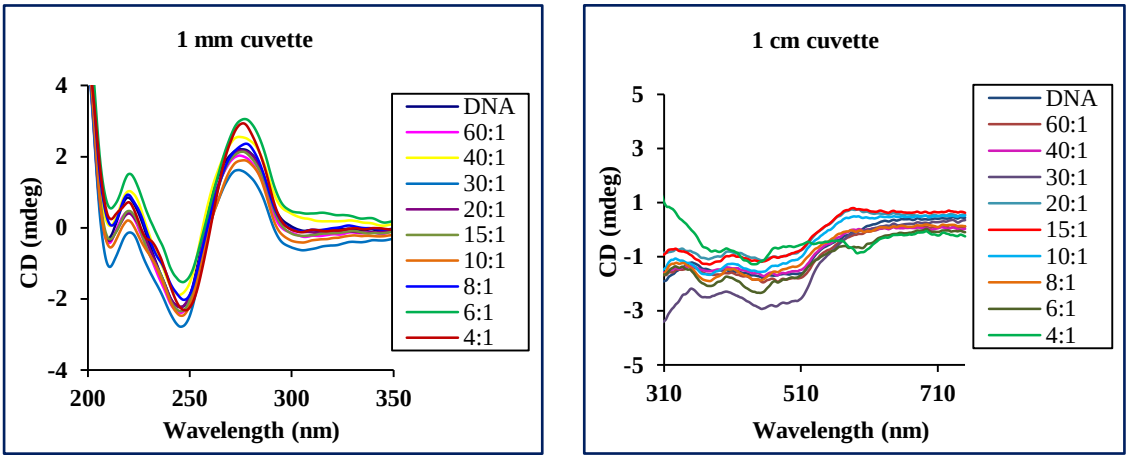

Figure 3.5 CD spectra of ct-DNA in 1 cm and 1 mm cuvettes in the presence of $[Fe_2(L_1)_3]Cl_4$ complex.

The CD spectrum of the complex with DNA shows that the DNA has retained its B-conformation upon interacting with the iron(II) cylinder. There are slight changes in the intensity of the CD signal as the concentration of the complex is increased, however

these changes are not significant indicating that the cylinder binds to DNA and does not trigger any notable conformational alterations in the DNA structure. These changes in intensities of CD signals are initiated by the occupancy of several binding sites by the complex. There are three weak induced CD signals observed at ~ 330 and 413 nm (transitions from the ligand) and ~ 604 nm (MLCT) at high concentrations of the complex which confirm binding of the cylinder to ct-DNA.

The LD experiment can give information about the binding mode of the $[Fe_2(L_1)_3]Cl_4$ complex to ct-DNA. The LD spectrum of the $[Fe_2(L_1)_3]Cl_4$ complex with ct-DNA is illustrated in Figure 3.6 (a).

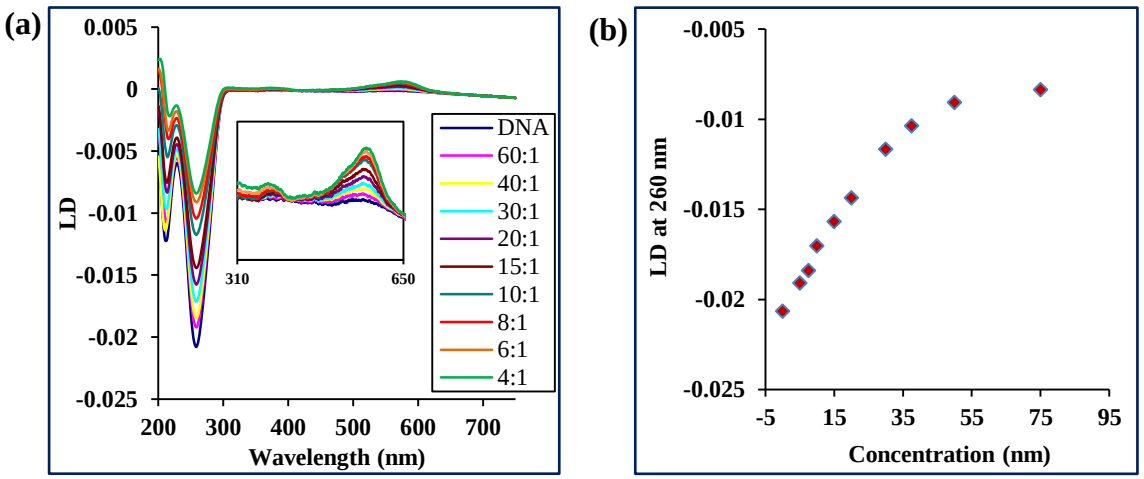

Figure 3.6 (a) LD spectrum of $[Fe_2(L_1)_3]Cl_4$ complex with ct-DNA **(b)** Change in LD signal at 260 nm at various complex concentrations.

When titrations of the $[Fe_2(L_1)_3]Cl_4$ complex to ct-DNA are performed, a decrease in the magnitude of the LD signal with respect to free DNA is observed at 260 nm indicating kinking/coiling of the DNA. The plot in Figure 3.6 (b) demonstrates changes in LD signal at various concentrations of the complex. At 4:1 ratio of DNA base:$[Fe_2(L_1)_3]Cl_4$, a 59 % DNA orientation loss is observed compare with 90 % in

case of the parent iron(II) cylinder.[7, 8] Flow LD orients DNA parallel to the direction of the flow and when the complex is bound to DNA in a specific orientation there is an induced LD signal observed in the MLCT region. The presence of induced LD signals in the spectrum at ~ 385 and 580 nm corresponding to iron(II) complex transitions confirms binding of the cylinder to DNA and this binding occurs in a specific orientation.

3.5.2 DNA binding studies of $[Fe_2(L_3)_3]Cl_4$

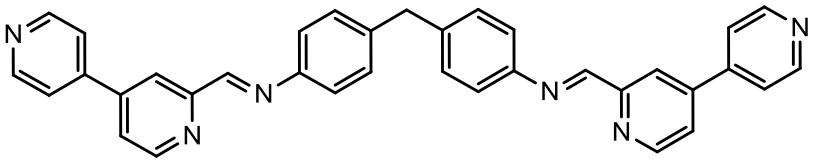

L_3

The $[Fe_2(L_3)_3]Cl_4$ complex is a water soluble compound. The stability of the complex in water was studied by UV/Vis spectroscopy over a 12 hour period (Fig. 3.7).

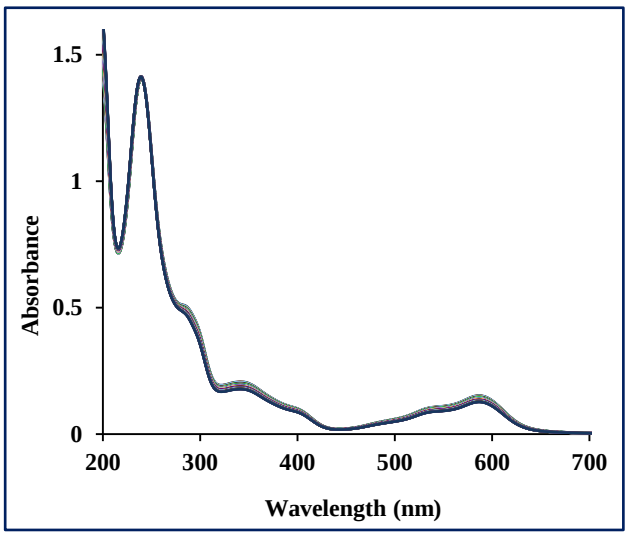

Figure 3.7 UV/Vis stability test spectrum of $[Fe_2(L_3)_3]Cl_4$ recorded in water for 12 hours.

The UV/Vis stability test spectrum reveals that the $[Fe_2(L_3)_3]Cl_4$ complex undergoes degradation. There is a decrease in absorbance corresponding to the MLCT transition at 586 nm. However, the changes observed are not significant indicating the process of decomposition is relatively slow (decrease in UV/Vis absorption signal by ~ 5 % in 12 hours). Nevertheless fresh solutions of the complex were made up for the DNA binding studies and used immediately.

The CD spectrum of $[Fe_2(L_3)_3]Cl_4$ gives a flat line as the compound exists as a racemic mixture. CD titrations of the complex to ct-DNA were performed at varying ratios of DNA bases:complex at constant DNA concentration (Fig. 3.8).

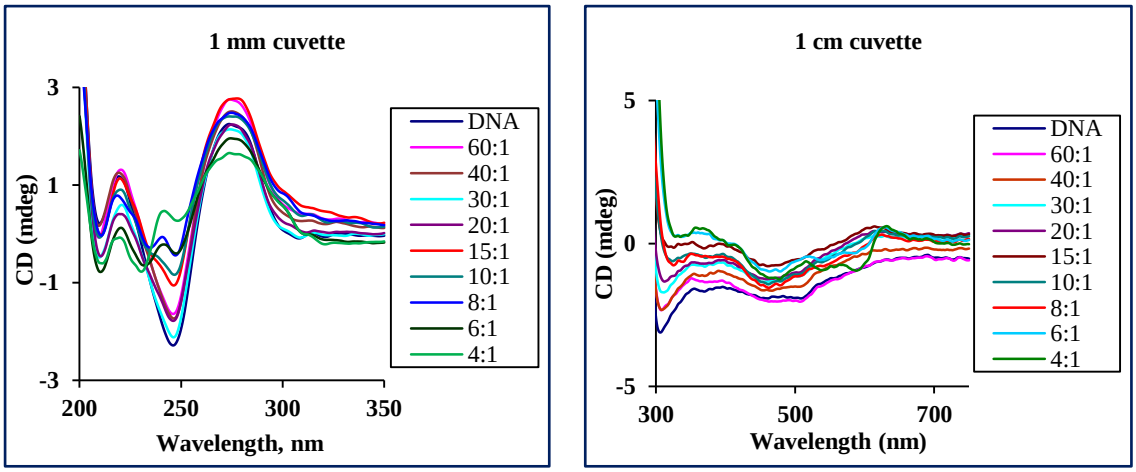

Figure 3.8 CD spectra of ct-DNA in 1mm and 1cm cuvettes in the presence of $[Fe_2(L_3)_3]Cl_4$ complex.

On addition of the complex to ct-DNA, changes in the intensity of the CD band at 248 nm indicate binding of the cylinder to ct-DNA. The binding of the complex does not affect the secondary structure of the B-DNA. A dramatical change in DNA CD signal is observed at a ratio of DNA:complex 15:1 which results into a significant

perturbation of the DNA signal at 248 nm which could be due to DNA-ligand interactions. At high concentrations of the complex an induced CD signal is observed at ~ 630 nm corresponding to the MLCT which confirms binding of the $[Fe_2(L_3)_3]Cl_4$ complex to DNA.

The LD titration experiment of $[Fe_2(L_3)_3]Cl_4$ was performed at constant ct-DNA concentration. The recorded spectrum is shown in figure 3.9 (a).

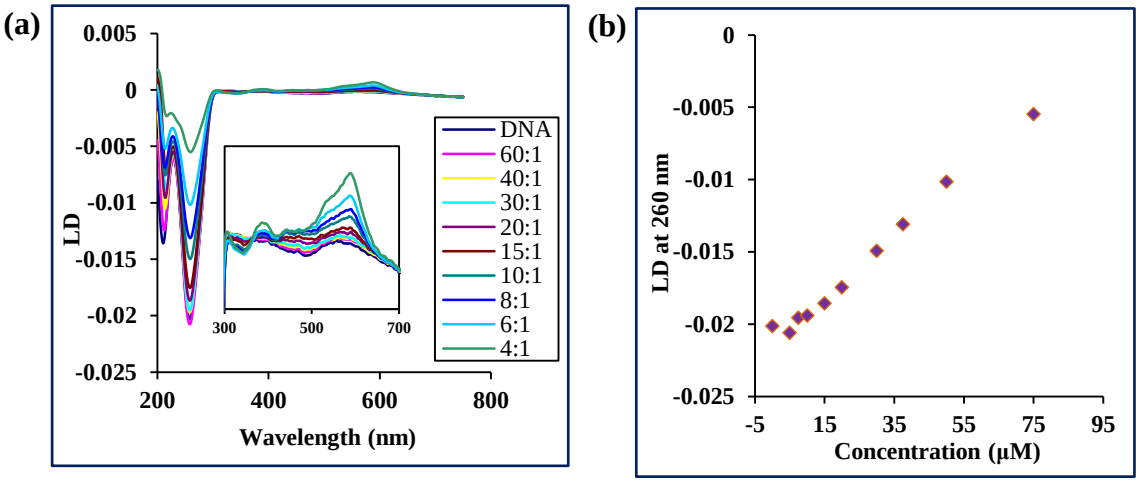

Figure 3.9 (a) LD spectrum of $[Fe_2(L_3)_3]Cl_4$ complex with ct-DNA **(b)** Change in LD signal at 260 nm versus concentration of $[Fe_2(L_3)_3]Cl_4$ complex.

Upon titration of the complex to ct-DNA a significant loss of the signal is observed at 260 nm as a result of changes in DNA orientation induced by the binding of the complex to ct-DNA. The change in the LD signal versus loading of the complex is depicted in Figure 3.9 (b). The reduction of the LD signal indicates that binding of the complex causes kinking/coiling of the DNA. At 4:1 ratio of DNA base:$[Fe_2(L_3)_3]Cl_4$, a ~ 73 % DNA orientation loss is observed compare with 59 % of the previously discussed $[Fe_2(L_1)_3]Cl_4$ complex, showing that the $[Fe_2(L_3)_3]Cl_4$ compound coils/kinks

DNA more effectively. The complex is bound to DNA in a specific orientation which is indicated by the presence of two induced positive bands in the spectrum at ~ 393 and ~ 594 nm that arise from cylinder transitions that occur parallel rather than perpendicular to the direction of the average DNA orientation.

3.5.3 DNA binding studies of $[Fe_2(L_4)_3]Cl_4$

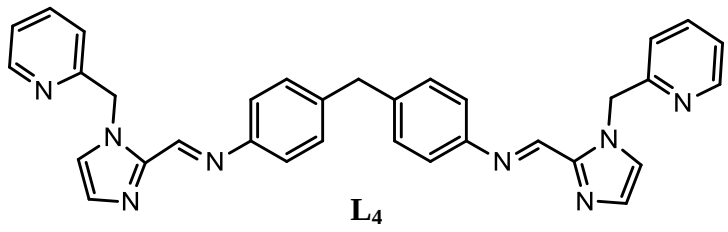

L_4

The synthesised $[Fe_2(L_4)_3]Cl_4$ complex is soluble in methanol and poorly in water. Upon addition of water the complex undergoes rapid degradation. The stability test of $[Fe_2(L_4)_3]Cl_4$ was recorded in methanol for 12 hours (Fig. 3.10).

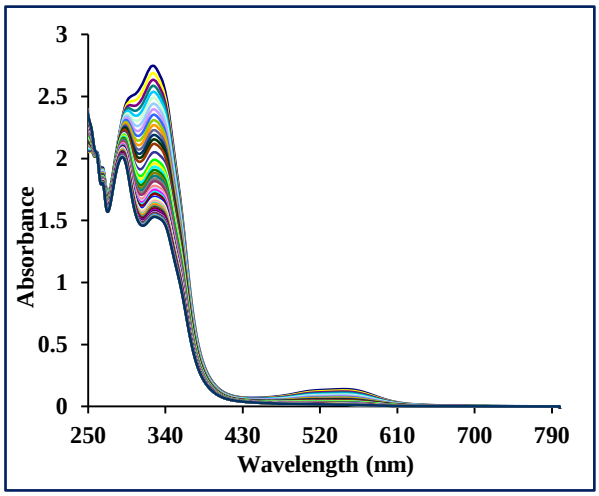

Figure 3.10 UV/Vis stability test spectrum of $[Fe_2(L_4)_3]Cl_4$ recorded in methanol for 12 hours.

The UV/Vis spectrum reveals a decrease in the intensity of the absorption at ~ 553 nm (MLCT), ~ 295 nm and ~ 331 nm as the $[Fe_2(L_4)_3]Cl_4$ complex suffers degradation. Despite the instability of the $[Fe_2(L_4)_3]Cl_4$ complex in water, CD and LD titrations were performed to explore the DNA binding properties of the compound. The complex itself might be stabilised by binding and interacting with DNA as the parent iron(II) cylinder.[9] $[Fe_2(L_4)_3]Cl_4$ is poorly soluble in water therefore to prepare a stock solution of the complex it was dissolved in methanol and then diluted with water (~ 5 % methanol solution). A fresh stock solution was prepared before the addition of the complex to ct-DNA and was kept refrigerated on ice. The CD titrations of the complex to ct-DNA have been performed at constant DNA concentration (Fig. 3.11).

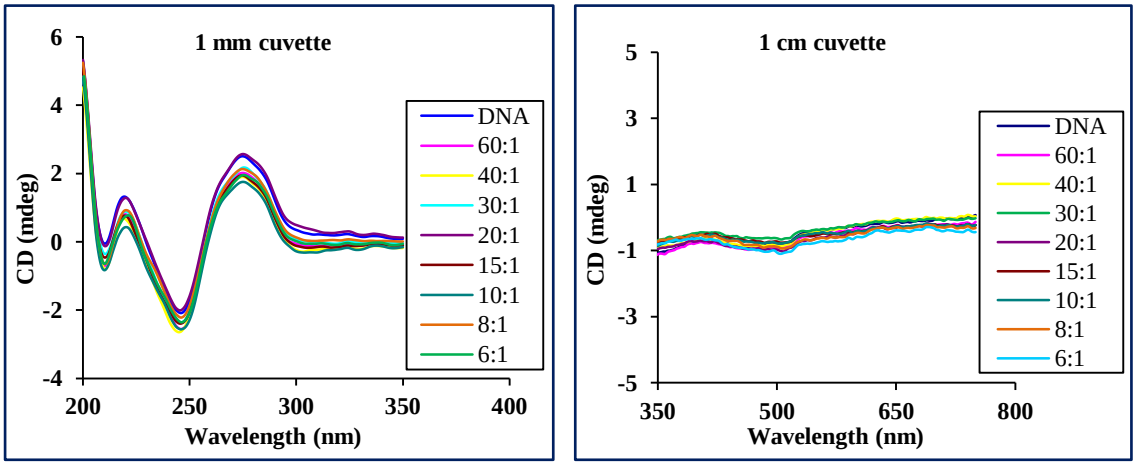

Figure 3.11 CD spectra of ct-DNA in 1cm and 1mm cuvettes in the presence of $[Fe_2(L_4)_3]Cl_4$ complex.

The CD spectrum shows that on addition of the $[Fe_2(L_4)_3]Cl_4$ complex to ct-DNA there is a slight perturbation in CD signal observed. However these changes are insignificant, suggesting interaction of the ligand with a DNA as the complex falls apart

in the solution and no stabilisation occurs. This is also demonstrated by the absence of an induced CD signal in the MLCT region.

Flow LD titrations were performed at constant concentration of ct-DNA. The characteristic negative signal between 220 and 300 nm confirms B-conformation of the DNA (Fig. 3.12). As in the case of the CD experiment, no induced LD signal is observed. A small loss of the signal at 260 nm could be a result of interactions with the ligand L_4. The CD and LD experiments reveal that no binding of the $[Fe_2(L_4)_3]Cl_4$ complex is observed due to instability in aqueous solution.

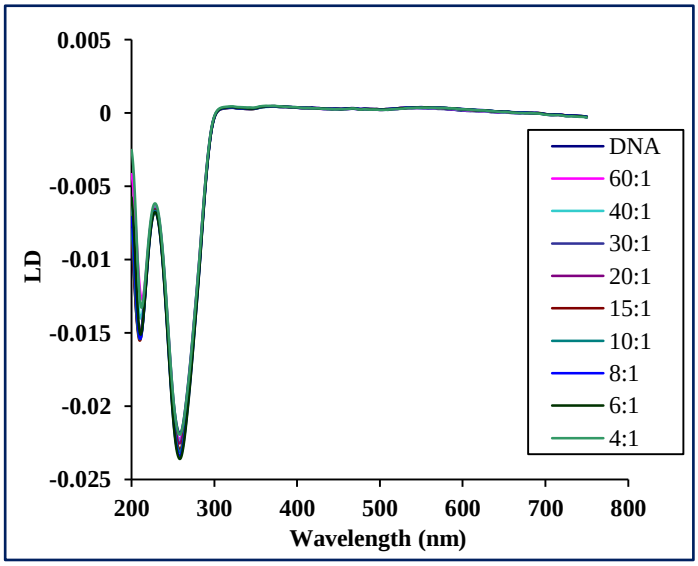

Figure 3.12 LD spectrum of $[Fe_2(L_4)_3]Cl_4$ complex with ct-DNA.

3.5.4 DNA binding studies of $[Ni_2(L_4)_3]Cl_4$

The synthesised $[Ni_2(L_4)_3]Cl_4$ complex is soluble in water and is suitable for DNA-binding studies. The stability of the helicate in water was examined for 11 hours (Fig. 3.13).

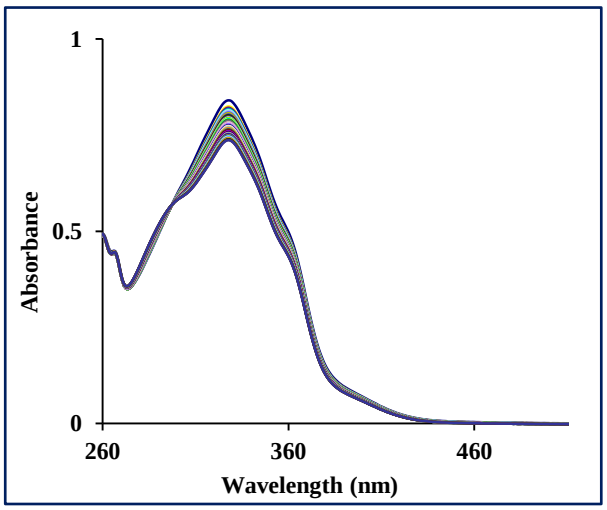

Figure 3.13 UV/Vis stability test spectrum of $[Ni_2(L_4)_3]Cl_4$ recorded in methanol for 11 hours.

The UV/Vis spectrum demonstrates that the absorption band at ~ 330 nm is gradually decreasing (by ~ 12 % in 11 hours) indicating slow degradation of the complex.

CD titrations of $[Ni_2(L_4)_3]Cl_4$ complex to ct-DNA were recorded at constant concentration of the DNA. At high loadings of the complex to DNA precipitation of the polynucleotide was observed. Therefore the stock concentration of the helicate was decreased from 600 μM to 400 μM. The CD spectrum of the $[Ni_2(L_4)_3]Cl_4$ complex is displayed in Figure 3.14.

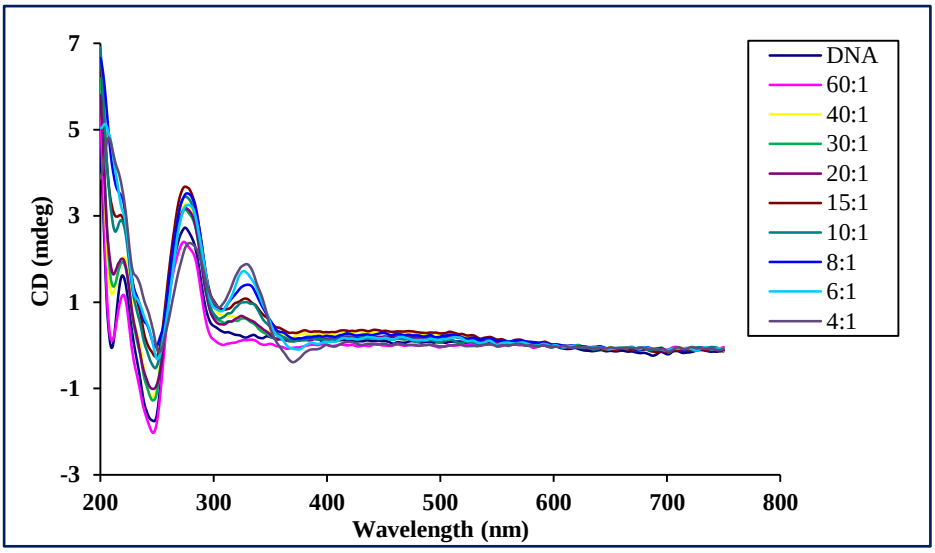

Figure 3.14 CD spectra of ct-DNA in 1mm cuvette in the presence of $[Ni_2(L_4)_3]Cl_4$ complex.

The CD spectrum demonstrates that the characteristic B-DNA pattern is retained during the titrations. Changes in the intensities of the CD band indicate binding of the complex to DNA. On addition of the nickel(II) helicate to ct-DNA a positive induced CD signal at ~ 330 nm is observed which also confirms binding of the helicate to DNA. The change in CD signal at 248 and 330 nm plotted versus concentration is shown in Figure 3.15.

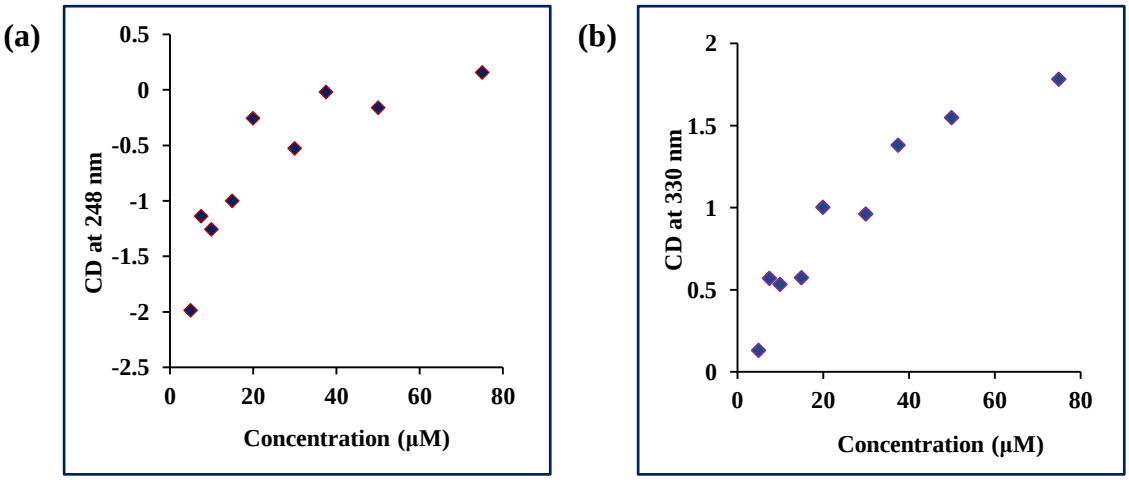

Figure 3.15 CD signal plotted versus concentration at **(a)** 248 nm **(b)** 330 nm.

Flow LD titrations were performed at constant concentration of ct-DNA. A characteristic negative LD signal of DNA was observed between 220 to 300 nm. The addition of the nickel(II) triple-stranded helicate affects the spectroscopy of ct-DNA (Fig. 3.16 (a)).

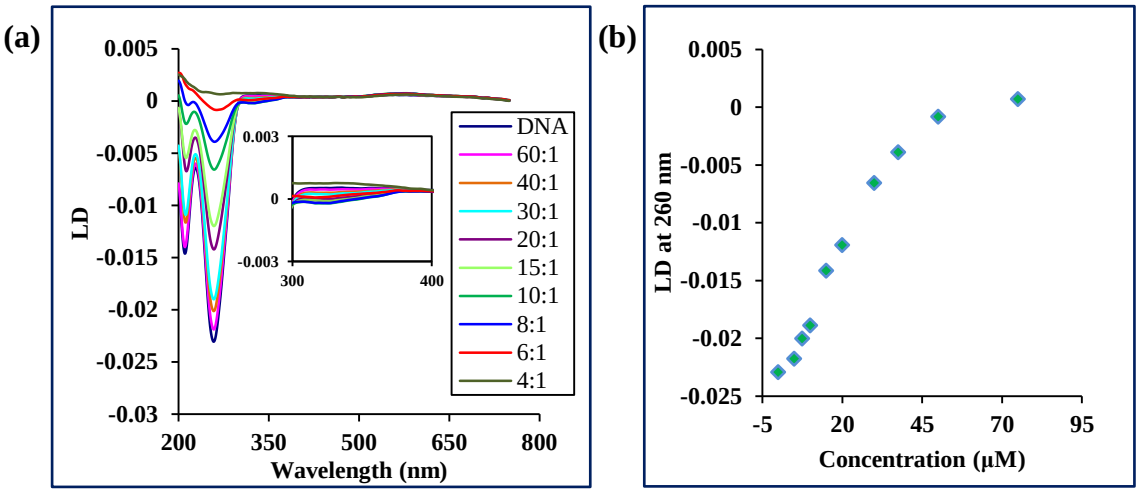

Figure 3.16 (a) LD spectrum of $[Ni_2(L_4)_3]Cl_4$ complex with ct-DNA **(b)** Change in LD signal at 260 nm versus concentration of $[Ni_2(L_4)_3]Cl_4$ complex.

The induced LD signal, which appears as a positive band at ~ 330 nm corresponds to cylinder transitions and indicates that these transitions are oriented more parallel rather than perpendicular. The loss of the signal at 260 nm demonstrates a change in the DNA orientation suggesting that the binding of the complex causes kinking/coiling of the DNA. The change in DNA LD signal plotted versus complex concentrations is shown in Figure 3.15 (b). Interestingly, at 4:1 ratio the intensity of the LD band at 260 nm is decreased by 97 %. The obtained results demonstrate that the $[Ni_2(L_4)_3]Cl_4$ complex coils ct-DNA more effectively than $[Fe_2(L_1)_3]Cl_4$, $[Fe_2(L_3)_3]Cl_4$, $[Fe_2(L_4)_3]Cl_4$ and the parent iron(II) cylinder.

In this section of the chapter 3, CD and LD DNA binding studies of $[Fe_2(L_1)_3]Cl_4$, $[Fe_2(L_3)_3]Cl_4$, $[Fe_2(L_4)_3]Cl_4$ and $[Ni_2(L_4)_3]Cl_4$ were discussed. The results of these studies demonstrate that the complexes $[Fe_2(L_1)_3]Cl_4$, $[Fe_2(L_4)_3]Cl_4$ and $[Ni_2(L_4)_3]Cl_4$ bind to DNA and cause alterations in its orientation, although the conformation of the B-DNA is retained. There are no significant changes in the CD and LD spectra of the $[Fe_2(L_4)_3]Cl_4$ complex as it undergoes slow degradation. Binding of $[Fe_2(L_4)_3]Cl_4$ and $[Ni_2(L_4)_3]Cl_4$ compounds to DNA causes more effect to its orientation than $[Fe_2(L_1)_3]Cl_4$. This can be visualised by comparing changes in the intensities of LD signals at 260 nm as a result of increased drug loading (Fig. 3.17).

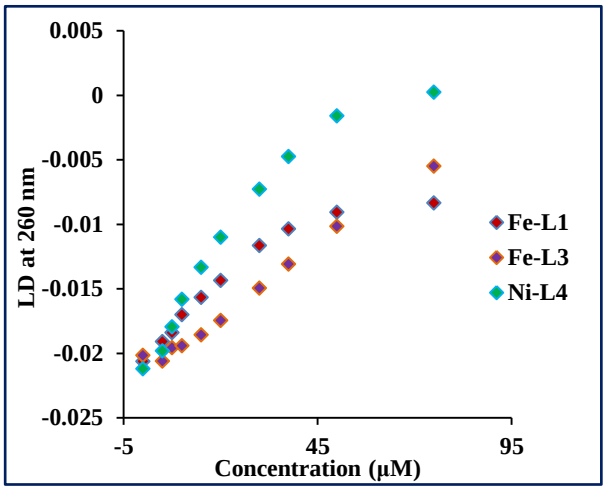

Figure 3.17 Changes in the intensities of LD signal at 260 nm of Fe-L1 = $[Fe_2(L_1)_3]Cl_4$, Fe-L3 = $[Fe_2(L_3)_3]Cl_4$ and Ni-L4 = $[Ni_2(L_4)_3]Cl_4$ versus concentration.

The graph demonstrates that in the presence of $[Ni_2(L_4)_3]Cl_4$ the DNA molecule is less oriented and loss of the LD signal at 260 nm is more dramatic than in the case of other complexes.

The compounds were further investigated for their ability to unwind plasmid DNA and stabilise DNA three-way junction structures.

3.6 Agarose gel electrophoresis studies

3.6.1 Introduction

Agarose gel electrophoresis is a common technique used to separate biomolecules such as DNA, RNA and proteins based on their size, charge or conformation.[10] DNA fragments can be separated by applying an electric field which causes the molecules to migrate through the pores of the gel. The shorter DNA fragments move faster than the longer ones. The conformation of the DNA is also crucial. In this work plasmid DNA pBR322 which contains 4361 base pairs was used. Plasmid pBR322 is a double-stranded circular DNA that can be found in bacteria. The plasmids exist predominantly in a supercoiled conformation but there are also open circular and linear forms. These three various conformations of the plasmid will move with different speeds through the agarose gel.[11] The supercoiled form moves faster than the open form whereas the linear form has an intermediate speed of migration (Fig. 3.18).

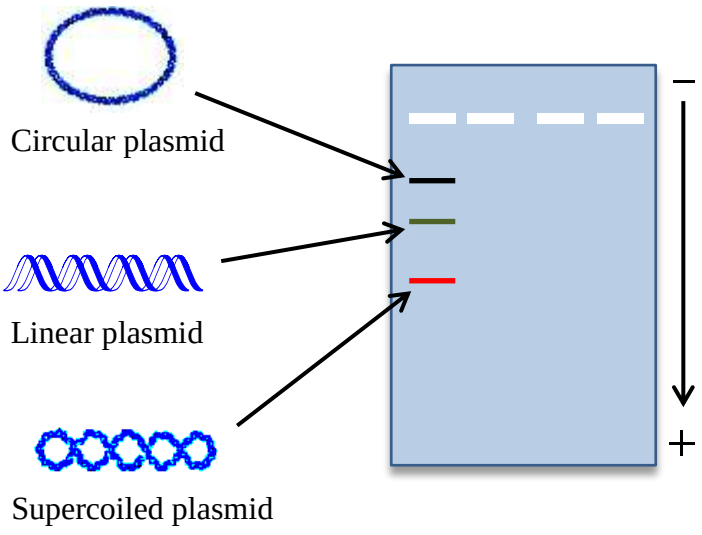

Figure 3.18 Schematic representation of agarose gel electrophoresis of different conformations of plasmid DNA.

In this work the agarose gel electrophoresis technique was used to determine the ability of the synthesised compounds to unwind supercoiled plasmid DNA. The compounds were incubated with plasmid DNA for 1 hour at various ratios of DNA base pairs:helicate (Table 3.0). During the gel electrophoresis experiment the negatively charged DNA fragments move towards a positively charged electrode with a speed of migration depending on the conformation and size of the DNA. Visualisation of the gel bands is achieved by staining the gel with ethidium bromide and placing the gel under UV-light. When ethidium bromide is intercalated between the base pairs of DNA it luminesces upon exposure to UV-light. The gel bands were detected using a UVIPro Platinum 2.0 system.

Well	1	2	3	4	5	6	7	8	9	10	11	12
Base pairs:helicate	control	25:1	20:1	15:1	10:1	8:1	6:1	5:1	4:1	3:1	2:1	control

Table 3.0 Ratios of plasmid DNA base pairs:helicate used in the experiment

3.6.2 Results and discussion

Ultrapure water was used to prepare various concentrations of the complexes $[Fe_2(L_1)_3]Cl_4$, $[Fe_2(L_3)_3]Cl_4$, and $[Ni_2(L_4)_3]Cl_4$. The compound $[Fe_2(L_4)_3]Cl_4$ and platinated complex $[Fe_2(L_1)_3]Cl_4$ were not soluble in water and therefore were dissolved in 2 % DMSO/water solutions. During the experiment the concentration of the complex was increased from 25:1 to 2:1 base pairs:helicate. The gel electrophoresis experiment was run for 3 hours at 120 V. The electrophoretic mobility of the plasmid DNA with synthesised compounds is shown in Figure 3.19.

(a) $[Fe_2(L_1)_3]Cl_4$

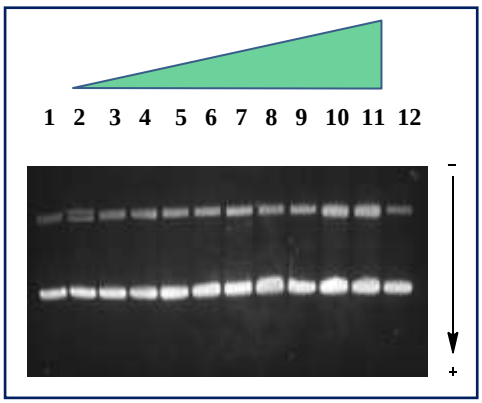

(b) $[Fe_2(L_3)_3]Cl_4$

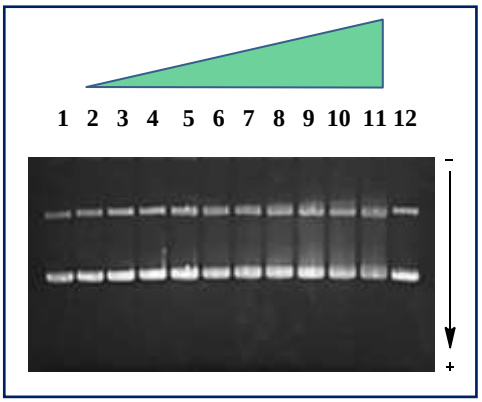

(c) $[Ni_2(L_4)_3]Cl_4$

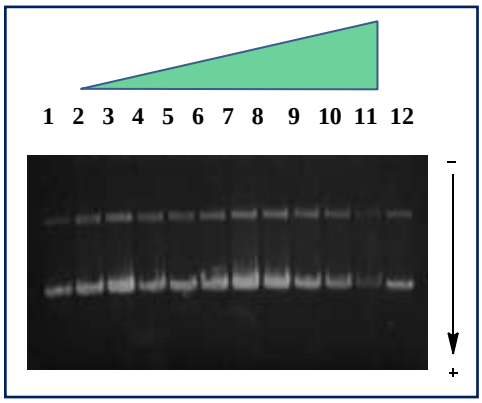

(d) $[Fe_2(L_4)_3]Cl_4$

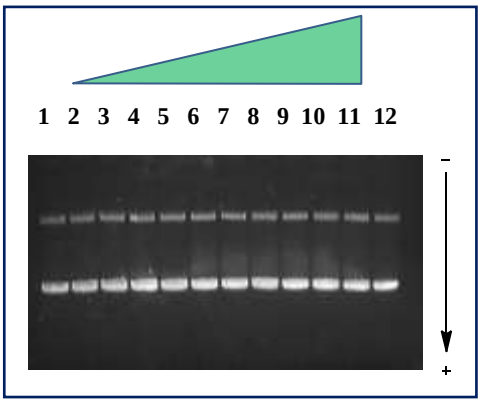

(e) $[Fe_2(L_1)_3]Cl_4$ with attached cisplatin

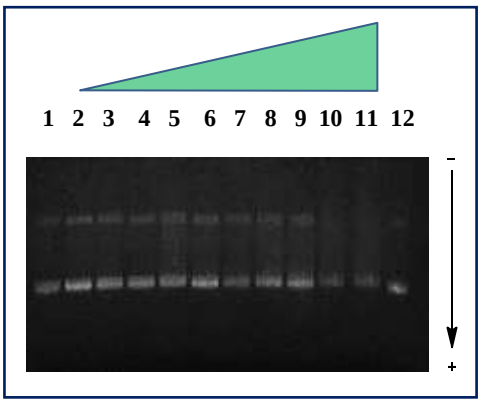

Figure 3.19 Agarose gel electrophoresis of pBR322 with **(a)** $[Fe_2(L_1)_3]Cl_4$ **(b)** $[Fe_2(L_3)_3]Cl_4$ **(c)** $[Ni_2(L_4)_3]Cl_4$ **(d)** $[Fe_2(L_4)_3]Cl_4$ **(e)** $[Fe_2(L_1)_3]Cl_4$ with attached cisplatin.

At low concentrations of the complex two conformations of plasmid are observed open circular and supercoiled. As the concentration of the complexes is increased there are no significant changes in the electrophoretic mobility of the supercoiled plasmid DNA detected. A slight blurring of the band corresponding to the supercoiled form is found for $[Fe_2(L_3)_3]Cl_4$ and $[Fe_2(L_1)_3]Cl_4$ with attached cisplatin suggesting a small decrease in the speed of migration of supercoiled DNA. Remarkably, there was no unwinding observed for the complex with attached cisplatin. Cisplatin itself causes unwinding of the DNA by 13 º (Fig. 3.20 (a)) by forming covalent bonds with purine DNA bases.[12, 13] In the case of $[Fe_2(L_1)_3]Cl_4$ with attached cisplatin, the coordination of DMSO solvent molecules to cisplatin could affect the DNA unwinding.

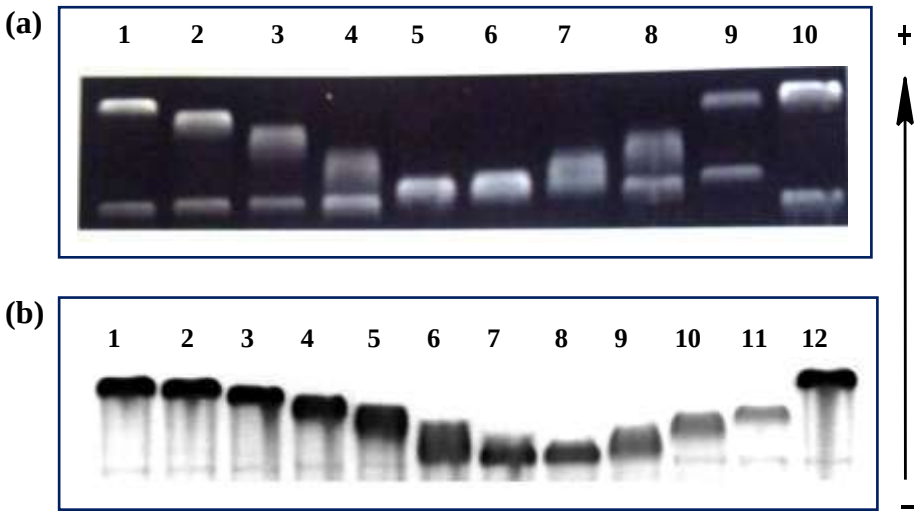

Figure 3.20 Unwinding of plasmid DNA by **(a)** Cisplatin (lanes 1 and 2 control (non-modified DNA); lanes 2-9 cisplatin:DNA base ratio: 0.033, 0.050, 0.063, 0.083, 0.100, 0.125, 0.167, 0.250)[13] **(b)** Iron(II) parent cylinder (lanes 1 and 12 control (non-modified DNA); lanes 2-11: cylinder:base ratio = 0.008, 0.015, 0.023, 0.027, 0.030, 0.034, 0.038, 0.046, 0.053, 0.061, respectively).[14]

Interestingly, the dinuclear iron(II) parent helicate effectively unwinds plasmid DNA by 27 º (Fig. 3.20 (b)).[14] The unwinding angle ϕ can be calculated using the following formula:

$$\phi = -18\sigma/r_{b(c)}$$

σ – superhelicity constant, $\mathbf{r_{b(c)}}$ – the ratio of the complex bound per nucleotide when supercoiled and open circular bands of plasmid co-migrate. The number of complex molecules bound per nucleotide was taken to be equal to the mixing ratios based on the assumption that all molecules of the compound present in the sample are completely bound to the DNA. The superhelicity constant for plasmid was found to be – 0.059.[14]

The absence of plasmid DNA unwinding in the case of the synthesised $[Fe_2(L_1)_3]Cl_4$, $[Fe_2(L_3)_3]Cl_4$, $[Fe_2(L_4)_3]Cl_4$, $[Ni_2(L_4)_3]Cl_4$ complexes can be associated with the instability of compounds at high temperature, the bulky size or the nature of the helicates.

3.7 Recognition of DNA three-way junction

3.7.1 Introduction

DNA encodes the genetic information of most living systems and is an attractive target for therapeutic treatment of many diseases, including cancer, which originate at the DNA level. Synthetic molecules that are able to recognise unusual DNA structures are of great interest for their inherent specificity. Thus, for example, synthetic iron(II) supramolecular helicate developed by Hannon and co-workers recognises DNA three way junction structures.[15]

DNA junction structures are formed when two or more helices meet in one point. DNA junctions play an important role in many biological processes. The DNA four-way

junction, for instance, is a key intermediate in homologous recombination. Three-way junctions (3WJ) are the simplest and most prevalent of junctions and consist of three double helical strands connected at the junction point. Three-way junctions can be found both in RNA and DNA. In RNA these branched structures are involved in splicing and translation processes whereas in DNA they arise transiently during the process of DNA replication. Three-way junctions have been discovered to be present as intermediate structures in Huntington`s disease and myotonic dystrophy type 1.[16]

Using an inexpensive approach Hannon *et al.* synthesised a tetracationic iron(II) triple-stranded helicate which binds to the DNA major groove and induces intramolecular DNA coiling. When the complex was crystallised with a DNA palindromic hexanucleotide 5`-d-(CGTACG)-3`, molecular recognition of the DNA-three way junction was observed with a helicate located in the centre of the junction (Fig. 3.21).[17]

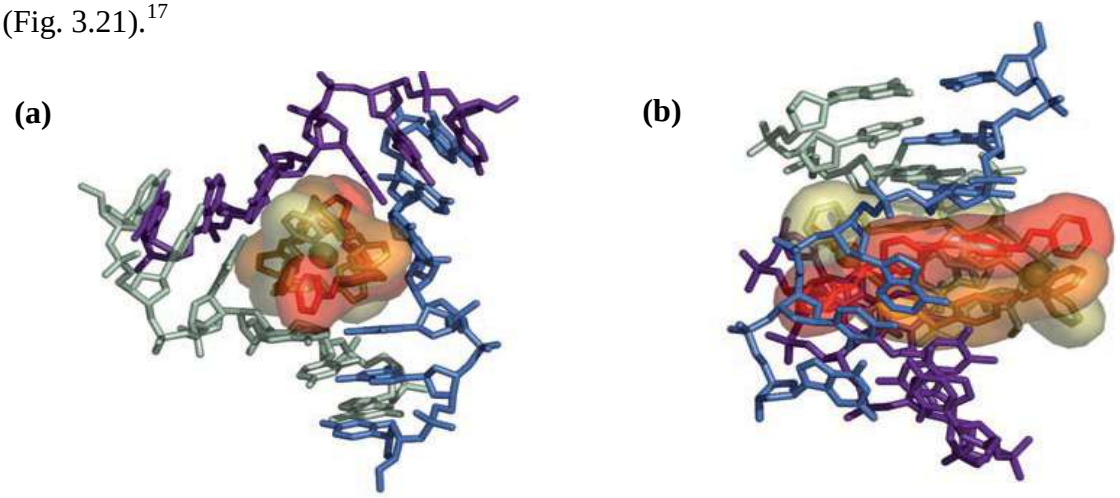

Figure 3.21 Crystal structure of iron(II) tetracationic helicate with palindromic hexanucleotide **(a)** Top view of the helicate-DNA complex **(b)** Side view of the helicate-DNA complex.[17]

The structure of the helicate does not undergo any conformational changes upon binding to the DNA junction. Non-covalent interactions play a key role in binding of the

iron(II) cylinder in the core cavity of the junction. The cylinder is positively charged and therefore is attracted to the negatively charged sugar-phosphate backbone of the DNA via electrostatic interactions (Fig. 3.22 (a)).

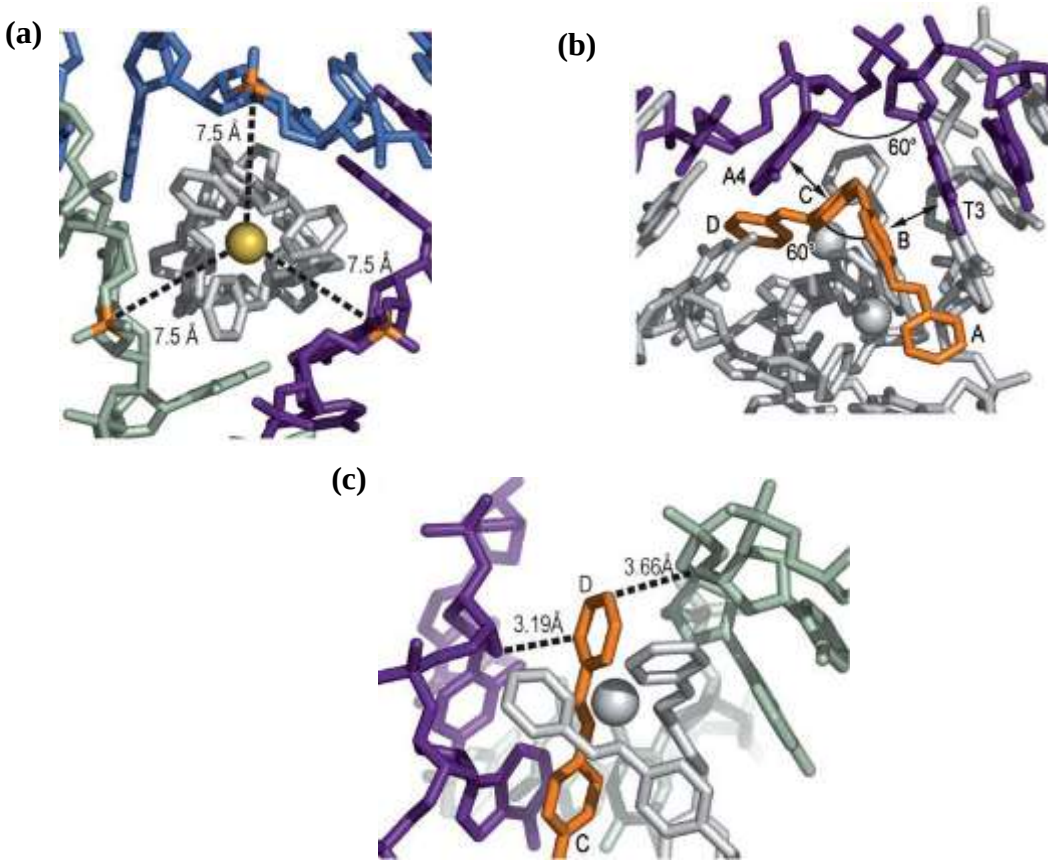

Figure 3.22 Noncovalent recognition of the DNA three-way junction by the iron(II) helicate **(a)** Electrostatic interactions between positively charged helicate and negatively charged DNA junction **(b)** π-π Stacking interactions between phenyl rings B and C and central T_3 and A_4 bases of the junction **(c)** Interaction of terminal phenyl ring D with minor groove of the DNA.[16]

The phenyl rings of the helicate form extensive π-π stacking interactions with adenine and thymine bases of the DNA three-way junction (Fig. 3.22 (b)). Due to the

three-fold symmetry of the cylinder which corresponds the three-fold symmetry of the DNA junction, these stacking interactions are repeated three times. The terminal pyridine rings of the supramolecular structure are located in the minor groove and are sandwiched between two opposite sugar-phosphate moieties of the DNA (Fig. 3.22 (c)). Hydrogen bonding was found to be present between the imine hydrogen adjacent to the terminal phenyl rings D and the N_3 nitrogen of the adenine. The non-covalent interactions present between the helicate and the DNA-three way junction stabilise the structure.

As the DNA three-way junction is relevant to the replication fork formed during the process of replication of DNA, molecules that are able to recognise this type of DNA structure have potential to be used as therapeutics in treatment of various diseases. By binding to the cavity of the junction the potential drug may cease the replication resulting in cell apoptosis. Key characteristics of the DNA-recognition motif of the drug are the shape and the size of the molecule which should perfectly match that of the target. In the case of the iron(II) supramolecular helicate it has the right dimensions to fit the hydrophobic cavity of a DNA three-way junction. Changing the structure of the cylinder can alter the binding properties of the complex.[17]

In this section of chapter 3 the recognition of DNA three-way junctions by the $[Fe_2(L_1)_3]Cl_4$, $[Fe_2(L_3)_3]Cl_4$, $[Fe_2(L_4)_3]Cl_4$, $[Ni_2(L_4)_3]Cl_4$ complexes, in comparison with their parent analogues, using the gel electrophoresis technique will be explored.

3.7.2 Results and discussion

3.7.2.1 Overview

The recognition of the DNA three-way junction by the synthesised compounds was examined using the polyacrylamide gel electrophoresis technique (PAGE). PAGE is used in the analysis of short sequences of DNA and the sensitivity of this method is achieved by the radioactive labelling of one of the strands of the DNA. In this work one strand of the oligonucleotide was labelled with γ-phosphate of ATP containing radioactive phosphorus-32. Phosphorus-32 has a short half-life and it decays with emission of β-radiation. The penetrating properties of β-particles are higher than those of α-particles and therefore β-radiation can be easily detected outside of the analysed sample. The oligonucleotide was labelled at the 5` terminus and the reaction was catalysed by bacteriophage T4 polynucleotide kinase.[18]

The PAGE experiment was performed using the facilities of the Functional Genomics and Proteomics Unit of the School of Bioscience at the University of Birmingham. A 14-mer nonpalindromic oligonucleotide was used to form a DNA three-way junction with seven base pairs per arm (Fig. 3.23 (a)). This junction structure was found to be the minimum length of DNA required for a three-way junction lacking unpaired bases to be stable enough to perform a gel electrophoresis experiment on a native gel at low temperatures (~ 5 ºC).[19] The autoradiogram of the gel was obtained by exposing the radiogel to a phosphor imaging plate and reading it with Molecular imager FX. In the absence of the supramolecular helicate no DNA junction should be observed on the autoradiogram, just a single strand of the DNA, whereas in the presence of the

cylinder the stabilisation of the DNA three-way junction should occur giving rise to a band on the autoradiogram (Fig. 3.23 (b)).

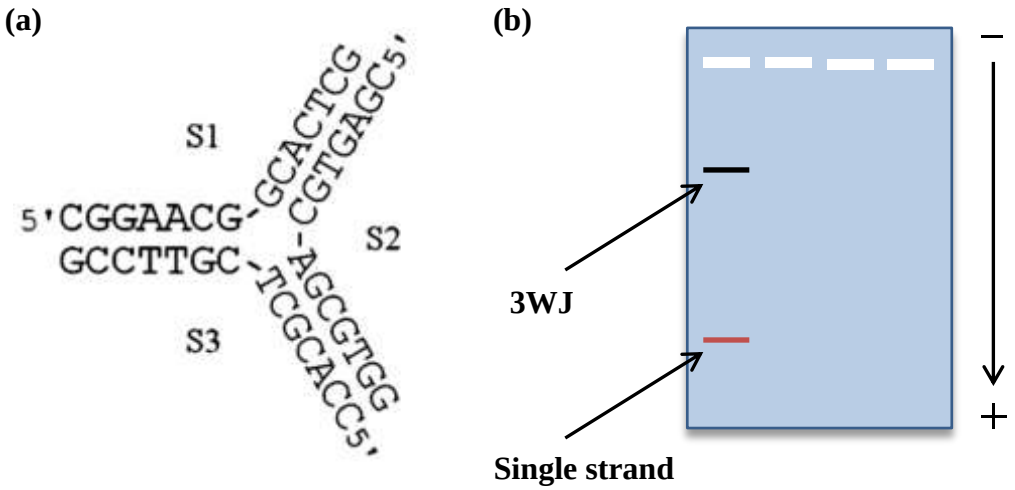

Figure 3.23 (a) Oligonucleotide sequences used for DNA three-way junction formation **(b)** Schematic representation of polyacrylamide gel electrophoresis experiment.

3.7.2.2 Recognition and stabilisation of DNA three-way junction by helicates

The synthesised compounds $[Fe_2(L_1)_3]Cl_4$, $[Fe_2(L_3)_3]Cl_4$, $[Fe_2(L_4)_3]Cl_4$ and $[Ni_2(L_4)_3]Cl_4$ were incubated with nonpalindromic sequences of the DNA and PAGE experiments were performed to analyse the samples. The autoradiogram for complexes $[Fe_2(L_3)_3]Cl_4$ and $[Fe_2(L_4)_3]Cl_4$ is shown in Figure 3.24. The S3* oligonucteotide strand was labelled with radioactive ^{32}P. Wells containing oligonucleotides S3*, S3*+S2, S3*+S2+S1 and S3*+S2+S1 with magnesium chloride or parent cylinder $[Fe_2(Lp)_3]Cl_4$ were used as a control. Magnesium ions and the parent cylinder are known to promote the formation of DNA three-way junctions and stabilise them.[19]

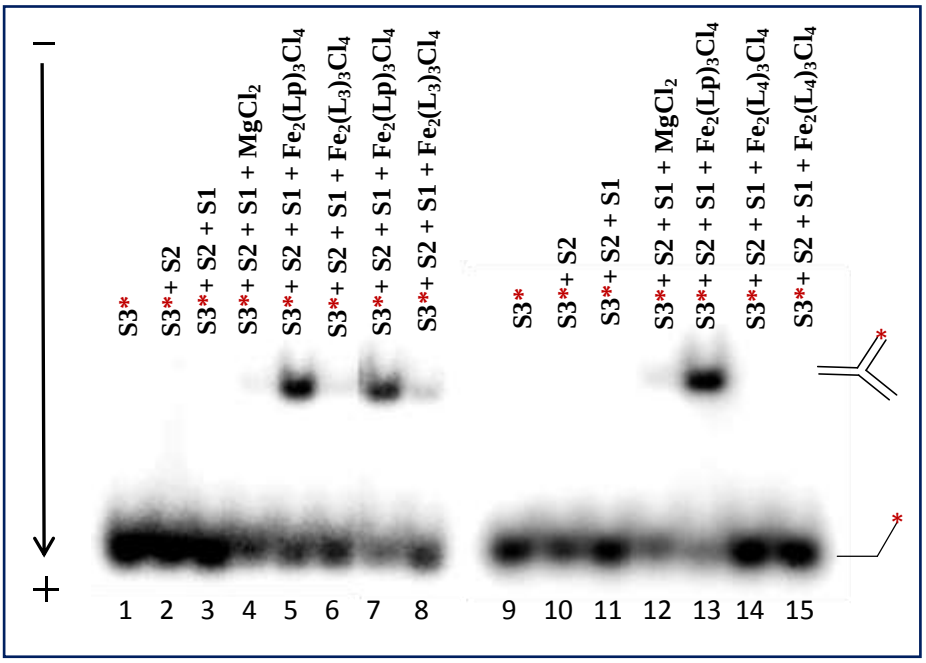

Figure 3.24 Autoradiogram of PAGE experiment with complexes $[Fe_2(L_3)_3]Cl_4$ and $[Fe_2(L_4)_3]Cl_4$. Lanes 1-4 and 9-12 correspond to S3*, S3*+S2, S3*+S2+S1, S3*+S2+S1+$MgCl_2$ respectively. Lanes 5-8: S3*+S2+S1 with parent cylinder $[Fe_2(Lp)_3]Cl_4$ (Lp = parent ligand) and $[Fe_2(L_3)_3]Cl_4$; lanes 13-15: S3*+S2+S1 with $[Fe_2(Lp)_3]Cl_4$ and $[Fe_2(L_4)_3]Cl_4$. DNA: complex ratio used in the experiment was 3:1.

The autoradiogram demonstrates that the $[Fe_2(L_3)_3]Cl_4$ complex promotes the formation of the DNA three-way junction. The observed bands are very weak compared to the bands of the parent analogue. The $[Fe_2(L_4)_3]Cl_4$ complex did not form the 3WJ structure apparently due to the instability of the complex in water. In order to calculate the percentage of DNA 3WJ formed for each complex, the intensities of the gel bands were quantified utilising the quantity one programme and calculated using the following formula:

$$\% \ 3WJ = (I_{3WJ}/(I_{ss} + I_{3WJ})) * 100$$

$\mathbf{I_{3WJ}}$ and $\mathbf{I_{ss}}$ are the intensities of the gel bands corresponding to the DNA three-way junction and the single stranded DNA respectively. The bar graph displayed in the Figure 3.25 shows the percentage of DNA 3WJ formed for complexes $[Fe_2(L_3)_3]Cl_4$ (Fe-L_3) and $[Fe_2(Lp)_3]Cl_4$ (Fe-Lp).

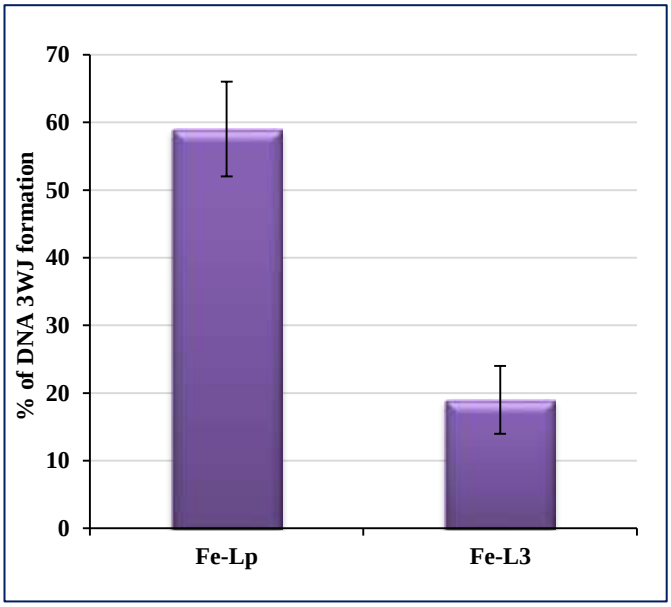

Figure 3.25 Bar graph displaying the percentage of DNA 3WJ formed by complexes $[Fe_2(L_3)_3]Cl_4$ (Fe-L_3) and $[Fe_2(Lp)_3]Cl_4$ (Fe-Lp).

The graph demonstrates that the Fe-L_3 complex induces the formation of ~ 20 % DNA 3WJs compared to the parent analogue which is more effective and forms ~ 60 % of 3WJs. The dimensions of the helicate are crucial criteria for binding of the complex to the core cavity of the junction. By introducing various substituents onto the pyridine ring of the ligand we can alter the binding properties of the helicate.

The autoradiogram recorded for complexes $[Fe_2(L_1)_3]Cl_4$ and $[Ni_2(L_4)_3]Cl_4$ is shown in Figure 3.26. The compounds were analysed in comparison with their parent analogues.

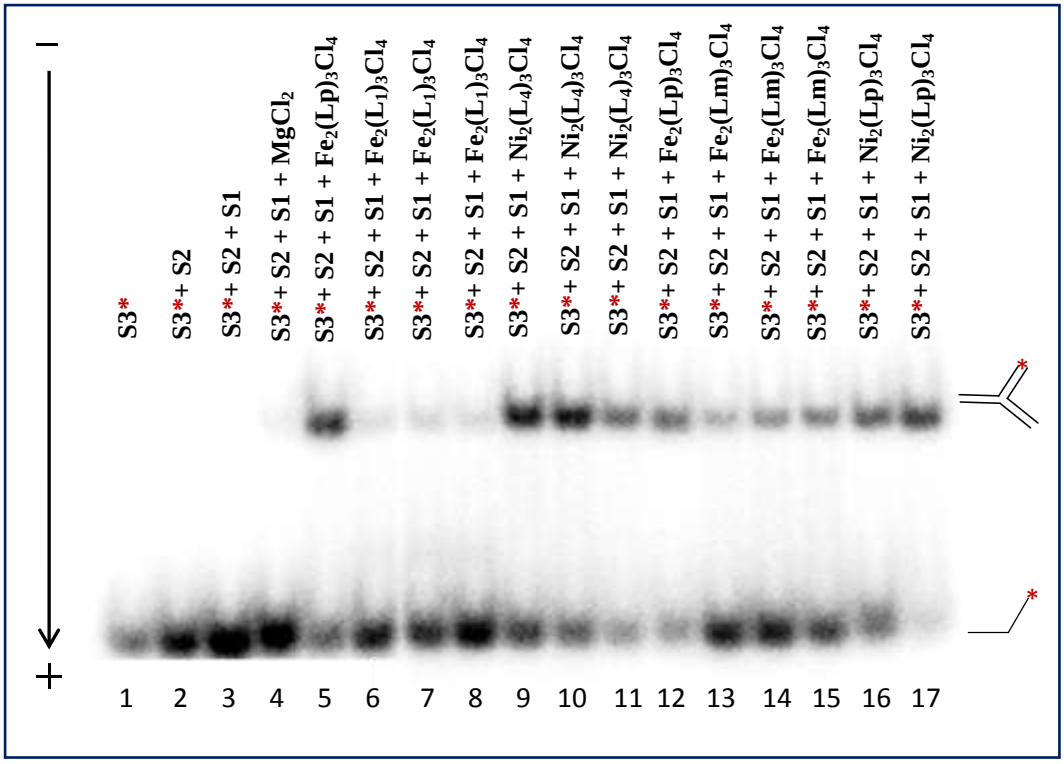

Figure 3.26 Autoradiogram of PAGE experiment of complexes $Fe_2(L_1)_3]Cl_4$ and $[Ni_2(L_4)_3]Cl_4$ in comparison with $[Fe_2(Lp)_3]Cl_4$, $[Ni_2(Lp)_3]Cl_4$ (Lp = parent ligand), $[Fe_2(Lm)_3]Cl_4$ (Lm = parent ligand with methyl group in place of imine hydrogen). Lanes 1-4: S3*, S3*+S2, S3*+S2+S1, S3*+S2+S1+$MgCl_2$. Lanes 5 and 12: S3*+S2+S1 with $[Fe_2(Lp)_3]Cl_4$; lanes 6-8: S3*+S2+S1 with $[Fe_2(L_1)_3]Cl_4$; lanes 9-11: S3*+S2+S1 with $[Ni_2(L_4)_3]Cl_4$; lanes 12-14: S3*+S2+S1 with $[Fe_2(Lm)_3]Cl_4$; lanes 16-17: S3*+S2+S1 with $[Ni_2(Lp)_3]Cl_4$. DNA:complex ratio used in the experiment is 3:1.

The autoradiogram reveals that all of the complexes form DNA 3WJs however with different effectiveness. In order to compare the obtained results the intensities of the gel bands were quantified (Fig. 3.27).

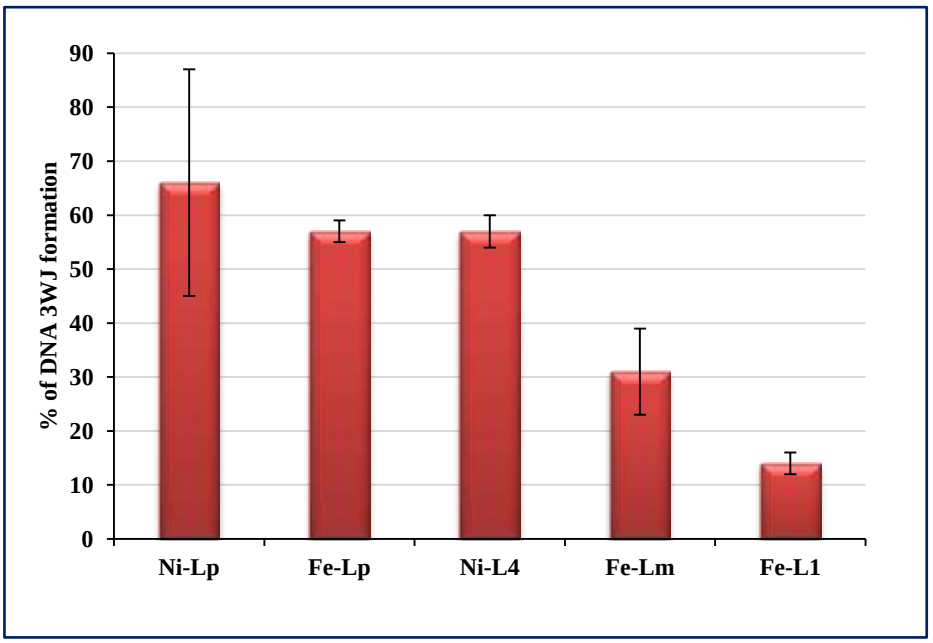

Figure 3.27 Bar graph displaying the percentage of 3WJ formed by $[Ni_2(Lp)_3]Cl_4$ (Ni-Lp), $[Fe_2(Lp)_3]Cl_4$ (Fe-Lp), $[Ni_2(L_4)_3]Cl_4$ (Ni-L_4), $[Fe_2(Lm)_3]Cl_4$ (Fe-Lm), $[Fe_2(L_1)_3]Cl_4$ (Fe-L_1) complexes.

The graph demonstrates that the Ni-Lp and Ni-L_4 complexes promote the formation of the DNA 3WJ comparable to the parent cylinder Fe-Lp, whereas the Fe-Lm and Fe-L_1 compounds showed less percentage of the junction formed. This could be the result of replacing the imine hydrogen with a more sterically demanding methyl group. Thus, for example, Siriporn Phongtongpasuk from Hannon`s group examined the parent cylinder with phenyl and pyridine groups at the imine position of the parent ligand (Fig. 3.28 (a, b)) by PAGE experiment.

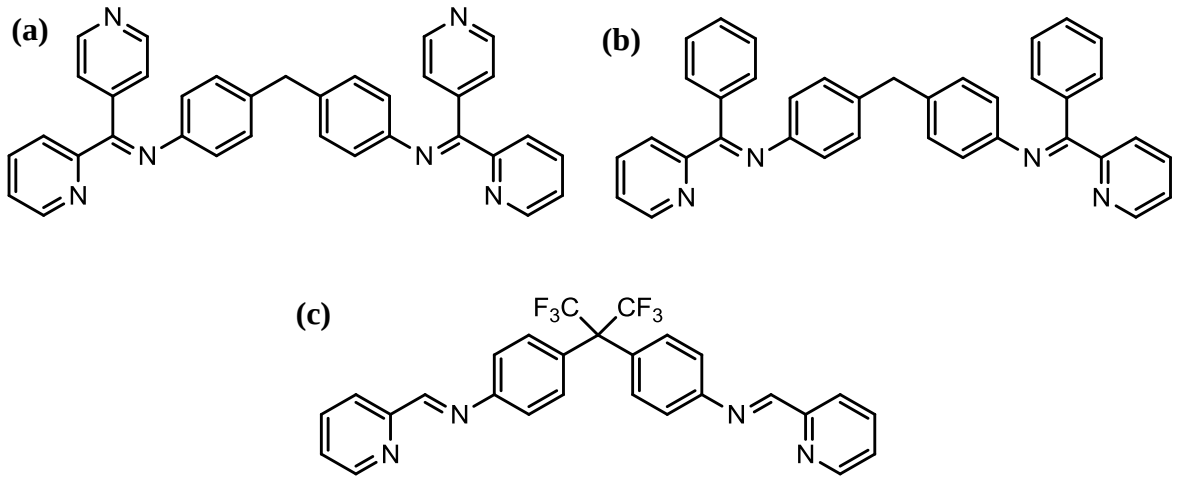

Figure 3.28 Chemical structures of ligands with various substituents **(a)** with pyridine ring at the imine position **(b)** with phenyl ring at the imine position **(c)** with bulky CF_3 groups in the middle of the spacer.

The results demonstrated that the parent cylinder with the phenyl substituent promoted the formation of DNA 3WJ though less effectively than the parent complex. No 3WJ was formed by the complex with the pyridine group at the imine position.[20] Brabec *et al.* have previously shown that the parent cylinder with bulky CF_3 groups introduced in the middle of the spacer in the ligand (Fig. 3.28 (c)) did not induce the formation of 3WJ structures as the diameter of the cylinder was too big to fit into the cavity of the junction.[19] These examples demonstrate that various substituents on the parent ligand can affect the formation and stabilisation of the DNA three-way junction.

The effect of different metal ions on the formation of the DNA 3WJ was investigated by PAGE experiment using iron(II), nickel(II) and cobalt(II) parent compounds which were synthesised according to a published literature procedure.[21] The results of the experiments are shown in Figure 3.29.

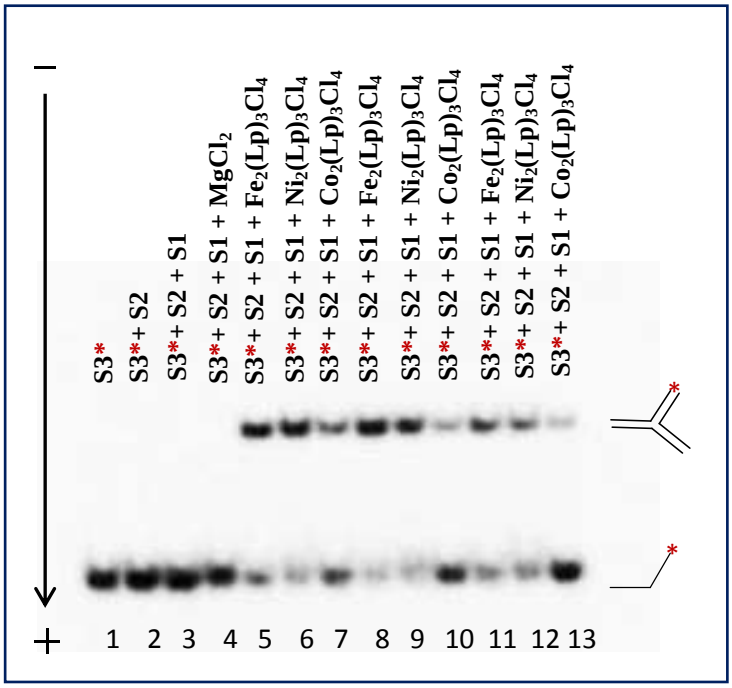

Figure 3.29 Autoradiogram of PAGE experiment of iron(II), nickel(II) and cobalt(II) parent compounds. Lanes 1-4: S3*, S3*+S2, S3*+S2+S1, S3*+S2+S1+$MgCl_2$. Lanes 5, 8, 11: S3*+S2+S1 with $[Fe_2(Lp)_3]Cl_4$; lanes 6, 9, 12: S3*+S2+S1 with $[Ni_2(Lp)_3]Cl_4$; lanes 7, 10, 13: S3*+S2+S1 with $[Co_2(Lp)_3]Cl_4$.

All the complexes were found to induce the formation of the DNA 3WJ, however for the iron(II) and nickel(II) compounds more intense 3WJ gel bands were observed. Quantification of the gel (Fig. 3.30) supported the obtained results.

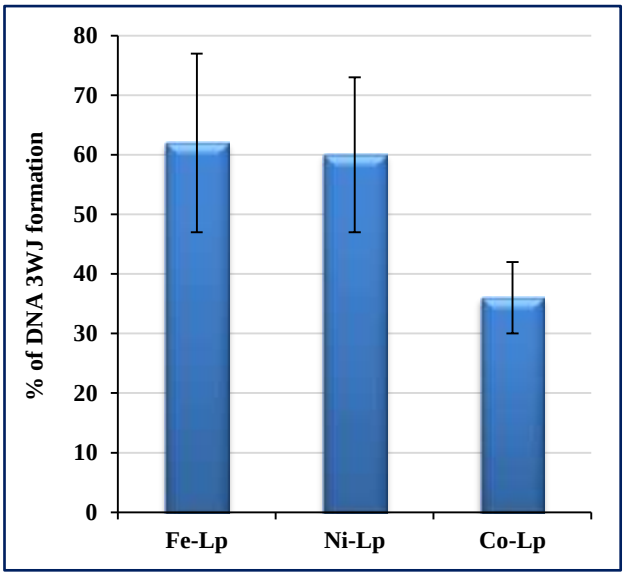

Figure 3.30 Bar graph displaying the percentage of DNA 3WJ formed by $[Fe_2(Lp)_3]Cl_4$ (Fe-Lp), $[Ni_2(Lp)_3]Cl_4$ (Ni-Lp) and $[Co_2(Lp)_3]Cl_4$ (Co-Lp) parent cylinders.

The percentage of DNA 3WJ formed for the cobalt cylinder was lower, ~ 36 %, compared to the nickel and iron cylinders ~ 60 % and ~ 62 % respectively. Such a significant difference in the percentage of 3WJ formation could be a result of low stability of cobalt(II) complex in aqueous solution. In order to confirm the proposed hypothesis, UV/Vis stability tests were performed over a 12-hour period on iron(II), nickel(II) and cobalt(II) parent complexes. The recorded spectra are shown in Figure 3.31.

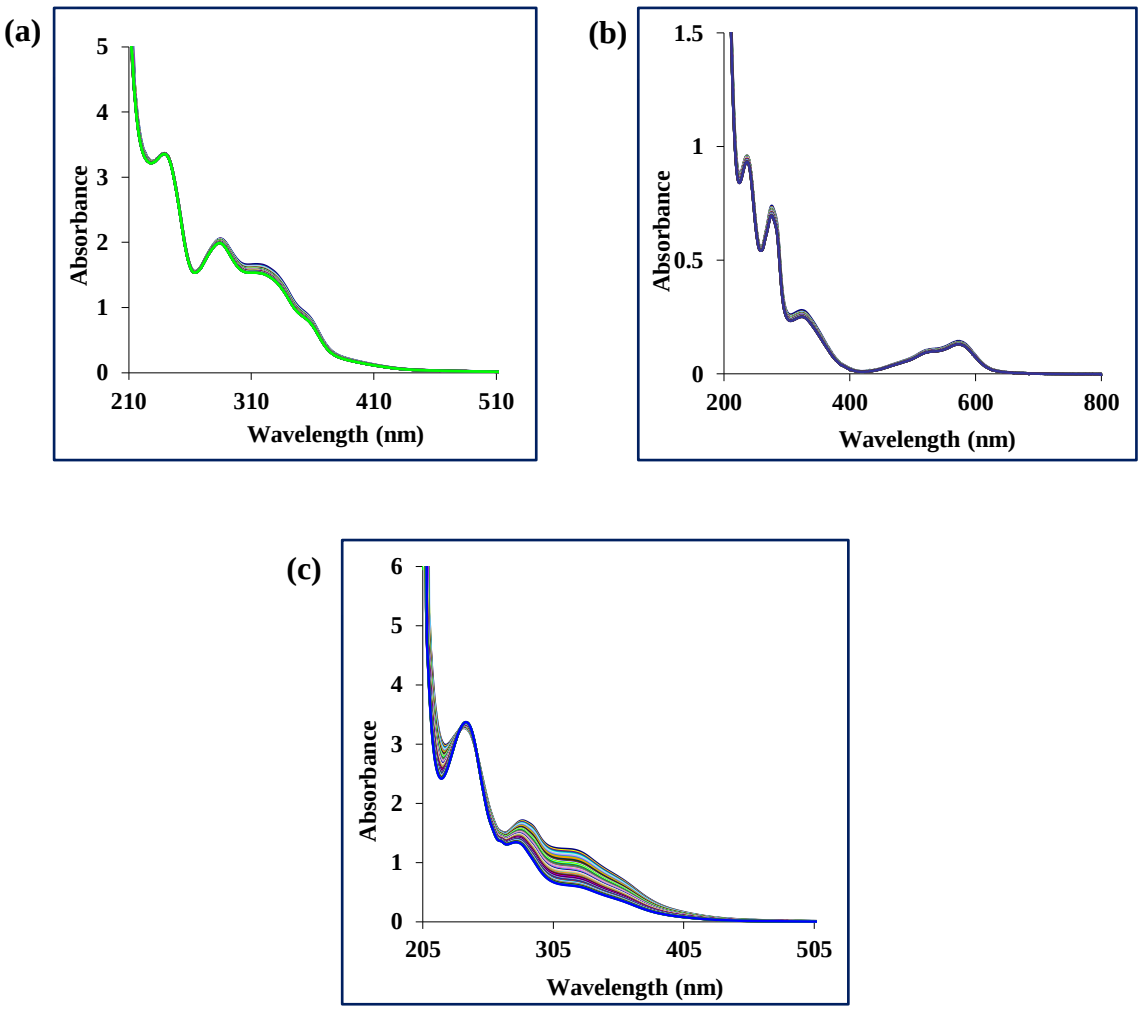

Figure 3.31 UV/Vis stability test spectra recorded in water over a 12-hour period for **(a)** $[Ni_2(Lp)_3]Cl_4$ **(b)** $[Fe_2(Lp)_3]Cl_4$ **(c)** $[Co_2(Lp)_3]Cl_4$.

The recorded UV/Vis spectra confirm that the $[Co_2(Lp)_3]Cl_4$ complex is less stable than the iron(II) and nickel(II) analogues and suffers degradation. $[Ni_2(Lp)_3]Cl_4$ and $[Fe_2(Lp)_3]Cl_4$ compounds are relatively stable over a 12 hour period although slight changes in the spectra are also observed. Thereby, low stability of cobalt(II) parent compound in aqueous solution explains the lower percentage of 3WJ formation in comparison with iron(II) and nickel(II) parent cylinders.

3.8 Conclusions

In this chapter various techniques such as circular and linear dichroism, UV/Vis spectroscopy and gel electrophoresis were applied to analyse the DNA binding properties and stability of the synthesised complexes. All the compounds were relatively stable aside from the $[Fe_2(L_4)_3]Cl_4$ complex which degrades rapidly in water. The CD titrations to ct-DNA revealed that the $[Fe_2(L_3)_3]Cl_4$, $[Fe_2(L_1)_3]Cl_4$ and $[Ni_2(L_4)_3]Cl_4$ complexes bind to the DNA which was further confirmed by the LD experiment. At high concentrations of the drug loading a loss of LD signal was observed as well as induced LD signals in the MLCT region indicating binding of the complexes to ct-DNA in a specific orientation and bending/coiling it. The loss of LD signal in the DNA region was more significant for complexes $[Fe_2(L_3)_3]Cl_4$ and $[Ni_2(L_4)_3]Cl_4$ with a nickel(II) complex leading to a 97 % loss of the signal at 260 nm at 4:1 ratio. Moreover, high concentrations of the nickel complex caused precipitation of ct-DNA.

The agarose gel electrophoresis results demonstrate that none of the synthesised complexes unwind plasmid DNA which can be related to the nature of the compounds or their instability at high temperatures. The data obtained from the PAGE experiments reveal that the $[Fe_2(L_1)_3]Cl_4$, $[Fe_2(L_3)_3]Cl_4$, and $[Ni_2(L_4)_3]Cl_4$ complexes induce the formation of the DNA 3WJ. The percentage of the 3WJ formed by the nickel complex was comparable to its iron(II) and nickel(II) parent analogues. The $[Fe_2(L_1)_3]Cl_4$ and $[Fe_2(L_3)_3]Cl_4$ compounds were less effective in the formation of the DNA 3WJ than the $[Ni_2(L_4)_3]Cl_4$ complex which can be elucidated by the influence of various substituents on the structure of the ligand. It was previously shown that the presence of substituents in the structure of the ligand as well as the shape and size of the cylinder affect the

binding properties of the complexes to the DNA 3WJ.[19] The $[Fe_2(L_4)_3]Cl_4$ complex did not promote the formation of the junction structure for the reason of instability in aqueous solution. The effect of different metal ions on the formation of the DNA 3WJ was investigated using iron(II), cobalt(II), nickel(II) parent cylinders. The cobalt(II) complex promoted lower percentage of 3WJ formation compared to the iron(II) and nickel(II) parent compounds due to the poor stability in aqueous solution. Both nickel(II) and iron(II) are relatively stable and induced ~ 60 % of 3WJ.

The focus of the next chapter is the cytotoxic activity of the synthesised complexes using an MTT colorimetric assay.

3.9 References:

1. N. P. Farrell in: J. A. McCleverty, T. J. Meyer, *Comprehensive Coordination Chemistry II*, vol. 9, Elsevier Ltd., Oxford, 2004.

2. M. J. Hannon, V. Moreno, M. J. Prieto, E. Moldrheim, E. Sletten, I. Meistermann, C. J. Isaac, K. J. Sanders and A. Rodger, *Angew. Chem., Int. Ed.*, 2001, **40**, 879-884.

3. A. Oleksi, A. G. blanco, R. Boer, I. Uson, J. Aymami, A. Rodger, M. J. Hannon, M. Coll, *Angew. Chem,. Int. Ed.*, 2006, **45**, 1227-1231.

4. T. Owen, *Fundamentals of modern UV-visible spectroscopy: Primer*, Agilent technologies, Germany, 2000.

5. J. Kypr, I. Kejnovska, D. Renčiuk, M. Vorlíčková, *Nucleic Acids Res.*, 2009, **37**, 1713-1725.

6. A. Rodger and B. Nordén, *Circular and linear dichroism*, Oxford University press, New York, 1997.

7. M. J. Hannon, V. Moreno, M. J. Prieto, E. Moldrheim, E. Sletten, I. Meistermann, C. J. Isaac, K. J. Sanders, A. Rodger, *Angew. Chem., Int. Ed.*, 2001, **40**, 879-884.

8. S. Vitorino, PhD thesis, University of Birmingham, 2011.

9. I. Meistermann, V. Moreno, M.J. Prieto, E. Moldrheim, E. Sletten, S. Khalid, P.M. Rodger, J.C. Peberdy, C.J. Isaac, A. Rodger and M.J. Hannon, *Proc. Natl. Acad. Sci., USA*, 2002, **99**, 5069-5074.

10. D. S. Kryndushkin, I. M. Alexandrov, M. D. Ter-Avanesyan, V. V. Kushnirov, *J. Biol. Chem.*, 2003, **278**, 49636-49643.

11. K. Triantafillidi, K. Karidi, O. Novakova, J. Malina, A. Garoufis, *Dalton. Trans.*, 2011, **40**, 472-483.

12. S. F. Bellon, J. H. Coleman, S. J. Lippard, *Biochemistry*, 1991, **30**, 8026-8035.

13. M. Huxley, PhD Thesis, University of Warwick, 2006.

14. J. Malina, M. J. Hannon, V. Brabec, *Nucleic Acids Res.*, 2008, **36**, 3630-3638.

15. M. J. Hannon, *Chem. Soc. Rev.*, 2007, **36** 280-295.

16. S. Muhuri, K. Mimura, D. Miyoshi, N. Sugimoto, *J. Am. Chem. Soc.*, 2009, **131**, 9268-9280.

17. A. Oleksi, A. G. Blanco, R. Boer, I. Uson, J. Aymami, A. Rodger, M. J. Hannon, M. Coll, *Angew. Chem., Int. Ed.*, 2006, **45**, 1227-1231.

18. C. C. Richardson, in *Procedures in nucleic acid research*, eds. G. L. Cantoni and D. R. Davies, Harper and Row, New York, Edn., 1971, Vol. 2, 815-828.

19. J. Malina, M. J. Hannon, V. Brabec, *Chem. Eur. J.*, 2007, **13**, 3871-3877.

20. S. Phongtongpasuk, PhD Thesis, University of Birmingham, 2010.

21. C. Painting, PhD Thesis, University of Warwick, 1999.

Chapter 4

Biological studies *in vitro*

4.1 Introduction

The evaluation of the biological activity of synthesised compounds is of great importance as it determines whether the synthesised molecule can be used as a potential drug. The biological effects of the compounds are explored using various assays. The cytotoxic activity of the drug, for example, can be assessed by using the LDH assay[1] (lactate dehydrogenase cell viability assay, measures integrity of the membrane), the SRB assay[2] (the method used to determine the antitumour activity of the molecule by measuring cellular proteins), the MTT colorimetric assay[3] (used to assess cell viability) etc. In this work the MTT assay was used to assess the antitumour activity of the synthesised complexes by measuring the inhibitory effect of the compounds on the proliferative activity of various cell lines.

4.2. Cell culture

4.2.1 Cell growth

To study the potential anticancer activity of the synthesized compounds *in vitro*, cytotoxic experiments were carried out using different human cancer cell lines: MDA-MB-231 human breast adenocarcinoma, SKOV-3 human epithelial ovarian carcinoma, A2780 human epithelial ovarian carcinoma and A2780cisR cisplatin-resistant human epithelial ovarian carcinoma. Cells were grown as monolayers in complete growth medium (RPMI 1640 or DMEM depending on a cell line) in tissue culture flasks in a humidified incubator at 37 ºC, 5 % CO_2 to simulate *in vivo* conditions.[4] The growth medium provides essential nutrients such as amino acids, fatty acids, sugars, ions, trace

elements, vitamins, and etc. that are essential for cell division and maintenance of the chemical environment for the cell.

Cells go through several growth phases. The initial phase is the quiescent or lag phase when cells recover from subculture, attach, and spread. The cells then enter the log phase where the number of cells begins to increase exponentially and they have the highest metabolic activity. The stationary phase is the phase where number of cells is constant, this is characteristic of a confluent population (where all growth surfaces are covered), the growth rate then slows down or stops. When cells reach their confluency they undergo a process called "cell splitting" or subculturing. Ideally, cells should be split when they are in a semi-confluent state and are still in the log phase. Cells that are not subcultured and are allowed to grow to a confluent state can sometime lag for a long period of time and some may never recover. Most cells are split (or at least fed) three times a week. In order to split cells, they are detached from the surface of the flask by trypsinization. The resultant cell suspension is then divided into fresh cultures.[5]

4.2.2 Cell counting and treatment

Determining the correct number of cells is crucial in performing accurate experiments. A device used for counting the number of cells per unit volume of a suspension is called a counting chamber or hemocytometer (Fig. 4.0), as originally it was designed to count blood cells.6 The central platform of the hemocytometer is divided into two counting grids. Each 3 x 3-mm grid is etched on a mirror-like surface. The grid is divided into large nine squares and each square has a surface area of 1 x 1 mm. The four corner squares and the central square are used for cell counting. Cells are counted in selected squares in a way that the total number of cells is 100 or so (it is

necessary in order to get good statistics). The cells should be uniformly distributed and not overlap each other. If the cells overlap the gridline, a cell is counted if it overlaps the top or right gridline and not counted if it overlaps the bottom or left gridline.[5, 6]

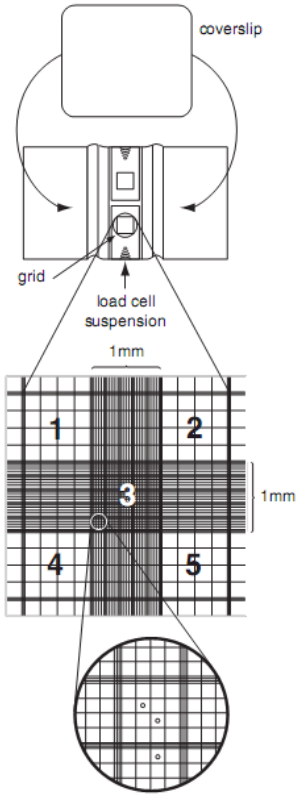

Figure 4.0 Hemocytometer (improved Neubauer) with a cover slip.[6]

To count the number of cells per 1 mL ($\mathbf{N_{Cells/mL}}$) the following formula is used:

$$\mathbf{N_{Cells/mL} = N_A \times 10^4 \times dilution\ factor}$$

$\mathbf{N_A}$ - average number of cells per square, $\mathbf{10^4}$ - volume correction factor for the hemocytometer.

To assess the number of viable cells trypan blue is used (Fig. 4.1). Trypan blue is a diazo dye. It is a vital stain that colours dead cells blue whereas living cells with an intact membrane do not absorb the dye and thus are not coloured.[7]

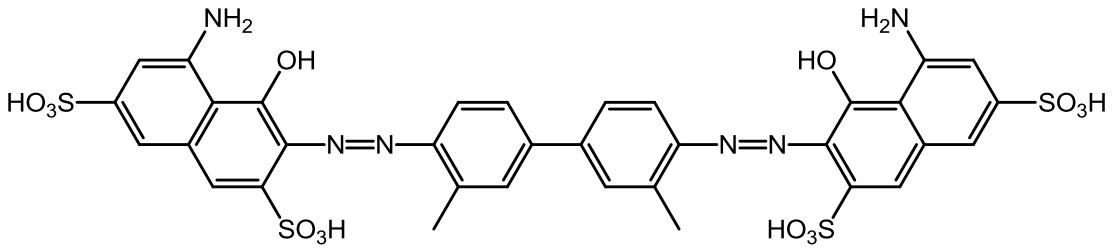

Figure 4.1 Structure of trypan blue.

To calculate the percentage of viable cells (**Cv**) the following equation is used:

$$\mathbf{Cv = N_L/N_{Tot} \times 100}$$

$\mathbf{N_L}$ - number of living cells, $\mathbf{N_{Tot}}$ - number of total cells counted.

To calculate the number of cells needed for an experiment to seed in a 96 flat-bottom well plate the following formula is used:

$$\mathbf{V_S = N_R/N_C \times V_M}$$

$\mathbf{V_S}$ - volume of cell suspension for seeding, $\mathbf{N_R}$ - number of cells per 1 mL required (depends on the cell density and is defined experimentally; for different cell lines this value varies), $\mathbf{N_C}$ - number of viable cells per 1 mL counted with hemocytometer, $\mathbf{V_M}$ - volume of medium per plate.

100 µL of suspension with the correct amount of cells is then distributed with a multichannel micropipette in each well of a 96 well microtiter plate and the plates are placed in the incubator for 24 hours to allow adhesion. The cells are then treated with various concentrations of complexes (200 µM, 100 µM, 50 µM, 25 µM, 12.5 µM) and incubated for 72 hours. After 72 hours of incubation the MTT assay is performed.

4.2.3 MTT assay

To examine cell proliferation and viability, the MTT colorimetric assay is used. The MTT assay also helps to determine the cytotoxicity of the synthesized compounds as they can inhibit or stimulate cellular growth and viability. The MTT assay was first introduced by Mossman as a quantitative measure of mammalian cell survival and proliferation.3 MTT or 3-(4,5-Dimethylthiazol-2-yl)-2,5-diphenyltetrazolium bromide is a yellow tetrazolium salt which is converted into a purple formazan by dehydrogenases in the mitochondria of living cells (Fig. 4.2 (a)). The ability of cells to reduce MTT indicates the mitochondrial integrity which can be interpreted as a measure of cell viability.

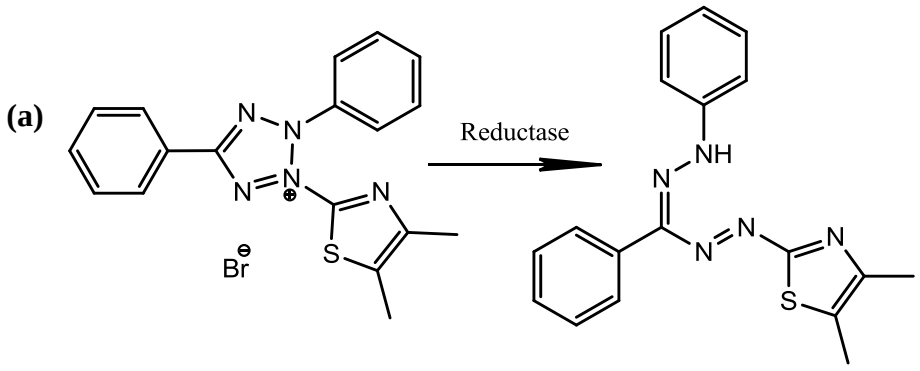

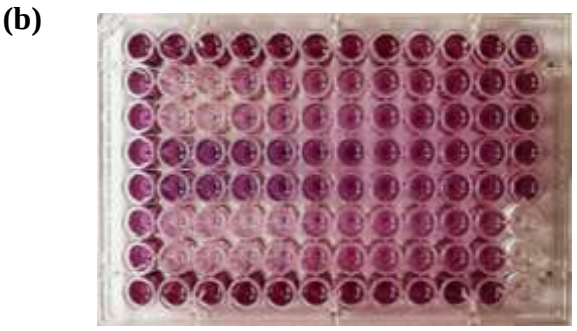

Figure 4.2 (a) Reduction of MTT to formazan **(b)** 96-Well plate with dissolved formazan crystals.

The MTT assay interpretation is based on the principle that the amount of formazan produced is proportional to the number of live cells. The formed purple crystals of formazan can be measured by a spectrophotometer plate reader after solubilization with DMSO (Fig. 4.2 (b)).[8] The absorbance of the coloured solution of formazan can be quantified by measuring at a certain wavelength, usually between 500-600 nm.[9, 10]

In this work, after dissolving the formed purple crystals of formazan with DMSO the absorbance at 590 nm was recorded using a plate reader machine (BioRad). The results obtained from cells treated with a compound were compared with results of untreated control cells, and the effectiveness of the agent was defined through the production of a dose-response curve.

4.2.4 Dose-response curve and IC_{50}

The potency of a compound or a drug is defined by the IC_{50} value. An IC_{50} or inhibitory concentration is the concentration of a compound required to inhibit a given biological process by half. IC_{50} values are important as they give information about the biological activity of a compound. The lower the IC_{50}, the higher the biological activity of the drug or compound and the lower the concentration of drug that is required to inhibit the maximum biological response.[11]

To calculate IC_{50} values a dose-response curve is produced. The x-axis represents different concentrations of the drug whereas the y-axis represents the response to the drug or compound (percentage cell growth). The IC_{50} value is then obtained from the point at which cell growth is inhibited by 50 %.

In this work the Microsoft Office Excel program was used to plot the dose-response curve and calculate IC_{50} values. An example of dose-response curve produced for cisplatin is displayed in Figure 4.3.

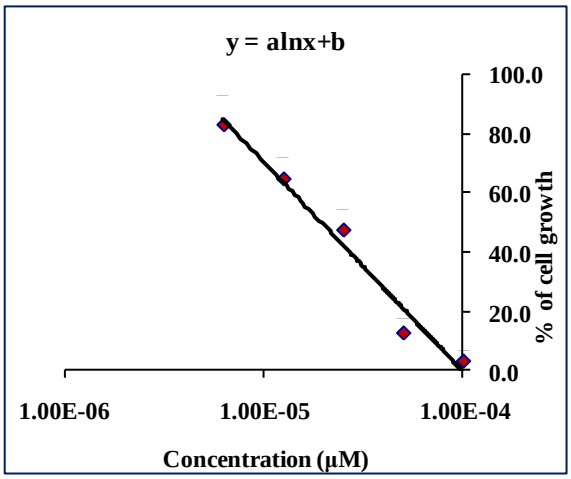

Figure 4.3 Dose-response curve for cisplatin in MDA-MB-231 cell line.

Change of the x-axis of the graph to natural logarithm allows better fitting of the dose-response curve to a straight line. Compounds with IC_{50} values higher than 100 µM were considered to be inactive. All experiments were repeated at least three times to ensure the consistency of the IC_{50} values. The data were then averaged and standard deviation (SD) was calculated. The evaluation of biological activity of synthesized complexes was carried out using the facilities of the School of Biosciences at the University of Birmingham provided by Prof. Kevin Chipman, Dr. Chris Bunce and Dr. Nikolas Hodges.

4.3 Results and discussion

A number of compounds were tested for anticancer activity, some of these were prepared in this thesis and others supplied by other researchers in the group. The compounds supplied by others are discussed first and then the complexes of this thesis.

4.3.1 Cytotoxic activity of the peptide conjugated iron(II) cylinders

Iron(II) peptide conjugated helicates were synthesised by Lucia Cardo from Hannon`s group, by attaching short amino acids to the iron(II) cylinder (Fig. 4.4) in order to improve the specificity of the metal complexes to DNA. The compounds were provided as their water soluble chloride salts for biological testing in cancer cell lines.

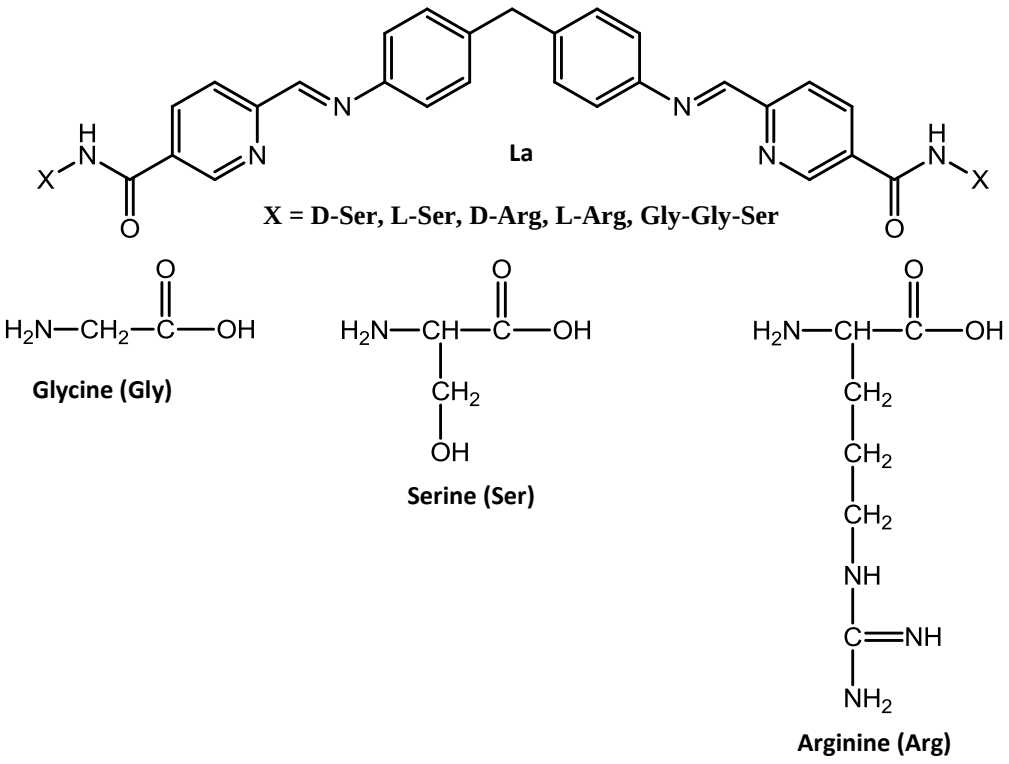

Figure 4.4 Chemical structures of ligand La, developed by Lucia Cardo, and conjugated amino acids.

Amino acids are components of proteins and play an important role in the recognition of specific sites of the DNA.[12, 13] Most sequence-specific DNA binding proteins bind in the major groove by using a simple secondary structure, usually an α-helix, which is complementary to the structure of the B-DNA major groove.[14] The amino acid sequences employed were chosen from those that can be found in natural systems and take part in DNA recognition. The peptides were conjugated to the cylinder at the 5-position of the pyridine ring after considering possible steric constraints. The compounds were shown to bind to the DNA and induce DNA bending/coiling[15] as well as promote DNA three-way junction formation, with arginine conjugates being more effective than the other compounds of this series.

The cytotoxic activity of cylinder-peptide conjugates was explored using A2780 ovarian and MDA-MB-231 breast cancer cell lines. The iron(II) parent complex and cisplatin were used as controls. The results of the experiments are shown in Table 4.0 and chart (Fig. 4.5).

Compound	MDA-MB-231, IC_{50} (μM)	A2780, IC_{50} (μM)
D-Arg	26±1	6±3
L-Arg	35±7	9±2
D-Ser	29±3	5±2
L-Ser	23±1	7±3
Gly-Gly-Ser	34±6	9±2
Parent cylinder	27±3	14±2
Cisplatin	27±3	4±2

Table 4.0 IC_{50} values of peptide-conjugated cylinders.

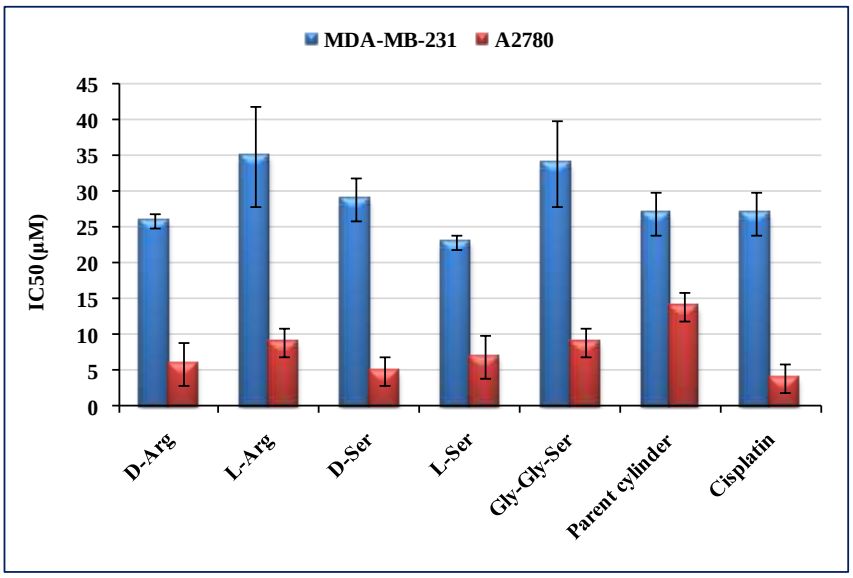

Figure 4.5 Schematic illustration of IC_{50} values from Table 4.0. The data represent mean values ± 1SD of three repeats.

The obtained IC_{50} values reveal that all of the peptide-cylinder conjugates possess antineoplastic activity. D-Arg and L-Arg iron(II) complexes are not stable in aqueous solution and gradually degrade, however low stability did not affect their cytotoxic profile. The activity of the complexes in the MDA-MB-231 cell line is similar however the IC_{50} values for the L-Arg and Gly-Gly-Ser cylinders were slightly higher. This could be due to lower affinity of the Gly-Gly-Ser conjugate to DNA shown by CD and LD studies.[15] The L-Arg complex forms the helicate in a P-conformation which causes the complex to be a slightly less effective DNA binder and this could affect the activity of the complex. The conjugated cylinders showed a good cytotoxic profile in ovarian cancer cell line A2780. The IC_{50} values for these complexes in A2780 cells were lower than those of the parent cylinder and comparable with cisplatin. The components of the ligand (the 4,4'-methylene dianiline spacer and peptide functionalised aldehydes) were also tested for potential anticancer activity by MTT assay. The results demonstrated

IC_{50} values higher than 100 μM indicating that the activity of the complexes arises just from the conjugate cylinders themselves.

4.3.2 Cytotoxic activity of Pt(II) and Pd(II) non-helical complexes

Several platinum(II) and palladium(II) complexes, synthesised by Philipp von Grebe a PhD student from Professor Bernhard Lippert`s group at the University of Dortmund, Germany, were supplied for evaluation of their cytotoxic activity. The structures of the complexes are shown in Figure 4.6.

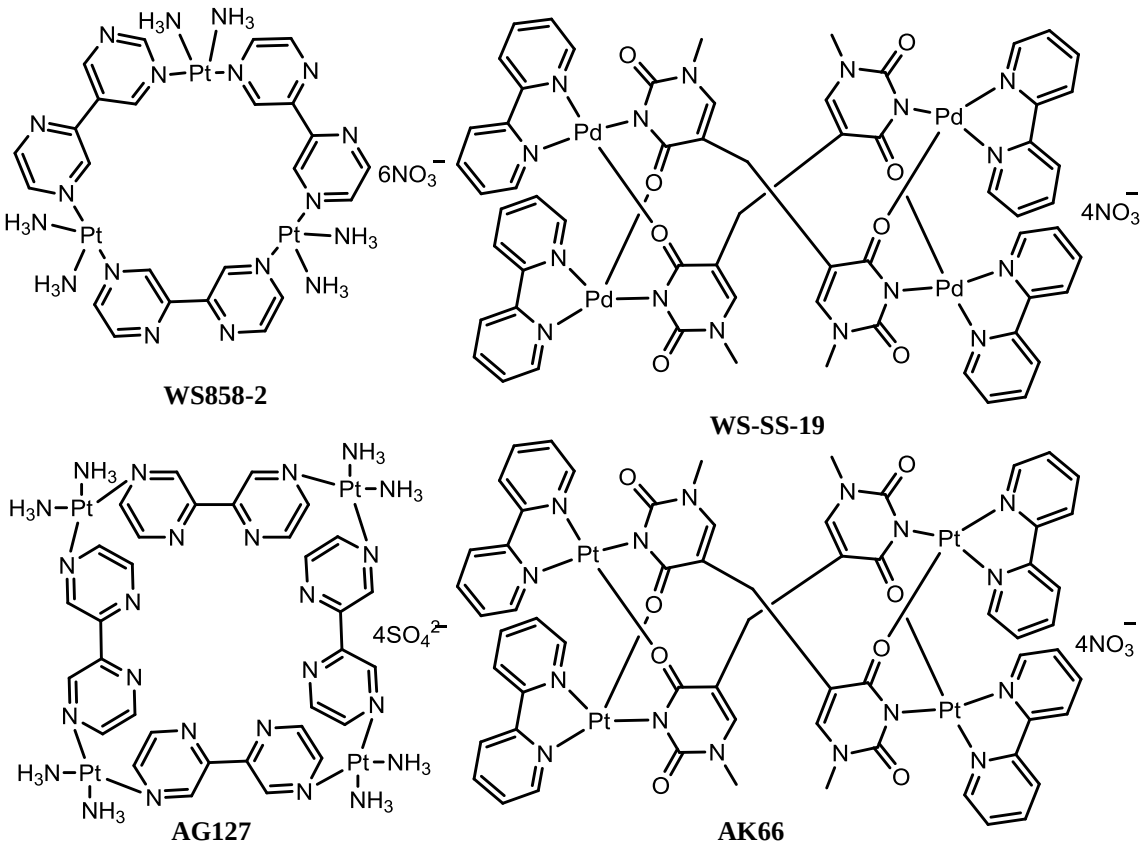

Figure 4.6 Structures of platinum(II) and palladium(II) complexes synthesised by Philipp von Grebe.

These compounds are supramolecular polycations of very different structure to the cylinders and with cyclic polyaromatic frameworks they may either fit into the major groove or bind at a DNA junction point. To this extent they are intriguing comparisons for the metal complexes being explored herein. A related tetraplatinum supramolecular square octacations has been shown to bind to quadruplex DNA[16] and to be cytotoxic to cancer cell lines.[17]

Moreno *et al.* reported studies on antitumour properties of supramolecular platinum squares (Fig. 4.7).[17]

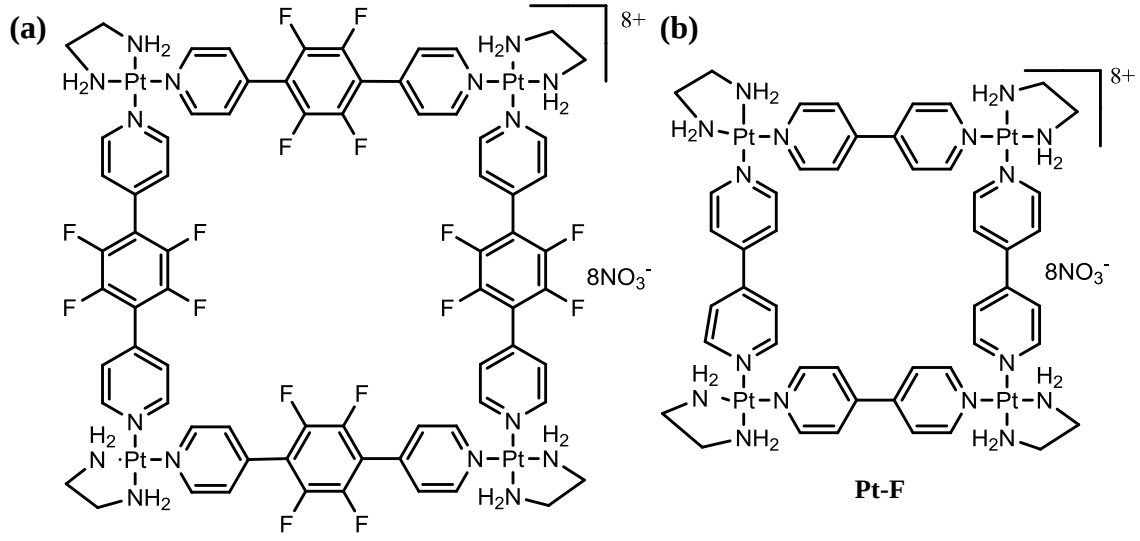

Pt-M **Pt-F**

Figure 4.7 Supramolecular squares tested for anticancer activity **(a)** Moreno platinum square (Pt-M) **(b)** Fujita platinum square (Pt-F).

The anticancer activity of these two platinum complexes was explored by MTT assay in HL-60 leukemia cell line. The results of the experiments as IC_{50} values are presented in Table 4.1 and chart (Fig. 4.8).

Compound	HL-60 IC_{50} (μM)
Pt-M	5 ± 2
Pt-F	3±1
Fe-Lp	18±3
Cisplatin	2±1

Table 4.1 IC_{50} values (μM) of supramolecular platinum squares[17] in comparison with Hannon iron(II) supramolecular helicate[18] (Fe-Lp) and cisplatin.

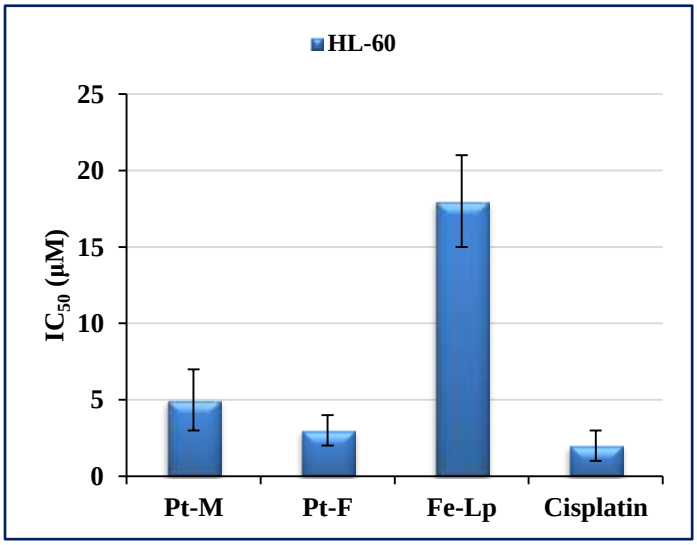

Figure 4.8 Schematic illustration of IC_{50} values from Table 4.1.

As it is listed in Table 4.1 and shown in the chart (Fig. 4.8) compound Pt-F exhibits cytotoxic activity comparable to that of cisplatin and they are approximately two-fold more active than compound Pt-M. It is unsurprising, because according to CD studies compound PT-F modifies the secondary and tertiary structures of DNA more

dramatically than compound PT-M apparently due to its smaller size.[17] The iron(II) supramolecular helicate is 3- to 5-fold less active in HL-60 cells than Pt-F and Pt-M.

Reports on biological studies of supramolecular cyclic polycations are relatively rare due to poor solubility in aqueous solutions. Therefore it was intriguing to perform cytotoxicity tests on compounds supplied by P. von Grebe which are water soluble polynuclear metal complexes.

The MTT assay of the platinum(II) and palladium(II) compounds was performed on A2780cisR, MDA-MB-231 and SK-OV-3 cancer cell lines. The results of the experiments are displayed in Table 4.2 and chart (Fig. 4.9).

Compound	A2780cisR IC_{50} (μM)	MDA-MB-231 IC_{50} (μM)	SK-OV-3 IC_{50} (μM)
AG127	13±3	>100	79[1]
AK66	23±8	>100	>100
WS858-2	18±1	>100	>100
WS-SS-19	18±3	14±5	17±4
Fe-Lp	13±2[19]	27±3	54±6
Cisplatin	6±2	23±5	10±3

Table 4.2 IC_{50} values (μM) of platinum(II) and palladium(II) complexes synthesised by Philipp von Grebe in comparison with Hannon iron(II) cylinder (Fe-Lp) and cisplatin.

[1] Only one experiment was performed with this complex due to insufficient quantities.

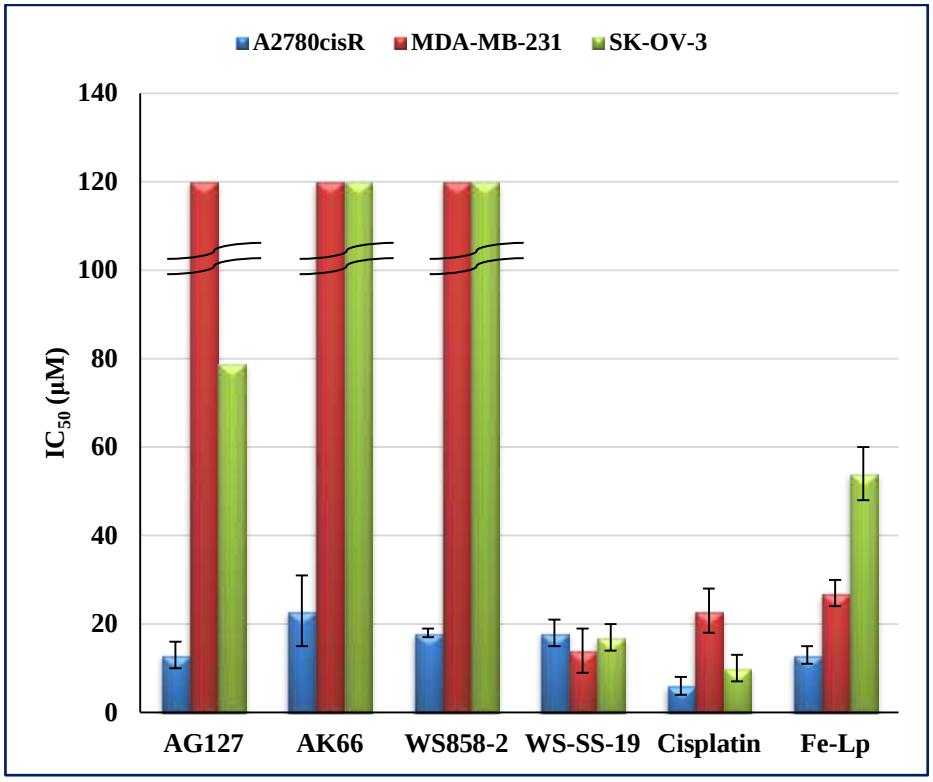

Figure 4.9 Schematic illustration of IC_{50} values from Table 4.2. The data represent mean values ± 1SD of three repeats.

The results of the assay demonstrate that all of the compounds are active in the A2780cisR cell line. Interestingly, the WS-SS-19 complex is the only compound of these series that showed good antitumour activity in MDA-MB-231 (IC_{50} values lower than cisplatin) and SK-OV-3 cells whereas the rest of the complexes were found to be inactive. Palladium metal complexes are generally considered to be less active than their platinum counterparts due to rapid hydrolysis of leaving groups, promoting the formation of very reactive species that are unable to reach their pharmacological targets. Increased structural integrity of a palladium drug can be reached by stabilising the molecule with a strong coordination to a nitrogen ligand and a suitable leaving group, leading to a higher activity.[20] Palladium metal complexes are known to be capable of

interacting with DNA enabling formation of the cross-links, inhibition of DNA synthesis as well as inducing apoptosis.[21] There is evidence that some palladium compounds can bind to an electron transport protein, cytochrome c, in mitochondria which is involved in the apoptosis process and acts as a death messenger. The compounds alter its conformation and cause release of the protein from its biological membrane.[22] Though the complex AG127 showed slight activity in the SK-OV-3 cell line, there is not enough evidence to prove the activity of this complex as the MTT experiment was performed only once due to an insufficient amount of the compound.

4.3.3 Cytotoxic activity of Rh(III) complexes.

Rhodium(III) complexes were provided by Susana Vitorino from Hannon`s group who synthesized and characterized these metal compounds. Dinuclear Rh(III) single stranded complexes are formed by linking together two Rh(III) metal centers with a bis-bidentate L_{azo} ligand and attaching a diimine (phen or bpy) ligand. The mononuclear Rh(III) complexes are based on a 2-phenylazopyridine ligand with an attached diimine ligand (Fig. 4.10). The bidentate ligand L_{azo} was chosen instead of the analogous imine ligand due to its greater stability.[23]

Works of Sheldrick and Lorenz *et al.* have shown that rhodium complexes are capable of inhibiting cell proliferation and thus possess antineoplastic activity.[24, 25] For this reason the synthesized Rh(III) complexes were investigated for their potential antitumour properties.

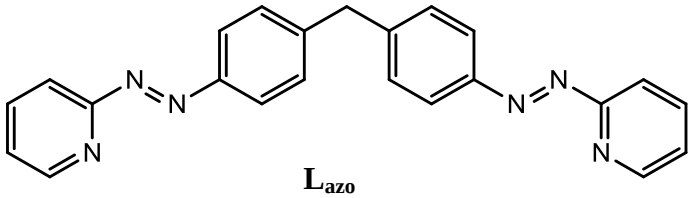

L_{azo}

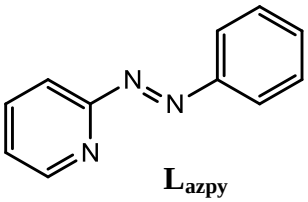

L_{azpy}

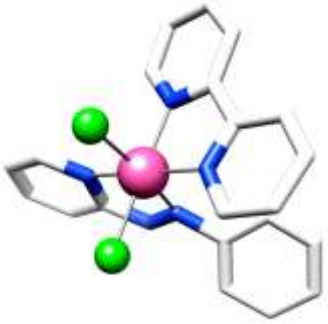

cis-($Rh_2(L_{azpy})(bpy)Cl_2$]Cl

(Rh-Bpy)

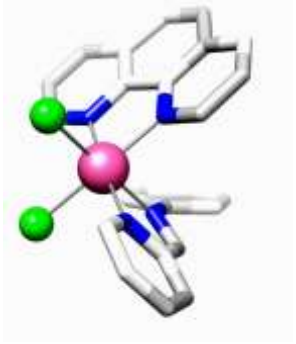

cis-($Rh_2(L_{azpy})(phen)Cl_2$]Cl
(Rh-Phen)

rac-($Rh_2(L_{azo})(phen)_2Cl_2$]$Cl_2$ (Isomer I)
and meso-isomer (Isomer II not shown)

Figure 4.10 Crystal structures of the Rh(III) complexes used for biological evaluation.[23]

The MTT assay of the Rh(III) compounds was performed on A2780 and MDA-MB-231 cancer cell lines. The results of the experiments are displayed in Table 4.3 and chart (Fig. 4.11).

Compound	A2780 IC_{50} (μM)	MDA-MB-231 IC_{50} (μM)
Isomer I	>100	65±5
Isomer II	>100	57±14
Rh-Bpy	>100	>100
Rh-Phen	26±2	23±2
Cisplatin	4±3	26±3

Table 4.3 IC_{50} values of the Rh(III) complexes synthesised by Susana Vitorino.

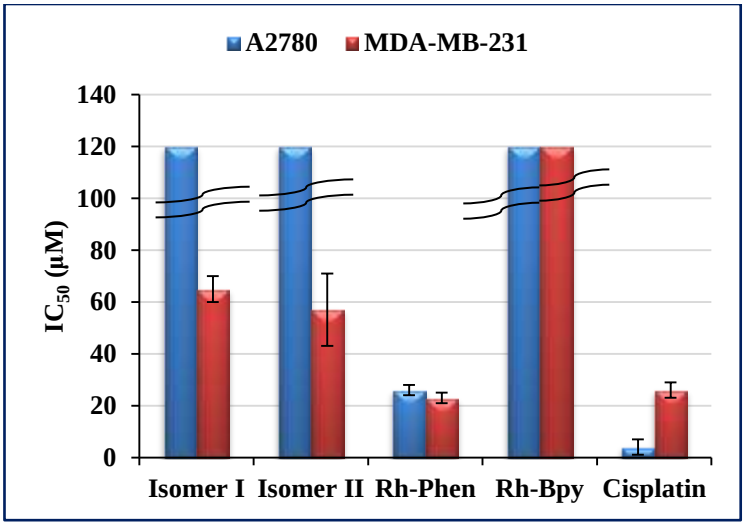

Figure 4.11 Schematic illustration of IC_{50} values from Table 4.3. The data represent mean values ± 1SD of three repeats.

The results of the MTT assay demonstrate that the mononuclear Rh(III) compound with attached phenanthroline ligand is the most effective cytotoxic agent among the tested rhodium complexes. The compound exhibited a good antitumour

profile in both cell lines with IC_{50} values comparable to that of cisplatin in the MDA-MB-231 cell line. Remarkably, DNA binding studies and gel electrophoresis showed that the complex did not significantly perturb the DNA structure or cause DNA plasmid unwinding as did its dinuclear analogues. According to the data obtained, it may be concluded that DNA is not the primary target of the Rh-Phen complex and the cytotoxic activity of the complex is associated with another cellular mechanism. One of the possible mechanisms is the suppression of DNA synthesis via inhibition of enzymes which take part in the DNA synthesis.[26] Some rhodium complexes are also known to cause oxidative damage to mitochondrial DNA which promotes specific changes in protein-DNA interactions and is thus identified by the mitochondrial protein machinery.[27] It is striking that the Rh-Bpy analogue did not exhibit any activity in cancer cell lines. By substituting the phenanthroline ligand with 2,2'-bipyridine, the biological activity of the complex was dramatically affected. The activity of the Rh-Phen complex can also be linked to the ligand. Phenanthroline itself is highly cytotoxic towards neoplastic cell lines. The IC_{50} values of phenanthroline in L1210 (cisplatin-sensitive murine leukemia) and A498 (human kidney adenocarcinoma) cancer cell lines are reported as 4.5, and 5.5 μM respectively. In leukemia cell lines phenanthroline is less active than cisplatin, whereas in other cell lines it shows 3.3- and 2.5-fold enhanced activity.[28]

Dinuclear Rh(III) compounds Isomer I and Isomer II exhibited moderate antitumour activity in the MDA-MB-231 cell line and no activity in the SK-OV-3 cell line. Both compounds were shown to bind to ct-DNA and cleave plasmid DNA. Thus the activity of these complexes can be associated with their ability to interact with a DNA or inhibit DNA synthesis.

4.3.4 Antitumour activity of supramolecular helicates with additional metal-binding units.

Turning to the compounds prepared in this thesis: the antineoplastic activity of $[Fe_2(L_1)_3]Cl_4$, $[Fe_2(L_1)_3]Cl_4$ with attached cisplatin, $[Fe_2(L_3)_3]Cl_4$, $[Fe_2(L_4)_3]Cl_4$ and $[Ni_2(L_4)_3]Cl_4$ was evaluated using MDA-MB-231 and SK-OV-3 cancer cell lines and compared to the parent analogues $[Fe_2(Lp)_3]Cl_4$, $[Ni_2(Lp)_3]Cl_4$ and $[Co_2(Lp)_3]Cl_4$. As an aide-mémoire the structures of L_1, L_3, L_4, Lp ligands are presented in Figure 4.12.

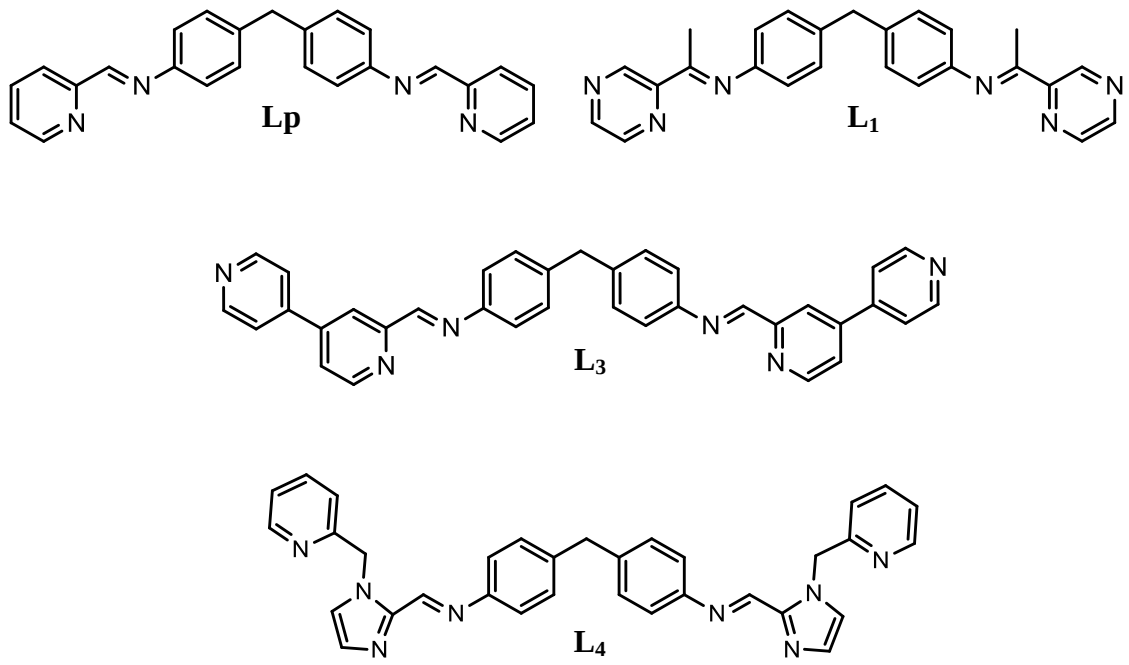

Figure 4.12 Structures of L_1, L_3, L_4 and Lp ligands.

The results of the MTT experiments are displayed in Table 4.4 and chart (Fig. 4.13).

Compound	SK-OV-3 IC_{50} (μM)	MDA-MB-231 IC_{50} (μM)
Fe-L_1	>100	>100
Fe-L_1Pt	-	39±19
Fe-L_3	21±6	17±1
Ni-L_4	52±5	55±10
Fe-L_4	>100	58±15
Fe-Lp	54±6	27±3
Ni-Lp	>100	>100
Co-Lp	10±6	10±1
Cisplatin	11±1	32±4

Table 4.4 IC_{50} values for a range of the helicates.

The Fe-L_1Pt compound was partially dissolved in DMEM medium and was not soluble in RPMI-1640 medium. Therefore evaluation of the cytotoxic activity of this complex was performed only using MDA-MB-231 cell line. To help to solubilise the compound an ultrasonicator was used. The Fe-L_4 complex was dissolved by addition of 2 % DMSO due to its insolubility in medium.

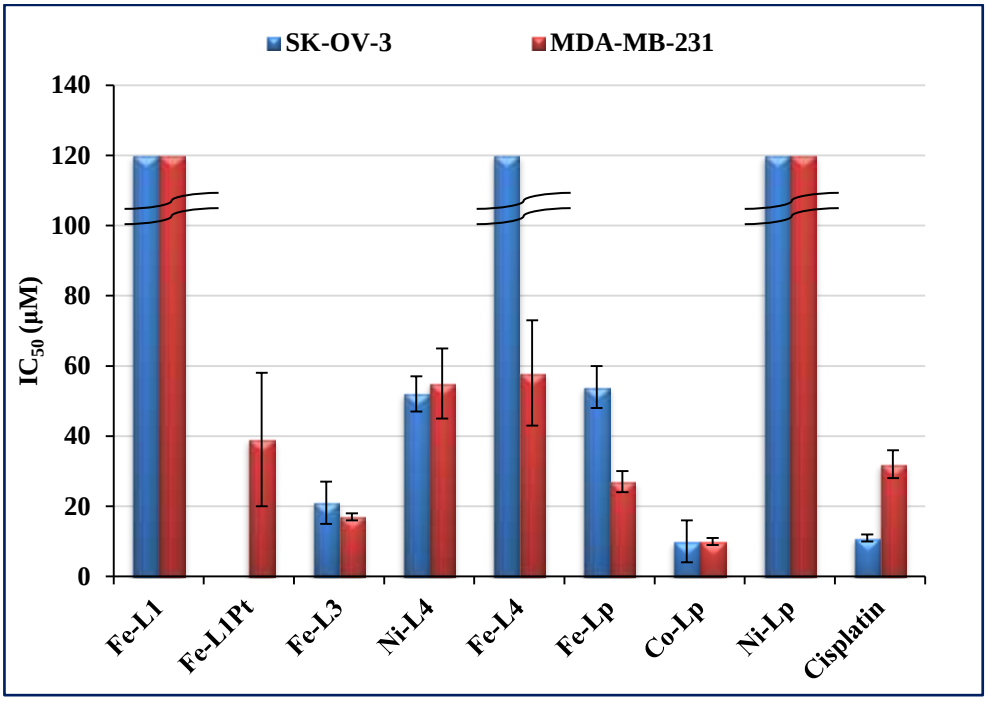

Figure 4.13 Schematic illustration of IC_{50} values from Table 4.4 (Fe-L_1 = $[Fe_2(L_1)_3]Cl_4$, Fe-L_1Pt = $[Fe_2(L_1)_3]Cl_4$ with attached cisplatin, Fe-L_3 = $[Fe_2(L_3)_3]Cl_4$, Ni-L_4 = $[Ni_2(L_4)_3]Cl_4$, Fe-L_4 = $[Fe_2(L_4)_3]Cl_4$, Fe-Lp = $[Fe_2(Lp)_3]Cl_4$, Co-Lp = $[Co_2(Lp)_3]Cl_4$, Ni-Lp = $[Ni_2(Lp)_3]Cl_4$). The data represent mean values ± 1SD of three repeats.

The obtained data reveals that the Fe-L_3 and Co-Lp complexes are the most active of all tested compounds of these series in both cancer cell lines. It should be noted that the Fe-L_3 complex showed an excellent antitumour profile in the MDA-MB-231 cell line with IC_{50} values two-fold lower than cisplatin. The activity of the compound can be attributed to its ability to interact with DNA. CD and LD studies demonstrated that the complex is an effective DNA binder, however according to the results from gel electrophoresis experiments, the Fe-L_3 helicate induces a low percentage of DNA three-way junction and does not unwind plasmid DNA when compared to its parent analogue Fe.Lp. This suggests that other cellular mechanisms may be involved which are

responsible for the antiproliferative activity of this compound. Thus, for instance, the antineoplastic activity of some iron(II) complexes is linked to DNA damage by active radical species produced by the compounds. Iron(II) ions are thought to be converted in cancer cells to iron(III) ions which are then involved in the production of active hydroxyl radicals.[29]

The Co-Lp complex exhibits potent antiproliferative activity in both cancer cell lines with IC_{50} values three-fold lower for MDA-MB-231 cells and comparable to cisplatin in SKOV-3 cancer cells. According to the gel electrophoresis results, the cobalt cylinder promoted a lower percentage of DNA three-way junction formation than the iron and nickel analogues which can be elucidated by its low stability in the aqueous solution. The activity of the cobalt complex can be linked to different cellular mechanisms. Cobalt compounds are known to form reactive oxygen species in an hypoxic tumour environment which attack the biomolecules of cancer cells such as lipids, proteins and DNA.[30] Thus treatment of cancer cells with cobalt complexes produces DNA strand breaks. Numerous breaks in DNA strands trigger the cellular death pathways. In addition, cobalt(II) compounds were found to be enzyme topoisomeraseII poisons. Topoisomerases are enzymes that control the unwinding and winding of DNA to facilitate DNA replication and recombination. TopoisomeraseII poisons convert topoisomeraseII from an essential enzyme to a cellular toxin that produces strand breaks in the genetic material.[31] Additional testing is required to elucidate the activity of the cobalt helicate and understand the mechanism of its action.

The nickel parent cylinder was found to be inactive in both cell lines which is striking as the ability of the complex to induce the formation of a DNA three-way junction is comparable to that of its iron counterpart. Remarkably, Qu *et al.* performed

MTT assay with M and P enantiomers of nickel parent cylinder on K562 leukemia cell line and both of the enantiomers were found to be active with IC_{50} values of 55 μM for P-enantiomer and 60 μM for M enantiomer.[32] The activity of the complexes was attributed to the ability of these compounds to inhibit telomerase activity and up regulate of p21 and p16 expression which are key effectors of cellular senescence.

The Ni-L_4 complex effectively inhibited cell proliferation in both cancer cell lines. CD and LD studies and gel electrophoresis experiments confirmed that the complex is an effective DNA binder and promoter of DNA 3WJ structures. According to literature reports, the activity of nickel compounds is associated with the ability to suppress DNA replication through inhibition of DNA polymerase *α* activity and transcription processes *in vitro* and *in vivo* and causing a non-random assault on DNA resulting in chromosomal aberrations.[33] Moreover, nickel complexes are known to bind proteins that are associated with DNA and are capable of cleaving DNA in the presence of oxidising agents through a production of reactive radical species. Although nickel is in the same group as platinum, it has not been shown significant anticancer properties. The ligands used to form nickel complexes can improve the biological properties of nickel.[34] This could be one of the reasons why the Ni-L_4 complex exhibited activity in cancer cell lines. The synthesised ligand L_4 is based on imidazole units linked to pyridine by an alkyl group. Imidazole derivatives are known to possess anti-inflammatory, antibacterial and anticancer properties.[35] Thus, for example, N-fused aminoimidazoles showed potent anticancer activities in kidney and breast cancer cell lines with low toxicity to normal cells.[36]

The iron(II) complex of L_4 showed moderate activity in the MDA-MB-231 cell line and no activity in the SK-OV-3 cell line. The stability of the complex did not affect

the activity of the compound. It can be suggested that the complex falls apart in the medium and the structural components of the cylinder inhibit cell proliferation by affecting various cellular processes.

Interestingly, the Fe-L_1 compound is not active in any of the cell lines used in the experiments. The absence of inhibitory activity on cancer cell growth can be attributed to lower affinity of the complex to ct-DNA. CD and LD studies demonstrated that the complex binds to the DNA in a less effective way than parent analogue or Fe-L_3. The complex did not show any DNA plasmid unwinding and caused ~ 15 % of DNA 3WJ formation. However, the Fe-L_1 compound with attached cisplatin showed antitumour activity in MDA-MB-231 cell line with IC_{50} values comparable to cisplatin. From the obtained results it can be concluded that the activity of the platinated iron(II) complex arises just from cisplatin alone.

In order to examine whether the iron(II) helicate mixed with cisplatin induces synergysm in activity, additional testing was performed by mixing 200 μM of parent iron(II) cylinder with 50 μM of cisplatin. The activity of the prepared mixture was tested in SK-OV-3 and A2780 cancer cell lines. The results of the experiments are presented in Table 4.5 and chart (Fig. 4.14).

Compound	SK-OV-3, IC_{50} (μM)	A2780, IC_{50} (μM)
Fe-Lp:cisplatin (4:1)	30±3	4±1
Fe-Lp	54±6	14±2
Cisplatin	8±3	4±2

Table 4.5 IC_{50} values of Fe-Lp:cisplatin mixture (Fe-Lp = $[Fe_2(Lp)_3]Cl_4$).

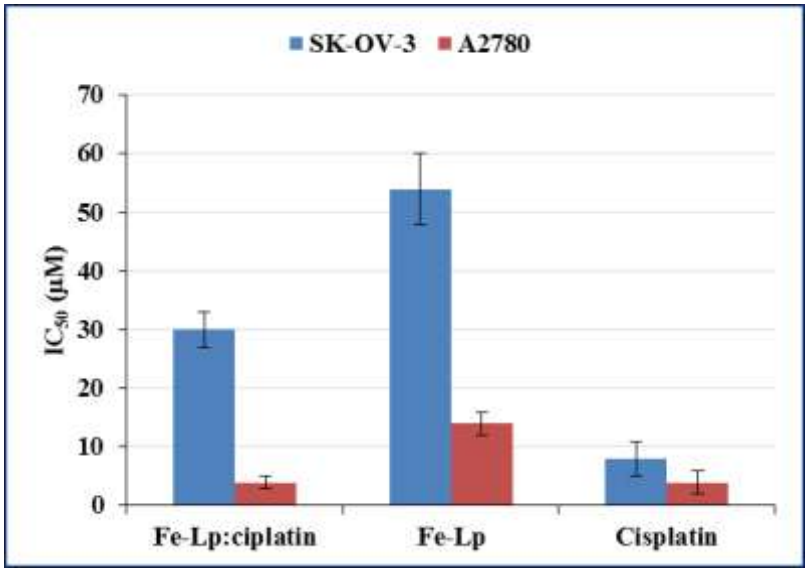

Figure 4.14 Schematic illustration of IC_{50} values from Table 4.5. The data represent mean values ± 1SD of three repeats.

The IC_{50} values of the iron(II) parent cylinder mixed with cisplatin show improved cytotoxic activity in both cancer cell lines compared to those of the cylinder alone, however there was no synergism of the two components observed. Interestingly, in A2780 cell line the IC_{50} value of the FeLp:cisplatin mixture is comparable to that of cisplatin in contrast to SK-OV-3 cells where no such effect was present. Additional testing is required to support the obtained results.

4.4 Conclusions

The biological evaluation of cytotoxic activity of a series of compounds was performed using MTT colorimetric assay. The IC_{50} values calculated gave preliminary information about the antiproliferative activity of the synthesised complexes. Modifications in ligand structure as well as variations in metal ions affected biological

activity and properties of compounds. The cytotoxic activity of most of the tested compounds was comparable to or lower than cisplatin. Only three compounds, palladium(II) complex WS-SS-19, cobalt(II) complex $[Co_2(Lp)_3]Cl_4$ and iron(II) helicate $[Fe_2(L_3)_3]Cl_4$, were more toxic than cisplatin in the MDA-MB-231 cancer cell line. The $[Fe_2(L_1)_3]Cl_4$ compound with attached cisplatin exhibits antitumour activity in MDA-MB-231 cells, however the activity arises just from cisplatin itself. It should be noted that the results obtained by *in vitro* testing may not correspond to results obtained by *in vivo* testing, as the environment of the experiments is different and many other factors should be taken into account. Additional experiments are required to be performed in order to understand cellular uptake and the mechanism of action of the synthesised compounds.

4.5 References:

1. T. Decker, M. L. Lohmann-Matthes, *J. Immunol. Methods,* 1988, **115**, 61-9.

2. V. Vichai, K. Kirtikara, *Nat. Protoc.*, 2006, **1**, 1112-1116.

3. T. Mosmann, *J. Immunol. Methods*, 1983, **65**, 6-24.

4. P. Price, T. J. McMillan, *Canc. Res.*, 1990, **50**, 1392-1396.

5. J. P. Mather, P. E. Roberts, *Introduction to cell and tissue culture Theory and Technique*, Plenum Press, New York, 1998.

6. M. C. Phelan , *Curr. Protoc. Cell Biol.*, 1998, **1.1**, 1.1-1.1.10.

7. A. E. Jablonski, W. H. Humphries IV, C. K. Payne, *J. Phys. Chem. B*, 2009, **113**, 405-408.

8. J. Skowroñ, L. Zapór, *Int. J. Occup. Safety Ergonomics*, 2004, **10**, 147-156.

9. F. Denizot, R. Lang, *J. Immunol. Methods*, 1986, **89**, 271-277.

10. A. P. Wilson, *Cytotoxicity and Viability Assays in Animal Cell Culture: A Practical Approach*, 3rd ed., Oxford University Press, Oxford, 2000.

11. D. C. Swinney, *Nature reviews. Drug discovery*, 2004, **3**, 801-808.

12. R. Rohs, X. Jin, S. M. West, R. Joshi, B. Honig, R. S. Mann, *Annu. Rev. Biochem.*, 2010, **79**, 233-269.

13. C. Yanover and P. Bradley, *Nucleic Acids Res.*, 2011, 1-13.

14. B. J. Chapman, *Advances in DNA Sequence-Specific Agents*, Elsevier Science B. V., Netherlands, 2002.

15. L. Cardo, PhD Thesis, University of Birmingham, 2010.

16. R. Kieltyka, P. Englebienne, J. Fakhoury, C. Autexier, N. Moitessier, H. F. Sleiman, *J. Am. Chem. Soc.*, 2008, **130**, 10040-10041.

17. M. Mounir, J. Lorenzo, M. Ferrer, M. J. Prieto, O. Rossell, F. X. Avile`s, V. Moreno, *J. Inorg. Biochem.*, 2007, **101**, 660-666.

18. A. C. G. Hotze, N. J. Hodges, R. E. Hayden, C. Sanchez-Cano, C. Paines, N. Male, M.-K. Tse, C. M. Bunce, J. K. Chipman, M.J. Hannon, *Chemistry & Biology*, 2008, **15**, 1258-1267.

19. Unpublished data from A. J. Pope, University of Birmingham.

20. A. S. Abu-Surrah and M. Kettunen, *Curr. Med. Chem.*, 2006, **13**, 1337-1357.

21. R. Kontek, K. Matławska-Wasowska, U. Kalinowska-Lis, B. Kontek, J. Ochocki, *Acta Pol. Pharm.*, 2011, **68**, 127-136.

22. S. Emami, H. Ghourchian, A. Divsalar, Int. J. Biol. Macromol., 2011, **48**, 243-248.

23. S. Vitorino, PhD thesis, University of Birmingham, 2011.

24. M. Dobroschke, Y. Geldmacher, I. Ott, M. Harlos, L. Kater, L. Wagner, R. Gust, W. S. Sheldrick, A. Prokop, *Chem. Med. Chem.*, 2009, **4**, 177-187.

25. S. Wirth, C. J. Rohbogner, M. Cieslak, J. Kazmierczak-Baranska, S. Donevski, B. Nawrot, I. P. Lorenz, *J. Biol. Inorg. Chem.*, 2010, **15**, 429-440.

26. N. Katsaros, A. Anagnostopoulou, *Crit. Rev. Oncol. Hemat.*, 2002, **42**, 297-308.

27. E. J. Merino, J. K. Barton, *Biochemistry*, 2008, **47**, 1511-1517.

28. S. Roy, K. D. Hagen, P. U. Maheswari, M. Lutz, A. L. Spek, J. Reedijk, and G. P. van Wezel, *ChemMedChem*, 2008, **3**, 1427-1434.

29. I. Ott, R. Gust, *Arch. Pharm. Chem. Life Sci.*, 2007, **340**, 117-126.

30. S. P. Osinsky, I. Ya. Levitin, A. L. Sigan, L. N. Bubnovskaya, I. I. Ganusevich, L. Campanella, and P. Wardmand, *Russ. Chem. Bull., Int.Ed.*, 2003, **52**, 2636-2645.

31. E. L. Baldwin, J. A. Byl, N. Osheroff, *Biochemistry*, 2004, **43**, 728-735.

32. Ha. Yu, C. Zhao, Y. Chen, M. Fu, J. Ren, X. Qu, *J. Med. Chem.*, 2010, **53**, 492-498.

33. D.-D. Li, J.-L. Tian, Y.-Y. Kou, W. Gu, X. Liu, and S.-P. Yan, *Z. Anorg. Allg. Chem.*, 2009, **635**, 2297-2301.

34. S. S. Matkar, l. A. Wrischnik, P. R. Jones, U. Hellmann-Blumberg, *Biochem. Biophys. Res. Commun.*, 2006, **343**, 754-761.

35. S. M. Sondhi, J. Singh, P. Roy, S. K. Agrawal, A. K. Saxena, *Med. Chem. Res.*, 2011, **20**, 887-897.

36. A. T. Baviskar, C. Madaan, R. Preet, P. Mohapatra,V. Jain, A. Agarwal, S. K. Guchhait, C. N. Kundu, U. C. Banerjee, P. V. Bharatama, *J. Med. Chem.*, 2011, DOI: 10.1021/jm200235u.

Chapter 5

Conclusions and future work

5.1 Conclusions

As highlighted in chapter 1, supramolecular chemistry is a powerful tool in the creation of fascinating and complex metallo-supramolecular architectures by utilising spontaneous self-assembly processes which occur though molecular recognition of the structural components.[1, 2] Simple metal-ligand interactions allow the development of synthetic supramolecular assemblies with interesting biological properties that have potential to be used as therapeutic agents.

In chapter 2, the synthesis of novel supramolecular helicates and attempts to combine them with cisplatin have been described. Additional metal-binding units were introduced onto the surface of the helicates to afford coordination of a cisplatin moiety however attempts to attach cisplatin to the helicates were unsuccessful due to instability of the synthesised compounds. Remarkably, the introduction of a methyl group in the imine position of one of the helicates improved the stability and allowed the formation of the complex with cisplatin to be achieved. Nevertheless the main drawback of this compound was poor solubility in water and instability at room temperature.

A fluorescent europium(III) helicate was synthesised as an attractive bioprobe however poor yield and insolubility in water were the main drawbacks in performing DNA binding studies and other biological experiments therefore they were not pursued further.

In chapter 3, stability tests and DNA binding studies of the synthesised helicates were investigated. The UV/Vis stability experiment revealed that most of the compounds undergo slow degradation upon standing in water. CD and LD studies demonstrated that the helicates bind to DNA inducing alterations in DNA orientation, however retaining its B-conformation. The gel experiments have shown that the

synthesised helicates do not unwind plasmid DNA however they induce the formation of DNA three-way junction structures with the nickel complex being the most effective. As DNA three-way junction structures represent the replication fork formed during the replication process, compounds that bind to and stabilise these structures can possibly affect cellular processes leading to apoptosis.

In chapter 4, the cytotoxic activity of a series of compounds provided by co-workers and synthesised helicates described in this work were explored using the MTT colorimetric assay. The evaluation of antineoplastic activity revealed that most of the compounds were active in cancer cell lines but less active than cisplatin. Only three compounds, the palladium(II) complex provided by Philipp von Grebbe from Professor Bernhard Lippert group, cobalt complex $[Co_2(Lp)_3]Cl_4$ and the synthesised iron(II) helicate $[Fe_2(L_3)_3]Cl_4$, were more cytotoxic in the MDA-MB-231 cell line than cisplatin. When combined supramolecular cylinder and cisplatin in one molecule the cytotoxic effect seemed to be just from cisplatin as the cylinder modification had turned off its activity. Interestingly, tests with cisplatin simply mixed with cylinder showed some activity enhancement in both cancer cell lines compared to that of cylinder alone, however there was no synergism of the two components observed.

5.2 Future work

In this work the synthesis of novel supramolecular helicates was described. The structural similarity with parent complex was retained whilst additional metal binding units were employed onto the ligand structure to afford additional coordinative binding. Upon binding of the anticancer agent to the helicates they fell apart. The instability problems could be overcome by synthesising analogous ruthenium complexes.

Ruthenium compounds are known to be much more stable and inert than their iron counterparts. The stability of the helicates can be partially improved by introducing alkyl substituents in the imine position of the ligand which are known to induce the positive inductive effect and stabilise the molecule. This explains, for instance, the relative stability of the synthesised $[Fe_2(L_1)_3]Cl_4$ complex alone as well as with attached cisplatin.

An interesting approach would be the synthesis of an iron or ruthenium helicate based on 4-(1H-imidazol-1-yl)-2-pyridinecarboxaldehyde as a potent antineoplastic activity was found for its derivatives.[3] The attempts to synthesise this complex through a multiple-step procedure have already been made however they were unsuccessful. An alternative two-step synthesis could be performed (Scheme 5.0).

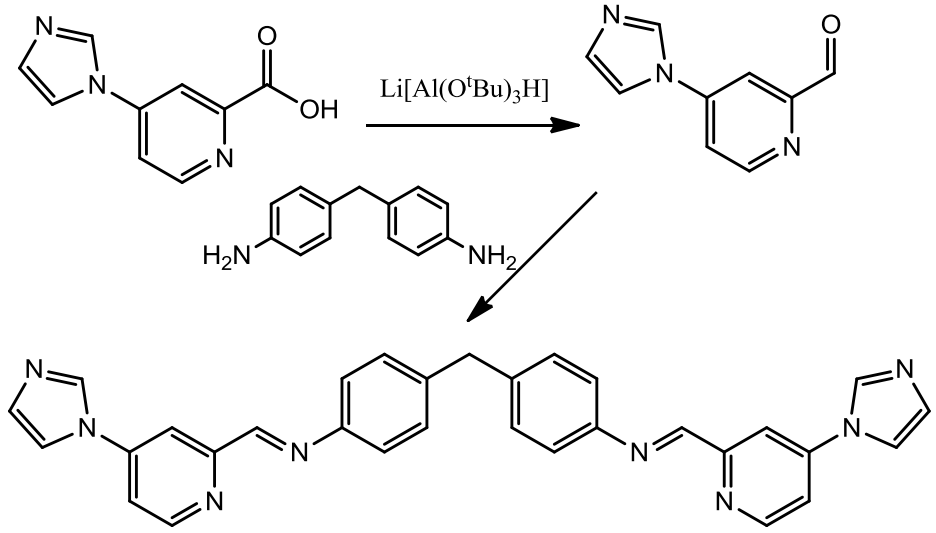

Scheme 5.0 Proposed synthesis of 4-(1H-imidazol-1-yl)-2-pyridinecarboxaldehyde based helicate.

4-(1H-imidazol-1-yl)-2-pyridinecarboxylic acid can be reduced to the corresponding aldehyde by a reported procedure using lithium tri(tert-butoxy)aluminum

hydride.[3] The obtained aldehyde can then be reacted with 4,4'-methylene dianiline to form the ligand.

The poor water solubility of some of the synthesised compounds limits their application. In order to overcome this negative effect, the structure of the molecule could be modified by reducing lipophilicity or introducing solubilising moieties which are polar functional groups such as alcohol, sulfonic acid, phosphate groups, amine, carboxylic acids, etc. These groups are capable of increasing solubility of a compound by interacting with water molecules by means of the hydrogen bonds.[4]

In chapter 4, the activity of the synthesised complexes was assessed in various cancer cell lines by the MTT assay. Additional testing can be performed to measure cellular uptake of the compounds. The cellular uptake of non-luminescent complexes is measured by inductively coupled plasma mass spectrometry (ICP-MS) and atomic absorption spectroscopy (AAS).[5] Flow cytometry[6] and confocal microscopy[7] could be employed to measure the cellular uptake of luminescent compounds. Comet assay can be used for the measurement of DNA damage caused by active radical species produced by some of the complexes.[8] Further studies are required to understand the mechanism of action and difference in activity of the synthesised compounds in various cancer cell lines.

5.3 References:

1. J. M. Lehn, *Chem. Soc. Rev.*, 2007, **36**, 151-160.

2. J. Vicens, Q. Vicens, *J. Incl. Phenom. Macrocycl. Chem.*, 2009, **65**, 221-235.

3. T. Fujisawa, T. Sato, *Organic Syntheses*, 1988, **66**, 116-120.

4. D. B. Troy, *Remington: The Science and Practice of Pharmacy*, 21st ed., Lippincott Williams & Wilkins, Philadelphia, 2006.

5. C. A. Puckett, R. J. Ernst, J. K. Barton, *Dalton Trans.*, 2010, **39**, 1159-1170.

6. M. E. Jiménez-Hernández, G. Orellana, F. Montero, M. T. Portolés, *Photochem. Photobiol.*, 2000, **72**, 28-34.

7. C. P. Montgomery, B. S. Murray, E. J. New, R. Pal, D. Parker, *Acc. Chem. Res.*, 2009, **42**, 925-937.

8. O. Ostling, K. J. Johannson, *Biochem. Biophys. Res. Commun.*, 1984, **123**, 291-298.

Chapter 6

Experimental

6.1 General

All chemicals and reagents were purchased from Sigma-Aldrich, Fisher Scientific, Fluorochem, Appollo Scientific, Alfa Aesar, Fluka and were used without further purification. All reactions were performed under an atmosphere of nitrogen unless otherwise stated. ^{1}H NMR spectra were obtained by using ACIII-300, AVIII-400, and DRX 500 Bruker spectrometers. The spectra were recorded in deuterated solvents purchased from Goss Scientific and analysed by MestReNova software. The experiments on recording ^{1}H NMR experiments at variable temperatures were performed by Dr. Neil Spencer. Electrospray Ionisation (ESI) analyses were performed by Mr. Peter Ashton and Mr. Nick May on a Micromass LCT Time of Flight Mass Spectrometer in a positive and negative ionisation mode. Matrix-Assisted Laser Desorption Ionization (MALDI) data were recorded using a Bruker Bi-flex MALDI Time of Flight mass spectrometer. Elemental analyses were performed on a CE Instruments EA1110 elemental analyser by Mrs. Lianne Hill. X-ray crystal structure data were obtained by the National Crystallography Service in Southampton using Bruker-Nonius KappaCCD diffractometers and analysed by Dr. Louise Male at the University of Birmingham. UV/Visible spectra were recorded on a Cary 5000 Varian spectrophotometer using 1 cm quartz cuvettes. IR spectra were obtained using a Perkin Elmer Spectrum 100 FT-IR Spectrometer. High-pressure liquid chromatography (HPLC) was carried out with an assistance of Mr. Graham Burns on a Dionex Summit HPLC system with a Summit P580P high pressure binary gradient pump and a Summit UVD 170s UV/VIS Multi-Channel Detector with Prep flow cell. Fluorescence experiments were conducted on a FS920 steady state fluorimeter with a Xe lamp (Xe900) and F900 software with the assistance of Doctor Dave Lewis.

6.2 Synthesis of L_1[1]

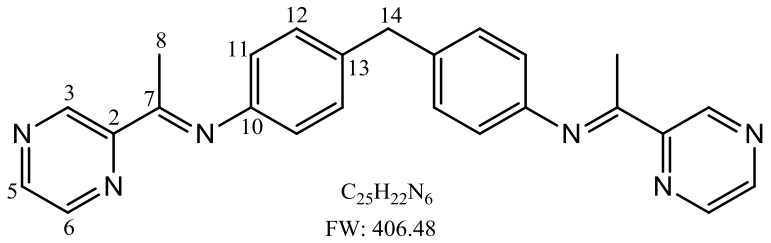

To a stirred solution of acetylpyrazine (90 mg, 0.74 mmol) in methanol (10 mL), 4,4'-methylenedianiline (70 mg, 0.37 mmol) and a few drops of acetic acid was added. The reaction was heated to reflux for 3 hours, cooled and the solvent reduced *in vacuo* to yield a yellow oil. The NMR spectrum revealed that the resulting mixture contained the desired product which was contaminated with unreacted starting materials and half-ligand. Attempts to purify the ligand by column chromatography failed. Therefore a one pot direct synthesis of the complex was carried out without isolation of the pure ligand.

^{1}H NMR (300 MHz, CD_3CN, 298 K): δ = 9.67 (d, 2H, J = 1.1 Hz, H_3), 8.78 (s, 2H, $H_{5/6}$), 8.77 (s, 2H, $H_{5/6}$), 7.39 - 7.35 (m, 8H, H_{11}, H_{12}), 4.07 (s, 2H, H_{14}), 2.46 (s, 6H, H_8).

Mass Spectrum (ESI): m/z = 429 $[C_{25}H_{22}N_6 + Na]^+$

6.2.1 Synthesis of $[Fe_2(L_1)_3](PF_6)_4$[1]

To a stirred solution of acetylpyrazine (90 mg, 0.74 mmol) in methanol (20 mL), a methanolic solution (3 mL) of 4,4'-methylenedianiline (73 mg, 0.37 mmol) and a few drops of acetic acid was added. The reaction was heated under reflux for 3 hours. Iron(II) chloride tetrahydrate (50 mg, 0.25 mmol) was added and the reaction mixture was maintained at the same temperature for 1h. The resulting purple solution was cooled down, concentrated *in vacuo* and placed in H-tubes with a saturated methanolic

solution of ammonium hexafluorophosphate for crystal growth. After 5 days dark purple crystals were collected, washed with methanol and dried *in vacuo* (52 mg, 29 %).

^{1}H NMR (300 MHz, CD_3CN, 298 K): δ = 9.66 (s, 2H, H_3), 8.80 (d, 2H, J = 2.6 Hz, $H_{5/6}$), 7.38 - 7.35 (m, 4H, $H_{5/6}$, $H_{11/12}$), 6.75 (d, 2H, J = 7.7 Hz, $H_{11/12}$), 5.56 (d, 2H, J = 7.7 Hz, $H_{11/12}$), 4.64 (d, 2H, J = 7.7 Hz, $H_{11/12}$), 4.02 (s, 2H, H_{14}), 2.45 (s, 6H, H_8).

Mass Spectrum (ESI): *m/z* = 332 $[Fe_2(C_{25}H_{22}N_6)_3]^{4+}$

Elemental analysis calculated (%) for $[Fe_2(C_{25}H_{22}N_6)_3](PF_6)_4 \bullet H_2O$; C, 46.7; H, 3.5; N, 13.1. Found: C, 46.2; H, 3.4; N, 13.2.

IR: 3648 (br), 1590 (w), 1504 (w), 1466 (w), 1412 (w), 1339 (w), 1381 (w), 1223 (w), 1175 (w), 819 (s), 786 (m), 760 (m), 741 (m), 555 (s) cm^{-1}.

UV/Vis (CH_3CN), λ (ε/$mol^{-1}dm^3cm^{-1}$): 227 (97500), 278 (65600), 570 (16500) nm.

6.2.2 Combining $[Fe_2(L_1)_3](PF_6)_4$ with cisplatin.

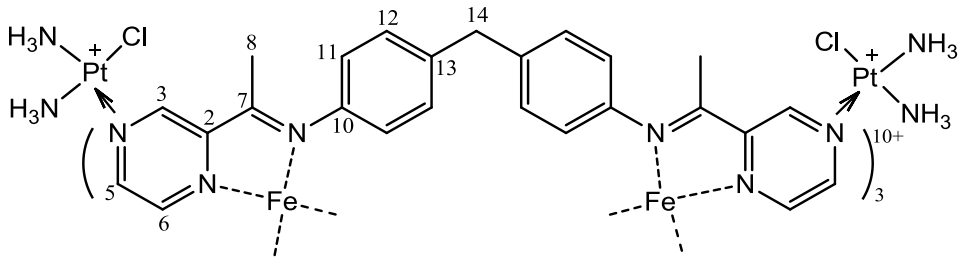

To a solution of *cis*-diamminedichloroplatinum(II) (10 mg, 0.033 mmol) in DMF (1 mL) a solution of silver nitrate (5.4 mg, 0.032 mmol) in DMF (1 mL) was added. The mixture was stirred overnight at room temperature with light exclusion. The white precipitate of silver chloride that had formed was removed by filtration through celite. The filtrate was cooled to -18 °C using propan-2-ol/dry ice bath. $[Fe_2(L_1)_3](PF_6)_4$ complex (11 mg, 0.005 mmol) in DMF (2 mL) was added dropwise over a period of 10

min. The reaction was stirred for 3 hours at -18 °C and then 1 hour at room temperature. The solvent was removed under reduced pressure and the residue was washed with methanol, acetonitrile and ether and dried *in vacuo* to yield the desired complex as a blue solid (17 mg, 79 %).

^{1}H NMR (300 MHz, d_6-DMF, 298 K): δ = 10.12 (s, 2H, H_3), 9.23 (t, 2H, *J* = 3.9 Hz, $H_{5/6}$), 8.25 (d, 2H, *J* = 3.9 Hz, $H_{5/6}$), 7.59 (d, 2H, *J* = 7.7 Hz, $H_{11/12}$), 6.85 (d, 2H, *J* = 7.7 Hz, $H_{11/12}$), 6.12 (d, 2H, *J* = 7.7 Hz, $H_{11/12}$), 5.35 (s, 6H, N$\underline{H}_3$), 4.97 (s, 6H, N$\underline{H}_3$), 4.78 (d, 2H, *J* = 7.7 Hz, $H_{11/12}$), 4.13 (s, 2H, H_{14}), 2.94 (s, 6H, H_8).

Elemental analysis calculated (%) for $[Fe_2(C_{25}H_{22}N_6(Pt_2Cl_2(NH_3)_4))_3](PF_6)_4(NO_3)_6$: C, 23.3; H, 2.7; N, 13.0. Found: C, 23.5; H, 2.8; N, 13.0.

IR: 3210 (br), 3107 (br), 1658 (w), 1599 (w), 1503 (m), 1324 (br), 1221 (w), 1187 (w), 1112 (w), 1080 (w), 1039 (w), 827 (s), 789 (m), 740 (w), 674 (w), 695 (w), 556 (s) cm^{-1}.

UV/Vis (DMF), λ (ε/$mol^{-1}dm^3cm^{-1}$): 344 (35900), 599 (9400), 695 (6800) nm.

6.2.3 Synthesis of cis-bis(dimethylsulphoxide)dichloroplatinum(II)[2]

Potassium tetrachloroplatinate(II) (285 mg, 0.70 mmol) was dissolved in water (3 mL). To the resulting red aqueous solution dimethylsulfoxide (167 mg, 2.1 mmol) was then added. The mixture was left standing overnight at room temperature to form yellow crystals. The crystalline solid was filtered off, washed with ice cold water, ethanol and diethyl ether and dried *in vacuo* (214 mg, 74 %).

^{1}H NMR ($CDCl_3$, 300 MHz, 298 K): δ = 3.56 (s, 12H, C$\underline{H}_3$).

Elemental analysis calculated (%) for $C_4H_{12}PtCl_2S_2O_2$: C, 11.4; H, 2.9. Found: C, 11.7; H, 2.7.

IR: 3037 (w), 3010 (m), 2917 (m), 1399 (m), 1314(m) 1299(m), 1153 (s), 1130 (s), 1016(s), 981 (m), 941 (m), 736 (m), 765 (w), 689 (m) cm^{-1}.

6.2.4 Combining $[Fe_2(L_1)_3]Cl_4$ with *cis*-bis(dimethylsulphoxide)dichloro-platinum(II).

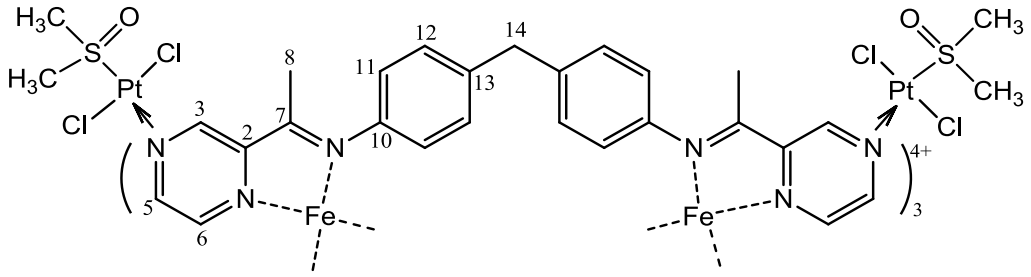

Before performing the experiment the $[Fe_2(L_1)_3](PF_6)_4$ complex was converted to $[Fe_2(L_1)_3]Cl_4$ using chloride form of Dowex 1x8 ion exchange resin. To a suspension of cis-bis(dimethylsulphoxide)dichloroplatinum(II) (43 mg, 0.10 mmol) in methanol (5 mL), a solution of $[Fe_2(L_1)_3]Cl_4$ (25 mg, 0.021 mmol) in methanol (3 mL) was added dropwise over a period of 10 minutes and the mixture was stirred at room temperature for 24 hours. The resulting violet precipitate was collected by filtration and washed with methanol and ether and dried *in vacuo* (47 mg, 78 %).

^{1}H NMR (CH_3CN, 300 MHz, 298 K): δ = 9.72 (s, 2H, H_3), 8.90 (d, 2H, J = 3.1 Hz, $H_{5/6}$), 7.44 (m, 4H, $H_{5/6}$, $H_{11/12}$), 6.79 (dd, 2H, J = 8.2, 2.3 Hz, $H_{11/12}$), 5.61 (dd, 2H, J = 8.2, 2.3 Hz, $H_{11/12}$), 4.68 (dd, 2H, J = 8.2, 2.3 Hz, $H_{11/12}$), 4.07 (s, 2H, H_{14}), 3.30 (d, 12H, J = 5.4 Hz, $C\underline{H}_3$ (DMSO)), 2.52 (d, 6H, J = 4.5 Hz, H_8).

IR: 3503 (br), 3005 (w), 2917 (w), 1592 (m), 1502 (m), 1465 (m), 1411 (m), 1376 (m), 1337 (m), 1302 (m), 1221 (m), 1186 (m), 1128 (s), 1020 (s), 921 (w), 838 (m), 787 (m), 733 (w) cm^{-1}.

6.3 Synthesis of L_2

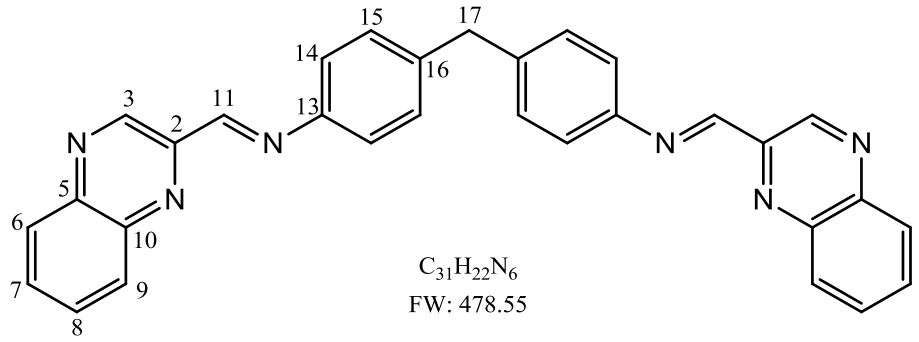

To a solution of quinoxaline-2-carboxaldehyde (100 mg, 0.58 mmol) in methanol (10 mL), 4,4'-methylendianiline (58 mg, 0.29 mmol) in methanol (2 mL) was added dropwise and the reaction mixture was stirred at room temperature overnight. The yellow precipitate that had formed was filtered off, washed with methanol and dried *in vacuo* (76 mg, 55 %).

^{1}H NMR ($CDCl_3$, 300 MHz, 298 K) δ = 9.75 (s, 2H, H_3), 8.83 (s, 2H, H_{11}), 8.21 – 8.11 (m, 4H, H_6, H_9), 7.87 – 7.79 (m, 4H, H_7, H_8), 7.40 – 7.30 (m, 8H, H_{14}, H_{15}), 4.13 (s, 2H, H_{17}).

^{13}C NMR ($CDCl_3$, 400 MHz, 298 K): δ = 158.1 ($2C_{11}$), 148.9 ($2C_2$), 148.4 ($2C_{13}$), 144.1 ($2C_3$), 142.9 ($2C_{5/10}$), 141.9 ($2C_{5/10}$), 140.6 ($2C_{16}$), 130.9 ($2C_7$), 130.4 ($2C_8$), 129.9 ($4C_{14/15}$), 129.6 ($2C_6$), 129.4 ($2C_9$), 121.6 ($4C_{14/15}$), 41.2 ($2C_{17}$).

Melting point: 243 – 245 °C

Mass spectrum (ESI): *m/z* = 501 $[C_{31}H_{22}N_6 + Na]^+$

Elemental analysis calculated (%) for $C_{31}H_{22}N_6$: C, 77.8; H, 4.6; N, 17.6. Found: C, 77.5; H, 4.6; N, 17.6.

IR: 3023 (br), 1623 (w), 1552 (w), 1492 (m), 1464 (w), 1415 (w), 1369 (w), 1319 (w), 1201 (m), 1113 (m), 1126 (m), 1012 (m), 976 (m), 960 (m), 898 (m), 860 (m), 845 (m), 818 (m), 761 (s), 638 (w), 603 (m) cm^{-1}.

6.3.1 Synthesis of $\{[Ag(C_{31}H_{22}N_6)](PF_6)\}_n$

Ligand L_2 (50 mg, 0.10 mmol) and silver acetate (17 mg, 0.10 mmol) were refluxed in methanol (10 mL) for 3 hours with light exclusion. The resulting yellow solution was filtered and the filtrate treated with a saturated solution of ammonium hexafluorophosphate. The yellow precipitate that had formed was collected by filtration, washed with methanol and diethyl ether and dried *in vacuo* (49 mg, 66 %).

^{1}H NMR (300 MHz, d_6-DMF, 298 K): δ = 9.80 (s, 2H, H_3), 9.79 (s, 2H, H_{11}), 8.34 (d, 2H, J = 8.5 Hz, H_6), 8.19 (d, 2H, J = 8.5 Hz, H_9), 8.07 (H_7 signal is evident in the edge of the solvent peak), 7.86 (t, 2H, J = 7.5 Hz, H_8), 7.78 (d, 4H, J = 8.2 Hz, $H_{14/15}$), 7.43 (d, 4H, J = 8.2 Hz, $H_{14/15}$) 4.07 (s, 2H, H_{17}).

Mass Spectrum (ESI): m/z = 1317 $[[Ag_2(C_{31}H_{22}N_6)_2](PF_6)]^+$, 586 $[Ag_2(C_{31}H_{22}N_6)_2]^{2+}$.

Elemental analysis calculated (%) for $\{[Ag(C_{31}H_{22}N_6)](PF_6)\}_n$: C, 50.9; H, 3.0; N, 11.5. Found: C, 50.8; H, 2.9; N, 11.4.

IR: 3655 (br), 1590 (w), 1495 (w), 1370 (w), 1344(w), 1214 (w), 1128 (m), 1024 (w), 940 (w), 874 (w), 829 (s), 775 (m), 760 (m), 625 (w), 610 (w), 556 (s) cm^{-1}.

UV/Vis (DMF), λ (ε/$mol^{-1}dm^3cm^{-1}$): 354 (55800) nm.

6.3.2 Synthesis of $[Cu_2(L_2)_2](PF_6)_2$

To a stirred solution of the ligand L_2 (50 mg, 0.10 mmol) in methanol (10 mL) $[Cu(MeCN)_4](PF_6)$ (39 mg, 0.10 mmol) was added to give a dark brown solution . The reaction mixture was heated under reflux overnight and then cooled to room temperature. The brown precipitate that had formed was filtered off, washed with methanol and ether and dried *in vacuo* (38 mg, 54 %).

^{1}H NMR (CD_3CN, 300 MHz, 298 K): δ = 9.64 (s, 2H, $2H_{11}$), 9.60 (s, 2H, H_3), 8.27 (d, 2H, J = 8.4 Hz, H_6), 7.93 (t, 2H, J = 7.6 Hz, H_7), 7.78 (br s, 2H, H_9), 7.65 (br t, 2H, J = 8.0 Hz, H_8), 7.49 (d, 4H, J = 8.2 Hz, $H_{14/15}$), 7.24 (d, 4H, J = 8.2 Hz, $H_{14/15}$), 3.89 (s, 2H, H_{17}).

Mass Spectrum (ESI): m/z = 542 $[Cu_2(C_{31}H_{22}N_6)_2]^{2+}$

Elemental analysis calculated (%) for $[Cu_2(C_{31}H_{22}N_6)_2](PF_6)_2$: C, 54.2; H, 3.2; N, 12.2. Found: C, 54.4; H, 3.6; N, 11.7.

IR: 3649 (w), 3034 (w), 1606 (w), 1572 (w), 1518 (m), 1489 (m), 1463 (w), 1421 (w), 1367 (m), 1340 (m), 1173 (w), 1214 (m), 1129 (m), 1028 (m), 944 (m), 831 (s), 759 (s) cm^{-1}.

UV/Vis (CH_3CN), λ (ε/$mol^{-1}dm^3cm^{-1}$): 250 (80500), 349 (56500), 577 (2200) nm.

6.4 Ligand L_3

6.4.1 Synthesis of 2-methyl-4,4'-bipyridine[3, 4]

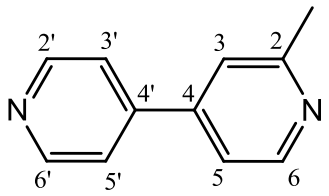

$C_{11}H_{10}N_2$
FW: 170.21

4,4'-bipyridine (15.6 g, 100 mmol) was dissolved in a solution of 98 % sulfuric acid (5 mL) in water (70 mL). Subsequently, acetic acid (30 g, 483 mmol) and a solution of silver nitrate (1.70 g, 10 mmol) in water (20 mL) were added to the solution of bipyridine. The resulting mixture was heated to 110 °C and maintained at that temperature for 30 min. At this point ammonium persulfate (22.8 g, 100 mmol) was added portionwise. When the vigorous evolution of carbon dioxide had finished, the solution was heated at reflux for 30 min, allowed to cool, and made alkaline to a pH value of about 8 by the addition of ammonia. The reaction products were extracted with diethyl ether (6 x 150 mL). The combined extracts were dried over $MgSO_4$ and evaporated in vacuo, to yield a yellow solid. The crude yellow solid was purified by a Dionex Summit HPLC system using a Phenomenex C_{18} column (250 mm x 30 mm) packed with Luna 10 μm using water-methanol (60:40) as an eluent. The desired product was obtained as an off white solid (2.8 g, 17 %).

^{1}H NMR ($CDCl_3$, 300 MHz, 298 K): δ = 8.60 – 8.73 (m, 6H, H_6, $H_{2'}$, $H_{6'}$), 7.52 – 7.32 (m, 8H, H_3, $H_{3'}$, H_5, $H_{5'}$), 2.65 (s, 3H, CH_3).

^{13}C NMR ($CDCl_3$, 400 MHz, 298 K): δ = 159.5 (C_2), 150.5 ($C_{2'}$, $C_{6'}$), 150.0 (C_6), 145.8 (C_4, $C_{4'}$), 121.4 ($C_{3'}$, $C_{5'}$), 120.9 (C_5), 118.5 (C_3).

Melting point: 89 – 92 °C (lit.[4] 92 - 93 °C).

Mass Spectrum (EI): m/z = 170 $[C_{11}H_{10}N_2]^+$

Elemental analysis calculated (%) for $C_{11}H_{10}N_2$: C, 77.6; H, 5.9; N, 16.5. Found: C, 77.6; H, 5.8; N, 16.6.

IR: 3398 (br), 3030 (m), 2920 (w), 1944 (w), 1593 (s), 1537 (m), 1474 (m), 1447 (w) 1394 (m), 1293 (m) , 1218 (m), 1080 (w), 1065 (w), 987 (m), 860 (m), 815 (s), 750 (w), 739 (w), 666 (w), 618 (s), 601 (m), 552 (m) cm^{-1}.

6.4.2 Synthesis of (Z)-2-methyl-(N-dimethylaminovinyl)-[4,4']-bipyridine

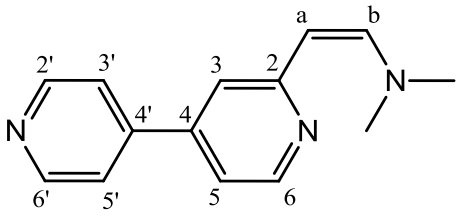

$C_{14}H_{15}N_3$
FW: 225.29

To a stirred solution of 2-methyl-4,4'-bipyridine (1g, 5.9 mmol, 1 equiv.) in DMF (10 mL), tert-butoxybis(diethylamino)methane (3 mL, 14.8 mmol, 2.5 equiv.) was added. The reaction mixture was heated to 140 °C and maintained at that temperature for 18 h. On cooling to room temperature the orange-brownish solution was hydrolyzed with water (20 mL) and extracted with dichloromethane (5 × 20 mL). The organic layers were collected and dried over $MgSO_4$ and the solvent was removed under reduced pressure. The resulting orange solid was recrystallized from dichloromethane-pentane to give the desired product as an orange crystalline material (Yield: 0.37 g, 28 %).

^{1}H NMR ($CDCl_3$, 300 MHz, 298 K): δ = 8.69 (dd, 2H, *J* = 4.5, 1.7 Hz, $H_{2'}$, $H_{6'}$), 8.41 (d, 1H, *J* = 5.2 Hz, H_6), 7.56 (d, 1H, *J* = 13.2 Hz, H_b), 7.51 (dd, 2H, *J* = 4.5, 1.7 Hz, $H_{3'}$, $H_{5'}$), 7.09 (dd, *J* = 1.7, 0.8 Hz, H_3), 7.01 (dd, 1H, *J* = 5.2, 1.7 Hz, H_5), 5.23 (d, 1H, *J* = 13.2 Hz, H_a), 2.92 (s, 6H, $C\underline{H}_3$).

^{13}C NMR ($CDCl_3$, 400 MHz, 298 K): δ = 159.8 (C_2), 150.3 ($C_{2'}$, $C_{6'}$), 149.7 (C_6), 146.7 ($C_{4/4'}$), 145.4 ($C_{4/4'}$), 144.4 (C_b), 121.4 ($C_{5'}$, $C_{3'}$), 116.6 (C_3), 115.1 (C_5), 95.7 (C_a), 40.6 ($2CH_3$).

Melting point: 122 – 126 °C

Mass Spectrum (EI): *m/z* = 226 $[C_{14}H_{15}N_3 + H]^+$

Elemental analysis calculated (%) for $C_{14}H_{15}N_3$: C, 74.6; H, 6.7; N, 18.6. Found: C, 74.5; H, 6.5; N, 18.4.

IR: 3077 (w), 2913 (w), 2804 (w), 1625 (m), 1579 (s), 1524 (s), 1501 (m), 1467 (m), 1423 (s), 1405 (m), 1361 (s), 1290 (m), 1215 (m), 1183 (m), 1102 (m), 1066 (m), 985 (m), 960 (m), 878 (m), 861 (m), 829 (s), 795 (s), 778 (m), 671 (m), 638 (m), 611 (m) cm^{-1}.

6.4.3 Synthesis of 2-formyl-[4,4']-bipyridine[5]

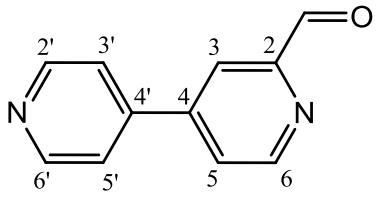

$C_{11}H_8N_2O$
FW: 184.19

(Z)-2-methyl-(N-dimethylaminovinyl)-[4,4']-bipyridine (100 mg, 0.44 mmol) and an

aqueous solution of sodium periodate (0.34 g, 1.6 mmol) were stirred in THF (60 mL) at 40°C for 18h. After cooling to room temperature, the solvent was removed under reduced pressure. The residue was dissolved in DCM (20 mL), washed with water (2 × 30 mL), dried ($MgSO_4$) and the solvent was removed *in vacuo*. Purification by column chromatography using silica and a mixture of DCM-Methanol (97:3) as an eluent gave the desired aldehyde as a white solid (54 mg, 66 %).

^{1}H NMR ($CDCl_3$, 300 MHz, 298 K): δ = 10.17 (s, 1H, C<u>H</u>O), 8.92 (dd, 1H, *J* = 5.0, 0.8 Hz, H_6), 8.79 (dd, 2H, *J* = 4.5, 1.7 Hz, $H_{2'}$, $H_{6'}$), 8.23 (dd, 1H, *J* = 1.9, 0.8 Hz, H_3), 7.78 (dd, 1H, *J* = 5.0, 1.9 Hz, H_5), 7.60 (dd, 2H, *J* = 4.5, 1.7 Hz, $H_{3'}$, $H_{5'}$).

^{13}C NMR ($CDCl_3$, 400 MHz, 298 K): δ = 193.0 (<u>C</u>HO), 153.7 (C_2), 151.1 (C_6), 150.9 ($C_{2'}$, $C_{6'}$), 146. 9 ($C_{4/4'}$), 144.4 ($C_{4/4'}$), 125.3 (H_5), 121.3 ($C_{3'}$, $C_{5'}$), 119.2 (C_3).

Mass Spectrum (EI): *m/z* = 184 $[C_{11}H_8N_2O]^+$

Elemental analysis calculated (%) for $C_{11}H_8N_2O{\cdot}0.4H_2O$: C, 69.0; H, 4.6; N, 14.6. Found: C, 69.1; H, 4.6; N, 14.1.

IR: 3042 (br), 2922 (w), 2858 (m), 1964 (w), 1708 (s), 1591(m), 1536 (m), 1473 (w), 1408 (m), 1375 (w), 1311(w), 1227 (w), 1197 (m), 1058 (w), 990 (m), 904 (m), 872 (w), 819 (s), 740 (m), 670 (m), 661 (m), 598 (m), 611 (s) cm^{-1}.

6.4.4 Synthesis of L_3

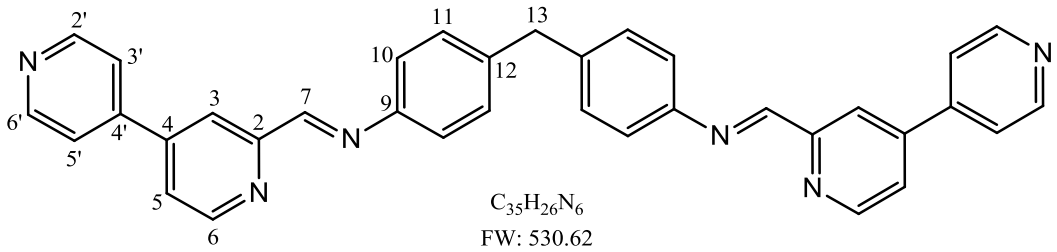

To a stirred solution of 2-formyl-[4,4']-bipyridine (27 mg, 0.15 mmol) in ethanol (2 mL) at room temperature, an ethanolic solution of 4,4'-methylendianiline (14.5 mg, 0.73 mmol) was added dropwise. The reaction mixture was stirred for 24 hours at room temperature and the resultant yellow precipitate was collected by filtration, washed with cold ethanol and diethyl ether and dried *in vacuo* (26 mg, 67 %).

^{1}H NMR ($CDCl_3$, 300 MHz, 298 K): δ = 8.84 (dd, 2H, J = 5.1, 0.8 Hz, H_6), 8.80 (dd, 4H, J = 4.5, 1.7 Hz, $H_{2'}$, $H_{6'}$), 8.72 (s, 2H, H_7), 8.51 (dd, 2H, J = 1.8, 0.8 Hz, H_3), 7.67 (dd, 4H, J = 4.5, 1.7 Hz, $H_{3'}$, $H_{5'}$), 7.64 (dd, 2H, J = 5.1, 1.8 Hz, H_5), 7.32 (H_{10}, H_{11} signals are evident in the edge of the solvent peak), 4.09 (s, 2H, H_{13}).

^{13}C NMR ($CDCl_3$, 400 MHz, 298 K): δ = 159.6 ($2C_7$), 155.7 ($2C_2$), 150.8 ($2C_{2'}$, $2C_{6'}$), 150.5 ($2C_6$), 148.8 ($2C_9$), 146.4 ($2C_{4/4'}$), 146.2 ($2C_{4/4'}$), 140.0 ($2C_{12}$), 129.9 ($4C_{10/11}$), 122.6 ($2C_5$), 121.5 ($4C_{10/11}$, $2C_{3'}$, $2C_{5'}$), 119.3 ($2C_3$), 41.1 (C_{13}).

Melting point: 143 – 145 °C

Mass Spectrum (EI): m/z = 553 $[C_{35}H_{26}N_6 + Na]^+$

IR: 3343 (br), 3221 (br), 1668 (w), 1626 (w), 1590 (m), 1536 (m), 1502 (m), 1473(m), 1404 (m), 1352 (w), 1193 (w), 1072 (m), 992 (m), 929 (w), 851 (m), 817 (s), 779 (w), 736 (w), 655 (w), 616 (s), 582 (w) cm^{-1}.

6.4.4.1 Synthesis of $[Fe_2(L_3)_3](PF_6)_4$

To a stirred solution of L_3 (21 mg, 0.0395 mmol) in methanol (1 mL), a methanolic solution of iron(II) chloride tetrahydrate (5.3 mg, 0.027 mmol) was added dropwise to give a dark violet solution. The mixture was stirred for 3 hours at room temperature and then treated with a saturated solution of ammonium hexafluoropfosphate to form a violet precipitate. The violet solid was collected by vacuum filtration, washed with methanol and diethyl ether and dried *in vacuo* (23 mg, 75 %).

^{1}H NMR (CD_3CN, 300 MHz, 298 K): δ = 8.95 (br s, 2H, H_7), 8.92 (br s, 6H, H_6, $H_{2'}$, $H_{6'}$), 8.07 (br d, 2H, J = 4.2 Hz, H_5) 7.92 (br s, 4H, $H_{3'}$, $H_{5'}$), 7.53 (br d, 2H, J = 3.9 Hz, H_3), 7.01 (br s, 4H, $H_{10/11}$), 5.63 (br s, 4H, $H_{10/11}$), 4.07 (br s, 2H, H_{13}).

Mass Spectrum (EI): m/z = 426 $[Fe_2(C_{35}H_{26}N_6)_3]^{4+}$

Elemental analysis calculated (%) for $[Fe_2(C_{35}H_{26}N_6)_3](PF_6)_4 \bullet 2H_2O$: C, 54.4; H, 3.6; N, 10.5. Found: C, 54.1; H, 3.6; N, 10.9.

IR: 3365 (br)**,** 3035 (br), 1595 (m), 1502 (m), 1471 (m)**,** 1409 (m), 1303 (w), 1203 (w), 1246 (w), 1110 (br), 1072 (w), 1017 (m), 815 (s), 745 (w) cm^{-1}.

UV/Vis (CH_3CN), λ (ε/$mol^{-1}dm^3cm^{-1}$): 241sh (108600), 287sh (41700), 586sh (15100) nm.

6.5 Ligand L_4

6.5.1 Synthesis of 1-pyridine-2-ylmethyl-1H-Imidazole carboxaldehyde[6, 7]

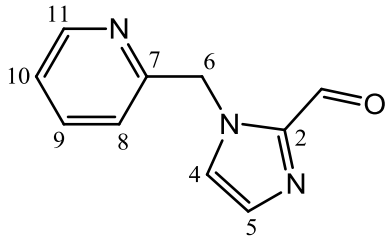

$C_{10}H_9N_3O$
FW: 187.20

To a stirred solution of 2-imidazolecarboxaldehyde (0.55 g, 5.67 mmol) and 2-(bromomethyl)pyridine hydrobromide (1.58 g, 6.24 mmol) in DMF (20 mL), *N,N* – diisopropylethylamine (3.0 mL, 17.01 mmol) was added. The reaction mixture was heated at 80 ºC overnight. After cooling to room temperature, the reaction was quenched with a saturated aqueous solution of $NaHCO_3$ (20 mL) and extracted with DCM (4 x 20 mL). The combined organic layers were washed with brine (30 mL), dried ($MgSO_4$), filtered, and concentrated under reduced pressure to afford brown oil. The crude mixture was purified by a Dionex Summit HPLC system using a Phenomenex C_{18} column (250 mm x 21.2 mm) packed with Luna 10 μm on a solvent gradient starting from 100 % water to 33 % of acetonitrile over 30 minutes to give the desired product as a yellow powder (0.13 g, 14 %).

^{1}H NMR ($CDCl_3$, 300 MHz, 298 K): δ = 9.82 (d, 1H, *J* = 0.9 Hz, C<u>H</u>O), 8.55 (ddd, 1H, *J* = 4.8, 1.7, 0.9 Hz, H_{11}), 7.66 (td, 1H, *J* = 7.7, 1.8 Hz, H_9), 7.37 (br s, 1H, $H_{4/5}$), 7.32 (1H, d, *J* = 0.9 Hz, $H_{4/5}$), 7.19 - 7.25 (m, 2H, H_{10}, H_8), 5.71 (s, 2H, H_6).

^{13}C NMR ($CDCl_3$, 400 MHz, 298 K): δ = 180.3 (CHO), 153.3 (C_7), 147.8 (C_{11}), 141.2 (C_2), 135.3 (C_9), 130.0 ($C_{4/5}$), 125.2 ($C_{4/5}$), 121.3 (C_{10}), 120.4 (C_8), 50.4 (C_6).

Mass Spectrum (EI): *m/z* = 187 $[C_{10}H_9N_3O]^+$

Melting point: 52 – 54 °C

Elemental analysis calculated (%) for $C_{10}H_9N_3O$: C, 64.2; H, 4.8; N, 22.0. Found: C, 64.1; H, 4.7; N, 22.0.

IR: 3103 (w), 2844 (w), 1672 (s), 1586 (m), 1569 (m), 1472 (m), 1412 (s), 1336 (m), 1303 (m), 1253 (m), 1287 (m), 1148 (m), 994 (m), 916 (m), 803 (m), 771 (s), 758 (s), 724 (m), 688 (m), 596 (m) cm^{-1}.

6.5.2 Synthesis of L_4

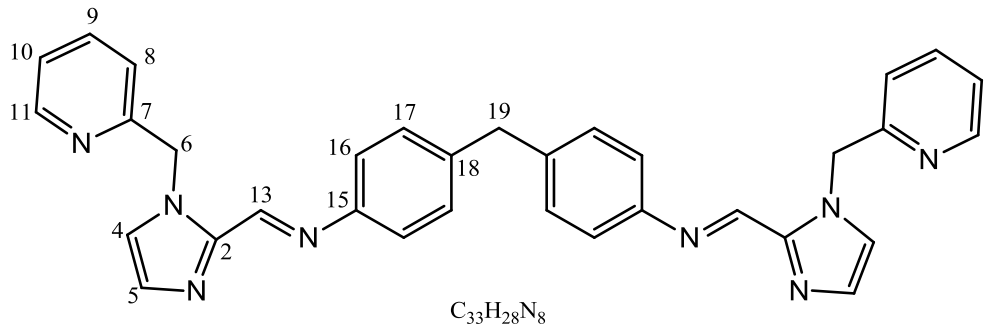

$C_{33}H_{28}N_8$
FW: 536.63

An ethanolic solution of 4,4'-methylendianiline (15.4 mg, 0.077 mmol) was added dropwise to a solution of imidazole-2-carbaxaldehyde (29 mg, 0.155 mmol) in ethanol (5 mL). The reaction mixture was stirred at room temperature overnight. The off-white precipitate that had formed was collected by filtration, washed with cold ethanol and ether and dried *in vacuo* (25 mg, 59 %).

^{1}H NMR ($CDCl_3$, 300 MHz, 298 K): δ = 8.60 (ddd, 2H, *J* = 4.8, 1.7, 0.9 Hz, H_{11}), 8.57 (s, 2H, H_{13}), 7.62 (td, 2H, *J* = 7.7, 1.8 Hz, H_9), 7.29 ($H_{4/5}$ signal is evident on the edge of the solvent peak), 7.25 (br s, 2H, $H_{4/5}$), 7.23 - 7.19 (m, 6H, H_{10}, $H_{16/17}$), 7.14 – 7.03 (m, 6H, H_8, $H_{16/17}$), 5.99 (s, 4H, H_6), 4.00 (s, 2H, H_{19}).

^{13}C NMR ($CDCl_3$, 400 MHz, 298 K): δ = 156.8 ($2C_7$), 150.5 ($2C_{11}$), 149.5 ($2C_{13}$), 148.8 ($2C_2$), 143.2 ($2C_{15}$), 139.6 ($2C_{18}$), 136.9 ($2C_9$), 130.7 ($2C_{4/5}$), 129.7 ($4C_{16/17}$), 125.2 ($2C_{4/5}$), 122.6 ($2C_{10}$), 121.8 ($2C_8$), 121.1 ($4C_{16/17}$), 52.7 ($2C_6$), 41.0 (C_{19}).

Mass Spectrum (EI): *m/z* = 559 $[C_{33}H_{28}N_8 + Na]^+$

Melting point: 168 – 170 °C

Elemental analysis calculated (%) for $C_{33}H_{28}N_8$: C, 73.9; H, 5.3; N, 20.9. Found: C, 73.6; H, 5.7, N, 21.2.

IR: 3094 (w), 3048 (w), 1625 (m), 1594 (m), 1570 (m), 1502 (m), 1467 (m), 1436 (m), 1279 (m), 1208 (m), 1106 (m), 1048 (m), 996 9m), 851 (m), 877 (s), 787 (m), 765 (s), 745 (s), 712 (m), 698 (m), 605 (m) cm^{-1}.

6.5.2.1 Synthesis of $[Fe_2(L_4)_3](PF_6)_4$

To a stirred solution of L_4 (17 mg, 0.032 mmol) in ethanol (5 mL), an ethanolic solution of iron(II) chloride tetrahydrate (4.2 mg, 0.021 mmol) was added dropwise and the mixture was stirred at room temperature for 30 minutes. The resulting solution was treated with a saturated solution of ammonium hexaphlorophosphate and the purple precipitate that formed was collected by filtration, washed with methanol and diethyl ether and dried *in vacuo* (19 mg, 79 %).

^{1}H NMR (CD_3CN, 300 MHz, 298 K): δ = 15.19 (s, 2H, $H_{4/5}$), 13.65 (s, 4H, $H_{4/5,}$ H_{13}), 8.66 (dd, 2H, *J* = 2.7, 1.1 Hz, H_{11}), 7.89 (td, 2H, *J* = 7.2, 1.1 Hz, H_9), 7.35 - 7.19 (m, 4H, H_8, H_{10}), 6.93 (br s, 4H, $H_{16/17}$), 6.57 (br s, 4H, $H_{16/17}$), 4. 69 (d, 2H, *J* = 15.4 Hz, $H_{6a/b}$), 3.30 (s, 2H, H_{19}), 3.02 (d, 2H, *J* = 15.4 Hz, $H_{6a/b}$).

Mass Spectrum (EI): m/z = 430 $[Fe_2(C_{33}H_{28}N_8)_3]^{4+}$, 622 $[[Fe_2(C_{33}H_{28}N_8)_3](PF_6)]^{3+}$, 1006 $[[Fe_2(C_{33}H_{28}N_8)_3](PF_6)_2]^{2+}$.

Elemental analysis calculated (%) for $[Fe_2(C_{33}H_{28}N_8)_3](PF_6)_4 \bullet 3H_2O$: C, 50.5; H, 3.9; N, 14.3. Found: C, 50.6; H, 3.7, N, 13.8.

IR: 3354 (w), 3124 (w), 3062 (w), 1615 (m), 1594 (m), 1502 (m), 1479 (m), 1438 (s), 1330 (w), 1288 (m), 1208 (m), 1132 (m), 1016 (w), 967 (m), 899 (m), 819 (m), 752 (s), 688 (m), 592 (m) cm^{-1}.

UV/Vis (CH_3OH), λ (ε/$mol^{-1}dm^3cm^{-1}$): 268 (57600), 295 (79100), 331 (86900), 553 (2400) nm.

6.5.2.2 Synthesis of $[Ni_2(L_4)_3]Cl_4$

To a stirred solution of ligand L_4 (18 mg, 0.034 mmol) in methanol (5 mL), nickel(II) chloride hexahydrate (5.3 mg, 0.022 mmol) in methanol (2 mL) was added and the mixture was refluxed overnight. After cooling to room temperature diethyl ether was added, the resulting orange precipitate was collected by filtration, washed with diethyl ether and dried *in vacuo* (12 mg, 57 %).

Mass Spectrum (EI): *m/z* = 432 $[Ni_2(C_{33}H_{28}N_8)_3]^{4+}$, 588 $[[Ni_2(C_{33}H_{28}N_8)_3]Cl]^{3+}$, 898 $[[Ni_2(C_{33}H_{28}N_8)_3]Cl_2]^{2+}$.

Elemental analysis calculated (%) for $[Ni_2(C_{33}H_{28}N_8)_3]Cl_4 \bullet 8H_2O$: C, 59.1; H, 5.0; N, 16.7. Found: C, 59.5; H, 5.0; N, 16.8.

IR: 3344 (br), 3053 (w), 1592 (m), 1532 (w), 1484 (m), 1437 (s), 1331 (m), 1292 (m), 1210 (m), 1134 (m), 997 (w), 969 (m), 904 (m), 861 (w), 815 (w), 752 (s) cm^{-1}.

UV/Vis (H_2O), λ (ε/$mol^{-1}dm^3cm^{-1}$): 260 (32600), 328 (55600) nm.

6.6 Ligand L_5

6.6.1 Synthesis of 2,6-pyridinecarboxylic acid monobenzyl ester[8, 9]

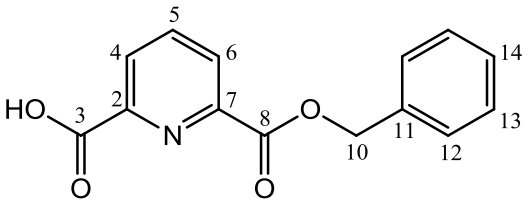

$C_{14}H_{11}NO_4$
FW: 257.24

To a stirred solution of ion exchange resin DOWEX 50W-X8 H^+ 20-50 mesh in BnOH (120 mL) was 2,6-pyridinedicarboxylic acid (11.5 g, 69 mmol) was added and the mixture was heated to 150 Cº for 1.5 hour. The reaction mixture was then cooled; the ion exchange resin was filtered off and washed twice with toluene. The filtrate was extracted with saturated aqueous $NaHCO_3$ (4 x 400 mL). The aqueous layers were combined, acidified with H_2SO_4 and extracted with DCM (3 x 200 mL). The organic layers were combined, washed with brine (400 mL), dried over $MgSO_4$ and evaporated in *vacuo*. The desired product was obtained by recrystallization from AcOEt (100 mL) and hexane (500 mL) as a white powder (4.22 g, 24 %).

^{1}H NMR ($CDCl_3$, 300 MHz, 298 K): δ = 8.44 – 8.37 (m, 2H, H_4, H_6), 8.12 (t, 1H, J = 7.8 Hz, H_5), 7.53 - 7.35 (m, 5H, H_{12}, H_{13}, H_{14}), 5.48 (s, 2H, H_{10}).

^{13}C NMR ($CDCl_3$, 400MHz, 298K): δ = 163.7 (C_3), 163.6 (C_8), 146.8 (C_2), 146.6 (C_7), 139.6 (C_5), 135.0 (C_{11}), 128.9 (C_6), 128.8 ($2C_{13,}$ $2C_{14}$), 128.6 (C_{12}), 127.0 (C_4), 68.1 (C_{10}).

Melting point: 130 – 131 °C (lit.[8] 132 – 133 °C)

Mass Spectrum (EI): m/z = 256 $[C_{14}H_{11}NO_4 - H]^+$

Elemental analysis calculated for (%) $C_{14}H_{11}NO_4$: C, 65.4; H, 4.3; N, 5.4. Found: C, 65.4; H, 4.2; N, 5.6.

IR: 3064 (w), 2880 (br), 2559 (br), 1736 (s), 1695 (s), 1575 (m), 1467 (w), 1499 (w), 1467 (m), 1417 (m), 1329 (m), 1289 (m), 1244 (s), 1152 (s), 1084 (m), 994 (m), 958 (m), 941 (m), 856 (m), 839 (w), 797 (w), 784 (w), 754 (s), 728 (s), 711 (s), 691 (s), 648 (m), 584 (w), 570 (w) cm^{-1}.

6.6.2 Synthesis of 6-(quinoline-6-ylcarbamoyl) picolinate

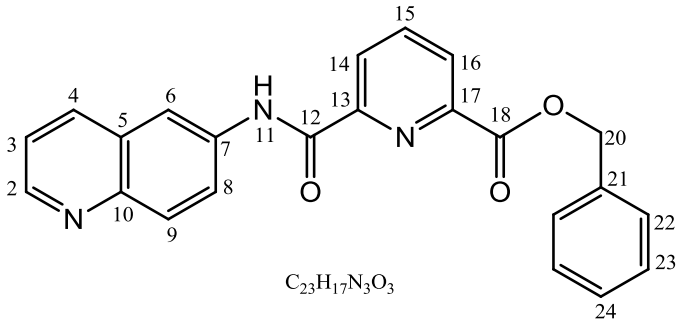

$C_{23}H_{17}N_3O_3$

FW: 383.40

To a stirred solution of 6-aminoquinoline (0. 56 g, 3.9 mmol) in 30 mL anhydrous THF, HOBt (0.53, 3.9 mmol) and monobenzyl ester (1 g, 3.9 mmol) were added at 0 ºC. After stirring for 30 min at 0 ºC, EDCI•HCl (0.79 g, 4.1 mmol) followed by triethylamine (0.57 mL, 4.1 mmol) were added and the mixture was stirred for an additional 30 min at 0 ºC and then at room temperature for 18h. The insoluble material was filtered off and the solvent removed under reduced pressure. Purification of the crude mixture by flash column chromatography on silica, using 2 % methanol in DCM solution as an eluent, gave the desired product as a white solid (0.78 g, 52 %).

^{1}H NMR ($CDCl_3$, 500 MHz, 298 K): δ = 10.31 (s, 1H, NH), 8.87 (dd, 1H, *J* = 4.1, 1.4 Hz, H_2), 8.60 (d, 1H, *J* = 2.3 Hz, H_6), 8.51 (d, 1H, *J* = 7.7 Hz, H_{14}), 8.31 (d, 1H, J = 7.7 Hz, H_{16}), 8.17 (d, *J* = 8.1 Hz, H_4), 8.12 (d, *J* = 9.0 Hz, H_9), 8.08 (t, 1H, *J* = 7.8 Hz, H_{15}), 7.85 (dd, 1H, *J* = 9.0, 2.3 Hz, H_8), 7.55 (d, 2H, *J* = 7.3 Hz, H_{22}), 7.49 - 7.38 (m, 4H, H_3, H_{23}, H_{24}), 5.52 (s, 2H, H_{20}).

^{13}C NMR ($CDCl_3$, 500MHz, 298K): δ = 163.9 (C_{18}), 161.4 (C_{12}), 149.8 (C_{13}), 149.5 (C_2), 146.5 (C_{17}), 145.7 (C_{10}), 138.9 (C_{15}), 135.8 (C_4), 135.3 (C_7, C_{21}), 130.3 (C_9), 128.8 (C_5), 128.7 ($2C_{23}$), 128.6 (C_{24}), 128.3 ($2C_{22}$), 127.6 (C_{16}), 125.5 (C_{14}), 123.3 (C_8), 121.6 (C_3), 116.2 (C_6), 67.7 (C_{20}).

Melting point: 143 – 145 °C

Mass Spectrum (EI): *m/z* = 383 $[C_{23}H_{17}N_3O_3]^+$

Elemental analysis calculated (%) for $C_{23}H_{17}N_3O_3$: C, 72.1; H, 4.5; N, 11.0. Found: C, 72.1; H, 4.3; N, 10.9.

IR: 3461 (w), 3220 (br), 1727 (s), 1670 (m), 1627 (w), 1574 (m), 1540 (s), 1498 (m), 1468 (m), 1448 (m), 1430 (m), 1381 (m), 1364 (m), 1294 (s), 1238 (s), 1221 (m), 1164 (m), 1143 (m), 1112 (w), 1077 (m), 1032 (w), 1001 (m), 947 (m), 925 (m), 908 (m), 873 (m), 840 (m), 797 (m), 755 (s), 742 (s), 718 (m), 698 (s), 687 (s), 651 (m), 589 (m) cm^{-1}.

6.6.3 Synthesis of 6-(quinoline-6-ylcarbamoyl) picolinic acid

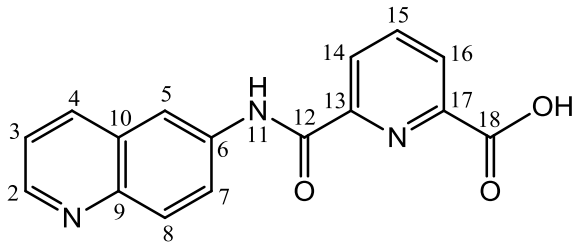

$C_{16}H_{11}N_3O_3$
FW: 293.28

6-(quinoline-6-ylcarbamoyl) picolinate (0.60 g, 1.57 mmol) was stirred in a mixture of MeOH/THF (10 mL, 1:1) with 10 % Pd/C catalyst (0.1 equivalent) at room temperature under a hydrogen gas atmosphere. The completion of the reaction was followed by TLC. The solution was filtered through a pad of celite to remove the catalyst and the solvent was evaporated under reduced pressure to give the desired product as a yellow solid (0.33 g, 72 %).

^{1}H NMR (d_6-DMSO, 500 MHz, 298 K): δ = 11.7 (s, 1H, NH), 8.84 (dd, 1H, J = 4.1, 1.5 Hz, H_2), 8.56 (d, 1H, J = 2.2 Hz, H_5), 8.45 (dd, 1H, J = 7.2, 1.7 Hz, H_{14}), 8.37 - 8.32 (m, 2H, H_4, H_{16}), 8.29 (t, 1H, J = 7.7 Hz, H_{15}), 8.15 (dd, 1H, J = 9.1, 2.3 Hz, H_7), 8.07 (d, 1H, J = 9.1 Hz, H_8), 7.52 (dd, 1H, J = 8.3, 4.2 Hz, H_3).

^{13}C NMR (d_6-DMSO, 500 MHz, 298 K): δ = 165.0 (C_{18}), 161.8 (C_{12}), 149.5 (C_2), 149.0 (C_{13}), 146.8 (C_{17}), 145.1 (C_9), 140.1 (C_{15}), 135.9 (C_6), 135.6 (C_4), 129.5 (C_8), 128.2 (C_{10}), 127.1 (C_{16}), 125.6 (C_{14}), 124.2 (C_7), 121.9 (C_3), 116.9 (C_5).

Melting point: decomposes above 292 °C

Mass Spectrum (EI): m/z = 293 $[C_{16}H_{11}N_3O_3]^+$

Elemental analysis calculated for (%) $C_{16}H_{11}N_3O_3$: C, 65.5; H, 3.8; N, 14.3. Found: C, 65.2; H, 4.0; N, 14.1.

IR: 3377 (br), 3209 (br), 3051 (br), 1678 (w), 1622 (w), 1594 (m), 1502 (m), 1476 (m), 1437 (m), 1357 (w), 1287 (w), 1207 (w), 1131 (w), 996 (w), 826 (m), 750 (m) 555 (s) cm^{-1}.

6.6.4 Synthesis of L_5

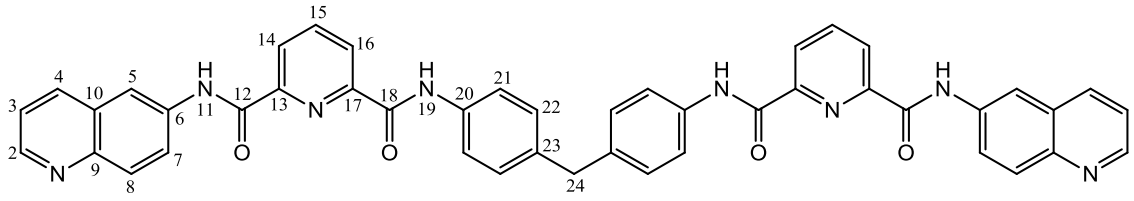

$C_{45}H_{32}N_8O_4$
FW: 748.79

To a stirred solution of 4,4'- diaminodiphenylmethane (93 mg, 0.47 mmol) in THF (15 mL), 6-(quinoline-6-ylcarbamoyl)picolinic acid (300 mg, 1.0 mmol) was added followed by HOBt (133 mg, 0.99 mmol) at 0 °C and the resulting mixture was stirred for 15 minutes at the same temperature. EDCI•HCl (189 mg, 0.98 mmol), triethylamine (0.14 mL, 0.98 mmol) and DMAP (69 mg, 0.57 mmol) were then added to the reaction mixture and the solution was stirred for 18h at room temperature The insoluble material was filtered off and the solvent was removed under reduced pressure. The residue was purified by flash column chromatography on silica, using 5 % methanol in DCM solution as an eluent, to afford L_5 as a white powder (140 mg, 37 %).

^{1}H NMR (d_6-DMSO, 400 MHz, 298 K): δ = 11.34 (s, 2H, H_{11}), 11.09 (s, 2H, H_{19}), 8.86 (dd, 2H, J = 4.1, 1.5 Hz, H_2), 8.68 (d, 2H, J = 2.2 Hz, H_5), 8.48 - 8.38 (m, 6H, H_4, H_{14}, H_{16}), 8.33 (t, 2H, J = 7.7 Hz, H_{15}), 8.23 (dd, 2H, J = 9.1, 2.2 Hz, H_7), 8.11 (d, 2H, J =

9.1 Hz, H_8), 7.80 (d, 4H, *J* = 8.4 Hz, $H_{21/22}$), 7.54 (dd, 2H, *J* = 8.3, 4.2 Hz, H_3), 7.36 (d, 4H, *J* = 8.4 Hz, $H_{21/22}$), 4.02 (s, 2H, H_{24}).

^{13}C NMR (d_6-DMSO, 400 MHz, 298 K): δ = 162.0 ($2C_{12}$), 161.5 ($2C_{18}$), 149.5 ($2C_2$), 149.0 ($2C_{13}$), 148.6 ($2C_{17}$), 145.1 ($2C_9$), 140.0 ($2C_{15}$), 137.5 ($2C_{20}$), 136.0 ($2C_6$, $2C_{23}$), 135.7 ($2C_4$), 129.4 ($2C_8$), 129.0 ($4C_{21/22}$), 128.2 ($2C_{10}$), 125.4 ($2C_{14}$, $2C_{16}$), 125.3 ($2C_7$), 121.9 ($2C_3$), 121.4 ($4C_{21/22}$), 117.2 ($2C_5$), 40.1 (C_{24}).

Melting point: 250 – 252 °C

Mass Spectrum (EI): *m/z* = 771 $[C_{45}H_{32}N_8O_4 + MeOH]^+$

Elemental analysis calculated (%) for $C_{45}H_{32}N_8O_4$: C, 72.2; H, 4.3; N, 15.0. Found: C, 71.7; H, 4.8; N, 14.7.

IR: 3303 (br), 3229 (br), 1686 (m), 1658 (m), 1587 (m), 1525 (s), 1445 (m), 1409 (m), 1380 (m), 1322 (m), 1220 (m), 1114 (m), 1128 (m), 1072 (m), 1000 (m), 929 (m), 871 (m), 829 (m), 719 (m), 677 (m), 649 (m) cm^{-1}.

6.6.4.1 Synthesis of $[Eu_2(L_5)_3]Cl_6$

To a flask containing a solution of $CH_3OH/CHCl_3$ (8 mL, 1:1), ligand L_5 (26 mg, 0.035 mmol) and europium(III) chloride hexahydrate (8.5 mg, 0.023 mmol) were added and the resulting mixture was heated under reflux for 24 hours. The mixture was cooled down to room temperature, and the resulting pale yellow solid was collected by filtration, washed with ether and dried in *vacuo* (7.8 mg, 24 %).

Elemental analysis calculated (%) for $[Eu_2(C_{45}H_{32}N_8O_4)_3]Cl_6 \bullet 3CHCl_3 \bullet H_2O$: C, 52.9; H, 3.2; N, 10.7. Found: C, 52.6; H, 3.5; N, 10.3.

IR: 3209 (br), 3085 (br), 2618 (br), 1627 (br), 1583 (s), 1554 (m), 1510 (m), 1434 (m), 1375 (m), 1279 (m), 1110 (br), 1019 (s), 945 (w), 820 (w), 759 (m), 729 (m) cm^{-1}.

UV/Vis (DMSO), λ (ε/mol^{-1}dm^{3}cm^{-1}): 308 (84700) nm.

6.7 Experimental procedure for DNA binding studies

All experiments were carried out using ultrapure water (molecular biology reagent). Stock solutions of calf thymus DNA (ct-DNA) (10 mg per 20 mL), sodium chloride (40 μM), and sodium cacodylate (4 μM) were prepared and stored frozen until the day of the experiment. Fresh samples containing ct-DNA (300 μM), sodium chloride (20 mM) and sodium cacodylate (2 mM) were prepared on the day of the experiment. In order to determine the concentration of ct-DNA the absorbance spectrum of the DNA sample was recorded. The absorbance at 260 nm, with a known molar extinction coefficient of ε = 6600 mol^{-1} dm^3 cm^{-1}, was identified and the concentration of ct-DNA was calculated using the Beer-Lambert Law.

Circular Dichroism (CD) spectra were recorded in 1 cm and 1 mm cuvettes using a Jasco J-715 spectropolarimeter. Titrations of the complex with the solution of ct-DNA were carried out at constant concentration of DNA. In order to keep the concentration of the DNA constant during the experiment, a stock solution with a double concentration of ct-DNA (600 μM) and buffer (NaCl 40 μM and 4 μM sodium cacodylate) was prepared. After adding X μL of the metal complex solution to the 300 μM ct-DNA, X μL of ct-DNA stock of double concentration (600 μM) was added. The concentration of the metal complex was increased during the experiment. By varying the concentration of the metal complex, different ratios of DNA base/metal complex with a range from 60:1 to 4:1 were obtained.

Linear dichroism (LD) spectra were collected on a Jasco J-715 spectropolarimeter adapted for LD measurements. The concentration of ct-DNA for the experiment was

determined in a similar way as described above for the CD experiment. Unlike in the CD experiment, a flow cuvette cell consisting of two cylinders with an annular gap of 0.5 mm, giving a 1 mm path length, was used for LD measurements. The speed of the cuvette rotation during the spectra measurements was maintained at approximately 1200 rpm. The DNA concentration was kept constant throughout the experiment.

6.8 Experimental procedure for agarose gel electrophoresis

Plasmid DNA pBR322 was purchased from Fermentas and kept frozen until the day of use. To prepare the gel 2 g of agarose was dissolved in 200 mL of Tris-Acetate EDTA (1X) buffer (TAE) by heating in a microwave for a few minutes and then the gel was allowed to cool down and set. The plasmid was dissolved in ultrapure water and the complex was added to the solution. The total prepared solution of 20 μL contained 2 μL of pBR322 (stock concentration was 0.5 μg/μL), 1.03 to 12.83 μL of the complex solution (stock concentration was 60 μM) and was made up with water. Compounds that were not very soluble in water were dissolved in 1 - 5 % DMSO/water solution. The samples were incubated for 1 hour at 37 ºC. After incubation, 4 μL of loading buffer containing 30 % glycerol, 0.05 % bromophenol blue and 0.025 % cyanol xylene was added to each sample and 18 μL of the prepared solutions was loaded on the agarose gel. The gel experiment was performed using an Amersham Biosciences HE99X Maxi submarine kit. The gel was run in TAE (1X) buffer at a constant voltage of 120 V (6 Vcm^{-1}) for 180 minutes. After the electrophoresis was finished, the gel was stained with ethidium bromide (0.5 mg mL^{-1}) for 10 - 15 minutes. The gel was visualized using an UVidoc Platinum System (UViDoc, Cambridge, UK) at 312 nm.

6.9 Experimental procedure for polyacrylamide gel (PAGE)

6.9.1 Radioactive labelling

4.8 μL of ultrapure water, 1 μL of 10x bacteriophage T4 polynucleotide kinase buffer, 1.2 μL of 100 μM oligonucleotide (S3), 1 μL of bacteriophage T4 polynucleotide kinase (purchased from New England Biolab) and 2 μL of γ-^{32}P ATP (6000 Ci/mmol) (obtained from Perkin Elmer) were mixed together in an eppendorf and incubated at 37 ºC for 40 minutes. In order to deactivate the action of polynucleotide kinase the solution was then heated to 80 ºC and maintained at that temperature for 3 minutes. A QIAquick nucleotide removal kit (QIAGEN) was used to purify the radioactive-labelled DNA fragments from unreacted ATP. 10 volumes of PN buffer were added to 1 volume of the reaction sample. Then the solution was introduced onto a QIAquick spin column with a 2 mL collection tube and the mixture was centrifuge for 1 minute at 6000 rpm. The flow-through was discarded after centrifugation. The QIAquick spin column was introduced into a new collection tube and 500 μL of PE buffer was added. The mixture was centrifuged at 6000 rpm and the flow-through was discarded. The addition of 500 μL PE buffer was repeated. The column was then centrifuged at 13,000 rpm for 1 minute to remove the remaining buffer. The column was placed into an eppendorf and 30 μL of ultrapure water was added onto the column. The solution was allowed to stand for 5 minutes and then was centrifuged at 13,000 rpm for 2 minutes to obtain an 4 μM stock solution of radiolabelled DNA.

6.9.2 Polyacrylamide gel preparation

To prepare 15 % native polyacrylamide gel, 100 mL of 10X buffer containing 892 mM of tris(hydroxymethy) amino methane and 890 mM of boric acid was mixed with 375 mL of 40 % acrylamide (29:1) (from Geneflow) and 525 mL of ultra-pure water. The 15 % native gel was prepared before the experiment and kept at 4 ºC. On the day of the experiment 50 mL of 15 % gel was mixed with 250 μL of 10 % (w/v) ammonium persulphate and 25 μL of tetramethylenediamine (TEMED) in a 50 mL falcon centrifuge tube. The prepared solution was poured onto the set of glass plates and the gel was left to polymerise for 30 – 40 minutes. Before use in the experiment, the excess residues of the gel were removed and each well of the gel was first washed with water and then with a TB running buffer.

6.9.3 PAGE electrophoresis experiment

The oligonucleotide sequences used in the experiments, S1: CGGAACGGCACTCG, S2: CGAGTGCAGCGTGG, S3: CCACGCTCGTTCCG, were purchased from Eurofins (Germany). 2 μM stock solutions of oligonucleotide strands S1, S2 and S3 were prepared. The oligonucleotide sequences were mixed with the complexes in TB buffer containing 89 mM tris(hydroxymethy) amino methane, 89 mM boric acid and 1 M sodium chloride. The prepared samples were incubated for 1 hour at room temperature and then placed on ice for 15 - 20 minutes. 5 μL of 30 % glycerol was added to each eppendorf and 13 μL of each sample was loaded onto 15 % polyacrylamide gel. The experiment was performed for 4 hours at 120 V using Gel System equipment (Thermo Scientific, UK). The gel was exposed on a phosphor imaging plate for 1 - 16 hours

depending on how fresh the radioactive ATP was used. The radiogel image was obtained from a Molecular imager FX (Bio-Rad). The quantification of the gel was carried out using the Quantity One programme.

6.10 Cell Culture

6.10.1 Materials and Methods

DMEM and RPMI medium and FBS were obtained from Invitrogen. Antibiotic antimycotic solution, L-glutamine, trypsin-EDTA, HEPES buffer ((4-(2-hydroxyethyl)-1-piperazineethanesulfonic acid) solution, sodium pyruvate, MTT (3-(4,5-Dimethylthiazol-2-yl)-2,5-diphenyltetrazolium bromide) and DMSO were obtained from Sigma-Aldrich, UK. Tissue culture flasks and 96 well microtiter plates were obtained from Appleton Woods, UK. A2780, A2780cisR, MDA-MB-231 and SK-OV-3 cell lines were purchased from the Health Protection Agency, European collection of cell cultures (ECACC). All reagents for cell culture were autoclaved before use. Manipulations with cells were carried out in sterile conditions in a class 1 tissue culture hood (Aura B4, Bio Air, Italy).

6.10.2 Cell growth conditions

Different types of media were used for different cell lines. A2780, A2780cisR and SK-OV-3 ovarian cancer cell lines were grown in Roswell Park Memorial Institute medium (RPMI-1640) and the MDA-MB-231 cell line in Dulbecco`s Modified Eagle`s medium (DMEM). The media was supplemented with 10 % FBS, 1 % L-glutamine, 1 % HEPES buffer, 1 % sodium pyruvate and 1 % antibiotic. Phenol red is added to media as a pH indicator. Cells were grown as monolayers in medium and maintained in an incubator

(MCO-15AC, Sanyo, Japan) at 37 C° and humidified atmosphere (5 % CO_2, 95 % air). Cells were refreshed every 2 days and regularly checked for the absence of contamination.

6.10.3 Medium preparation

70 mL of fresh medium was removed from the bottle (500 mL, purchased from Initrogen) and discarded. 5 ml of antibiotic antimycotic, 15ml of GSH (5 mL of L-glutamine, 5 mL of sodium pyruvate, 5 mL of HEPES buffer) and 50 mL of FBS (fetal bovine serum) were added to the medium.

6.10.4 Defrosting cells

Cells were kept in a cryovessel in liquid nitrogen. To defrost the cells they were taken out of the cryovessel and warmed up to 37 °C in a water bath. The cells were added to a falcon centrifuge tube and resuspended with fresh medium. The cells with medium were then placed in flasks (15 mL of cells with medium for 75 cm^2 flask) and left overnight in the incubator to attach to the flask surface. The next day medium was refreshed to remove DMSO, which is a component of a freezing medium, and cells were placed in the incubator for growing.

6.10.5 Cell passaging

Medium, Trypsin-EDTA solution and PBS were warmed to 37 ºC in a water bath before use. Cells were taken out of the incubator and medium was removed from the flask. Cells were washed with 10 mL of PBS solution and then 2.5 mL (for 75 cm^2 flasks) of trypsin-EDTA solution was added. The flask with cells was then placed in the incubator

for 3 - 4 minutes. The cells were detached from the flask surface by gently hitting the flask with a hand. The action of trypsin was neutralized by addition of medium 3 times volume of trypsin (7.5 mL). The suspension of cells with medium was transferred to a 50 mL falcon tube and cells were centrifuged at 1000 rpm at 25 ºC for 7 minutes. The medium was removed from the tube and discarded. The formed pellet of cells was resuspended in fresh medium and cells were split depending on cell density and type of cell line (1:3 to 1:6 for MDA-MB-231; 1:2 to 1:3 SK-OV-3; 1:3 to1:6 A2780; 1:5 to 1:20 A2780cisR). Cells with fresh medium were placed in the incubator for growing.

6.10.6 Cell counting and seeding

The procedure for cell passaging was performed before cell counting was carried out. The pellet of cells formed as a result of centrifugation was resuspended in 1 mL of fresh medium and the cells were counted using an improved Neubauer counting chamber. To count cells, 190 µL of Trypan blue dye was added to an eppendorf. 10 µL of cell suspension was added and the solution was mixed well. 10 µL of the cells with dye was introduced on to each side of the counting chamber and cell counting was performed using a microscope. The amount of cells necessary for the experiment was calculated and aliquots with a right amount of cells in the medium were prepared. MDA-MB-231 and SK-OV-3 cell lines were seeded at a density of 8000 – 10000 cells per well, A2780 and A2780cisR cell lines were seeded at a density of 4000 – 6000 cells per well. 100 µL of the prepared aliquots of cells in medium was seeded in each well of the 96 flatbottom mocrititer well plates. Plates were incubated at 37 ºC for 24 hours to allow cells to attach to the flask surface before treatment with the synthesized compounds.

6.10.7 Cell testing procedure

200 μM stock solutions of the metal complexes in medium were prepared. After the plates had been incubated for 24 hours they were treated with 100 μL of six different concentrations of the complex (200 μM, 100 μM, 50 μM, 25 μM, 12.5 μM). 100 μL of fresh medium was added to the control wells and the plates were incubated for 72 hours.

6.10.8 MTT assay

After 72 hours of incubation, 50 μL of MTT solution (5 mg/mL in PBS) was added to each well of the plate except for 3 wells of the control and then incubated for a further 2 hours. Medium with MTT was removed subsequently and formed purple crystals of formazan were dissolved by the addition of 200 μL of DMSO in each well of the plate. The plates were left for 15 minutes to ensure full solubilisation of the purple crystals. The absorbance was measured using a microplate reader (Bio Rad) set at 590 nm.

6.10.9 Cells freezing procedure

When cells were no longer needed they were frozen gradually by placing in a freezer at -70 ºC and then in a cryovessel with liquid nitrogen. The procedure for freezing cells is similar to the one of cell passaging, however after the centrifugation and removal of the medium, the cells were resuspended in a 10 % DMSO/FBS solution. 1 mL of cells in freezing medium was placed in a cryovial and frozen.

6.11 References:

1. M. Pascu, F. Tuna, E. Kolodziejczyk, G. I. Pascu, G. Clarkson and M. J. Hannon, *Dalton. Trans.*, 2004, 1546-1555.

2. M. Huxley, PhD thesis, University of Warwick, 2006.

3. A. Barltrop and A. C. Jackson, *J. Chem. Soc., Perkin Trans. 2*, 1984, 367-371.

4. C.-L. Chen, J. M. Ellsworth, A. M. Goforth, M. D. Smith, C.-Y. Su and H.-C. zur Loye, *Dalton Trans.*, 2006, 5278-5286.

5. HE Chemical Co., Ltd., China.

6. J. L. Moore, S. M. Taylor and V. Soloshonok, *ARKIVOC*, 2005, **VI**, 287-292.

7. G. J. Bridger, R. T. Skerlj, A. Kaller, C. Harwig, D. Bogucki, T. Wilson, J. Crawford, E. J. McEachern, B. Atsma, S. Nan *et al.*, *PCT Int. Appl.*, 2003,WO 2003055876 A1 20030710.

8. Y. Hamuro, S. J. Geib, and A. D. Hamilton, *J. Am. Chem. Soc.*, 1997, **119**, 10587-10593.

9. F. Stomeo, C. Lincheneau, J. P. Leonard, J. E. O'Brien, R. D. Peacock, C. P. McCoy, T. Gunnlaugsson, *J. Am. Chem. Soc.*, 2009, **131**, 9636-9637.

Appendix

A - Crystallographic data of the $[Cu_2(L_2)_2](PF_6)_2$ complex

Empirical Formula	$C_{62}H_{44}Cu_2N_{12}$, $2PF_6$	
Formula Weight	1374.11	
Temperature	120(2) K	
Wavelength	0.71073 Å	
Crystal System	Monoclinic	
Space Group	P 2_1	
Unit Cell Dimensions	a = 10.633(2) Å	α = 90°
	b = 20.396(4) Å	β = 99.966(9)°
	c = 16.328(3) Å	γ = 90°
Volume	3487.5(12) $Å^3$	
Z	2	
Density (calculated)	1.309 Mg/m^3	
Absorption Coefficient	0.733 mm^{-1}	
Crystal Size	0.18 x 0.05 x 0.02 mm^3	
Reflections Collected	19669	
Independent Reflections	10977 [R(int) = 0.0799]	
Data / Restraints / Parameters	10977 / 1240 / 827	
Goodness-of-fit on F^2	1.175	
Final R indices [I>2sigma(I)]	R_1 = 0.1580, wR_2 = 0.3775	
R indices (all data)	R_1 = 0.2483, wR_2 = 0.4239	
Largest diff. Peak and hole	0.662 and -0.849 $e.Å^{-3}$	

B - Crystallographic data of the $[Fe_2(L_4)_3](PF_6)_4$ complex

Empirical Formula	$C_{99}\ H_{84}\ Fe_2\ N_{24},\ 4(P\ F_6)$	
Formula Weight	2448.25	
Temperature	120(2) K	
Wavelength	0.71073 Å	
Crystal System	Triclinic	
Space Group	P-1	
Unit Cell Dimensions	a = 14.6717(4) Å	γ = 66.665(2)°
	b = 18.6418(5) Å	β = 83.538(2)°
	c = 22.0009(4) Å	γ = 80.3500(10)°
Volume	5439.9(2) $Å^3$	
Z	2	
Density (calculated)	1.495 Mg/m^3	
Absorption Coefficient	0.429 mm^{-1}	
Crystal size	0.20 x 0.08 x 0.05 mm^3	
Reflections collected	74537	
Independent reflections	19136 [R(int) = 0.0847]	
Data / restraints / parameters	19136 / 2060 / 1624	
Goodness-of-fit on F^2	1.084	
Final R indices [I>2sigma(I)]	R_1 = 0.1032, wR_2 = 0.1782	
R indices (all data)	R_1 = 0.1676, wR_2 = 0.2127	
Largest diff. peak and hole	1.035 and -0.766 $e.Å^{-3}$	

C - Crystallographic data of the $[Ni_2(L_4)_3](PF_6)_4$ complex

Empirical Formula	$C_{99}\ H_{84}\ N_{24}\ Ni_2,\ 4(PF_6)$	
Formula Weight	2463.42	
Temperature	120(2) K	
Wavelength	0.71073 Å	
Crystal System	Triclinic	
Space Group	P -1	
Unit Cell Dimensions	a = 13.3692(9) Å	α = 113.514(3)°
	b = 22.2187(16) Å	β = 102.465(3)°
	c = 22.4798(18) Å	γ = 97.137(4)°
Volume	5811.4(7) $Å^3$	
Z	2	
Density (calculated)	1.408 Mg/m^3	
Absorption Coefficient	0.476 mm^{-1}	
Crystal size	0.05 x 0.05 x 0.02 mm^3	
Reflections Collected	68732	
Independent Reflections	20085 [R(int) = 0.2118]	
Data / restraints / parameters	20085 / 1612 / 1481	
Goodness-of-fit on F^2	1.023	
Final R indices [I>2sigma(I)]	R_1 = 0.1796, wR_2 = 0.3672	
R indices (all data)	R_1 = 0.3444, wR_2 = 0.4462	
Largest diff. peak and hole	0.824 and -0.519 $e.Å^{-3}$	